ABSTRACT

Title of Dissertation:	CHARACTERIZING THE ROLE OF THE PHOSPHOENOLPYRUVATE-DEPENDENT PHOSPHOTRANSFERASE SYSTEM ENZYME II LOCI IN THE PATHOGENESIS OF THE GROUP A STREPTOCOCCUS
	Ganesh Sundar, Doctor of Philosophy, 2017
Dissertation directed by:	Dr. Kevin S. McIver, Professor, Department of Cell Biology and Molecular Genetics

The Group A Streptococcus (GAS, *Streptococcus pyogenes*) is a Gram-positive human pathogen that must adapt to unique host environments in order to survive. Links between sugar metabolism and virulence have been demonstrated in GAS, where mutants in the phosphoenolpyruvate-dependent phosphotransferase system (PTS) exhibited Streptolysin S (SLS)-mediated hemolysis during exponential growth. This early onset hemolysis correlated with an increased lesion size and severity in a murine soft tissue infection model when compared with parental M1T1 MGAS5005. To identify the PTS components responsible for this phenotype, we insertionally inactivated the 14 annotated PTS EIIC-encoding genes in the GAS MGAS5005 genome to functionally characterize each EIIC. It was found that a few EIIs had a limited influence on PTS sugar metabolism, whereas others were promiscuous. The mannose-specific EII locus exhibited the most influence on PTS sugar metabolism. Importantly, the mannose-specific EII also acted to prevent the early

onset of SLS-mediated hemolysis. These roles were not identical in two different M1T1 GAS strains, highlighting the versatility of the PTS to adapt to strain-specific needs. This is further illustrated by the fructose-specific EII, which is important for survival in whole human blood for MGAS5005, but not 5448. The mannose-specific EII can transport glucose in other pathogens, but the route of glucose utilization is unknown in GAS. MGAS5005 mutants were generated in a non-PTS glucose transporter (GlcU) and a glucokinase (NagC) of an annotated non-PTS glucose metabolic pathway. Since Δ*ptsI*, Δ*nagC*, and Δ*glcU* all grow to some extent in glucose, it is evident that glucose can be metabolized both by PTS and non-PTS routes. . However, the route of glucose utilization affects overall pathogenesis, as Δ*nagC* survives like WT in whole human blood, whereas *ptsI* is unable to survive. Subcutaneous infection of mice with Δ*nagC* did not exhibit increased lesion size, although these lesions are more severe than MGAS5005 due to the early onset of hemolysis. Overall this suggests that the routes of glucose metabolism greatly influence SLS-mediated hemolysis. These results highlight that PTS carbohydrate metabolism plays an important role for GAS pathogenesis in both the skin and whole human blood, through the actions of EIIs.

CHARACTERIZING THE ROLE OF THE PHOSPHOENOLPYRUVATE PHOSPHOTRANSFERASE SYSTEM ENZYME II LOCI IN THE PATHOGENESIS OF THE GROUP A STREPTOCOCUS

by

Ganesh Sundar

Dissertation submitted to the Faculty of the Graduate School of the
University of Maryland, College Park, in partial fulfillment
of the requirements for the degree of
Doctor of Philosophy
2017

Advisory Committee:
Professor Kevin S. McIver, Ph.D, Chair
Professor Vincent T. Lee, Ph.D
Professor Daniel Nelson, Ph.D
Professor Richard Stewart, Ph.D
Professor Wade C. Winkler, Ph.D

Dedication

I would like to dedicate this dissertation to my friends and family who have helped me get to where I am today. I would especially like to dedicate this to my wife, Priyadarhisni Potapragada, for tolerating my long days and weekends in getting to this point. Your support has been tremendous in getting me over the finish line. I would also like to sincerely thank my sister and my parents for giving me the foundation to succeed. I would not be in this position today if you all did not set the tone for success, and sacrificed more than I can imagine to get me here.

Finally, I would like to dedicate this to two special people who are not here today. Bhavani Chiti: you taught me how to be myself, and to always attack my dreams with a sense of urgency and passion. Kutti Thatha: you taught me to love science, being one of the few scientists in our family.

Acknowledgement

I would like to acknowledge my lab members for all their help in getting me to this point. Between our coffee trips, lab lunches, gatherings at meetings and Kevin's house, and your scientific help, I would not have been able to get through graduate school successfully. Thank you all for everything you have done for me along the way, and I look forward to remaining friends for the rest of our lives. These 5 years have been extremely enjoyable. I would also like to acknowledge my commitee for everything science and non-science. Hopefully I have met your expectations as a graduate student. Finally, I want to acknowledge my mentor, Kevin. You taught me what it takes to succeed in this field, and have trained me to use my skills in my future. Thank you all tremendously.

Table of Contents

Table of Contents

Table of Contents

Table of Contents

Table of Contents

Table of Contents

Table of Contents

List of Tables

List of Figures

List of Figures

List of Figures

List of Abbreviations

Abbreviation	*Full term*
α	alpha
aa	amino acid
ABCs	Active Bacterial Core surveillance
ASPGN	acute post-streptococcal glomerulonephritis
ARF	acute rheumatic fever
ATP	adenosine triphosphate
β	beta
bp	base pair
BSA	bovine serum albumin
B. subtilis	*Bacillus subtilis*
C	Celsius
CcpA	catabolite control protein A
CCR	carbon catabolite repression
CDC	Center for Disease Control
CDM	chemically defined media
cDNA	complementary DNA
CFU	colony forming units
C. difficile	*Clostridium dificile*
Cm	Chlorampenicol
CovRS	control of virulence two-component system
cre	catabolite response element
CSF	cerebrospinal fluid
DEPC	diethyl pyrocarbonate
dH2O	distilled water
DHAP	Dihydroxyacetone phosphate
DMSO	Dimethyl sulfoxide
DNA	deoxyribonucleic acid
DNase	deoxyribonuclease
dNTPs	deoxyribonucleic acid triphosphate monomers
ED	Entner–Doudoroff Pathway
EI	Enzyme I
EII	Enzyme II
E.coli	*Escherichia coli*
FBP	fructose-1,6-bisphophate
FBS	Fetal Bovine Serum
g	gravity
g	gram
GAP	glyceraldehyde-3-phosphate
GAS	Group A Streptococcus
GBS	Group B Streptococcus
gDNA	genomic DNA
h	hour
H_2O_2	hydrogen peroxide
HA^2	hyaluronic acid
His, H	histidine
HK	histidine kinase
HMDB	human metabolite database
Hpr	histidine phosphocarrier
HprK/P	Hpr kinase/phosphatase
iGAS	invasive Group A Streptococcus

List of Abbreviations

ABBR.	*Full term*
i.p.	intraperitoneal
IVIG	intravenouse immunoglobulin
kb	kilobase
kDa	kilo-Dalton
KDPG	2-dehydro-3-deoxy-phosphogluconate
K. pneumoniae	*Klebsiella pneumoniae*
L	liter
LB	Luria-Bertani medium
M	molar
m	milli
μ	micro
MF	multiplication factor
Mga	multiple gene regulator of Group A streptrococcus
MOI	multiplicity of infection
M1T1	serotype of GAS most commonly found in North America
NADH	nicotinamide adenine dinucleotide
NCBI	National Center for Biotechnology Information
NEB	New England Biolabs
NETs	Neutrophil extracellular trap
NF	necrotizing faciitis
ng	nanograms
nM	nanomolar
OCD	obsessive compulsive disorder
OF	opacity factor
ORF	open reading frame
OV	omnilog values
PAMP	pathogen associated molecular patterns
PANDAS	pediatric autoimmune neuropsychiatric disorders associated with streptococcal infections
PCR	polymerase chain reaction
PCVR	PRD-containing virulence regulator
PEP	phosphoenolpyruvate
PMN	polymorphonuclear leuokocyte
PPP	Pentose-phosphate pathway
PRD	PTS regulatory domain
PTS	phosphoenolpyruvate-dependent phosphotransferase system
RBC	Reb blood cell
RNA	ribonucleic acid
RNA-seq	RNA-sequencing
RR	response regulator
RT	reverse transcriptase
SC	Sydenham's chorea
SDS	sodium dodecyl sulfate
Ser, S	serine
S. aureus	*Staphylococcus aureus*
S. gordonii	*Streptococcus gordonii*
Sp	Spectinomycin
S.pyogenes	*Streptococcus pyogenes*
S. pneumoniae	*Streptococcus pneumoniae*

List of Abbreviations

ABBR.	*Full term*
SLO	streptolysin O
SLS	streptolysin S
SRA	sequence read archive
STSS	streptococcal toxic shock syndrome
TCA	tricarboxylic acid cycle
TCS	two-component system
TE	tris/EDTA
THY	Todd-Hewitt yeast extract medium
TM	transmembrane
TraSH	transposon-site hybridization
UV	ultraviolet
WT	wildtype

Chapter 1: Literature Review

Historical perspective

In 1842, Ignaz Semmelweis demonstrated that you could reduce the mortality rate in hospital birthing wards by having the doctors wash their hands and cleaning the sheets between patients. This prevented the spread of puerperal fever, or more commonly known as childbed fever, which was the cause of the high mortality rate. Pasteur would later validate his work at a seminar in 1879 at the French Academy of Sciences, when he stated that the epidemic seen in hospital wards was the result of a chain-forming microbe that was being spread by the hospital staff from sick to healthy patients (Ferretti, 2016). Despite this notion, Semmelweis' work was generally ridiculed, and he died in an asylum from a blood infection 2 weeks after he was admitted (Ferretti, 2016). Pasteur was the first to isolate streptococcus from women with puerperal fever. However, the first mention of streptococcus was in 1874, when Theodor Billroth described the microbe found in wound infections (Ferretti, 2016). *Streptococcus* (twisted berry) *pyogenes* (pus-forming) officially got its name in 1884, when Friedrich Julius Rosenbach isolated this bacterium from suppurative lesions (Ferretti, 2016, Evans, 1936). In the 1920s, George and Gladys Dick showed that scarlet fever was associated with a sore throat caused by hemolytic streptococci that produced a secreted toxin that they referred to as Dick toxin (Ferretti, 2016). These important events set the foundation for research in streptococcal diseases that have plagued the world for centuries.

Classification of GAS

Streptococcus pyogenes is a Gram-positive human pathogen that forms chains during growth. GAS exhibits beta-hemolysis (complete lysis of red blood cells) when streaked on 5% sheep blood agar plates. It currently has no other known reservoirs outside of humans, is catalase negative, and does not form spores. Colonies are opaque and tend to be mucoid, especially in strains that express increased amounts of capsule (Martin, 2000).

GAS is also a facultative anaerobe, so it is still able to grow in the presence of oxygen. However, it does not contain a complete TCA cycle, so GAS relies mainly on glycolysis for the fermentation of sugars, usually leading to the production of lactic acid. GAS can be grown in the presence of many sugars; however, it is auxotrophic for multiple amino acids (Slade *et al*., 1951).

In 1933, Rebecca Lancefield was able to divide streptococcal species through surface antigens, splitting them into Groups from A to X, with the Group A Streptococcus isolated strains from human diseases (Ferretti, 2016). She later developed the Lancefield M-typing system, a serological antigen-antibody reaction system to identify distinct M types. M protein is a surface protein on GAS that has multiple functions, most notably in resistance to phagocytosis (Ferretti, 2016, Lancefield, 1962). To differentiate the M type of a strain, antisera from rabbits against different M types was incubated with the extraction of the M protein from a strain and monitored for the formation of precipitate (Facklam, 1999). Serum opacity factor typing can also be used, as some M-types produce opacity factor (OF, apoproteinase), which increases the opacity of mammalian serum (Facklam, 1999). T typing further classifies similar M types. T antigen is also detected by agglutination assays, and is often used in conjunction with M typing (Beall *et al.*, 1998). The serotype most prominently found in invasive and noninvasive infections in North America is M1T1.

Clinical perspective

GAS normally colonizes the nasopharyngeal mucosa or the skin of humans, as it is a strictly human pathogen. This leads to the development of pharyngitis and impetigo, which can be treated with antibiotics, and are generally self limiting. However, there are many strains that are invasive and can access sterile sites via the bloodstream, leading to more severe outcomes such as necrotizing fasciitis, scarlet fever, STSS and septicemia. Complications can also occur post infection with the development of streptococcal reactive arthritis, rheumatic fever, and glomerulonephritis. GAS infections have also been linked to

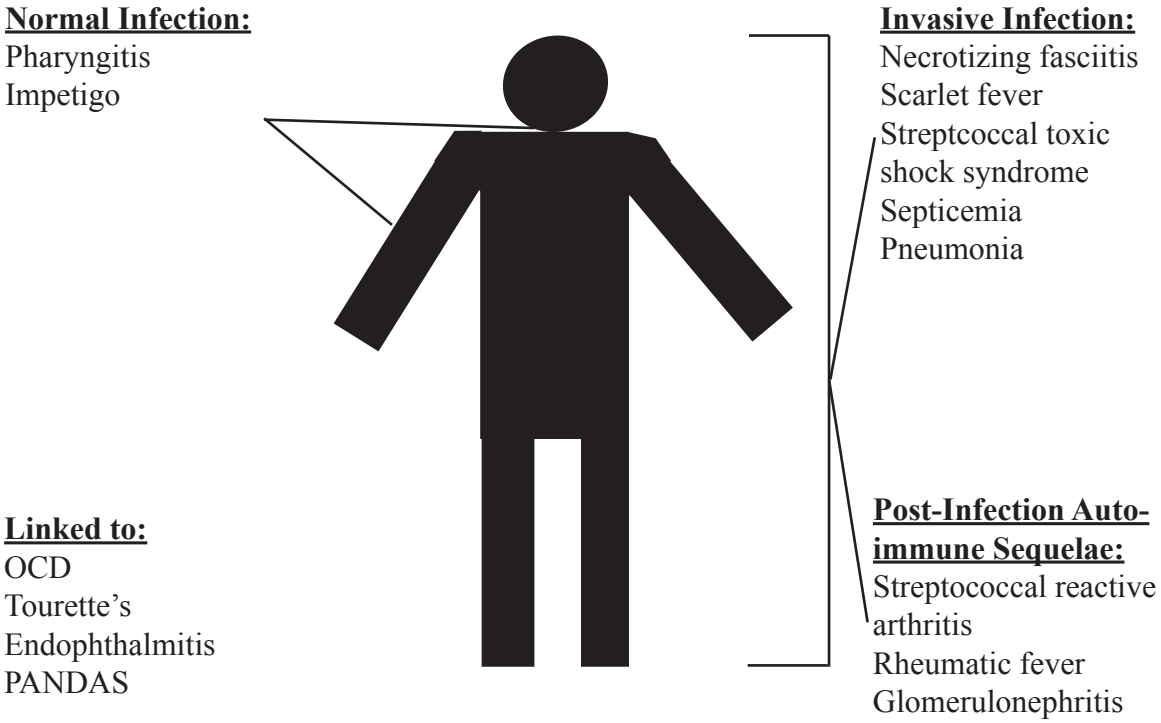

Figure 1.1 Examples of clinical manifestations of GAS infections. GAS infections are typically split into three disease categories. Each are shown here, with examples of typical clinical outcomes listed as examples below. Examples of neuropsychiatric disorders linked to GAS infections are also shown. Black lines depict areas of the human body that are usually affected in these conditions.

obsessive compulsive disorder (OCD), tourettes, endophthalmitis, and more controversially, pediatric autoimmune neuropsychiatric disorders associated with strepotcoccal infections (PANDAS) (**Fig 1.1**). Without a licensed vaccine against GAS, these infections lead to more than 500,000 deaths every year making it the 9th leading infectious cause of human mortality worldwide (Cunningham, 2008). The following section will look at some of the symptoms mentioned above in more detail.

Pharyngitis (Non Invasive). Pharyngitis develops when GAS colonies the throat, often noted by white spots visible to the eye. GAS is the cause of pharyngitis in 20-40% of children between 5-15 years old, most commonly in the winter or spring in the US. Pharyngitis is often accompanied with fever, pain while swallowing, and tender lymph nodes, but vomiting, abdominal pain, and edema of the tonsils can also occur. Symptoms

usually resolve within a week, although GAS is still present in the throat if antibiotics are not administered. Complications such as peritonsillar abscess, sinusitis, otitis media, and bacteremia can also occur from pharyngitis. Throat swabs are primarily used to diagnose GAS infections, and once confirmed, patients are given either penicillin (preferred) or cephalosporin (penicillin allergic patients) (Wessels, 2016).

Impetigo (Non Invasive). Infections of the skin usually result in impetigo, which is an infection of the outer keratin layer. These infections form crusty patches usually on the lower extremities and the face and occur in mostly tropical areas associated with poorer living conditions and declining personal hygiene practices. Like with pharyngitis, these infections are localized and are treated with penicillin. Complications can also occur, most notably acute glomerulonephritis (Stevens, 2016).

Necrotizing Fasciitis (Invasive). Invasive infections in the U.S. have become increasingly abundant after 1980, such as necrotizing fasciitis (NF), where GAS is able to penetrate into deeper tissues and destroy underlying layers. This spreads very quickly, (24-72 hours) from the site of infection, with extensive tissue necrosis and inflammation becoming more and more apparent (Stevens, 2016b). Mortality rates are between 70-80%, and many times removal of the infected tissue or amputation is the only course of treatment (Stevens, 2016b).

Streptococcal Toxic Shock Syndrome (Invasive). Streptococcal toxic shock syndrome (STSS) is when a GAS infection leads to systematic organ failure, typically through bacteremia as GAS moves from the site of infection to sterile sites. Many GAS toxins act as superantigens for T-cells, which leads to massive cytokine induction. STSS begins with fever, chills, nausea and vomiting. Pain begins to increase, along with disorientation, tachycardia, and tachypnea (Stevens, 2016b). In last phase of STSS, hypotension and organ failure begin. Because many patients only come into the hospital at this point, death usually occurs 24-48 hours post-admission (Stevens, 2016b). Once a patient is admitted

and confirmed to have STSS, they are treated with broad-spectrum antibiotics, put on ventilator, given intravenous immune globulin (IVIG), among other drastic measures (Stevens, 2016b). STSS rarely develops from pharyngeal infections (Stevens, 2016b).

Scarlet Fever (Invasive). Scarlet Fever can occur in combination with pharyngitis, where a red rash that feels like sandpaper begins to develop on the trunk of the body and spreads to the arms and legs. According to the CDC, scarlet fever symptoms include fever, headaches, swollen glands, nausea, vomiting, abdominal pain, and a strawberry tongue. Although still not well understood, these infections are treatable and usual resolve quickly (CDC). Streptococcal pyrogenic exotoxins are thought to play a primary role in the development of scarlet fever (Wessels, 2016). Although rare, GAS skin infections can also lead to the development of scarlet fever (Wessels, 2016).

Glomerulonephritis (Post-Infection). Acute poststreptococcal glomerulonephritis (APSGN) is an infection that occurs after GAS infection where nephritogenic immune complexes form in circulation or when the antigen and antibody collide in the glomeruli. These stimulate the activity of immune cells, leading to an inappropriate inflammatory response (Rodriguez-Iturbe, 2016). Treatment, outside of the treatment of the GAS infection, includes limiting salt and fluid intake (Rodriguez-Iturbe, 2016). Diuretics generally have mixed results, as some are beneficial, but most lead to additional complications (Rodriguez-Iturbe, 2016). APSGN can also lead to chronic kidney disease, impaired renal function, and persisting arterial stiffness (Rodriguez-Iturbe, 2016). The mortality rate for APSGN is around 30%; however, prognosis for children is usually very good (Rodriguez-Iturbe, 2016).

Acute Rheumatic Fever, ARF (Post-Infection). ARF is a post-infection complication that develops in children ages 5-15 as a result of a GAS pharyngeal infection only. The major criteria for diagnosis of ARF after a confirmed GAS infection are carditis, polyarthritis, chorea, subcutaneous nodules, and erythema marginatum, with only 2 of these

required for a positive diagnosis. ARF occurs when antibodies produced by B-cells against GAS, M protein, or GlcNAc bind to valve endothelium in the heart. Damaged endothelium recruit activated T cells that produce cytokines and infiltrate the heart valve, where they elicit a γ-interferon TH1 response. Autoimmune activity of T cells breaks down the heart valve, causing an increased immune response and impairing heart function. Repeated infections lead to scarring of the heart valve in patients, making them more susceptible to repeated bouts of ARF (Cunningham, 2016).

PANDAS (Post-Infection). A more controversial post-infection complication is the development of Pediatric Autoimmune Neuropsychiatric Disorders Associated with Streptocccal infections (PANDAS). The criteria for a PANDAS diagnosis is (1) OCD/tic, (2) Prepubertal symptom onset, (3) Acute onset of symptom, (4) Close timing of *S. pyogenes* infection and symptom onset, and (5) presence of neurologic abnormalities (Swedo *et al*., 1998). The controversy for this condition stems from the difficulty in reliably linking the cause of neuropsychiatric disorders to GAS infections. Different techniques may be used to test for GAS infections. Additionally, tics/OCD are the manifestation of complex processes and are hard to strictly associate to one trigger. Depending on the study, there is reported to be either an association, or no association between these two clinical manifestations (Murphy *et al.*, 2012, Bernstein *et al*., 2010, Kurlan *et al.*, 2008, Leckman *et al.*, 2011). However, antibody cross-reactivity between GAS and the brain occurs in some patients with Syndenham's chorea (SC) (Orefici *et al.,* 2016). These antibodies stimulate excess dopamine signaling in the brain, leading to the development of symptoms. PANDAS patients had similar antibodies against dopamine receptors as SC patients (Cox *et al.*, 2013). Associative evidence exists from animal models showing that the presence and absence of these antibodies help mediate SC and PANDAS. Whether these mechanisms actually link neuropsychiatric disorders to streptococcal infections is still controversial (Orefici *et al.,*2016).

Global distribution

A significant number of GAS infections occur around the world each year, leading to both mortality and economic loss as a result of treatment expenses. The 2010 Global Burden of Disease study estimated that 140,495,000 cases of impetigo occurred worldwide each year (Hay *et al*., 2014). Pharyngitis cases are harder to estimate, as there are high rates of throat colonization of GAS in school-aged children combined with misclassification of pharyngitis causes (Sanyahumbi *et al*, 2016). More severe clinical manifestations of GAS infections lead to more problematic infections, and afflict millions of people worldwide. Although estimates of acute rheumatic fever and glomerulonephritis vary widely based on the region of the world, the 2010 Global Burden of Disease study estimated over 34 million cases of rheumatic heart disease leading to over 345,000 deaths a year (Sanyahumbi *et al*, 2016).

Invasive cases in United States

The Active Bacterial Core surveillance (ABCs) set up by the CDC Emerging Infection Program network monitors the occurrence of invasive bacterial infections in 10 sites across the country to map disease trends (CDC, 1997-2014). From 1997-2014, invasive GAS (iGAS) infections in the elderly (>50 years old) have increased (**Fig. 1.2A**). The number of cases observed between the ages of 5-17 is relatively low. This would suggest that the elderly may be more susceptible to more invasive forms of GAS infections. Overall, the estimated number of national cases has increased, although the number of resulting deaths has stayed the same (**Fig. 1.2B**). Compared to two other commonly invasive streptococci [Group B Streptoccocus (GBS) and *S. pneumonaie*], the number of deaths has remained the same, indicating that therapeutic interventions are not improving to effectively treat invasive infections (**Fig. 1.2C**). Additionally, the number of overall cases of invasive disease has decreased for *S. pneumonaie*, but this has not been the case for GAS (**Fig. 1.2C**). With the estimated % of cases resulting in death remaining around

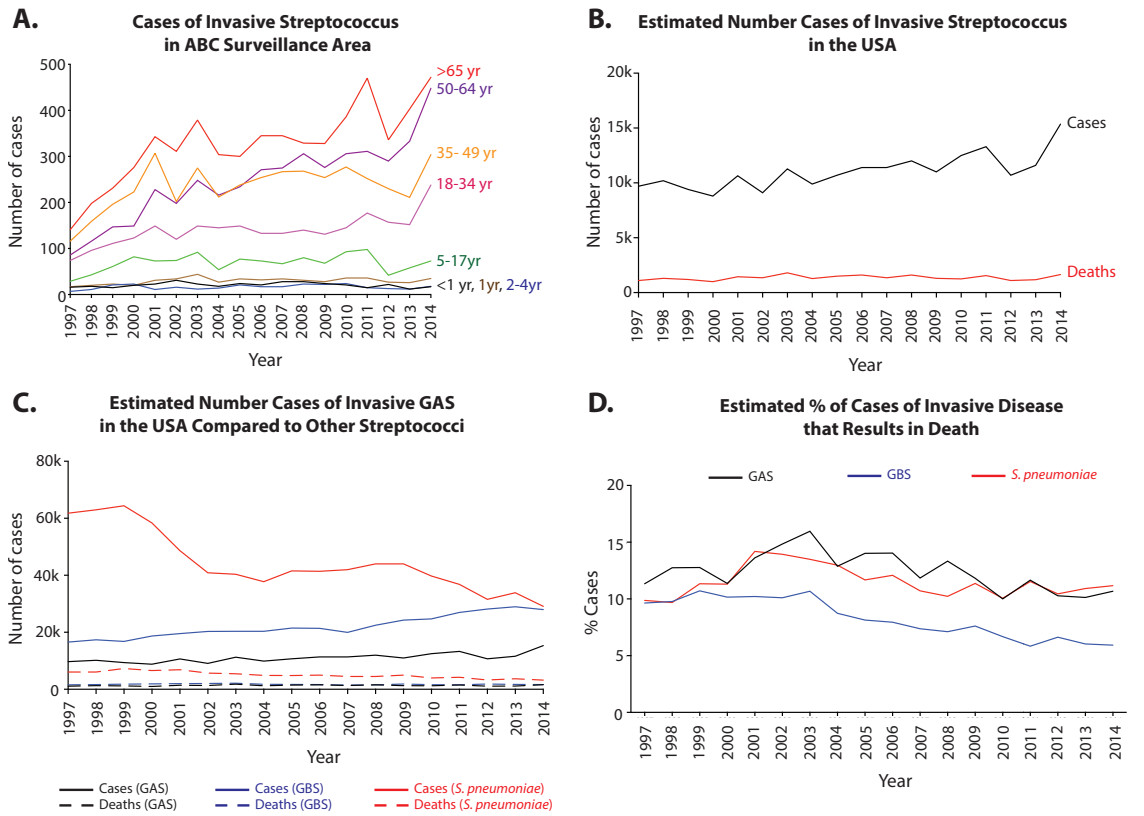

Figure 1.2 Trends of invasive streptococcal infections as determined by the CDC ABC program (https://www.cdc.gov/abcs/reports-findings/surv-reports.html). (A) Invasive GAS infections from 1997-2014 were graphed according to age group and the number of cases observed in each surveillance area. **(B)** Based on the data from the observed areas, the CDC estimated the number of invasive GAS infections that occur nationwide over the 17-year period. The black line represents the number of cases, whereas the red line depicts the estimated number of deaths. **(C)** The estimated number of cases and deaths for GAS (black) was compared to two other streptococcal species: (1) GBS (blue) and (2) *S. pneumoniae* (red). Solid lines illustrate the number of cases estimated, and the dotted lines represent the number of deaths estimated. **(D)** The CDC also estimated the % of deaths that resulted from invasive streptococcal infections. The same color scheme as observed in (C) was used.

10-15% for GAS over the last 17 years, increased understanding of the pathogenesis of iGAS strains is essential to improve therapeutic interventions (**Fig. 1.2D**).

Vaccine production

Currently, a licensed vaccine does not exist for GAS, with vaccine development hindered by the fact that a US federal ban existed from 1969 to 2006 that prevented testing of GAS vaccines in humans (Dale *et. al.*, 2016). This was the result of a trial in which 3

children were thought to develop ARF as a result of the vaccine, although this has been disputed by the trial authors (Dale *et. al.*, 2016). A 26-valent M protein based vaccine has completed phase I and II clinical trials, and has been shown to provide protective immunity for 79% of serotypes found in the United States (Dale *et. al.*, 2016). This vaccine has been shown to provide immunity without generating cross-reactive antibodies, a historically well-documented problem with the immune response to GAS infections in general (Hu *et al.*, 2002, Dale *et. al.*, 2016). Based on increasing epidemiological studies, a 30-valent M protein vaccine was developed, which accounted for 98% of the serotypes identified in North America, and for 78% of invasive disease in Europe (Dale *et. al.*, 2016). Although other targets have been used as the basis for development of a vaccine, such as fibronectin-binding protein (Kawabata *et al*., 2001), serum opacity factor (Courtney *et. al.*, 2003, Schulze *et. al.*, 2006), and SpeB (Kapur *et al*., 1994), these have not yet moved beyond animal studies (Dale *et. al.*, 2016). The development of vaccines has improved and shows promise, but there is still not an available vaccine for human use. Therefore, ongoing studies to find more beneficial therapeutic targets are essential.

Rise of the M1T1 clone

The rise of the M1T1 clone of GAS can be attributed to the acquisition of new genes that allow it to infect humans with greater persistence. M1T1 infections rose in the late 1980s, and have now frequently been isolated from invasive (iGAS) and noninvasive infections. Two prophages, encoding a superantigen (*speA2*) and a streptococcal nuclease (*sda1*), have been identified in M1T1 strains that diversify these clones from other M1 strains. The *speA2* reintroduction into M1T1 is thought to coincide with its global rise, as for 60 years before, M1 isolates did not have SpeA2. Sda1 degrades DNA neutrophil extracellular traps (NETs), which allow GAS to escape and invade host tissues. The SpeB cysteine protease degrades many GAS virulence factors important for virulence, thereby

decreasing virulence potential. However, invasive strains have much lower SpeB as the result of a spontaneous mutation in *covS*. The CovRS two-component system regulates around 15% of the genome, including many virulence genes. This increase in virulence gene expression, and the lower expression of *speB,* gives rise to more severe infections and the increased ability of M1T1s to survive in humans (Aziz & Kotb, 2008) M1T1 MGAS5005 (*cov*-) is a model strain isolated from the cerebrospinal fluid of a patient in Ontario in 1996 (Sumby *et al.*, 2005). This strain is used in this dissertation to study the dynamics of iGAS pathogenesis along with M1T1 5448, a *cov*+ isolate from a patient with necrotizing fasciitis in Ontario in 1994 (NCBI).

Antibiotic treatment

The Group A Streptococcus is still extremely sensitive to penicillin, and therefore remains the preferred drug for treatment. Confirmed GAS pharyngitis cases should be treated with a 10-day course of oral penicillin V, or amoxicillin, or a single dose of Benzathine penicillin injected intramuscularly. Those that have penicillin allergies are recommended to be given a 5-10 day course of cephalexin, cefadroxil, clindamycin, azithromycin, or clarithromycin orally. Although antibiotic resistance has been observed for many of the alternative antibiotics, no known cases of penicillin resistant GAS have been documented to date (CDC, https://www.cdc.gov/groupastrep/diseases-hcp/index.html).

Sugars present in the human body

Many sugars line the surface of cells and proteins, are present in tissues and biofluids of humans, and are consumed on a daily basis. Pathogens can utilize and often rely on these sugars to survive and grow in the host. Just as tissue types vary in different parts of the body, the availability of carbohydrates and metabolites vary as well. If a pathogen is able to use this as environmental cues, it could be used to determine where in the body it is located, and execute

Table 1.1. Presence of PTS sugars in Human Biofluids

	glucose	fructose	mannose	sucrose	mannitol	cellobiose	ascorbic acid	lactose	galactose	maltose	salicin	trehalose
Amniotic fluid							X					
Blood	X	X	X	X	X		X	X	X	X		
Breast Milk	X		X				X	X	X			
Cellular cytoplasm							X		X		X	
Cerebrospinal Fluid	X	X	X		X		X		X			
Feces	X	X	X	X	X			X	X	X		X
Saliva	X	X	X	X	X		X		X			
Urine	X	X	X	X	X		X	X	X	X		X

*Blue indicates biofluid potentially encountered during throat infection
*Red indicates biofluid encountered during blood sepsis
*Source data from HMDB (Wishart *et. al,* 2013, Wishart *et. al*, 2009, Wishart *et. al*, 2007)

the appropriate virulence program. Although we are still far-removed from those types of conclusions, it suggests that there is a host niche metabolic signature that pathogens can sense.

The phosphoenolpyruvate-phosphotransferase system (PTS) is a major carbon transport system in many bacteria that is responsible for the transport of specific sugars. These sugars are abundantly present and detected in many host tissues and biofluids (**Table 1.1, 1.3**), with 75% of GAS PTS sugars have been detected in human blood (**Table 1.1**) and 58% (7/12) of PTS sugars detected in saliva (**Table 1.1**) (Wishart *et. al,* 2013, Wishart *et. al*, 2009, Wishart *et. al*, 2007). The sugar content of saliva may be 67% given that maltose has been detected by other groups on mucins (Shelburne *et al*., 2008b). Surprisingly, galactose and ascorbic acid are present in the most number of biofluids (**Table 1.1**), although glucose is the most abundantly found. As expected, glucose is found in the highest concentration in both blood and saliva (**Table 1.2**). Mannose, fructose, mannitol, ascorbic acid, and galactose are also found in blood at a concentration about 1000-fold less than glucose, which indicates that, although very scarce, these sugars may potentially be available for GAS (**Table 1.2**). Sucrose is also detected in blood, but at minute concentrations (**Table 1.2**). Saliva has only 4 PTS carbohydrates that have been quantified; glucose is the most abundant,

Table 1.2 Concentrations (μM) of PTS sugars identified in the Human Biofluids

Sugar	Blood	CSF	Saliva
Glucose	**4781.13** ± 425.33 (10)	**3356.67** ± 1866.88 (3)	**287.73** ± 284.83 (6)
Fructose	**39.5** ± 12.02 (2)	**200** ± 56.57 (2)	-
Mannose	**51.5** ± 17.68 (2)	**44** ± 28.28 (2)	-
Sucrose	**1.8** (1)	-	**38** ± 19.80 (2)
Mannitol	**34** (1)	**4.875** ± 0.50 (4)	-
Cellobiose	-	-	-
Ascorbic Acid	**49.6** ± 25.58 (6)	**134.56** ± 39.51 (5)	**3.11** ± 4.24 (3)
Lactose	-	-	-
Galactose	**63.65** ± 34.86 (2)	**166** (1)	**83.46** (1)
Maltose	-	-	-
Salicin	-	-	-
Trehalose	-	-	-

*mean ± SD (number of studies)
* - (no values reported)
* source data from HMDB (Wishart *et. al,* 2013, Wishart *et. al*, 2009, Wishart *et. al*, 2007)

followed 3-fold less galactose (**Table 1.2**). PTS carbohydrates in the cerebrospinal fluid are important, since MGSA5005 was isolated from the CSF. Concentrations of glucose are reported to be similar to blood, with fructose and ascorbic acid at a concentration of 1000-fold less (**Table 1.2**)(Wishart *et. al,* 2013, Wishart *et. al*, 2009, Wishart *et. al*, 2007).

When we extend our outlook to PTS sugars that have been detected in any human tissue, it is evident that they are present in almost every part of the body (**Table 1.3**); however, very few tissues have the exact same PTS sugars present in the same combination and likely not at the same concentration (**Table 1.3**). The situation gets considerably more complex when one considers other metabolites that are present in these environments as well. Considering that CSF contains 440 metabolites, Urine contains 4060, Serum contains 4561, Saliva contains 1233, and Feces contains 695 (Wishart *et. al,* 2013, Wishart *et. al*, 2009, Wishart *et. al*, 2007), the uniqueness of the types of PTS sugars present in biofluids does not even begin to describe the complexity that potentially exists in the metabolome of these host environments. Therefore, a metabolic signature is more than possible, which could potentially allow pathogens to exploit this to successfully survive in the host.

Table 1.3 Presence of PTS sugars in Tissues

	glucose	fructose	mannose	sucrose	mannitol	cellobiose	ascorbic acid	lactose	galactose	maltose	salicin	trehalose
Adipose Tissue	X			X			X					
Adrenal Cortex	X						X					
Adrenal Gland	X											
Adrenal Medulla	X		X				X					
Beta Cell	X											
Bladder	X		X	X			X	X				
Brain	X				X		X		X			
Brain Plaques	X											
Epidermis	X		X	X			X					X
Erythrocyte							X					
Eye Lens	X						X					
Fetus	X											
Fibroblasts	X		X	X			X					X
Gonads	X						X					
Gut	X							X				
Heart							X					
Intestine	X		X	X		X	X	X				
Kidney	X		X	X						X		X
Liver	X	X					X		X	X		
Lung	X						X					
Lymphocyte							X					
Mouth	X			X								
Muscle	X		X	X			X	X				X
Myelin	X		X	X			X					
Nerve Cells	X			X								
Neuron	X			X			X					
Pancreas	X		X									
Placenta	X		X	X			X					
Platelet				X			X	X		X		X
Prostate	X	X	X	X			X		X			
Skin					X			X				
Sperm		X										
Spleen			X	X		X	X	X				
Stratum Corneum				X								
Testes			X									

*Blue indicates tissue potentially encountered during throat infection
*Red indicates tissue potentially encountered during blood sepsis
*Gold indicates tissue potentially encountered during skin infections
*Source data from HMDB (Wishart et. al, 2013, Wishart et. al, 2009, Wishart et. al, 2007)

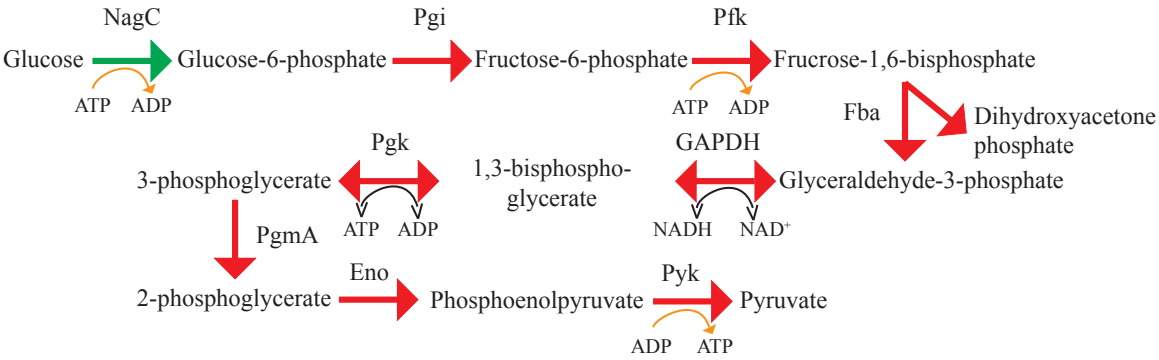

Figure 1.3 Glycolysis in GAS. Glycolytic intermediates are shown. Enzymes that carry out each reaction is shown above the arrows. Red arrows depict reactions where the enzyme was shown to be essential in GAS (Le Breton, *et. al,* 2015) and occur in the direction indicated, whereas green arrows were not. Orange curved arrows represent irreversible reactions. Black curved arrows can occur in both directions.

GAS carbon metabolism

Glycolysis

GAS relies heavily on glycolysis for the fermentation of incoming sugars. The pathway, outlined in **Figure 1.3**, is made up of almost entirely essential proteins, again highlighting its importance (Le Breton *et al*., 2015). The pathway begins when a glucokinase (Spy_1311) uses ATP to phosphorylate glucose to generate glucose-6-phosphate (G-6-P), which is then converted to fructose-6-phosphate (F-6-P) by phosphoglucose isomerase (Pgi). Phosphofructokinase (Pfk) then uses another ATP to phosphorylate F-6-P to create fructose-1,6-bisphosphate (FBP) that is then broken down into Dihydrooxyacetone phosphate (DHAP) and glyceraldehyde-3-phosphate (GAP) by fructose-bisphosphate aldolase (Fba). Glyceraldehyde-3-phosphate dehydrogenase (GAPDH) coverts GAP into 1-3-bisphoglycerate, generating nicotinamide adenine dinucleotide (NADH). This is then converted by phosphoglycerate kinase (Pgk) to 3-phosphoglycerate, which generates 1 ATP. Next, Phosphoglycerate mutase (PgmA) converts 3-phosphoglycerate to 2-phosphoglycerate with is then converted by enolase into phosphoenolpyruvate (PEP). The conversion of PEP to pyruvate generates an ATP, but this conversion can also be used

to phosphorylate Enzyme I (EI) to start PTS uptake of sugars. The enzymes of glycolysis are usually activated by divalent cations to allow for binding of the negatively charged phosphorylated sugars (Pancholi *et. al.,*2016). In all, this pathway produces 2 NADHs and 2 ATPs. Since GAS is a lactic acid bacterium, pyruvate is generally converted to lactate/ lactic acid by L-lactate dehydrogenase (Ldh).

Entner-Doudoroff

The Entner-Doudoroff pathway (ED), which was discovered in in *Pseudomonas saccharophila* in 1952, is an alternate to glycolysis that uses a different set of intermediates (Conway, 1992). Rather than cleaving fructose-1,6-bisphosphate by Fba to yield GAP and dihydroxyacetone phosphate, the ED pathway cleaves 2-dehydro-3-deoxy-phosphogluconate (KDPG) by the KDPG aldolase (Eda) to create GAP and pyruvate (Conway, 1992). The only two enzymes from this pathway that are present in GAS are Eda and the 2-dehydroxy-3-deoxygluconokinase, the latter of which creates KDPG (Pancholi *et. al.*, 2016). However, the enzymes required for glucose entry into the ED pathway are not annotated or have not been identified, therefore this pathway is largely incomplete. It is possible that GAS may scavenge 2-dehydroxy-3-deoxy-D-gluconate and use this incomplete pathway as another source of pyruvate, but this has not been extensively explored. Therefore, this significance of this pathway in GAS in currently unknown (Pancholi *et. al.*, 2016).

Pentose phosphate pathway

The pentose phosphate pathway (PPP) is an alternate pathway to glycolysis that metabolizes glucose-6-phosphate through an oxidative and non-oxidative branch that generates fructose-6-phosphate and glyceraldehyde-3-phosphate that can be fed back into glycolysis (Stincone *et al*., 2015). This pathway provides the cell with many precursors for the biosynthesis of nucleotides, amino acids, and vitamin B6 (Stincone *et al*., 2015). Like other pathways in GAS, except glycolysis, not all reactions in this pathway are

predicted to be intact. GAS contains a 6-phosphogluconate dehydrogenase, transaldolase, transketolase, and a Ribulose-5-P-4-epimerase, allowing GAS to produce fructose-6-phosphate and glyceraldehyde-3-phosphate from 6-phosphogluconate. However, the steps to convert glucose-6-phosphate into 6-phosphogluconate are absent and the role of PPP in GAS physiology remains to be seen.

TCA cycle

The tricarboxylic acid (TCA) cycle is an 8 protein metabolic pathway that is responsible for the degradation of Acetyl-CoA to generate 12 ATPs. GAS does not posses an intact TCA cycle, but the enzymes to generate Acetyl-CoA (AcoA/B–pyruvate dehydrogenase E1, AcoC-α-ketoacid dehydrogenase E2, and AcoL-dihydrolipoamide dehydrogenase) are present (Pancholi *et. al*., 2016). The functional significance of this is unknown, as no role for Acetyl-CoA generation has been attributed in GAS physiology (Pancholi *et. al*, 2016). The absence of a TCA cycle does mean that *Streptococcus pyogenes* relies heavily on glycolysis for the fermentation of incoming sugars to generate ATP.

The phosphoenolpyruvate-dependent phosphotransferase system (PTS)

The PTS is a carbohydrate transport system present in most bacteria that couples the translocation of an incoming sugar with its subsequent phosphorylation (Deutscher *et al*., 2006). The PTS is made up of two types of proteins, general and sugar specific. The general proteins Enzyme I (EI, *ptsI*) and HPr are cytosolic and are common to all the EIIs present in a bacterium. The sugar-specific proteins are Enzyme II complexes (EII) that are made up of two cytosolic components (EIIA and EIIB), as well as one or two membrane transporters (EIIC and EIID). To date, EIIDs are only found in the mannose-family EIIs (Deutscher *et al*., 2006).

EI is autophosphorylated at the expense of phosphoenolpyruvate (PEP), which will then phosphorylate HPr on its Histidine-15 residue. Subsequently Hpr-His-15 phosphorylates EIIA, which phosphorylates EIIB, followed by phosphorylation of the

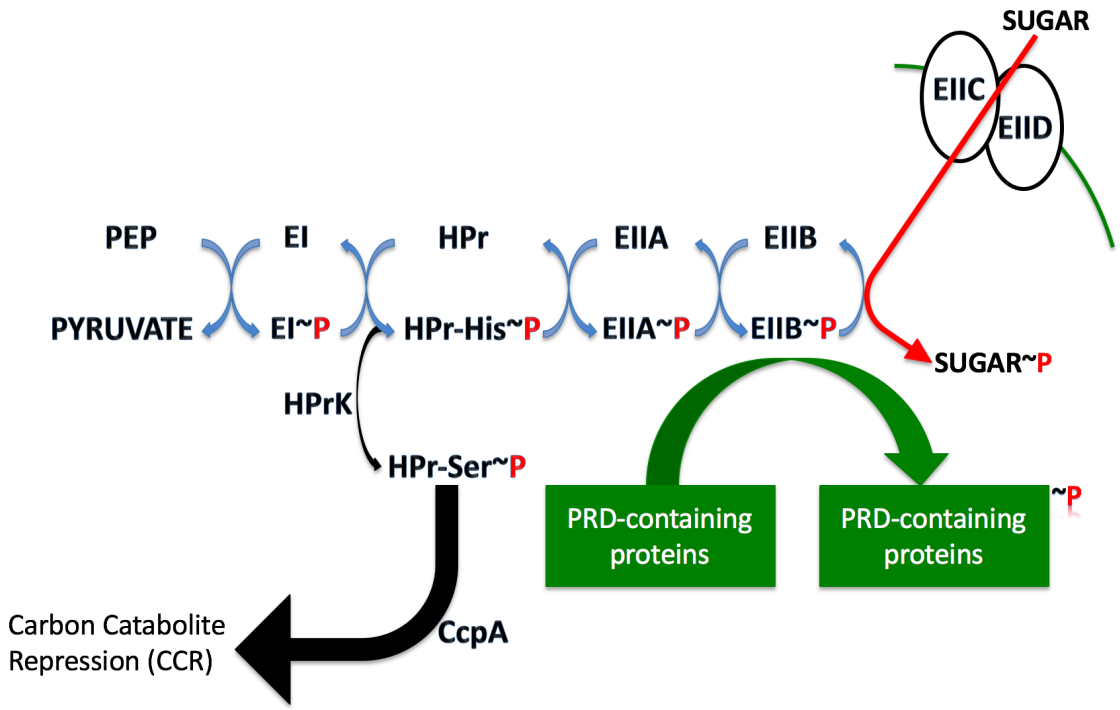

Figure 1.4 The PTS. Enzymes involved with PTS-mediated sugar transport and regulation are depicted. Blue arrows depict the phosphotransfer of a phosphate (red P) to each phosphocarrier protein or incoming sugar in the relay. Black arrows indicate the networks in the CcpA-mediated CCR pathway. The green arrows depict the modification of PTS-regulatory domain (PRD)-containing regulators as a way to affect global gene expression.

incoming sugar that is transported by EIIC/D (Deutscher *et al.*, 2006) (**Fig 1.4**). The phosphorelay also allows for the PTS to participate in signal transduction, as EIIBs can phosphorylate PTS-regulatory domains found within several transcriptional regulators in the absence of its inducing source (**Fig 1.4**). In addition, HPr can be phosphorylated on its Serine-15 residue in the presence of a preferred carbon source, and in conjunction with the carbon catabolite protein A (CcpA), can limit the expression of alternative metabolic pathways (carbon catabolite repression, CCR) (**Fig 1.4**). These two processes allow for the PTS to potentially influence the expression of a wide variety of genes.

Four EII Families. The four main families of EIICs are (1) Glucose-Fructose-Lactose, (2) Ascorbate-Galactitol, (3) Mannose, and (4) Dihydroxyacetone. The Glucose-Fructose-Lactose family is thought to be the original and largest family, with each

EIIC having 10 transmembrane (TM) domains (Saier, 2015). The EIIA, EIIB, and EIIC components in this family are not thought to coevolve. The Ascorbate-Galactitol family is made up of mostly fusion proteins, with each EIIC component containing 11 or 12 TM domains (Saier, 2015) . Not much is known about the Dihydroxyacetone family, other than that it appears the newest of all the EII families (Saier, 2015). The Mannose EII family is the only one that has an EIID component and, while other EIIB are phosphorylated on a cysteine residue, mannose family EIIB is phosphorylated on a histidine residue. In addition to transporting the most substrates of the EII families, it is also the most structurally unique (Saier, 2015). The significance of the mannose-specific EII, and the extensive role it plays in the physiology and virulence of many human pathogens will be discussed in later sections of this dissertation.

Predicted TM domains for MGAS5005 EIICs. Using the transmembrane (TM) prediction program Protter (http://wlab.ethz.ch/protter/start/), we predicted the number of TM domains in each EII present in the GAS genome to roughly predict which families are represented. We found three (Spy_0520; Spy_0782; Spy_1480) that belong to the mannose family, as these all have an EIID associated with their respective EIIC (**Table 1.4**). Six predicted EIIs appear to fall in the Ascorbate-Galactitol EII family (Spy_0475; Spy_0662; Spy_1542; Spy_1692), as these are fusion proteins (**Table 1.4**). However, the majority are annotated for sugars in the Glucose-Lactose-Fructose family, yet do not have the predicted number of TM domains characteristic of this family. Therefore, assigning families for each EII is problematic using just transmembrane domains and subunit compositions. Still, the predicted transmembrane domains reveal that EIIs tend to have between 10-12 transmembrane domains to facilitate sugar translocation (**Table 1.4**).

Comprehensive EII metabolic studies. Two studies in Gram-positive bacteria have looked deeply into characterizing each EII to assign sugar specificities. These studies highlight some key points into what may be observed in GAS.

Table 1.4 Plotter prediction of the number of transmembrane domains present in each EIIC/D.

Spy #	TM domains	Fusion**
148	11	No
475	10	ABC
520-1	11*	No
662	11	ABC
782-3	11*	No
1079	10	No
1399	11	No
1480-1	12*	No
1542	10	ABC
1633	8	BC
1663	9	No
1692	7	ABC
1744	11	No
1784	10	BC

*includes both EIIC and EIID
** If a fusion protein, subunits that are fused together with the EIIC are listed

In *S. pneumoniae,* 21 EIIs have been identified in the pan-genome (Bidossi *et al*., 2012). 26 strains of *S. pneumoniae* were compared, and surprisingly, each had different number of EIIs (between 15-20). This indicates that not only are there metabolic differences between species, but within strains. Additionally, the ability of each strain to ferment each tested sugar also varies. For the most part, EII annotations matched the experimentally verified substrates (Bidossi *et al.*, 2012). However, this is partly due to the fact that most mutants were only assessed for their ability to grow in the carbohydrate for which they were annotated, missing pleiotropic effects. As seen with many streptococci, the mannose-specific EII have the broadest range of substrates of all the EIIs (Bidossi *et al*., 2012).

Staphylococcus aureus has the most (29) encoded transporters (Vitko *et al*., 2016) compared to *Staphylococcus epidermidis* (16 transporters), *Staphylococcus haemolyticus* (20 transporters), and *Staphylococcus saprophyticus* (21 transporters). It also has the most unique number of transporters of the compared species with 10 (Vitko *et al*., 2016). *S. aureus* has 13 PTS-specific sugars, and 15 EIIs currently annotated in its genome. Annotations for these EIIs are very broad and appear to be annotated based on the family of EII and not a specific sugar, as in GAS MGAS5005 (Vitko *et al.*, 2016). Deletion of an EII leads to very

limited affects on growth, as most EII mutants only affect growth of *S. aureus* in one or two sugars. Because the annotations are broad, no comparison can be made on the accuracy of annotation versus function. However, this illustrates the need to experimentally verify sugar-specificities in strains when an EII's role is of interest.

Glucose metabolism

Glucose metabolism in GAS has not been studied in any detail; however, an in depth analysis of glucose metabolism has been done in *S. aureus*. Glucose transport in this pathogen is highly redundant, where a substantial decrease in growth and uptake of glucose was only observed when four transporter proteins (3 PTS, 1 non-PTS: GlcU) were mutagenized (Vitko *et al*., 2016). Even this quadruple mutant had residual glucose metabolism, indicating the potential for an unidentified transporter. This additional transporter is not a PTS EII, as a Δ*glk*Δ*ptsH-H15A* mutant (a strain that cannot transport glucose through the PTS or be phosphorylated by the glucokinase (GlK), does not grow on glucose, indicating that glucose in *S. aureus* is only metabolized via the PTS or by the glucokinase pathway (Vitko *et al*., 2016). This appears to be the case for GAS as well and is the focus of studies described in Chapter 7. Glucose transport and metabolism are highly redundant, as no single EII has ever been shown to be solely responsible for glucose transport. In addition, many bacteria posses alternate pathways to metabolize glucose separate from glycolysis, highlighting the extreme importance of glucose metabolism for pathogenic bacteria.

Mixed acid fermentation

Mixed acid fermentation occurs when ethanol, acetate, and formate are generated as the end products of fermentation. Pyruvate-formate lyase (Pfl) converts pyruvate to formate and Acetyl-CoA. Acetyl-CoA can then be converted into ethanol by alcohol dehydrogenase (AdhE), or into acetate by the enzyme acetate kinase. Phosphoenolpyruvate carboxylase can also convert PEP into oxaloacetate (Forster *et.al.*, 2014). GAS possesses genes that

are annotated to encode pyruvate-formate lyase (Spy_1569), alcohol dehydrogenase (Spy_0039), acetate kinase (Spy_0094), and PEP carboxylase (Spy_0505). Although little is known about the functions of these proteins, and if their annotations are appropriate, this suggests that GAS can generate alternative end products to lactic acid when a carbohydrate is metabolized and that pH alone is likely not the only readout for positive carbohydrate metabolism by a GAS strain.

Carbon catabolite repression (CCR)

Carbon catabolite repression is a condition induced in the presence of a preferred carbon source, usually glucose, where bacteria have developed several mechanisms to prevent either the expression or the activity of alternate carbon source metabolic enzymes to prevent the metabolism of less favorable carbon sources. In this section, two mechanisms of CCR will be explored.

i) Carbon Control Protein A (CcpA)-dependent CCR.

In GAS, this is the major form of catabolite repression. It occurs when the metabolism of a preferred carbon source produces high amounts of fructose-1,6-bisphosphate, which stimulates the kinase activity of the HprK kinase/phosphorylase that in turn phosphorylates Hpr on its serine-46 residue. Hpr(Ser-P) acts as a cofactor to CcpA, allowing CcpA to bind catabolite response elements (*cre*) to regulate expression of the target gene (Deutscher *et al.*, 1997). However, the presence of a *cre* site does not guarantee that CcpA is able to bind, as was shown for the *manLMN* and *arcABC* operons in *S. suis* (Willenborg *et al.*, 2014). When FBP levels are lower and phosphate levels increase, HprK acts as a phosphorylase and cleaves the phosphate off of the serine-46 residue, allowing for HPr to be phosphorylated on its histidine-15 residue to facilitate PTS uptake activity of alternate carbon sources; leading to the relief of CCR (Deutscher *et al*., 1997). HPr(Ser-P) has also been shown to elicit CCR on its own by binding to sugar permeases in certain bacteria (Saier *et al*., 1996), and is also required for growth on a wide range of sugars (Zeng & Burne, 2010).

In reality, this model is fairly simplistic, and the discovery of a fourth form of HPr has further complicated matters. HPr(Ser-P) is thought to greatly inhibit the phosphorylation of the histidine-15. However, HPr(Ser-P)(His-P) can build up in rapidly growing bacteria (Roy *et. al*., 2008). This does not occur in all bacteria, as those that are able to control intracellular pH do not have high levels of HPr(Ser-P)(His-P) (Bacilli and Enterococci) whereas those that do not regulate their intracellular pH have higher levels (Roy *et. al*., 2008). HPr(Ser-P)(His-P) is generated due to the high concentration of HPr(Ser-P) present in rapidly growing cells, which is able to be phosphorylated by EI at an acidic pH (Casabon *et. al.*, 2006). Although EI normally phosphorylates HPr, its preferred substrate, this doesn't occur as strongly at a lower pH, where HPr(Ser-P) phosphorylation by EI is enhanced (Casabon *et. al.*, 2006). It is unclear at the moment if HPr(Ser-P)(His-P) is able to interact with CcpA, but this can potentially add another wrinkle into CcpA-dependent CCR regulation. Interrogation of the role of HPr and HPrK is problematic, as both of the genes that encode these proteins (*ptsH* and *ptsK* respectively), are critical for *in vitro* growth in GAS (Le Breton *et al.*, 2015).

CcpA affects gene expression by binding to *cre* sites in the promoter region of many genes. The traditional consensus sequence in *Bacillus subtilis* is TGWAANCGNT, where W represents an A or a T, and N represents any base. A variable *cre* site (cre_{var}) was identified in *C. acetobutylicum*, which has the distinct feature of variable spacer regions (0-40 nt) that allow for increased variability in CcpA regulation (Yang *et al*., 2017). The consensus sequence for cre_{var} is Nx TGTAAA-Yx –TTTA CAMx, where N and M represent bases that complement each other, Y represents any base, and X represent the number of bases. Y_X represents the variable spacer region present in cre_{var}. Genes that contain cre_{var} generally encode proteins for substrate transport, metabolism, redox balancing, sporulation, or solvent production categories (Yang *et. al*., 2017). Another variable cre_2 is also present (TTTTCAAAAAATTTTC) and is usually found in genes associated with stationary phase

and are located mostly inside open reading frames (Willenborg *et al.,* 2014). With three types of *cre* sites, CcpA-dependent CCR is complex, and regulation of gene expression may have many layers to ensure efficient use of the nutrients available.

ii) EII-mediated CCR.

CCR can also occur by $EIIA^{Glc}$ in Gram-negative bacteria. In *E.coli*, $EIIA^{Glc}$ that is unphosphorylated can bind to other sugar permeases, namely the maltose, melibiose, and raffinose, lactose, galactose, and L-arabinose transporters (Chen *et. al.*, 2013, Deutscher *et. al.*, 2006). In the case of maltose, $EIIA^{Glc}$ that is unphosphoryalted will prevent the outward facing conformation of the maltose transporter which is required for maltose translocation, as well as inhibiting ATP hydrolysis (Chen *et. al.,* 2013). $EIIA^{Glc}$ also prevent glycerol metabolism by preventing glycerol kinase (GlpK) from phosphorylating glycerol to generate glycerol-3-phosphate (Deutscher *et. al.*, 2006). This is predicted to occur in GAS as well, although through EI rather than $EIIA^{Glc}$. Since this mode of CCR only occurs when the unphosphoryalted $EIIA^{Glc}$ binds to each transporter, cells are able to prioritize the metabolism of one sugar over others apart from CcpA-dependent CCR. This is because an unphosphoryalted $EIIA^{Glc}$ will only occur when glucose is being transported by its cognate EIIC (Deutscher *et. al.*, 2006). Binding of $EIIA^{Glc}$ to other membrane transporters has never been seen with Gram-positive bacteria.

This does not exclude the ability of EIIs to elicit CCR. In oral streptococci, ManL ($EIIAB^{man}$) is a well-characterized CcpA-independent CCR mechanism. In *S. mutans,* ManL helps change the expression profile when the external media goes from glucose-rich to glucose-poor (Moye *et. al.*, 2014). In *S. gordonii*, this is done by regulating the expression of several other EIIs, namely the fructose-specific EIIs (*fruA* and *levD*) (Tong *et al.*, 2011). In these cases, dephosphoryaltion of ManL due to sugar transport through ManM (EIIC) and ManN(EIID) elicits ManL-dependent CCR (Tong *et. al*., 2011). However, ManL-dependent CCR is limited to glucose and mannose in *S. mutans*, which is not the case in *S.*

gordonii (Tong *et al*., 2011). The mannose-specific EII in *S. pneumoniae* affects growth on many different non-preferred sugars and is thought to be the result of the transport of multiple sugars that stimulates the expression of other PTS operons specific for that sugar (Fleming & Camilli, 2016). In support of this, a Δ*manLMN* mutant failed to stimulate expression of the lactose-specific metabolic operon (Fleming & Camilli, 2016). However, *manLMN* has a higher affinity for glucose compared to lactose, and via inducer exclusion, can suppress the expression of the lactose-specific metabolic operon in the presence of glucose (Fleming & Camilli, 2016). Inducer exclusion is a common phenomenon observed in bacteria, where transport of a preferred carbon source, usually glucose, prevents the transport of another less preferred carbon source.

CcpA core regulon in GAS

The core CcpA regulon was recently compiled by DebRoy *et. al* (2016), compiling a list of differentially regulated genes in Δ*ccpA* mutants in MGAS2221 (M1), MGAS10870 (M3), and MGAS6180 (M28) using RNA-seq (DebRoy *et al*., 2016). Overall, 310-386 genes were identified as CcpA-regulated in each strain, with a core group of 173 genes (DebRoy *et al*., 2016). As expected, many transport and metabolism genes fell in the core CcpA regulon, including nine EIIs anticipated since PTS transport systems are generally specific for alternate carbohydrates (DebRoy *et al.,* 2016). However, in *S. suis* the CcpA regulon only includes four EIIs (Willenborg *et al.*, 2014). Although the largest number of genes affected by the deletion of *ccpA* involves carbohydrate metabolism, many also are involved in amino acid, nucleotide, and lipid metabolism (DebRoy *et al.*, 2016). In almost all cases, CcpA acts as a repressor to the core regulon genes identified, again illustrating the importance of CcpA to CCR in GAS.

Interestingly, only two virulence gene loci were identified in the core regulon. The first is *endoS*, encoding a secreted endoglycosidase (DebRoy *et al*., 2016) that is responsible for the processing of glycoproteins. The second is the 9-gene *sag* operon required for

Streptolysin S or SLS production (DebRoy *et al*., 2016), which is known to be catabolite repressed. However, the mechanism by which CcpA influences SLS expression appears to be indirect, as binding of CcpA to the *sag* promoter was only shown *in vitro* (Kinkel & McIver, 2008) but not *in vivo* (Kietzman & Caparon, 2010). The inclusion of the *sag* operon in the CcpA core regulon corroborates several observations that Δ*ccpA* exhibits early onset of hemolysis (Kinkel & McIver, 2008, Shelburne *et al.*, 2008a). CcpA has been linked to virulence in other pathogens as well. CcpA is required for the colonization of the nasopharynx and the lung. In *S. mutans,* it governs acid formation and tolerance. In *Clostridium perfringens,* it regulates (either directly or indirectly) the expression of enterotoxin. In *C. difficile*, CcpA regulates toxin production (Antunes *et al*., 2011). In *S. aureus* and *S. gordonii,* CcpA contributes to methicillin and penicillin resistance respectively (Gorke & Stulke, 2008). This illustrates that efficient metabolism of preferred carbohydrates is intimately tied with virulence.

Links between metabolism and virulence in Gram-positive pathogens

PTS carbohydrate metabolism is vital to the pathogenesis of many human pathogens. In this section, a few examples are highlighted in closely-related Gram-positive pathogens. In *S. aureus*, severely hampering the ability to utilize glucose leads to a dramatic reduction in lesion size and lower bacterial burden in a subcutaneous murine infection model (Vitko *et al*., 2016). The mannose-specific EII appears repeatedly as being important for virulence of other pathogens. In *Lactobacillus plantarum*, impairment of *manLMN* expression led to peroxide sensitivity (Stevens *et al*., 2010). In *S. mutans*, ManL helps biofilm formation and competence (Abranches *et al.*, 2006). ManLMN also affect virulence gene expression. In *L. monocytogenes*, dephosphorylated ManL depresses the activity of the virulence regulator PrfA, which in turn activates the expression of the virulence genes *hly* and *acta* (Ake *et al*., 2011). Similarly, ManN ($EIID^{man}$) prevents suislysin expression, which leads to the

absence of hemolysis (Lun *et al.*, 2004). One of the more interesting roles that the mannose-specific EII plays in virulence relates to bacteriocins. Many bacteria use bacteriocins when competing with other populations. The mannose-specific EII is known to be a target for class IIa bacterocins (Kjos *et al*., 2011), which are small peptides produced by lactic acid bacteria that inhibit growth. It also is a target for mutacins, as a Δ*manLMN* mutant in *S. salivarius* had reduced sensitivity to I-T9 and R-3B (Nicolas *et. al.* , 2010). The mannose-specific EII may play such a significant role, because it is constitutively expressed *in vivo* (Watanabe *et. al.*, 2013) and *in vitro* (Shelburne *et al*., 2008b, Fleming & Camilli, 2016).

The influence of metabolism is not just limited to the mannose-specific EII or mannose metabolism, as fructose metabolism also seems to play a large role in virulence. In *S. gordonii*, FruA (fructose-specific EII) senses high levels of fructose, switching cells from a sessile to planktonic phenotype, thereby aiding the formation of biofilms (Loo *et al*., 2003). In *S. iniae*,*fruA* is found only in five virulent strains that were studied, but was absent in five non-virulent strains (Pridgeon *et al*., 2013). *fruA* also is important for the ability of GAS to adjust to different blood-related stresses, which will be discussed in the next section. Deletion of the cellobiose-PTS reduces the virulence of *K. pneumoniae*, is attenuated in a *S. pneumonaie*/sepsis model and reduces survival in the nasopharynx, blood, ears, and lungs of mice (Wu *et. al.*, 2012, McAllister *et al.*, 2012). Sucrose metabolism perturbations lead to attenuation of *S. pneumoniae* in the nasopharynx (Iyer & Camilli, 2007). Maltose utilization promotes intestinal colonization by commensal and enterohemorraghic *E. coli* (Le Bouguenec *et. al.*, 2010). Preventing mannitol utilization hinders the ability of *S. aureus* to survive exposure to host antimicrobial fatty acids (Kenny *et al.*, 2013). RNA-seq from murine tissues following *i.p*. infection with Group G streptococci found the mannose, glucose, mannitol, cellobiose, sucrose, galactitol, β-glucoside, N-acetylglucosamine, and the N-acetylgalactoseamine PTS EIIs were upregulated over the course of 8 hours (Watanabe *et. al.*, 2013). This highlights the importance of sugar metabolism in the overall

pathogenic process.

GAS versus the host

S. pyogenes contains an arsenal of weapons to not only combat the host immune response, but also to coordinate expression of the appropriate virulence factors in order to survive during infection. Here, selected genes specifically involved in virulence that also have a connection with carbon metabolism are highlighted.

CovRS

CovRS is a two-component system in GAS, whose loss has been linked to the hypervirulent phenotype seen in many invasive strains. In the two strains used in this study, MGAS5005 is a spontaneous *covS* mutant whereas 5448 is wild type for *covRS.* CovRS specifically responds to Mg^{2+} and LL-37, but loses this ability as spontaneous mutations can occur when exposed to neutrophils. As a result, the repression of many virulence factors is lost, increasing the virulence potential of these strains (Federle *et al*., 1999, Heath *et al.*, 1999, Bernish & van de Rijn, 1999). One visible result of the loss of *covS* is a hypermucoid phenotype resulting from an increase in *hasA* expression (Levin & Wessels, 1998). The CovRS regulon also includes many metabolic genes, including those involved in mannose, maltose, and β-glucoside metabolism (Graham *et al*., 2002). As a result, a *covS* mutant may exhibit different metabolic capability over the course of infection that allows it to have a greater virulence potential.

SpeB

SpeB is a cysteine protease responsible for the degradation of many GAS and host proteins. It is translated as a 40 kDa immature protein, which is autocleaved to form a 28 kDa active protein (Hynes *et. al.*, 2016). Expression of *speB* is significantly induced after 3 days post infection in a subcutaneous murine infection model (Loughman & Caparon, 2006b). SpeB activity is also highest at a pH of 6.5 and low chloride concentration (Loughman &

Caparon, 2006a). *speB* is also catabolite repressed, as CcpA binds to the *speB* promoter (Kietzman & Caparon, 2010), although expression in GAS is affected by the PTS in a strain-specific manner. In GAS MGAS5005 and 5448AP, *speB* was lower in Δ*ptsI* mutant strains as compared to their parental strains. However, this was not the case for a *covS*$^{+}$ parental strain, where Δ*ptsI* had the same level of expression of *speB* as compared to 5448 (Gera, 2014).

Mga

Mga is a stand-alone regulator that controls the transcription of many virulence and metabolic genes in GAS, and is most active in late exponential to late-log phase (McIver, 2009). The Mga regulon encompasses genes that are both directly (core) and indirectly affected by Mga activity (Hondorp & McIver, 2007). The core Mga regulon is directly regulated by Mga and includes genes for adhesion and internalization such as M protein (*emm*) and fibronectin-binding surface adhesion (*fba*), immune evasion such as C5a peptidase (*scpA*) and secreted inhibitor of complement (*sic*) and its own expression (Hondorp & McIver, 2007). Many sugar utilization genes are indirectly regulated by Mga, including the mannose/fructose-specific EII (*ptsABCD*) and the fructose-specific EII (*fruRBA*); however, the Mga regulon can vary depending on the serotype (Valdes, 2016).

PTS-regulatory domains (PRDs) are phosphorylated by either EI/Hpr or EIIBs in the appropriate conditions. Mga is a PRD-containing virulence regulator (PCVR) that is able to alter its activity based on the phosphorylation status of PTS enzymes. EIIBs can phosphorylate PRDs in the absence of the inducing sugar, as the phosphate will reside on the EIIB rather than being passed onto a translocated sugar. Hpr-His~P can phosphorylate PRDs as well, which is prevented in the presence of a preferred carbon source as Hpr will be phosphorylated on its Serine residue in this situation. PRDs are present in many bacteria, specifically on antiterminators and activators, but have only been found on virulence regulators in Gram-positive bacteria (Stulke *et al*., 1998).

Mga in GAS has two PRDs. PRD1 has two conserved histidines that were shown to be phosphorylated by EI/Hpr (Hondorp *et al*., 2013). Phosphorylation of PRD1 is thought to inhibit Mga activity, as *in vitro* transcription of emm is higher when EI/Hpr is not phosphorylated (Hondorp *et al.*, 2013). EIIBs are thought to phosphorylate PRD2 in the absence of the inducing sugar (Hondorp *et al.*, 2013). As a result, mutations in the PTS alter Mga activity. A Δ*ptsI* mutant in the M4 GA40634, which cannot phosphorylate Mga on either PRD, has lower expression of the core regulon genes *arp* and *sof* (Hondorp *et al*., 2013), indicating a reduction in Mga activity. Additionally, an MGAS5005 Δ*ptsI* mutant had lower expression of *sic*. However, there appears to be strain specificity, as 5448AP.Δ*ptsI* has no effect on the expression of *emm* or *sic*, whereas 5448.Δ*ptsI* has increased expression of both genes (Gera, 2014).

Interestingly, not only is Mga activity affected by the PTS, but the Mga regulon itself can change depending on the nutrient conditions of the environment. The Mga regulon determined for GAS grown in THY differs significantly from the regulon when GAS was grown in low glucose C-media (Valdes, 2016).This includes the Streptolysin S (SLS) operon, which is Mga-regulated (most likely indirectly) in low glucose, but not in high glucose (Valdes, 2016). This appears to correlate with differences in PRD phosphorylation. Overall, this suggests that the PTS may signal virulence pathways through Mga to impact both virulence and sugar metabolism, an important concept that will be touched upon throughout this dissertation.

Sugar metabolism genes essential for virulence

Many PTS genes have also been demonstrated to be important for GAS pathogenesis. Maltose/maltodextrin metabolism was shown to be necessary for GAS colonization and disease burden in the mouse oropharynx (Shelburne *et al.*, 2008b). Fructose-metabolic genes have been found to be required for survival against neutrophil killing, a process that is explored more in Chapter 6 of this dissertation (Valdes *et al.*, 2016). Several metabolism

genes were identified in a whole genome mutagenesis screen for GAS survival in whole human blood, including the fructose-specific EII, the mannose-specific EII, and a sucrose-6-phosphate hydrolase (*scrB*)(Le Breton *et al.*, 2013). In a gene expression analysis of pathways critical for GAS survival in whole human blood, many carbohydrate metabolism genes appeared such as the mannose-specific EII (Graham *et al*., 2005). Furthermore, the expression levels varied over the course of 90 minutes, highlighting how GAS is able to adapt to quickly changing nutrient content (Graham *et al.*, 2005). Studies on blood related stresses have identified PTS genes as well. The GAS regulon in the presence of heme stress, a condition that is likely to occur with the lysis of RBCs, identified the fructose-specific EII and the lactose-specific EII as induced, while the mannose/fructose-specific EII was repressed (Sachla *et al.*, 2014).

Elimination of the PTS phosphorelay by deletion of the first enzyme in the pathway (EI) in GAS led to the early expression of the toxin Streptolysin S, (see below) rather than being expressed in late-log growth phase like its parental wild type strain (Gera *et al.,* 2014). This also resulted in larger more necrotic lesions at the site of infection in a subcutaneous murine skin infection model (Gera *et al.*, 2014). This suggests that the PTS mediates SLS activity *in vivo*.

Streptolysin S

SLS is a potent Class I bacterocin that lyses many host cells (Molloy *et al*., 2011, Nizet *et al.*, 2000). SLS-like toxins exist across many bacterial species, and are hardly unique to GAS. Although not all are bioactive like SLS, SLS-like clusters have been found in *Firmicutes, Spirochaetes,* and *Actinobacteria* (Molloy *et al.,* 2011). Many important pathogens such as *Listeria monocytogenes* and *S. aureus* also have regions of homology to the *sag* operon, although many of them have not been as extensively studied (Molloy *et al.*, 2011). Hemolysis associated with streptococcal infections was observed in the late 1800s,

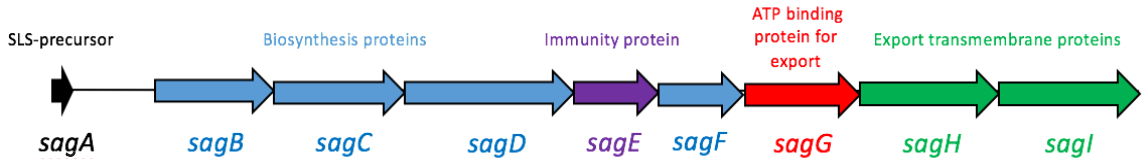

Figure 1.5 The *sag* operon in GAS. The gene names (below arrows), and encoded protein functions (above arrows, color coded) are shown respective to each gene in the *sag* operon. Arrows are color coded according to the encoded protein function, and are drawn to scale.

but SLS was not identified until the late 1930s (Todd, 1938).

SLS is encoded by a 9-gene operon that is responsible for extracellular release of mature SLS (**Fig. 1.5**). The operon consists of *sagA-F*, each encoding a protein responsible for a different step in SLS biosynthesis and transport. *sagA* encodes an immature SLS peptide that is further processed post-transcriptionally by SagBCD to create the SLS to be exported (Molloy *et al*., 2011). SagD forms a complex with SagBC to carry out the reaction, where SagC produces thiazoline and CH_3-oxazoline rings by removing water from the SLS-precursor peptide backbone (Molloy *et al.*, 2011). SagB then catalyzes a dehydrogenase reaction to remove the hydrogen to create an aromatic thiazole and CH_3-oxazole heterocycles (Molloy *et al*., 2011). The mature SLS is now structurally rigid, which allows for better binding to its targets (Molloy *et al*., 2011). SagGHI are thought to create an ABC transporter to export SLS, where SagG is the ATP-binding protein, and SagHI create the membrane channel. SagE is thought to be the immunity protein, but also hypothesized to cleave the leader sequence from SLS to make a bioactive SLS that is exported (Molloy *et al.*, 2011). Little is known about the role SagF plays, other than that it is membrane associated (Molloy *et al.*, 2011).

Many functions have been proposed for SLS, with the underlying theme being to help GAS survive in the host. The vast majority (99%) of GAS isolates have been shown to produce SLS (Molloy *et. al*, 2011), and Δ*sagA* mutants in many GAS strains were shown to be attenuated in different infection models (Datta *et. al.*, 2005). SLS has been associated with soft tissue injuries (Datta *et. al*., 2005), evasion of the immune system

through programmed cell death (Datta *et. al*., 2005, Goldmann *et. al*, 2009), translocation across the epithelial barrier (Sumitomo *et. al*, 2011), and in quorum-sensing (Lyon *et al*., 2001). The hallmark of SLS activity has been observed with the lysing of RBCs, which has been thought to occur to promote GAS to gain access to iron (heme) (Sachla *et. al*., 2014). This is supported by the fact that SLS expression is also stimulated by the presence of serum (unpublished).

Until recently, not much was known about the mechanism by which SLS lysed target cells, other than the process appeared to be osmotic. Higashi *et. al.* (2016) discovered that SLS actually interacts with membrane ion channels, where Cl^- ions are rapidly influxed into RBCs, which causes a massive influx of water and results in cell lysis. They showed that SLS interacts with a particular ion channel called Anion exchanger 1 (AE1 or band 3), which is almost exclusively and most abundantly found on RBCs (Higashi *et. al*, 2016). Anion channels on other host cells are now hypothesized to be targets for SLS, although no evidence has been presented that would confirm this assertion as of yet.

Triggers for SLS activity have long been a subject of study. When SLS was first discovered, it was found that potassium ions stabilize SLS, and that nucleic acids serve as a sufficient stimulant for SLS production (Bernheimer *et. al*, 1948). In addition, it was observed that SLS activity was also stimulated by maltose, trehalose, inulin, raffinose, mannose, and glucosamine to different extents (Bernheimer *et. al*, 1948). Most interestingly, it was noted that SLS activity was diminished in the presence of glucose and heme stress, the first suggestion that SLS is catabolite repressed (Bernheimer *et. al*, 1948, Sachla *et. al*., 2014).

Chapter 2: Overview

The Group A Streptococcus (GAS, *Streptococcus pyogenes*) is a Gram-positive human pathogen that must adapt to unique host environments in order to survive. Invasive GAS (iGAS) is able to infiltrate into sterile sites in a human, requiring a mechanism to integrate different environmental cues to coordinate an appropriate virulence expression program for each host niche. Although iGAS may not be as common as superficial infections that infect the throat and skin, they do lead to the development of more serious clinical symptoms such as necrotizing fasciitis and streptococcus toxic shock syndrome (STSS). Unlike superficial infections that are usually treated with antibiotics and are generally self-limiting, invasive infections are much more complicated to treat due to antibiotic access and effectiveness (Cunningham, 2000). Without a licensed vaccine, GAS continues to be a public health problem whose healthcare costs can reach millions of dollars per year (Pfoh *et. al.,*2008) and it ranks as the 9th leading infectious cause of human mortality (Carapetis *et al*., 2005).

One mechanism that bacteria employ to coordinate environmental nutrient availability with gene expression is through sugar metabolism and transport. Sugars and carbohydrate metabolic pathways have long been implicated in the virulence processes of many human pathogens (López-Garrido *et al*., 2015, Foster *et al*., 2003, Petzold *et al*., 2006, Lowe *et al*., 2009, Ngamskulrungroj *et al*., 2009, Tournu *et al*., 2013). Links between sugar metabolism and virulence have been demonstrated in GAS, where mutants in the phosphoenolpyruvate-dependent phosphotransferase system (PTS) exhibited premature Streptolysin S (SLS)-mediated hemolysis during exponential growth. This early onset hemolysis correlated with an increased lesion size and severity in a murine soft tissue infection model when compared with parental M1T1 MGAS5005 (Gera *et al*., 2014), a representative strain from the most commonly found GAS serotype in North American.

To identify the PTS components responsible for this phenotype, we insertionally

inactivated the 14 annotated PTS sugar transporter-encoding genes (Enzyme IIC components, EIICs) in the GAS MGAS5005 genome and subjected this library to metabolic and hemolysis assays to functionally characterize each EIIC. It was found that a few EIIs had a very limited influence on PTS sugar metabolism, whereas others were fairly promiscuous. Very few EIIs affected the metabolism of a sole carbon source, illustrating the inherent redundancy within the PTS for the transport and utilization of carbohydrates. 7 EIIs contribute to the early hemolytic phenotype seen in MGAS5005.Δ*ptsI*, which suggests that the regulation of SLS-mediated hemolysis may require many inputs. However, early hemolysis did not affect survival in whole human blood, as only two EIIs were found to be important for survival in this environment.

One of the main EIICs that contributed heavily to both GAS metabolism and hemolysis is the mannose-specific EII. The mannose-specific EII locus, encoded by *manLMN*, was expressed as a mannose-inducible operon that exhibited the most influence on PTS sugar metabolism, including mannose. Each individual subunit of the mannose-specific EII also affects the metabolism of PTS carbohydrates to different extents, with the EIID having the least influence. Importantly, components of the mannose-specific EII also acted to prevent the early onset of SLS-mediated hemolysis. Interestingly, these roles were not identical in two different M1T1 GAS strains, highlighting the possible versatility of the PTS to adapt to strain-specific needs. The mannose-specific EIICD mutant (Δ*manMN*) also exhibits more severe lesions in a subcutaneous murine infection model, although the lesion size is similar to that in MGAS5005.

Strain specificity also appeared when we functionally characterized the fructose-specific EII operon (*fruA*) in another M1T1 5448. Components of the predicted fructose metabolic operon (*fruRBA*), made up of the fructose-specific EII (*fruA*), a fructose-1-phosphate kinase (*fruB*), and the operon regulator (*fruR*) were implicated as essential for survival against neutrophil killing (Valdes *et al*., 2016). However, *fruA* was not one of

them, and was not important for survival in whole human blood. Interestingly, these *ex vivo* virulence-related phenotypes were not the same for a Δ*fruA* strain created in MGAS5005, highlighting again the divergent roles of the same protein in two different strains of the same serotype. In this study, we characterized the metabolic influence of FruA in 5448 and compared it to MGAS5005 to identify other points of variation. We also characterized under which conditions this metabolic operon is expressed in an effort to determine the cause behind its importance in GAS immune evasion (Valdes *et al*., 2016).

Although we managed to characterize two EIIs that are important for overall GAS pathogenesis and metabolism, we could not find an EII that fully explained the early hemolytic phenotype seen in MGAS5005.Δ*ptsI*. However, we did determine that hemolysis occurs only in low nutrient conditions, strengthened by the fact that MGAS5005.Δ*ccpA*, a mutant unable to initiate carbon catabolite repression (CCR), also exhibited early hemolysis. We hypothesized that perturbations in efficient glucose metabolism may be the cause for the misregulation of SLS-mediated hemolysis. The route of glucose utilization is unknown in GAS, therefore we made mutants in a non-PTS glucose transporter (*glcU*) and a glucokinase (*nagC*) of an annotated non-PTS glucose metabolic pathway. It is evident that glucose can be metabolized both by the PTS and non-PTS routes, as Δ*ptsI*, Δ*nagC*, and Δ*glcU* all grow to some extent in glucose. However, the route of glucose utilization affects overall pathogenesis, as forcing glucose to go through the PTS (Δ*nagC*) allows for survival of MGAS5005 in whole human blood, whereas absence of PTS (Δ*ptsI*) transport is detrimental to overall survival in whole human blood. In addition, components of the non-PTS glucose metabolic pathway influence the utilization of PTS carbohydrates, as Δ*glcU* does not grow similarly to WT in mannose, and Δ*nagC* has affected growth in many PTS sugars presented as the sole carbon source. Interestingly, all three mutants display the early onset of SLS-mediated hemolysis, although to largely different levels. Similar to Δ*ptsI*, Δ*nagC* also displayed

more severe lesions as compared to MGAS5005 in a murine skin infection model. However, unlike what was observed with Δ*ptsI*, these lesions were not significantly larger than those of wild type. Dissemination of all three strains was unaffected, as similar CFUs were obtained from the spleen 48 hours post infection (hpi). All of these data suggest that carbohydrate metabolism plays an extensive role in GAS pathogenesis.

Chapter 3: Materials and Methods

Bacterial strains and media

Media

GAS was grown in either Todd-Hewitt broth with 0.2% yeast extract (THY), Chemically defined medium (CDM, Alpha Biosciences), or C-media. Composition of all three medias are presented in **Appendix**. Freshly prepared sodium bicarbonate (59.51 μM) and L-cysteine (11.68 μM) were added to CDM before use. The carbon source for CDM or C-media was added at either 1% (all other PTS sugars) or 0.5% (glucose) prior to GAS inoculation. On occasion, various concentrations of glucose was used. Luria-Broth (LB) was used to grow *E.coli* strains. Kanamycin (Km) was used at 50 μg ml^{-1} for *E.coli* and at 300 μg ml^{-1} for GAS. Spectinomycin (Sp) was used at 100 μg ml^{-1} for both *E.coli* and GAS.

M1T1 strains

Bacterial strains used in this study are listed in **Table 3.1**.

E. coli strains

Bacterial strains used in this study are listed in **Table 3.1.**

Generation of the annotated EII mutant library in MGAS5005

Mutagenic temperature sensitive pCRS integrative plasmids were used to create the annotated EII mutant library as previously described (Le Breton & McIver, 2013, Le Breton *et al*., 2013). Briefly, ~500 bp region of homology to each EIIC was inserted into SmaI-cut pCRS to create a mutagenic plasmid (**Table 3.2**). The mutagenic plasmid was then transformed into electrocompetant MGAS5005 and plated at 30°C for 2 days with 5% CO_2. The resulting transformants were then transferred to THY/$Spec^{100}$ plates at 30°C (5% CO_2) for 1 day, passaged in THY/$Spec^{100}$ broth for 1 day at 37°C (5% CO2), then plated on THY/$Spec^{100}$ for 1 day.

Proper insertion of the mutagenic plasmid, which was checked for accuracy by BamH1 digestion and sequencing, was validated by PCR using specific validation primers

and the plasmid primers 1201, 1211, pvuIIR, and pvuIIF (**Table 3.2**). Rescue strains were generated for each mutant by passaging confirmed mutants twice in THY broth for 1 day each at 30°C, then plated on THY at 37°C (5% CO_2). Rescues were confirmed by checking for spectinomycin sensitivity.

Generation of mannose EII subunit mutants in the M1T1s MGAS5005 and 5448

Using the pSinS (*repA* deleted) mutagenic plasmid approach, stable insertional mutants were created in some of the mannose EII subunits (Le Breton *et al.*, 2015). Briefly, mutagenic pSinS plasmids were created by cloning ~500bp of a region of homology to an EII subunit into a SmaI-cut pSinS. BamH1 digestion and sequencing was used to determine insert orientation and accuracy. The mutagenic plasmids were then transformed into electrocompetent 5448 or MGAS5005 cells containing pHlpK (which provides the *repAts* gene to pSinS), and plated on THY/ Sp^{100}/Km^{300} at 30°C (5% CO_2) for 2 days. Transformants were then passaged in THY/ Sp^{100}/Km^{300} for 1 day, pelleted, resuspended and incubated in saline for 2 hours in a 37°C water bath, and plated on THY/Sp^{100} at 37°C (5% CO_2). Mutants showed spectinomycin resistance and kanamycin sensitivity, and were confirmed via PCR using specific mutant confirmation primers and either 1201 or 1211 (**Table 3.2**).

Generation of fructose metabolic operon mutants and Δ*sloR*

Allelic exchange to create nonpolar mutants of *fruR, fruB*, and *fruA* was employed. Briefly, the open reading frame of each gene was replaced with a cat cassette as previously described (Rose, 1988). The primers oAXSpy066(0-2).(2,3,5,6) (**Table 3.2**) were used to amplify the region up and downstream of the CDS with overlaps of the cat cassette, and ligated by PCR-splicing by overlap extension (SOE). The *cat* cassette was amplified using oCatFwd and oCatRev (**Table 3.2**). This PCR product was digested by SmaI and cloned into SmaI digested pCRS, creating each mutagenic plasmid (**Table 3.4**). The mutagenic plasmids were integrated into the GAS genome by double-crossover homologous

recombination and passaged to select for both the mutant and revertant strains. Mutants were selected for by looking for colonies that were Cm^R but Sp^S, indicating the successful exchange of the cat cassette for the selected gene as well as loss of the mutagenic plasmid. Revertant strains were selected as having sensitivity for both antibiotics, indicating loss of the mutagenic plasmid after the initial integration, leaving behind the intact gene. PCR was used to validate proper *cat* insertion in the mutants.

Mutagenesis of *sloR* was done with pCRK, using the same procedure as before when generating the EII mutant library. The only difference was the antibiotic used during passages, using kanamycin instead of spectinomycin. Again, mutants were confirmed using PCR using sloR luc F and 1211 (**Table 3.2**).

Generation of glucose metabolic pathway mutants

MGAS5005.Δ*glcU* (**Table 3.1**) was created by using the pCRS system described in the earlier section to create an polar insertional inactivation mutant. MGAS5005.Δ*nagC* (**Table 3.1**) was created using allelic exchange with the swap of *nagC* for a kanamycin resistant cassette (from pCRK). This cassette was introduced by pCRS, where GAS transformants were passaged in THY with Sp and Km for two days at 30°C. These cells were then passaged in THY with Km, plated, and screened for kanamycin resistance and spectinomycin sensitivity at 37°C. Revertants were saved that were sensitive to both drugs, indicating reversion to wildtype *nagC*. Km^{50} was used for passaging this strain, based on presumably weak expression of the kanamycin resistance gene. We created a MGAS5005.Δ*glcU*Δ*ptsI* by transforming a mutagenic pCRK plasmid with a region of homology corresponding to *glcU* into the MGAS5005.Δ*ptsI* strain (Gera *et al*., 2014). Positive double mutants were resistant to both Sp^{100} and Km^{300}.

DNA manipulations

Polymerase Chain Reaction (PCR) was performed using either Taq DNA

Table 3.1: Bacterial strains

Bacterial Strain	*Relevant genotype description*	*Reference*
E.coli		
DH5α	*hsdR17 recA1 gyrA endA1 relA1*	Hanahan *et. al*, 1983
S.pyogenes		
MGAS5005	M1T1	Sumby *et. al*, 2005
MGAS5005.Δ*ptsI* (Δ*ptsI*)	Δ*ptsI* mutant in MGAS5005	Gera *et. al*, 2014
MGAS5005.Δ*manLMN*	MGAS5005 i.i. of *manLMN*	Sundar *et. al*, 2017
MGAS5005.Δ*manMN*	MGAS5005 i.i. of *manMN*	Sundar *et. al*, 2017
MGAS5005.Δ*manN*	MGAS5005 i.i. of *manN*	Sundar *et. al*, 2017
MGAS5005.Δ$manLMN_R$	MGAS5005.Δ*manLMN* rescue	Sundar *et. al*, 2017
MGAS5005.Δ$manMN_R$	MGAS5005.Δ*manMN* rescue	Sundar *et. al*, 2017
MGAS5005.Δ$manN_R$	MGAS5005.Δ*manN* rescue	Sundar *et. al*, 2017
5448	M1T1	Chatellier *et. al*, 2000
5448.Δ*manLMN*	5448 i.i. of *manLMN*	Sundar *et. al*, 2017
5448.Δ*manMN*	5448 i.i. of *manMN*	Sundar *et. al*, 2017
5448.Δ*manN*	5448 i.i. of *manN*	Sundar *et. al*, 2017
5448.Δ$manLMN_R$	5448.Δ*manLMN* rescue	Sundar *et. al*, 2017
5448.Δ$manMN_R$	5448.Δ*manMN* rescue	Sundar *et. al*, 2017
5448.Δ$manN_R$	5448.Δ*manN* rescue	Sundar *et. al*, 2017
MGAS5005.Δ*nagC (ΔnagC)*	MGAS5005 i.i. of *nagC*	This study
MGAS5005.Δ*glcU (ΔglcU)*	MGAS5005 i.i. of *glcU*	This study
MGAS5005.Δ*glcU*Δ*ptsI*	MGAS5005 i.i. of *glcU*/a.e. of *ptsI*	This study
MGAS5005.Δ$nagC_R$	MGAS5005.Δ*nagC* revertant	This study
MGAS5005.Δ$glcU_R$	MGAS5005.Δ*glcU* revertant	This study
5448.Δ*fruR*	5448 a.e of *fruR*	Valdes *et. al*, 2016
5448.Δ*fruB*	5448 a.e of *fruB*	Valdes *et. al*, 2016
5448.Δ*fruA*	5448 a.e of *fruA*	Valdes *et. al*, 2016
5448.Δ$fruR_R$	5448.Δ*fruR* rescue	Valdes *et. al*, 2016
5448.Δ$fruB_R$	5448.Δ*fruB* rescue	Valdes *et. al*, 2016
5448.Δ$fruA_R$	5448.Δ*fruA* rescue	Valdes *et. al*, 2016
EII mutant library		
Δ3-keto-L-gulonate	MGAS5005 i.i. of Spy0148	Sundar *et. al*, 2017
Δβ-glucoside	MGAS5005 i.i. of Spy0475	Sundar *et. al*, 2017
ΔCellobiose-1	MGAS5005 i.i.of Spy1079	Sundar *et. al*, 2017
ΔCellobiose-2	MGAS5005 i.i. of Spy1744	Sundar *et. al*, 2017
ΔFructose	MGAS5005 i.i. of *fruA*	Sundar *et. al*, 2017
ΔGalactose	MGAS5005 i.i. of Spy1399	Sundar *et. al*, 2017
ΔLactose	MGAS5005 i.i. of *lacE.2*	Sundar *et. al*, 2017
ΔMaltose	MGAS5005 i.i. of *malT*	Sundar *et. al*, 2017
ΔMannitol	MGAS5005 i.i. of Spy1663	Sundar *et. al*, 2017
ΔMannose/Fructose	MGAS5005 i.i. of *ptsC*	Sundar *et. al*, 2017

Table 3.1 con't: Bacterial strains

Bacterial Strain	*Relevant genotype description*	*Reference*
EII mutant library con't		
ΔMannose (Δ*manMN*)	MGAS5005 i.i. of *manM*	Sundar *et. al*, 2017
ΔN-acetylgalactosamine	MGAS5005 i.i. of Spy520	Sundar *et. al*, 2017
ΔSucrose	MGAS5005 i.i. of *scrA*	Sundar *et. al*, 2017
ΔTrehalose	MGAS5005 i.i. of Spy1784	Sundar *et. al*, 2017
Δ3-keto-L-gulonate$_R$	Δ3-keto-L-gulonate rescue	Sundar *et. al*, 2017
Δβ-glucoside$_R$	Δβ-glucoside rescue	Sundar *et. al*, 2017
ΔCellobiose-1$_R$	ΔCellobiose-1 rescue	Sundar *et. al*, 2017
ΔCellobiose-2$_R$	ΔCellobiose-2 rescue	Sundar *et. al*, 2017
ΔFructoseR	ΔFructose rescue	Sundar *et. al*, 2017
ΔGalactose$_R$	ΔGalactose rescue	Sundar *et. al*, 2017
ΔLactose$_R$	ΔLactose rescue	Sundar *et. al*, 2017
ΔMaltose$_R$	ΔMaltose rescue	Sundar *et. al*, 2017
ΔMannitol$_R$	ΔMannitol rescue	Sundar *et. al*, 2017
ΔMannose/Fructose$_R$	ΔMannose/Fructose rescue	Sundar *et. al*, 2017
ΔMannose$_R$	ΔMannose rescue	Sundar *et. al*, 2017
ΔN-acetylgalactosamine$_R$	ΔN-acetylgalactosamine rescue	Sundar *et. al*, 2017
ΔSucrose$_R$	ΔSucrose rescue	Sundar *et. al*, 2017
ΔTrehalose$_R$	ΔTrehalose rescue	Sundar *et. al*, 2017

* i.i = Insertional Inactivation
** a.e.= allelic exchange

polymerase (NEB) for diagnostic assays, or using Accuprime Pfx (Life Technologies) for cloning. Both were carried our according to the manufacturer's protocol. Sequencing was done through Genewiz, Inc. Genomic DNA was extracted from GAS strains using the Master-Pure complete DNA and RNA purification kit for Gram-positive bacteria (Epicentre). Wizard Plus SV miniprep kit was used to extract plasmids from *E. coli*. DNA fragments from agarose gels or PCR reactions were purified using the Wizard SV gel and PCR cleanup kit (Promega).

Ligations were performed using a T4 ligase. Reactions were set up as a 16:1 ratio between insert and plasmid, and reactions were incubated in a 16^{o}C water bath for 1 day. Restriction digests were also performed for 2 hours in buffers and temperatures recommended by the manufacturer (NEB). Plasmids used are listed on **Table 3.4.**

Table 3.2: Primers used

Primer	*Sequence 5' to 3'*	*Target*
Amplification of region of homology for EII mutagenic plasmids		
Spy148L	CCC**GGATCC**ACCTGGAGCATTCAACCCAGCTAAGCAAGC	CDS of Spy148
Spy148R	CCC**GGATCC**TACAGCAACAGCACCAAGTGCAACTTG	
Spy475L	CCC**GGATCC**CGTTGCCTTTATTAACTTCT	CDS of Spy475
Spy475R	CCC**GGATCC**ACATGATAAATAGCGAGCAT	
Spy520L	CCC**GGATCC**TCGGCCCTGGTATCTTTGGTACCTTGATGGCTA	CDS of Spy520
Spy520R	CCC**GGATCC**TTGGAGGTAGGCTGCACAAACATAACCAAT	
Spy662L	CCC**GGATCC**TTCTAAAAATATTGTAGTAGA	CDS of Spy662
Spy662R	CCC**GGATCC**ACCGTTTGTTTCAACTTTAATAGCTACT	
Spy782L	CCC**GGATCC**TGGGGGCCTCTCTAGAAGCTCTTTTCCT	CDS of Spy782
Spy782R	CCC**GGATCC**ATGGCAAAACCGACAGCTGGAAGAAGGC	
Spy1079L	CCC**GGATCC**TATCGACATCAATGGCTATG	CDS of Spy 1079
Spy1079R	CCC**GGATCC**TTAACCGCAGGTGGTACATTAT	
Spy1399L	CCC**GGATCC**AAATTGGCTTCTGGGGCTCTAAGTTCT	CDS of Spy1399
Spy1399R	CCC**GGATCC**ATCATGCGAATCAAACGACCACGTGTGA	
Spy1480L	CCC**GGATCC**TTTCTGCAATTTTGGTCGTT	CDS of Spy1480
Spy1480R	CCC**GGATCC**AAAGTGGAAGCGTTCAATAC	
Spy1542L	CCC**GGATCC**TTTATGATGAAGGAAAGATTGATAAGG	CDS of Spy1542
Spy1542R	CCC**GGATCC**AAAACAATACCGATAATAGGATTACCC	
Spy1633L	CCC**GGATCC**GATTGTTCATACTACTTTAG	CDS of Spy1633
Spy1633R	CCC**GGATCC**TAAATGGAATAAAGAAAATTGGGTTCA	
Spy1663L	CCC**GGATCC**TTCGGAGAAATTGAGGGATTTGATTTATTTT	CDS of Spy1663
Spy1663R	CCC**GGATCC**GAGATTCATAATCTTGTTTGATTTGTT	
Spy1692L	CCC**GGATCC**CTCTTGTTGCCATTTGGTCTTCACCACA	CDS of Spy1692
Spy1692R	CCC**GGATCC**GCATTGCTGCAAACATAAATAGGTACT	
Spy1744L	CCC**GGATCC**GATGCTATCAGTAAGGTTTG	CDS of Spy1744
Spy1744R	CCC**GGATCC**GCATCTAGATTTGATAAGAG	
Spy1784L	CCC**GGATCC**CCAAAAACTGGGTTTGGGATTTTGGTTTCTTTACC	CDS of Spy1784
Spy1784R	CCC**GGATCC**AAGCAAAAACGGCTGACCCTTGAGCGATATTTGAA	
Validation primer for confirming EII mutants		
148mutant conf1	TGCTAGCTGACCTTTGG	5' of CDS of Spy148
475mutant conf1	GACCCCAAAAATAGCTGGTTC	5' of CDS of Spy475
520mutant conf1	CTCCTTGACCATCACGG	5' of CDS of Spy520
662mutant conf1	GCGTCTCTTAGAATCAGCGG	5' of CDS of Spy662
782mutant conf1	TTCCAATCGTCCTCAGCACC	5' of CDS of Spy782
1079mutant conf1	AAGAATTTGGTGGACGC	5' of CDS of Spy1079
1399mutant conf1	AACTTCACCCGTTAAAGGGC	5' of CDS of Spy1399

Table 3.2 con't: Primers used

Primer	*Sequence 5' to 3'*	*Target*
1480mutant conf#1	TGCTAGCTGACCTTTGG	5' of CDS of Spy1480
1542mutant conf#1	GACCCCAAAAATAGCTGGTTC	5' of CDS of Spy1542
1633mutant conf#1	CTCCTTGACCATCACGG	5' of CDS of Spy1633
1663mutant conf1	GCGTCTCTTAGAATCAGCGG	5' of CDS of Spy1663
1692mutant conf1	TTCCAATCGTCCTCAGCACC	5' of CDS of Spy1692
1744mutant conf#1	AAGAATTTGGTGGACGC	5' of CDS of Spy1744
1784mutant conf1	AACTTCACCCGTTAAAGGGC	5' of CDS of Spy1784
Mannose EII subunit mutagenesis and validation		
manL-F	CCC**GGATCC**CATGCCAAACGAAGGACCAG	CDS of *manL*
manL-R	CCC**GGATCC**GAAGGTCATCTTGAGCAACC	
manN-F	CCC**GGATCC**GCTTATGCACTTATCCCTGC	CDS of *manN*
manN-R	CCC**GGATCC**GTTTTCCAGGAAGGTCGATAG	
manM validation	GGTGTTACATTCGACGTCCG	5' of CDS of *manM*
manN validation	GGTGTTACATTCGACGTCCG	5' of CDS of *manN*
Mannose EII transcirptional operon		
manL-5'	CGACCTAGGTGTTACATTCG	CDS of *manL*
manM-5'	AATCGGTGGTGCGATGGTTG	CDS of *manM*
manM-3'	AGGGCAGTTGACAAAGTACG	
manN-5'	GCTATTGGTGGTATGAGCCT	CDS of *manN*
manN-3'	GGTCTTCAGGAGACGTATAC	
manO-3'	AATTCAAGGGCCTTGTCACC	CDS of *manO*
Fructose EII operon mutagenesis		
oAXSpy0660.5	CCC**GGATCC**CAGAGCTAGTTCACGCTAAAG	*fruR*
oAXSpy0660.2	TATCCAGTGATTTTTTTCTCCATGATTAATTGTTTTCGTTTTGATTTT	*fruR*
oAXSpy0660.3	CAGGGCGGGGCGTAATTTATACCGTGACCTTAAACCC	*fruR*
oAXSpy0660.6	CCC**GGATCC**AATTCGGTCTCTTCTTGTGAC	*fruR*
oAXSpy0661.1	CCC**GGATCC**ATTACTCAACTCCTCTGAGTC	*fruB*
oAXSpy0661.2	TATCCAGTGATTTTTTTCTCCATAATTCAATCACCTTTGCCTTTTC	*fruB*
oAXSpy0661.3	GATGAGTGGCAGGGCGGGGCGGCTTTCTCTGA TGACTTGGC	*fruB*
oAXSpy0661.4	CCC**GGATCC**TAGCTACTCCCATTTCTGCAG	*fruB*
oAXSpy0662.1	CCC**GGATCC**AAAGGTGATCAAGATACTCG	*fruA*
oAXSpy0662.2	TATCCAGTGATTTTTTTCTCCATCGTTTTTCTACCTCAACTTTATG	*fruA*
oAXSpy0662.3	GGCAGGGCGGGGCGTAAAAGGTAAAGAACTTTTTTCTTAC	*fruA*
oAXSpy0662.4	CCC**GGATCC**AAAATTAGTGAGTTGATACC	*fruA*

Table 3.2 con't: Primers used

Primer	*Sequence 5' to 3'*	*Target*
sloR InIn F	GGG**GGATCC**ATTCTTGTTTTAGCTATTTT	*sloR*
sloR InIn R	GGG**GGATCC**CCCAGCCACAAAACCTGGGA	*sloR*
Fructose EII transcriptional operon		
FruR RevTransF	TATGTCAAACAAACGACCGA	*fruR*
FruB RevTransF	TATGAAGAGTCAAAATCCAA	*fruB*
FruB RevTransR	GGGAAAGCTTAGTTTTCAAA	*fruB*
FruA RevTransR	ATCATAAAGAAGAGATCCGT	*fruA*
Luciferase and 5'RACE		
FruR luc_1	GGG**GGATCC**TTGTGAGCCTAGATTATGAG	*fruR*
FruR luc_4	GGG**CTCGAG**GATTAATTGTTTTCGTTTTG	
sloR luc F	GGG**GGATCC**GTCAAACTTCCTATATCTATCTT	*sloR*
sloR luc R	GGG**CTCGAG**ATACGAACCTCCTCATTGATAATAT	
FruR SP1	TCAGCACCTCCATGAACACG	*fruR*
FruR SP2	ATGTAGCCGTCCTTCTTGCT	*fruR*
FruR SP3	CCAACTCTCCTAGATCTCTA	*fruR*
Glucose pathway mutants mutagenic primers and validation		
oAX1311-1	CCC**GGATCC**AGAAATCCCTTTGACTGAA	*nagC*
oAX1311-2k	GGTGATATTCTCATTTTAGCCATGAGGTG	*nagC*
oAX1311-3k	ATTTTACTGGATGAATTGTTTTAGCCATG	*nagC*
oAX1311-4	CCC**GGATCC**TTGATGGCTGGTCTTGGCTC	*nagC*
Spy1856 F	CCC**GGATCC**GATGACACTGCAACTTTGG	*glcU*
Spy1856 R	CCC**GGATCC**CCAATGCCCCAAAGTAATC	*glcU*
oAX1311-V	CCATTACGACAATATTCCTTGG	5' of CDS of *nagC*
Spy1856 mutantconf1	GGTGTTACATTCGACGTCCG	5' of CDS of *glcU*
Realtime PCR		
manL M1T1 RT L	GGCGATCATCACTGGTCTC	*manL*
manL M1T1 RT R	TGTTCAACACCTGCACCAG	*manL*
manM M1T1 RT L	TCCCTGCAGCTCTTCTTGT	*manM*
manM M1T1 RT R	CCGATTTGCATACCTTCGT	*manM*
manN M1T1 RT L	TTGCCCTTGAAGAAGAACG	*manN*
manN M1T1 RT R	CAGCAAGAGGTCCCATCAT	*manN*

Table 3.2 con't: Primers used

Primer	*Sequence 5' to 3'*	*Target*
fruA M1 RT L	ACCGGGCTTAGTAGCTGGT	*fruA*
fruA M1 RT R	ACTTCTCCTCCTGCTGCAA	*fruA*
fruB M1 RT L	GTTCAGCGCCAGCTAATCT	*fruB*
fruB M1 RT R	TCACAAACCACCTGAGCAC	*fruB*
fruR M1 RT L	GTCAAACAAACGACCGATC	*fruR*
fruR M1 RT R	TCCAAGAAATGCCTTGTCA	*fruR*
ptsI M1 RT L	CGGAAACCAAGGAATGGAT	*ptsI*
ptsI M1 RT R	TGGCAAACCTGTTGTGGTT	*ptsI*
gyrA M1 RT-L	CGACTTGTCTGAACGCCAAAGTC	*gyrA*
gyrA M1 RT-R	ATCACGTTCCAAACCAGTCAAAC	*gyrA*
sloR M1T1 RT L	GTGAAGTAGGCGGAGCAAA	*sloR*
sloR M1T1 RT R	CGGCATAACCTGGAGACAC	*sloR*
Miscellaneous		
oCatFwd	ATGGAGAAAAAAATCACTGGATA	*cat*
oCatRev	TTACGCCCCGCCCTGCC	*cat*
oCatSeq1	TTCCA TGAGCAAACTGAAACG	*cat*
oCatSeq2	CAGGTTTTCACCGTAACACG	*cat*
1201	AACAGCTATGACCATGATTACG	*M13*
1211	GTTGTAAAACGACGGCCAGT	*M13*

* bp in bold denote restriction sites

** Underlined bp denote areas of overlap with a resistance cassette for PCR soeing

Transformation

Electrocompetent cell preparation

To prepare MGAS5005 and 5448 for transformation, we made electrocompetent cells as described earlier (Le Breton & McIver, 2013). Briefly, GAS strains were grown in THY + 20mM glycine at 37°C overnight. 7.5 mls of the overnight culture was added to 150 mls of THY + 20mM glycine and grown at 37°C until an OD_{600} of 0.2-0.4. Cells were then pelleted, washed in ice-cold EP-solution (100% glycerol) and pelleted again before a final

resuspension in glycerol. Cells were then stored at -80°C.

Electroporation

Plasmids used in this dissertation are listed in **Table 3.4**. To prevent arcing during electroporation, DNA was drop dialyzed with dH_2O on a 0.025 μm membrane filter (Millipore). This was done for either 30 minutes (*E.coli*) or 1 hour (GAS). Electroporation was performed using a GenePulser Xcell (BioRad). DNA was added to 100 μl of competent cells in a 2 mm cuvette placed on ice. The cuvette was then electroporated using 2.5 kV, 200 Ω and 25 μF for *E.coli*, or 1.75kV, 400 Ω and 25 μF for GAS. Cells were then transferred to 1 ml of LB (*E.coli*) and incubated shaking at 37°C for 1 hour, or to 10 mls of THY (GAS) and incubated statically at 30°C for 4 hours. Cells were then centrifuged at 6000g, resuspended in 100 μl of their respective medias, and plated on antibiotic selection.

Metabolic Assays

Growth Curves

GAS growth was monitored using the FLUOstar Omega microplate spectrophotometer (BMG). OD_{600} measurements were taken every 30 minutes for 24 or 48 hours. Plates were shaken for 10 seconds prior to each reading. Overnight cultures were grown in 10 mls of THY (with/without antibiotic), pelleted, and washed in saline. The OD_{600} of the cultures was then adjusted to 0.2 in saline. 50 μl of culture was added to each well of either a 24 or 48 well plate (Corning/Costar) containing CDM + 1% of a PTS carbohydrate (0.5% for glucose). Plates were sealed with plate tape (Bio-Rad), and then incubated in the microplate spectrophotometer for 24 or 48 hours.

Growth curves were analyzed by dividing the OD_{600} measurements of the mutant by the WT at each time point to generate a set of % WT. The median and interquartile range of this data set was calculated. Mutants were determined to have significant growth defects in carbon sources in which growth was more than 2 fold below WT. Mutants were determined to have growth above WT in carbon sources that have 2 fold growth above WT. ΔOD was

Table 3.3: Primer origin

Primer	*Reference*	*Primer*	*Reference*
Spy148L	Sundar *et. al*, 2017	manN-F	Sundar *et. al*, 2017
Spy148R	Sundar *et. al*, 2017	manN-R	Sundar *et. al*, 2017
Spy475L	Sundar *et. al*, 2017	manMvalidation	Sundar *et. al*, 2017
Spy475R	Sundar *et. al*, 2017	manNvalidation	Sundar *et. al*, 2017
Spy520L	Sundar *et. al*, 2017	manL-5’	Sundar *et. al*, 2017
Spy520R	Sundar *et. al*, 2017	manM-5’	Sundar *et. al*, 2017
Spy662L	Sundar *et. al*, 2017	manM-3’	Sundar *et. al*, 2017
Spy662R	Sundar *et. al*, 2017	manN-5’	Sundar *et. al*, 2017
Spy782L	Sundar *et. al*, 2017	manN-3’	Sundar *et. al*, 2017
Spy782R	Sundar *et. al*, 2017	manO-3’	Sundar *et. al*, 2017
Spy1079L	Sundar *et. al*, 2017	oAXSpy0660.5	Valdes *et. al*, 2016
Spy1079R	Sundar *et. al*, 2017	oAXSpy0660.2	Valdes *et. al*, 2016
Spy1399L	Sundar *et. al*, 2017	oAXSpy0660.3	Valdes *et. al*, 2016
Spy1399R	Sundar *et. al*, 2017	oAXSpy0660.6	Valdes *et. al*, 2016
Spy1480L	Sundar *et. al*, 2017	oAXSpy0661.1	Valdes *et. al*, 2016
Spy1480R	Sundar *et. al*, 2017	oAXSpy0661.2	Valdes *et. al*, 2016
Spy1542L	Sundar *et. al*, 2017	oAXSpy0661.3	Valdes *et. al*, 2016
Spy1542R	Sundar *et. al*, 2017	oAXSpy0661.4	Valdes *et. al*, 2016
Spy1633L	Sundar *et. al*, 2017	oAXSpy0662.1	Valdes *et. al*, 2016
Spy1633R	Sundar *et. al*, 2017	oAXSpy0662.2	Valdes *et. al*, 2016
Spy1663L	Sundar *et. al*, 2017	oAXSpy0662.3	Valdes *et. al*, 2016
Spy1663R	Sundar *et. al*, 2017	oAXSpy0662.4	Valdes *et. al*, 2016
Spy1692L	Sundar *et. al*, 2017	sloR InIn F	Valdes *et. al*, 2016
Spy1692R	Sundar *et. al*, 2017	sloR InIn R	Valdes *et. al*, 2016
Spy1744L	Sundar *et. al*, 2017	FruR RevTransF	Valdes *et. al*, 2016
Spy1744R	Sundar *et. al*, 2017	FruB RevTransF	Valdes *et. al*, 2016
Spy1784L	Sundar *et. al*, 2017	FruB RevTransR	Valdes *et. al*, 2016
Spy1784R	Sundar *et. al*, 2017	FruA RevTransR	Valdes *et. al*, 2016
148mutantconf1	Sundar *et. al*, 2017	FruR luc_1	Valdes *et. al*, 2016
475mutantconf1	Sundar *et. al*, 2017	FruR luc_4	Valdes *et. al*, 2016
520mutantconf1	Sundar *et. al*, 2017	sloR luc F	Valdes *et. al*, 2016
662mutantconf1	Sundar *et. al*, 2017	sloR luc R	Valdes *et. al*, 2016
782mutantconf1	Sundar *et. al*, 2017	FruR SP1	Valdes *et. al*, 2016
1079mutantconf1	Sundar *et. al*, 2017	FruR SP2	Valdes *et. al*, 2016
1399mutantconf1	Sundar *et. al*, 2017	FruR SP3	Valdes *et. al*, 2016
1480mutantconf#1	Sundar *et. al*, 2017	manL M1T1 RT L	Sundar *et. al*, 2017
1542mutantconf#1	Sundar *et. al*, 2017	manL M1T1 RT R	Sundar *et. al*, 2017
1633mutantconf#1	Sundar *et. al*, 2017	manM M1T1 RT L	Sundar *et. al*, 2017
1663mutantconf1	Sundar *et. al*, 2017	manM M1T1 RT R	Sundar *et. al*, 2017
1692mutantconf1	Sundar *et. al*, 2017	manN M1T1 RT L	Sundar *et. al*, 2017
1744mutantconf#1	Sundar *et. al*, 2017	manN M1T1 RT R	Sundar *et. al*, 2017
1784mutantconf1	Sundar *et. al*, 2017	fruA M1 RT L	Valdes *et. al*, 2016
manL-F	Sundar *et. al*, 2017	fruA M1 RT R	Valdes *et. al*, 2016
manL-R	Sundar *et. al*, 2017	fruB M1 RT L	Valdes *et. al*, 2016

Table 3.3 con't: Primer origin

Primer	*Reference*
fruB M1 RT R	Valdes *et. al*, 2016
fruR M1 RT L	Valdes *et. al*, 2016
fruR M1 RT R	Valdes *et. al*, 2016
ptsI	Gera *et. al,* 2014
ptsI	Gera *et. al,* 2014
gyrA M1 RT-L	Ribardo *et. al,* 2004
gyrA M1 RT-R	Ribardo *et. al,* 2004
sloR M1T1 RT L	Valdes *et. al*, 2016
sloR M1T1 RT R	Valdes *et. al*, 2016
oCatFwd	Valdes *et. al*, 2016
oCatRev	Valdes *et. al*, 2016
oCatSeq1	Valdes *et. al*, 2016
oCatSeq2	Valdes *et. al*, 2016
1201	Genewiz
1211	Genewiz
oAX1311-1	This study
oAX1311-2k	This study
oAX1311-3k	This study
oAX1311-4	This study
Spy1856 F	This study
Spy1856 R	This study
oAX1311-V	This study
Spy1856mutantconf1	This study

determined by deducting the initial OD_{600} from the max OD_{600}. Data presented is the average of at least 3 biological replicates, done in technical duplicates. Significance was determined by unpaired Student t test ($p\text{-value}<0.5$). In some cases, a Klett-Summerson colorimeter (A filter) was used to monitor growth. Rather than OD_{600}, growth was monitored using Klett units. Briefly, 10 mls of media was added to a Klett tube with each strain inoculated at 1:20 and grown at 37°C. Growth rates were calculated by dividing the ΔKlett from two timepoints during exponential growth.

ΔOD Assays

ΔOD calculated in certain cases (glucose test strip utilization assays) was performed in a different manner than described above. Overnight GAS cultures were added to 1:20 to 5 mls of either THY or CDM + PTS carbohydrate. 1 ml was removed from each tube, and the OD_{600} was measured. The final OD_{600} was then measured by allowing each tube to incubate at 37°C for 24 hours before removing another 1 ml. The initial OD_{600} was subtracted from the final OD_{600} to yield the ΔOD_{600} of the mutant strain grown in either in THY or CDM + a single PTS carbohydrate. Sugar concentration readings using the glucose test strips (AimStrip® Plus) were measured at both 0 and 24 hours.

Growth in whole human blood

A modified growth experiment was carried out in whole human blood to determine if low nutrient content lead to the activity of Streptolysin S. GAS strains were inoculated

Table 3.4: Plasmids used

Plasmids	*Relevant description*	*Reference*
pCRS	Temperature-sensitive conditional vector; Sp^R	Le Breton *et. al,*2013
pCRK	Temperature-sensitive conditional vector; Km^R	Le Breton *et. al,*2013
pSinS	Suicide plasmid for stable i.i.; Sp^R	Le Breton *et. al,*2015
pHlpK	Temperature-sensitive conditional helper vector; Km^R	Le Breton *et. al,*2015
pACYC	Vector containing Cm^R gene	
pKSM950	Spy0148 mutagenic plasmid; pCRS	Sundar *et. al*, 2017
pKSM951	Spy0475 mutagenic plasmid; pCRS	Sundar *et. al*, 2017
pKSM952	Spy0520 mutagenic plasmid; pCRS	Sundar *et. al*, 2017
pKSM953	*fruA* mutagenic plasmid; pCRS	Sundar *et. al*, 2017
pKSM954	*ptsC* mutagenic plasmid; pCRS	Sundar *et. al*, 2017
pKSM955	Spy1079 mutagenic plasmid; pCRS	Sundar *et. al*, 2017
pKSM956	Spy1399 mutagenic plasmid; pCRS	Sundar *et. al*, 2017
pKSM957	*manL* mutagenic plasmid; pSinS	Sundar *et. al*, 2017
pKSM958	*manM* mutagenic plasmid; pCRS	Sundar *et. al*, 2017
pKSM959	*manM* mutagenic plasmid; pSinS	Sundar *et. al*, 2017
pKSM960	*manN* mutagenic plasmid; pCRS	Sundar *et. al*, 2017
pKSM961	*manN* mutagenic plasmid; pSinS	Sundar *et. al*, 2017
pKSM962	*scrA* mutagenic plasmid; pCRS	Sundar *et. al*, 2017
pKSM963	*lacE.2* mutagenic plasmid; pCRS	Sundar *et. al*, 2017
pKSM964	Spy1663 mutagenic plasmid; pCRS	Sundar *et. al*, 2017
pKSM965	*malT* mutagenic plasmid; pCRS	Sundar *et. al*, 2017
pKSM966	Spy1744 mutagenic plasmid; pCRS	Sundar *et. al*, 2017
pKSM967	Spy1784 mutagenic plasmid; pCRS	Sundar *et. al*, 2017
pKSM968	*nagC* mutagenic plasmid with nonpolar Km^R; pCRS	This study
pKSM969	*glcU* mutagenic plasmid for i.i.; pCRS	This study
pKSM970	*glcU* mutagenic plasmid for i.i.; pCRK	This study
p5448.ΔfruR	Δ*fruR* mutagenic plasmid; nonpolar *cat*	Valdes *et. al*, 2016
p5448.ΔfruB	Δ*fruB* mutagenic plasmid; nonpolar *cat*	Valdes *et. al*, 2016
p5448.ΔfruA	Δ*fruA* mutagenic plasmid; nonpolar *cat*	Valdes *et. al*, 2016
pKSM720	GAS replicating plasmid with promoterless firefly luciferase (*luc*) and ribosomal binding site	Valdes *et. al*, 2016
pKSM944	GAS replicating plasmid with full length P*fru* driving expression of *luc*	Valdes *et. al*, 2016
pKSM945	GAS replicating plasmid with P*fru* no FruR consensus driving expression of *luc*	Valdes *et. al*, 2016
pKSM948	GAS replicating plasmid with P*sloR* driving expression of *luc*	Valdes *et. al*, 2016

1:20 in 10 mls fresh whole human blood, rotating for at least 6 hours. Samples were taken every hour from 0 h. The blood sugar concentration was taken using the glucose test strips using the procedure described earlier. Samples were then vortexed for 10 minutes, diluted,

and plated on THY for viable counts.

The API®50 CH system

The API®50 CH system (Biomérieux) was used to assess utilization of carbon sources by GAS using the procedure described previously (Valdes *et al.*, 2016). Briefly, strains were cultured overnight on blood agar plates, scraped and resuspended in 1 ml of saline, and vortexed for 3 minutes. Cultures were then diluted and added to 10 ml of API®50CHL medium (BioMérieux). This was then added to the 50 cupules in the assay kit, and incubated at 37°C (5% CO_2). Utilization scores were determined at both 24 and 48 hours, with each strain given either a "+" for utilization, and "+/-" for partial utilization, and a "-" for no utilization. To calculate the utilization scores for each strain for a particular carbon source, "+" was given a 1, "+/-" was given a 0.5, and "-" was given a 0. With two measurements per assay, scores for each carbon source ranged from 0-2.

Biolog Carbon Utilization Panel

Carbohydrate metabolic profiles of GAS strains was determined via the Biolog Omnilog (Biolog, Inc.) as previously described (Gera *et al.*, 2014). Briefly, the metabolic profile of each strain was assessed using the PM1 and PM2A carbon panels (96-well microplate). This system allows the interrogation of the utilization of 190 carbon sources, with each plate containing 95 carbon sources and one negative control. Each GAS strain was cultured on blood agar plates and resuspended in inoculating fluid (Biolog) to an OD_{600} of 0.14. 100 μl of the cell suspension was added to each well of the PM microplates before each plate was incubated at 37°C for 48h. Utilization of a carbon source was determined by a change in a colorimetric dye present in the inoculating fluid via an Omnilog X instrument located at the FDA center for Food and Applied Nutrition (CFSAN). The data was analyzed using the Omnilog software (Biolog).

Sugar Utilization Monitored by Glucose Test Strips

Sugar utilization was also monitored by the use of a blood glucose testing system (AimStrip® Plus). Although typically used to monitor blood sugar, we used this apparatus

to monitor sugar concentration of THY, CDM, and whole human blood during GAS growth. Values are given in mg/dl. Readings were taken by first inserting a test strip (AimStrip® Plus) into the monitor, placing the test strip into the culture to draw up liquid droplets, and waiting for 10 seconds for the final reading.

Influence Scores

The influence an EII has on the metabolism of a carbon source was illustrated by determining an Influence Score. The Influence Score is an arbitrary value assigned to each EII for each PTS carbohydrate, and has no bearing on the metabolic potential or efficiency. It is simply a qualitative method to visualize the potential impact an EII might have on the transport and metabolism of a carbon source by combining the results of all the growth and metabolic assays performed.

The **Influence Score** was calculated as followed:

Growth curve score = Median % WT of growth

ΔOD score = Mean of % WT of ΔOD_{600}

API score = % WT of utilization score

Influence score

0.5 [0.5 (**Growth curve score**) + 0.5 (**ΔOD score**)] + 0.5 (**API score**)

Luciferase Assays

Strains for luciferase assays were created as follows. P*fru* was amplified from 5448 gDNA using FruR_luc_1 and FruR_luc_4 primers (**Table 3.2**). The PCR fragments was digested using BglII/XhoI and ligated into pKSM720 cut with the same restriction enzymes (pKSM944; **Table 3.4**). A truncated P*fruR* was also amplified from 5448 gDNA using FruR_luc_2 and FruR_luc_4, which deletes the putative FruR binding site from the promoter region (**Table 3.2**). This PCR fragments was also digested and ligated in pKSM720(pKSM945), similarly to the full length P*fruR*. P*sloR* was amplified form 5448

gDNA using sloR_luc_F/R, digested and ligated in the same manner to form pKSM948 (**Table 3.4**).

The Luciferase assay was carried out as previously described (Valdes *et al*., 2016). 5448 and 5448.Δ*fruR* were transformed with the luciferase plasmids (**Table 3.1**). This was grown in CDM + 0.5% glucose or 1% fructose, mannose, or sucrose with spectinomycin at 37°C. 500 μL samples were taken every 30 kletts (beginning at 50), pelleted, supernatant was discarded, and samples were placed at 20°C overnight. Using a luciferase assay system (Promega), pellets were resuspended in lysis buffer. These were then normalized to cell units using the equation: 4.5(x ml)(65 Klett units/2), where x = sample volume. The luciferase assay was read using a Centro XS3 LB 960 luminometer (Berthold Technologies), into which 50 μl of Luciferin-D reagent was injected. Three biological replicates in each sugar was performed.

Hemolysis Assays

The hemolysis assay was carried out as previously described with some modifications (Gera *et al.*, 2014). GAS strains were grown in THY supplemented with 10% heat inactivated serum, with samples taken every hour for 8 hours. Samples were then pelleted and 50 μl of the cell free supernatant was added to 950 μl of difibrinated sheep red blood cells (RBCs). To prepare the RBCs, 500 μl was washed in phosphate-buffered saline (PBS) three times. Once the supernatant was added to the red blood cells, these cultures were incubated for 1 h at 37°C. The cultures were then centrifuged at 3000g to clear intact RBCs. The OD_{541} of the supernatant was measured to determine the release of hemoglobin from lysed RBCs. OD_{541} above 0.2 were considered positive RBC lysis. A modifies version of this assay was also carried out where samples were taken every 20 min, rather than every hour. Data shown is a combination of at least three biological replicates.

Virulence Assays

Lancefield Bactericidal Assay

GAS survival in whole human blood was assessed as previously described (Le Breton *et al*., 2013). Briefly, GAS was grown in THY to early mid-exponential phase (OD_{600} ~ 0.10) and is serially diluted in saline. 50 µl of a 10^{-4} dilution was added to 500 µl of fresh heparinized whole human blood. Blood donation was approved by the University of Maryland Institutional Review Board (IRB) (protocol 10-0735). Approved consent was obtained from each donor, and records have been archived. Once inoculated with GAS, the blood was rotated for 3h at 37°C. A multiplication factor was calculated by dividing the CFUs obtained after blood challenge by the initial CFU inoculation. Data are shown as percent wildtype, where multiplication factors of mutant strains were divided by the multiplication factors of the wildtype, multiplied by 100. Data are shown as the average of at least three biological replicates. Statistical significance was determined using an unpaired Student t test (p-value < 0.05).

Murine Infections

Animal work was performed in an AAALAC-accredited ABSL-2 facility at the University of Maryland, College Park. IACUC-approved protocols (R-16-05) for humane treatment of animal subjects in accordance with the Office of Laboratory Animal Welfare (OLAW) at NIH, Public Health Service, and the Guide for the Care and Use of Laboratory Animals guidelines were used. Extreme care was taken to limit the distress and pain to the animals.

The subcutaneous murine infection model was carried out as previously described (Gera *et al*., 2014). Overnight GAS cultures were used to inoculate 75 ml of THY at a 1:20 dilution. Cultures where then incubated at 37°C (5% CO_2) until late-logarithimic phase (Klett ~ 100). 5-7 week old female CD-1 mice (Charles River Laboratories) was inoculated with ~ 3 x 10^9 CFU ml^{-1}, as determined by microscope counts. Inoculation counts were then verified by plating for viable colonies on THY plates. Before infecting each mouse, they were anesthetized with ketamine and hair was removed from a 3 cm^2 area of one of

the haunches with Nair (Carter Products). A 100 μl of the GAS suspension in saline was injected subcutaneously. The mice were then monitored three times daily for 7 days, and were euthanized by CO_2 asphyxiation upon signs of morbidity. Image J was used to measure lesion sizes at 36 or 48 h post infection. Lesion severity was also determined by calculating the mean red pixel intensity among all the pixels present in the lesion selection. GraphPad Prism was used to analyze the data and an unpaired two-tailed Student t test was used to test for significance. Survival significance was determined by Mantel-Cox log rank test. The p-value was <0.5 for both statistical tests. CFUs from the extracted spleen were also calculated by resuspending spleens in 1 ml of PBS, disrupting the tissue, serially diluting the mixture, and then plating onto THY. Spleens were extracted 2 days post infection.

Cell culture

Human polymorphonuclear leukocytes (PMNs) or monocytes were isolated from heparinized blood of volunteer donors (IRB-approved protocol) using Polymorphprep (Axis-Shield) or Ficoll Paque plus (GE Healthcare), respectively, per the manufacturer's instructions. Contaminating red blood cells (RBCs) were removed by treatment with red cell lysis solution (Epicentre) and washing with Dulbecco's mod- ified phosphate-buffered saline (PBS) (Sigma). Isolated PMNs and monocytes were maintained in RPMI 1640 cell culture medium (HyClone) supplemented with 2.05 mM L-glutamine and 20% plasma from donor blood for the duration of the killing assay.

The human-derived promyelocytic leukemia HL60 (Sigma) cell line was maintained as indicated in the UAB-GBS-OPA protocol (http://www.vaccine.uab.edu/UAB-GBS-OPA.pdf). Briefly, the HL60 cell line was maintained in RPMI 1640 cell culture medium supplemented with 2.05 mM L-glutamine and 10% fetal bovine serum (FBS) (HyClone). Low-passage-number HL60 cells were differentiated into neutrophil-like cells for opsonophagocytic killing assays by supplementing culture medium with 1 M all-trans retinoic acid (ATRA) in dimethyl sulfoxide (DMSO) (3 mg/ml stock solution). PMNs,

monocytes, and HL60 cells were maintained at 37°C in 5% CO_2.

Opsonophagocytic killing assays

Isolated PMNs or differentiated HL60 cells were seeded at a density of 106 cells/ml in 24-well plates with RPMI 1640 cell culture medium supplemented with 2.05 mM L-glutamine. GAS strains were grown overnight, and cultures were diluted into fresh THY and grown to mid-log phase (OD_{600} of 0.4). Bacteria were opsonized prior to neutrophil challenge by resuspension in donor plasma (PMN assays) or FBS (HL60 assays) for 30 min at 37°C. GAS then was added to seeded neutrophils to the desired multiplicity of infection (MOI of 0.1 unless otherwise indicated) in a final volume of 1 ml RPMI 1640 cell culture medium (HyClone) plus 2.05 mM L-glutamine, 20% plasma, or FBS. Neutrophil-challenged bacteria were incubated at 37°C in 5% CO_2 for 2 h. GAS also was incubated in RPMI 1640 plus 2.05 mM L-glutamine, 20% plasma, or FBS in the absence of PMNs, monocytes, or differentiated HL60 cells for the purpose of survival comparison.

Following incubation, surviving GAS was harvested by collecting supernatants and neutrophils. Neutrophils were immediately lysed by resuspension in sterile H_2O, and the intracellular contents were pelleted and recombined with corresponding well supernatants for plating on THY agar to obtain total viable bacterial counts after overnight incubation at 37°C and 5% CO_2. The resistance of GAS to opsonophagocytic killing following neutrophil challenge was assessed by comparing CFU obtained from the plating of viable bacteria isolated from killing assays to CFU obtained from GAS incubation in cell culture media in the absence of neutrophils (CFU obtained from PMNs divided by CFU obtained from medium times 100). All survival indices are normalized to the survival of wild-type (100%) under the conditions tested. Data presented are the results of at least 3 biological replicates, each performed in triplicate, with P values determined by unpaired t test.

RNA Analysis

Reverse transcription PCR (RT-PCR) to determine transcriptional architecture

Total RNA isolated from GAS strains grown to late-logarithmic phase using

TritonX-100 isolation as described previously (Sung *et al*., 2003). Isolated RNA was then treated with DNaseI, as per manufacturer's protocol. RT-PCR was performed on 500 ng of DNase-treated RNA with M-MuLV reverse transcriptase (NEB) using the manufacturer's protocol. 3' primers for each gene was used in the reaction for 1 hour at 42^{o}C, followed by enzyme inactivation at 90^{o}C for 10 minutes to generate cDNA. PCR was then performed using Taq polymerase and the relevant primer pairs. PCR was set-up as follow: 5 minutes at 95^{o}C (initial activation); 45 cycles of 30 seconds at 95^{o}C, 3 minutes at 55^{o}C (60^{o}C for full operon cDNA), 1.5 minutes at 72^{o}C (PCR) and 5 min at 72^{o}C (final extension).

Quantitative real-time PCR (qRT-PCR)

qRT-PCR experiments were carried out on RNA extracted from GAS strains grown in various media conditions (Sung *et al.*, 2003). Each strain was grown to late-logarithmic phase, and RNA was isolated similarly to RNA isolated for RT-PCR. Isolated RNA was treated with DNaseI. 25 ng of treated RNA was added to SYBR green master mix with 6.5 µl of each gene specific real-time primer from a 20 nM stock solution. The experiment was carried out using the one-step protocol on a Light Cycler 480 (Roche). Primers were designed using (Robinson *et al.*, 2011) Primer 3 (http://biotools. umassmed.edu/bioapps/primer3_www.cgi). Data shown is the average of at least 3 biological replicates. Significance was determined by two-fold change in expression.

RNAseq

The following protocol was previously described in (Valdes *et al.*, 2016). For RNA transcriptome sequencing (RNA-Seq), total RNA was extracted using a Direct-zol RNA miniprep kit (Zymo Research) with a modified procedure to improve GAS cell disruption. Cells from frozen pellets were resuspended in 700 µl of TRIzol supplemented with approximately 300 mg of acid-washed glass beads (Sigma Life Science) and disrupted by vortexing for 5 min. Beads were collected by brief centrifugation, and cell lysate was used for RNA purification as recommended by the manufacturer. RNA samples were treated with the Turbo DNase-free kit (Life Technologies) to avoid gDNA contamination. A total

of 5 g of DNase-treated RNA was treated for rRNA removal using the Ribo-Zero magnetic kit (Epicentre) for Gram-positive bacteria, and rRNA-depleted RNA then was purified with the RNAClean XP kit (Agencourt). Sample quality was assessed using a 2100 Bioanalyzer (Agilent), and sample quantity was determined using a NanoDrop 8000 spectrophotometer (Thermo Scientific).

RNA-Seq directional libraries were generated using the ScriptSeq v2 RNA-Seq library preparation kit (Illumina) according to the manufacturer's recommendations. Briefly, 45 ng rRNA-depleted RNA was fragmented and used for reverse transcription with random primers containing a 5'-tagging sequence. The 5'-tagged cDNA then was modified at its 3' end by a terminal-tagging reaction to generate di-tagged, single-stranded cDNA that then was purified using the AMPure system (Agencourt). The purified di-tagged cDNA was used as a template to generate second-strand cDNA containing Illumina adaptor sequences, to incorporate index barcodes, and to amplify the library by limited-cycle PCR. The resulting RNA-Seq libraries were purified using the AMPure system (Agencourt), and RNA-Seq library quality was verified as described above. A rapid-run 100-bp single-read DNA sequencing then was performed at the Institute for Bioscience and Biotechnology Research (IBBR) Sequencing Facility at the University of Maryland, College Park, using the Illumina HiSeq 1500 platform. Data were generated in the standard Sanger FastQ format, and raw reads were deposited with the Sequence Read Archive (SRA) at the National Center for Biotechnology Information (accession number PRJNA297518).

Read quality was measured using FastQC (http://www.bioinformatics.babraham.ac.uk /projects/fastqc/), filtered and trimmed using trimmomatic (Bolger *et al.*, 2014), and mapped against the MGAS5005 genome (accession number CP000017) using bowtie (Langmead, 2010), bowtie2 (Langmead & Salzberg, 2012, Trapnell *et al.*, 2012), and tophat (Trapnell *et al.*, 2012) with options to allow one mismatch and randomly map multihit reads. The resulting alignments were converted to sorted BAM alignments (Li *et al*., 2009) and counted (Anders *et al*., 2015) by coding and intergenic region. Initial visualizations

of the sequencing mapping were performed using the Integrative Genomics Viewer (IGV) (Robinson *et al.*, 2011). Differential expression analyses were performed following the size-factor and quantile normalization of read counts, and batch effect estimation was taken into account by including the date in the Limma (Ritchie *et al.*, 2015) statistical model. The resulting metrics of expression were visualized using circos (Krzywinski *et al.*, 2009) and tested for ontology enrichment using KEGG (Ogata *et al.*, 1999), goseq (Young *et al.,* 2010), clusterProfiler (Yu *et al.,* 2012), GOstats (Beissbarth & Speed, 2004), and topGO (Alexa *et al.*, 2006). Raw reads were deposited in the Sequence Read Archive (SRA) at the National Center for Biotechnology Information under accession number PRJNA297518.

5' RACE

The following protocol was previously described in Valdes *et. al,* 2016. Reverse transcriptase PCR (RT- PCR) was carried out on 500 ng of total RNA with Moloney murine leukemia virus reverse transcriptase (NEB) according to the manufacturer's protocol using primers FruA RevTrans R and FruB RevTrans R (Table 3.2). Reverse transcription was performed for 1 h at 42°C using 1 μl of cDNA as a template in the reaction mix, followed by enzyme inactivation at 90°C for 10 min. The subsequent PCR was done with the following parameters: 5 min at 95°C (initial activation); 30 cycles of 30 s at 95°C, 30 s at 55°C, and 1.5 min at 72°C (PCR); and a final extension step of 5 min at 72°C. The 5'/3' RACE kit (Roche) was used according to the supplier's instructions. A 500-ng aliquot of DNase-treated total RNA was used to obtain the cDNA by primer extension with primer FruR SP1. Following the 3' tailing reaction with dATPs, the cDNA was amplified by PCR using the reverse primer FruR SP2 and oligo(dT) anchor (**Table 3.2**); the forward primer was supplied with the kit. The 5' end of the transcript then was determined by sequencing the PCR product using the primer FruR SP3 (**Table 3.2**).

Chapter 4: Characterization of the Contribution of individual EIICs to PTS carbohydrate metabolism, regulation of SLS-mediated hemolysis, and GAS survival in whole human blood

Portions of this chapter were published with the following authors: Ganesh S. Sundar, Emrul Islam, Kanika Gera, Yoann Le Breton and Kevin S. McIver (© 2016 John Wiley & Sons Ltd. Molecular Microbiology. doi: 10.1111/mmi.13573.).

Author contributions: GSS, KG, and KSM designed the study, GSS, YLB, and EI acquired and analyzed the data, and GSS, YLB, and KSM wrote the manuscript.

Data contribution: all data presented in this chapter were obtained by GSS

Introduction

Our previous work showed that a PTS null mutant (Δ*ptsI*) in the M1T1 GAS strain MGAS5005 resulted in an increased size and severity of lesions at the site of infection in a murine soft tissue infection model due to the early onset of Streptolysin S (SLS) expression and activity during growth (Gera *et al*., 2014). We hypothesized that this was the result of the lack of access by GAS to a particular set of carbohydrates that served as the signal for SLS expression. Individual carbohydrates have been shown to be signals that contribute to the expression of virulence factors in other pathogens. For example, *Salmonella enterica* uses L-arabinose to modulate the expression of genes in the *Salmonella* pathogenicity island 1, encoding a Type 3 secretion system critical during systemic infection (López-Garrido *et al*., 2015). Many fungal pathogens rely on carbohydrate metabolic pathways (trehalose in particular) for survival in different hosts (Foster *et al*., 2003, Petzold *et al*., 2006, Lowe *et al.*, 2009, Ngamskulrungroj *et al.*, 2009, Tournu *et al*., 2013) Therefore, this could be the case for GAS as well.

Enzyme II (EII) components provide the PTS with carbon specificity. Generally speaking, each EII transports and phosphorylates a small number of carbohydrates, except for the mannose-family EIIs which are known to have fairly broad substrates. However,

the sugar-specificity of each EII is typically assigned by sequence homology. In fact, the annotation of sugar-specific EII complexes in sequenced GAS genomes have seldom been experimentally verified. EII genes are often genes incorrectly annotated based on homology alone, exemplified by the initially annotated glucose-specific *malT* locus in M1 GAS that was shown experimentally to transport maltose (Shelburne *et al*., 2008b). In this study, we insertionally inactivated each predicted EIIC transporter gene present in the M1T1 MGAS5005 genome in order to characterize their metabolic profile and determined the EII complexes that contribute to the early expression of SLS observed in the Δ*ptsI* mutant.

The creation of an annotated PTS EII mutant library provides the ability to determine which sugars play an important role in different infection environments by uncovering any EIIs that are important for GAS survival in the host niches tested. To test this idea, we also screened the EIIC mutant library in whole human blood to uncover those EIICs that may play a role in survival in this important host environment. Identifying genes important for GAS survival in human blood is imperative, as iGAS travels from the local site of infection to other parts of the body through the bloodstream. Also, blood is a nutrient rich environment, so it is likely that EIIs may play a role in GAS survival. Several EIIs have already been shown to be upregulated in the presence of blood components (Sachla *et al.*, 2014), or whole human blood (Graham *et al*., 2005), making this increasingly likely. Additionally, several metabolic genes, including 3 EII subunits (Cellobiose EIIC, Fructose EIIABC, Mannose EIID), were essential for M1T1 GAS 5448 survival in whole human blood in a transposon mutagenesis screen (Le Breton *et al*., 2013). No such screen has ever been carried out with MGAS5005.

Results

Generation of an annotated EIIC mutant library in MGAS5005

We generated an annotated EIIC mutant library in the M1T1 MGAS5005 in order

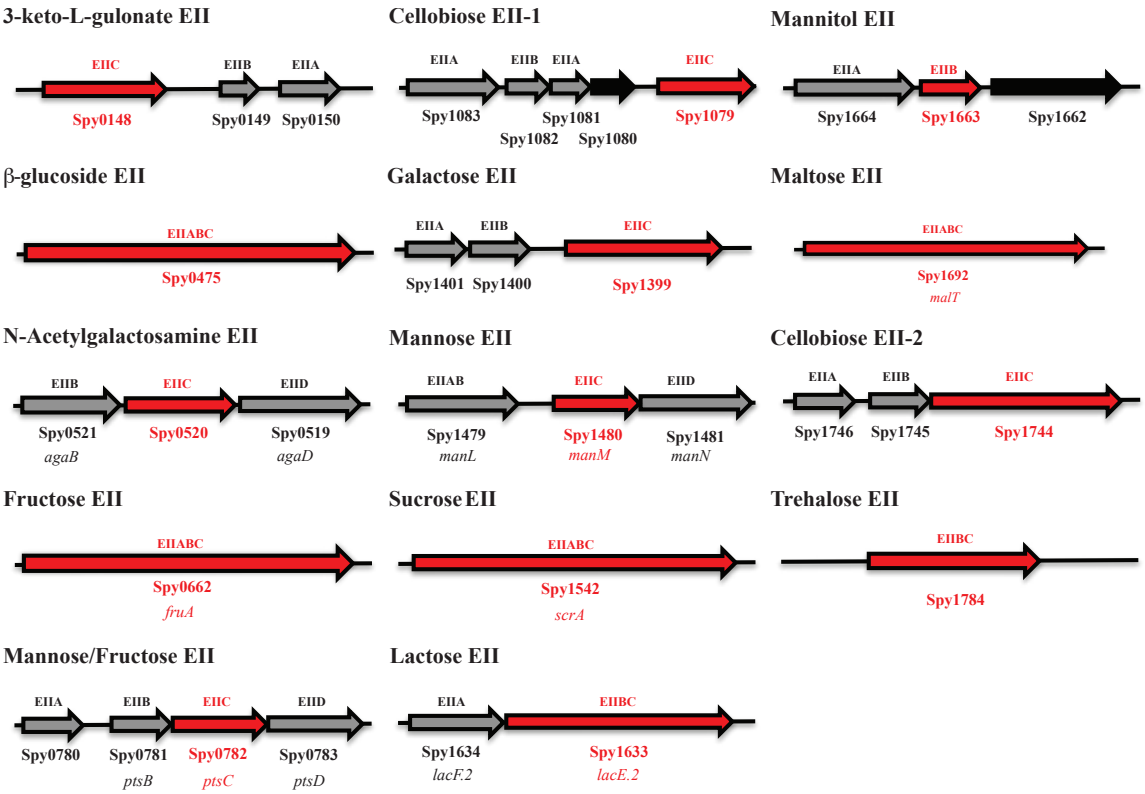

Figure 4.1 PTS EII present in the GAS M1T1 MGAS5005 annotated genome shown in predicted loci. Genes encompassing the sugar-specific EIIs are indicated in grey, and hypothetical genes are indicated in black. Sugar-specificities are based on annotation. EIICs are highlighted in red to represent those that were targeted for mutagenesis. Gene names are listed below the Spy numbers for those that are known. Since there are two predicted cellobiose EII loci, they are numbered 1 and 2 based on their order in the genome.

to experimentally verify the sugar specificities of each EII. We insertionally inactivated the gene encoding the EIIC transporter within all 14 annotated EII loci (**Fig 4.1**). The mutations were made with pCRS as indicated in chapter 3, so each mutation is polar, thereby potentially affecting the expression of downstream genes. The EIIB gene was mutagenized for the annotated mannitol-specific EII (Spy_1664/Spy_1663) since there is currently no annotated EIIC for this particular EII (**Fig 4.1**). Confirmed mutants were then used to create rescue strains as a control (see chapter 3).

EIIC library reveals inherent redundancy among PTS transporters for growth on PTS carbohydrates

To confirm the PTS carbohydrates utilized by wild type (WT) MGAS5005, it

was grown in chemically defined medium (CDM) with a given PTS carbohydrate as the sole carbon source (see chapter 3). MGAS5005 only grew on 8 of the 11 established PTS carbohydrates (Gera *et al*., 2014)(**Fig 4.2 A and B**); therefore, the 3 sugars not supporting growth of the wild type MGAS5005 (e.g., cellobiose, galactose and mannitol) were eliminated from further analysis (**Fig 4.2 A and B**). Although ascorbic acid was not known to be a PTS carbohydrate for GAS, a recent study found that the 3-keto- L-gulonate-specific EIIC (**Fig. 4.1**; Spy_0148) might actually transport ascorbic acid (Afzal *et al.*, 2015). In support of this, the MGAS5005.Δ*ptsI* mutant exhibited impaired growth compared with WT MGAS5005 in CDM + 1% ascorbic acid, indicating it is indeed a PTS-dependent carbohydrate for GAS (**Fig. 4.2 C**).

The MGAS5005 EIIC mutant library was then compared with WT MGAS5005 grown in CDM with each of the 9 PTS carbohydrates determined above. Growth data are shown in **Fig. 4.3 A–N and Fig. 4.4**, and summary of the data is shown in **Fig. 4.5**. Six of the EIIC mutants (**Fig. 4.1**; Δ3-keto-L-gulonate, ΔCellobiose(1), ΔGalactose, ΔLactose, ΔMannitol, ΔTrehalose) grew comparable to MGAS5005 in all PTS carbohydrates tested (**Fig. 4.5A**, all clear boxes). Four EIIC mutants (**Fig. 4.1**; Δβ-glucoside, ΔN-acetylgalactosamine, ΔFructose, ΔMaltose) grew better than MGAS5005 in at least one PTS carbohydrate (**Fig. 4.5A**, green boxes). In addition, four EIIC mutants (**Fig. 4.1**; Δβ-glucoside, ΔFructose, ΔMannose/Fructose, ΔMannose) exhibited altered growth compared with MGAS5005 in more than one carbohydrate (**Fig. 4.5A**, yellow/red/green boxes). Only the ΔSucrose EIIC mutant showed altered growth in the carbohydrate for which it was annotated to transport, strongly indicating redundancy for transport of any given sugar (**Fig. 4.5A**). In fact, salicin, maltose, and ascorbic acid, were the only PTS carbohydrates tested that did not show a significant defect in more than one EII mutant (**Fig. 4.5A**). Surprisingly, 2 EIIC mutants (ΔN-acetylgalactosamine, ΔFructose) showed increased growth profiles in glucose as compared with MGAS5005, which was unexpected

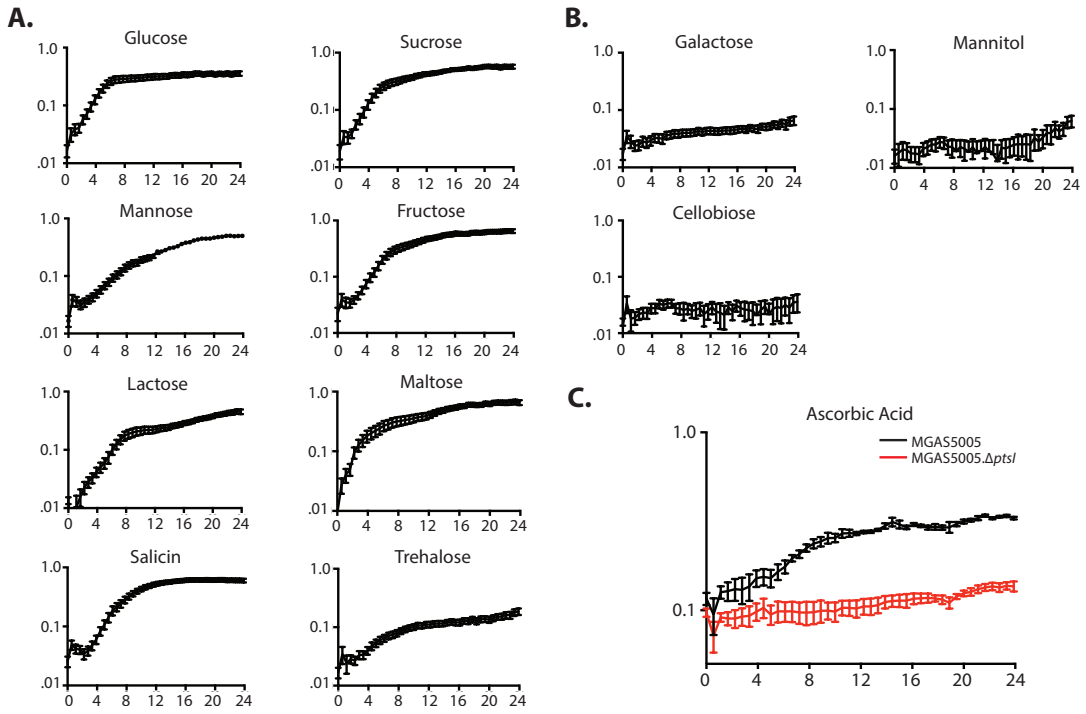

Figure 4.2. Growth profile of MGAS5005 in PTS carbohydrates. A) PTS carbohydrates that facilitate growth of MGAS5005 and used for the characterization of the EIIC mutant library. Growth was assayed a described in chapter 3. **B)** Three PTS carbohydrates unable to facilitate reasonable growth of MGAS5005 and were eliminated from further analysis. **C)** Growth of MGAS5005 and MGAS5005.Δ*ptsI* in CDM + 1% ascorbic acid.

given that the MGAS5005.Δ*ptsI* mutant lacking PTS signaling grows comparable to WT in glucose (**Fig. 4.5A**). Total yield (ΔOD_{600}) after 24h of growth was used as another indicator of the impact of each EIIC on growth in PTS carbohydrates (**Fig. 4.4** and **Fig. 4.5B**). Only two EIIC mutants (ΔGalactose, ΔCellobiose(2)) exhibited the same total yield as WT MGAS5005 in every PTS carbohydrate tested. Overall, most of the EIIC mutants grew to a different yield than MGAS5005 in multiple PTS carbohydrates, again suggesting that there is an inherent redundancy among the EIIs for carbohydrate transport. This is further supported by the fact that reductions in total yield of many EIIC mutants showed intermediate phenotypes, instead of a total loss of growth, which is not indicative of a system where a given transporter was responsible for a single carbohydrate transport (**Fig. 4.5B**).

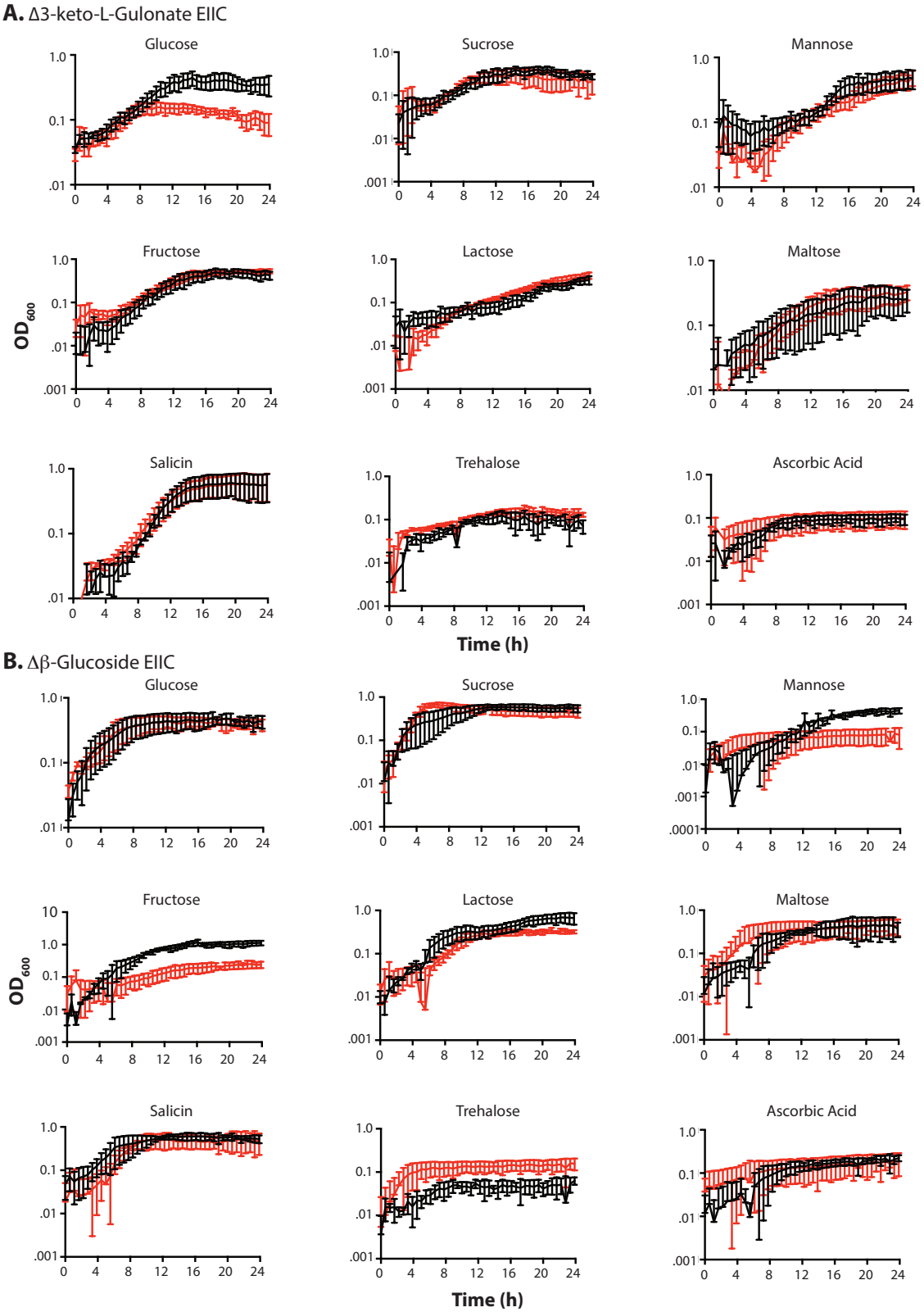
A. Δ3-keto-L-Gulonate EIIC
Glucose
Sucrose
Mannose
Fructose
Lactose
Maltose
Salicin
Trehalose
Ascorbic Acid
OD600
Time (h)
B. Δβ-Glucoside EIIC
Glucose
Sucrose
Mannose
Fructose
Lactose
Maltose
Salicin
Trehalose
Ascorbic Acid
OD600
Time (h)

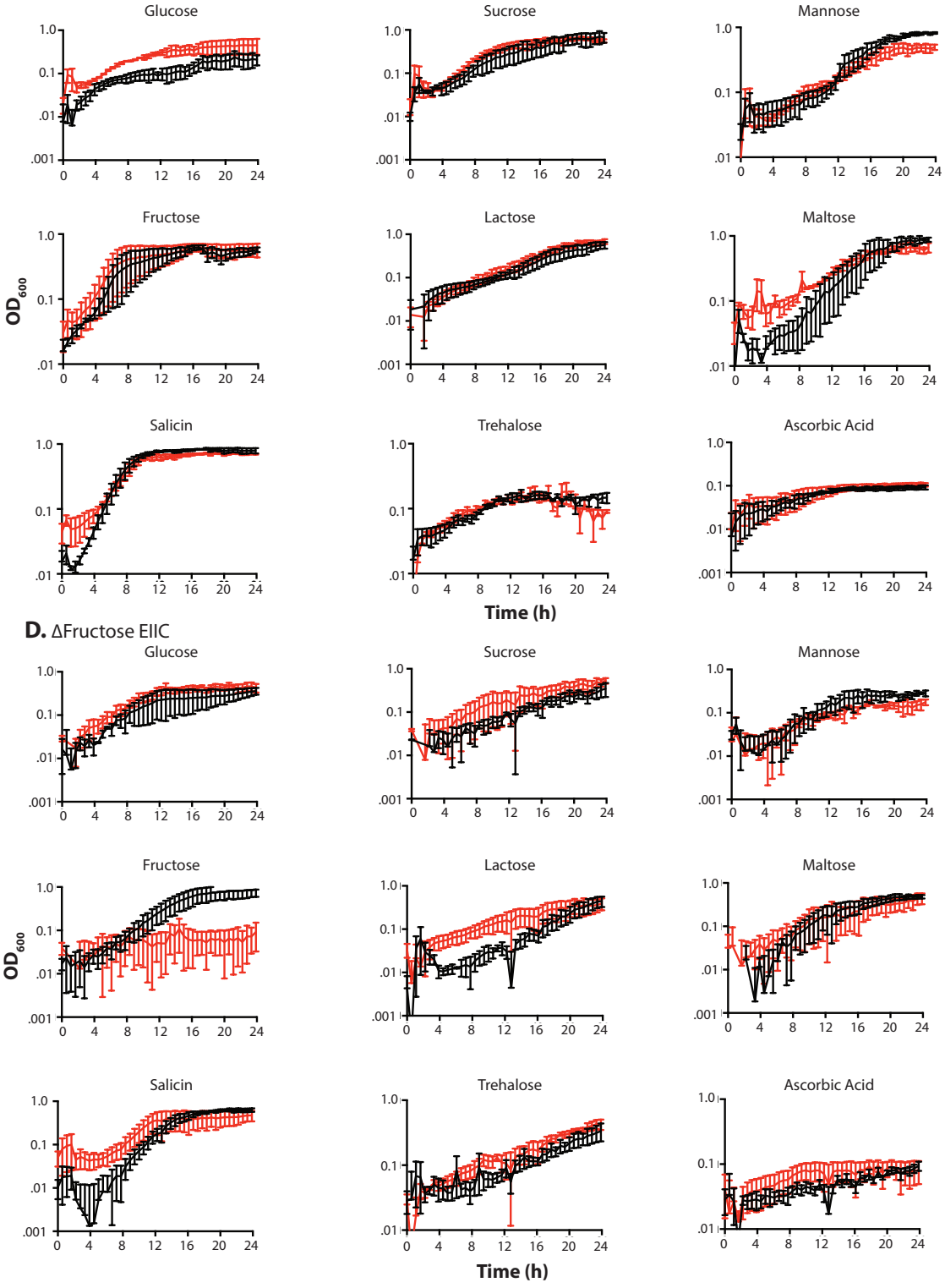
C. ΔN-Acetylgalactosamine EIIC
Glucose
Sucrose
Mannose
Fructose
Lactose
Maltose
Salicin
Trehalose
Ascorbic Acid
OD600
Time (h)
D. ΔFructose EIIC
Glucose
Sucrose
Mannose
Fructose
Lactose
Maltose
Salicin
Trehalose
Ascorbic Acid
OD600
Time (h)

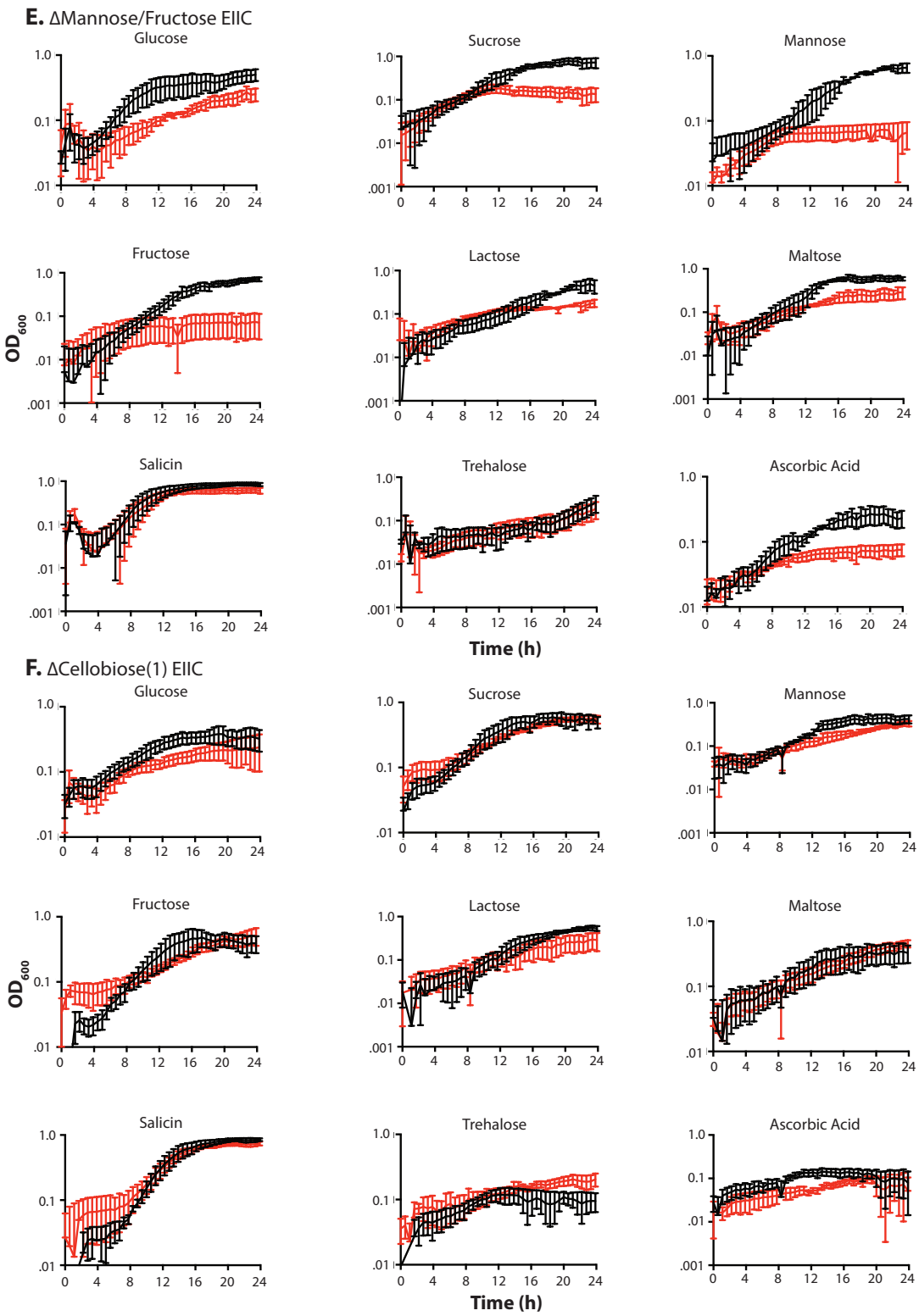
E. ΔMannose/Fructose EIIC
Glucose
Sucrose
Mannose
Fructose
Lactose
Maltose
Salicin
Trehalose
Ascorbic Acid
OD600
Time (h)
F. ΔCellobiose(1) EIIC
Glucose
Sucrose
Mannose
Fructose
Lactose
Maltose
Salicin
Trehalose
Ascorbic Acid
OD600
Time (h)

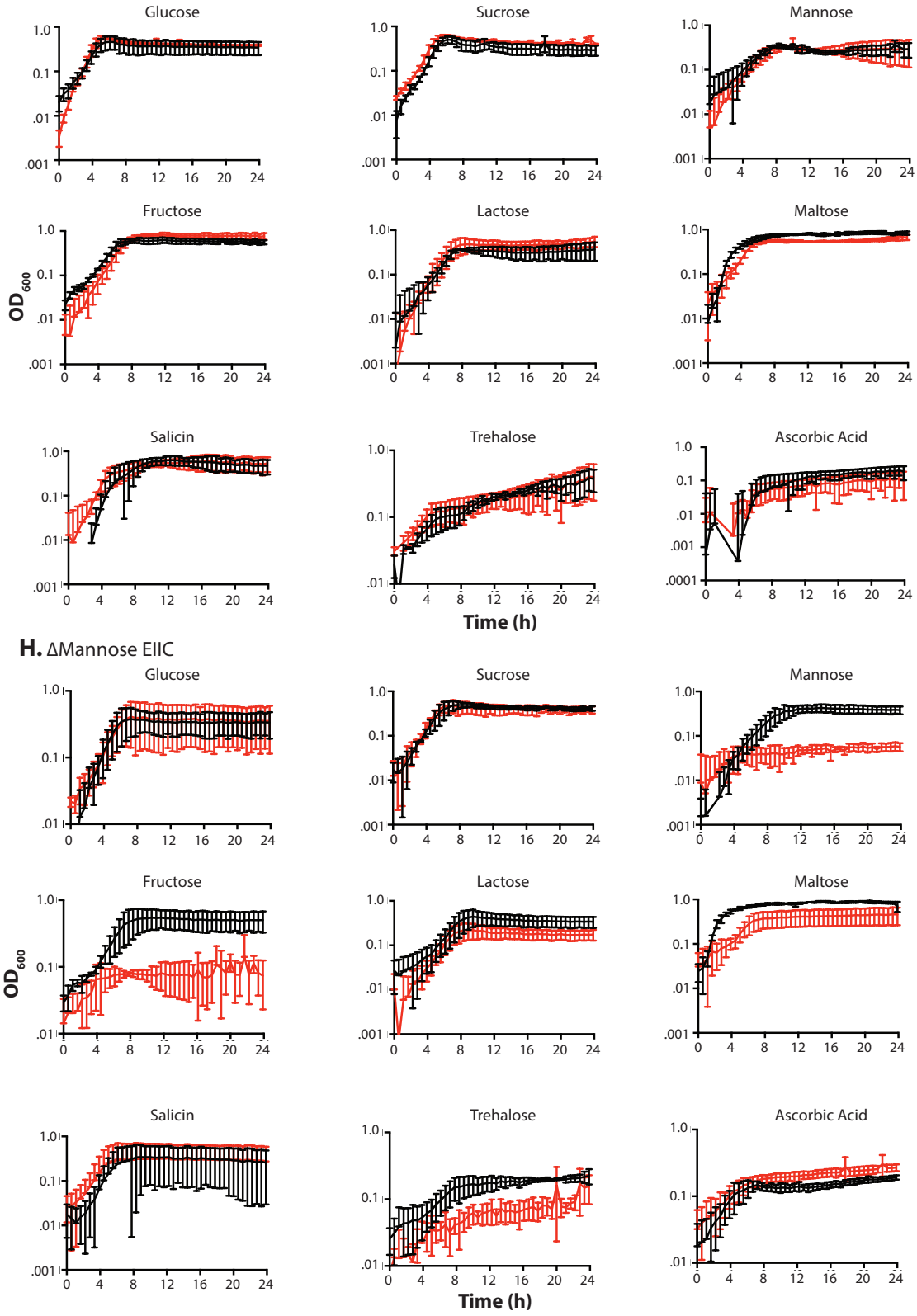
G. ΔGalactose EIIC
Glucose
Sucrose
Mannose
Fructose
Lactose
Maltose
Salicin
Trehalose
Ascorbic Acid
OD600
Time (h)
H. ΔMannose EIIC
Glucose
Sucrose
Mannose
Fructose
Lactose
Maltose
Salicin
Trehalose
Ascorbic Acid
OD600
Time (h)

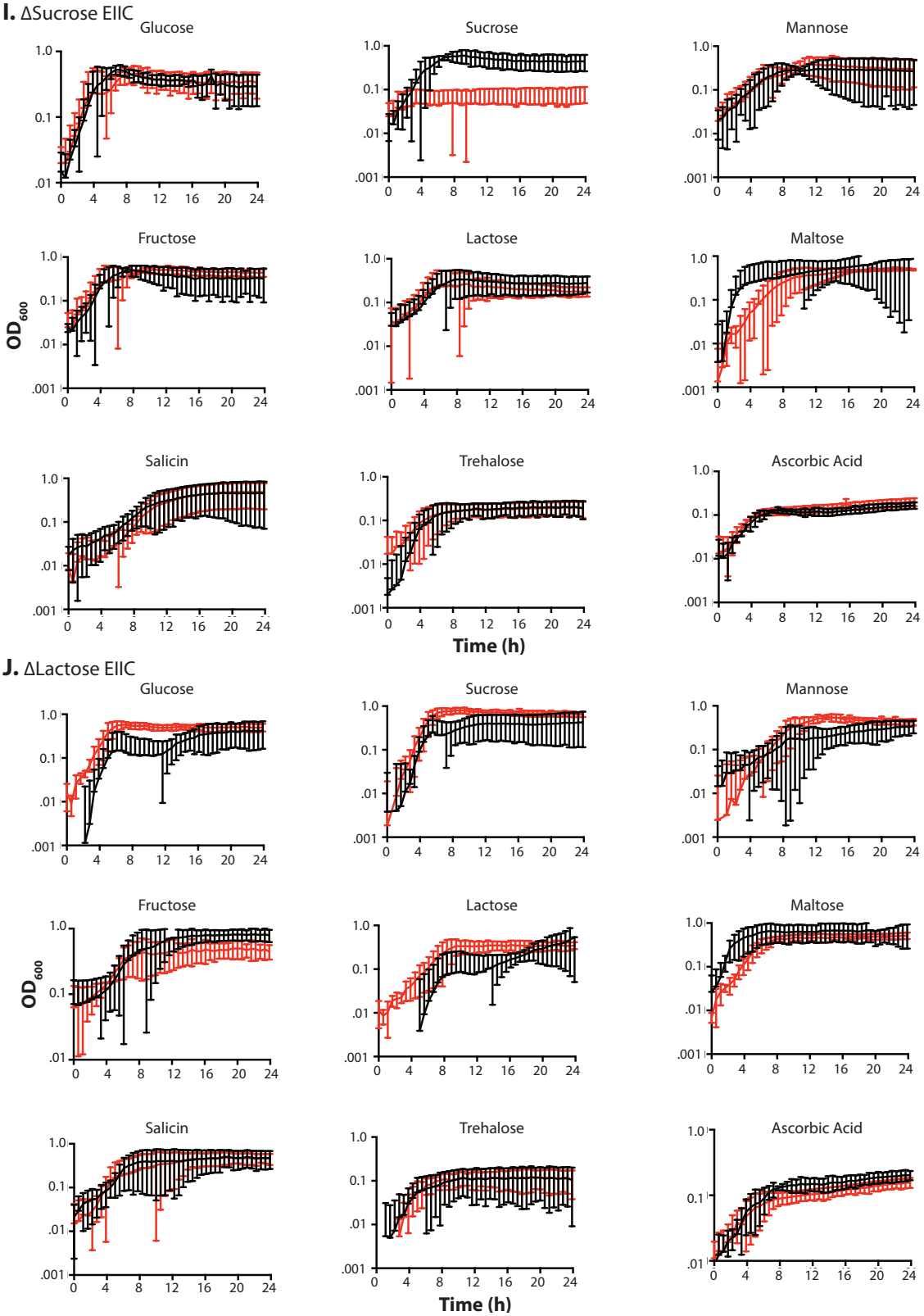
I. ΔSucrose EIIC
Glucose
Sucrose
Mannose
Fructose
Lactose
Maltose
Salicin
Trehalose
Ascorbic Acid
OD600
Time (h)
J. ΔLactose EIIC
Glucose
Sucrose
Mannose
Fructose
Lactose
Maltose
Salicin
Trehalose
Ascorbic Acid
OD600
Time (h)

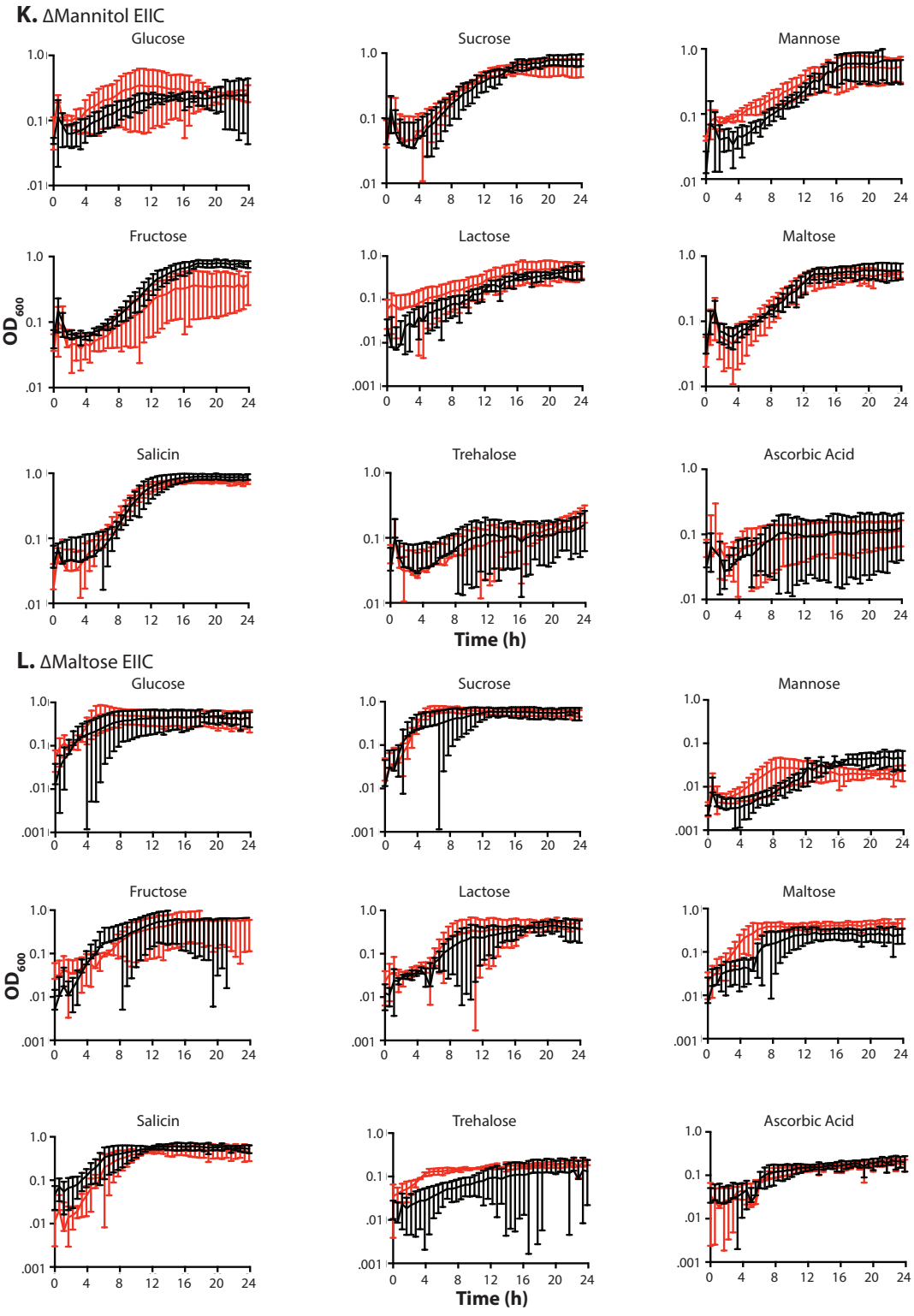
K. ΔMannitol EIIC
Glucose
Sucrose
Mannose
Fructose
Lactose
Maltose
Salicin
Trehalose
Ascorbic Acid
OD600
Time (h)
L. ΔMaltose EIIC
Glucose
Sucrose
Mannose
Fructose
Lactose
Maltose
Salicin
Trehalose
Ascorbic Acid
OD600
Time (h)

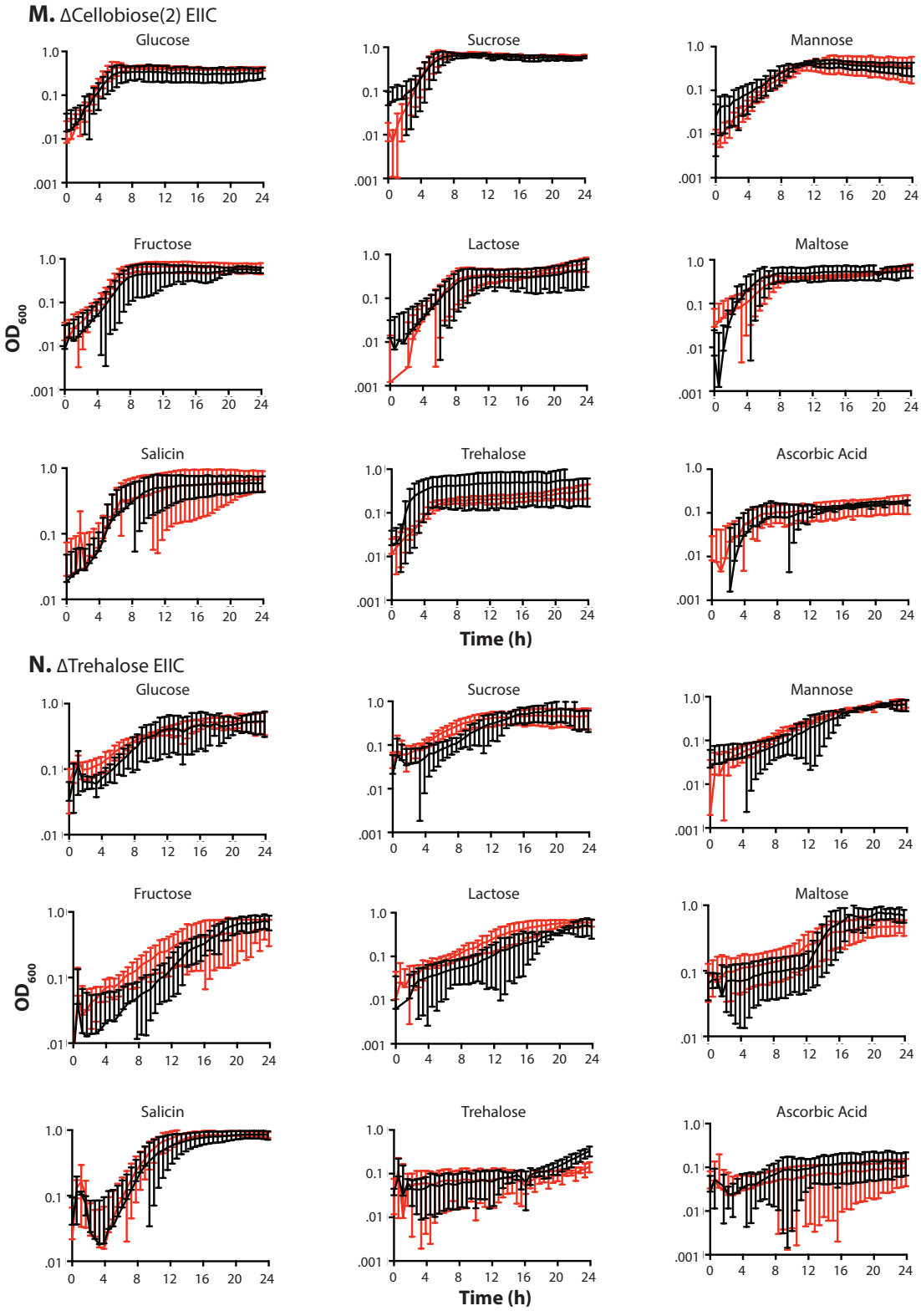
M. ΔCellobiose(2) EIIC
Glucose
Sucrose
Mannose
Fructose
Lactose
Maltose
Salicin
Trehalose
Ascorbic Acid
OD600
Time (h)
N. ΔTrehalose EIIC
Glucose
Sucrose
Mannose
Fructose
Lactose
Maltose
Salicin
Trehalose
Ascorbic Acid
OD600
Time (h)

O.

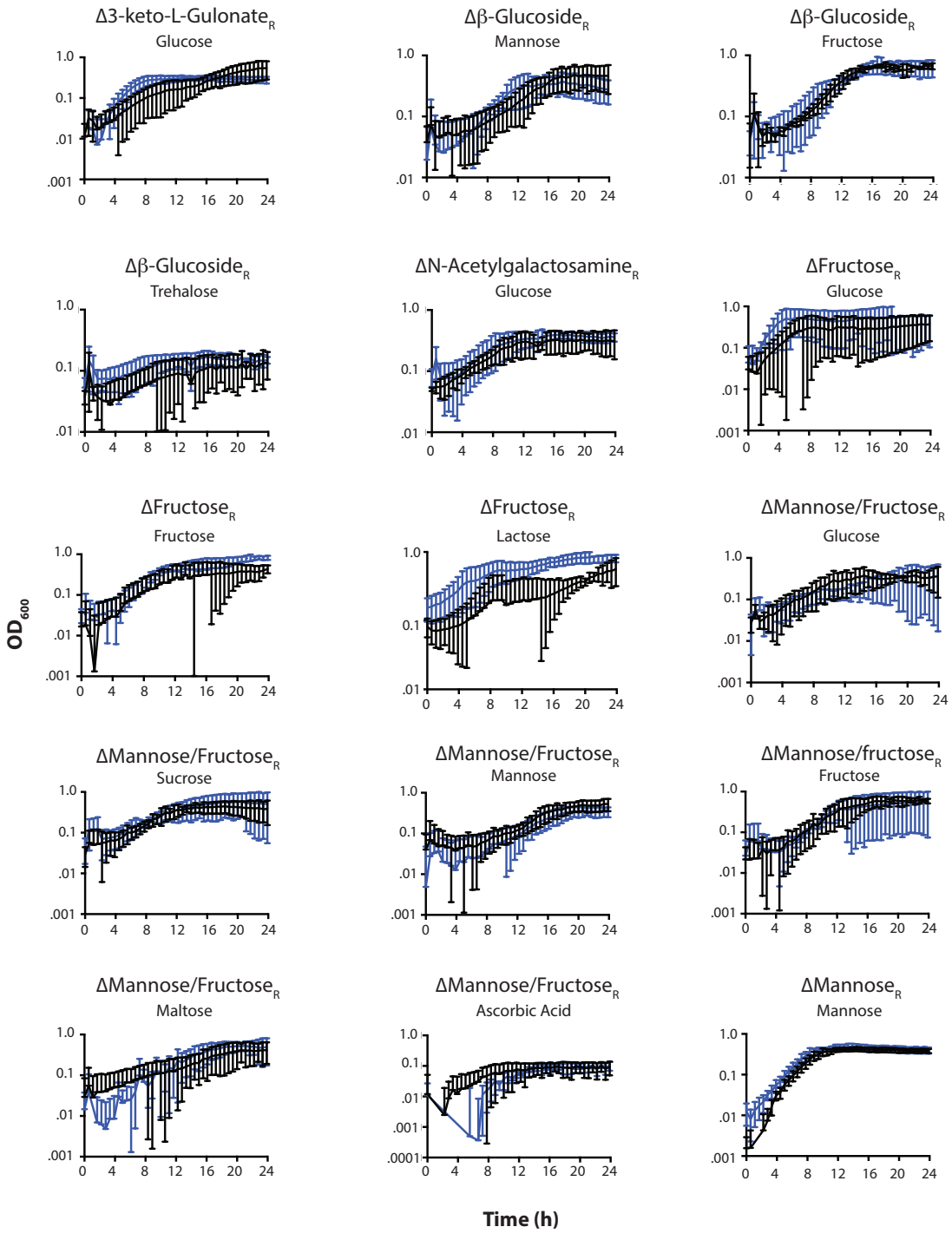
Δ3-keto-L-Gulonate$_R$
Glucose
Δβ-Glucoside$_R$
Mannose
Δβ-Glucoside$_R$
Fructose
Δβ-Glucoside$_R$
Trehalose
ΔN-Acetylgalactosamine$_R$
Glucose
ΔFructose$_R$
Glucose
ΔFructose$_R$
Fructose
ΔFructose$_R$
Lactose
ΔMannose/Fructose$_R$
Glucose
ΔMannose/Fructose$_R$
Sucrose
ΔMannose/Fructose$_R$
Mannose
ΔMannose/fructose$_R$
Fructose
ΔMannose/Fructose$_R$
Maltose
ΔMannose/Fructose$_R$
Ascorbic Acid
ΔMannose$_R$
Mannose
OD$_{600}$
Time (h)

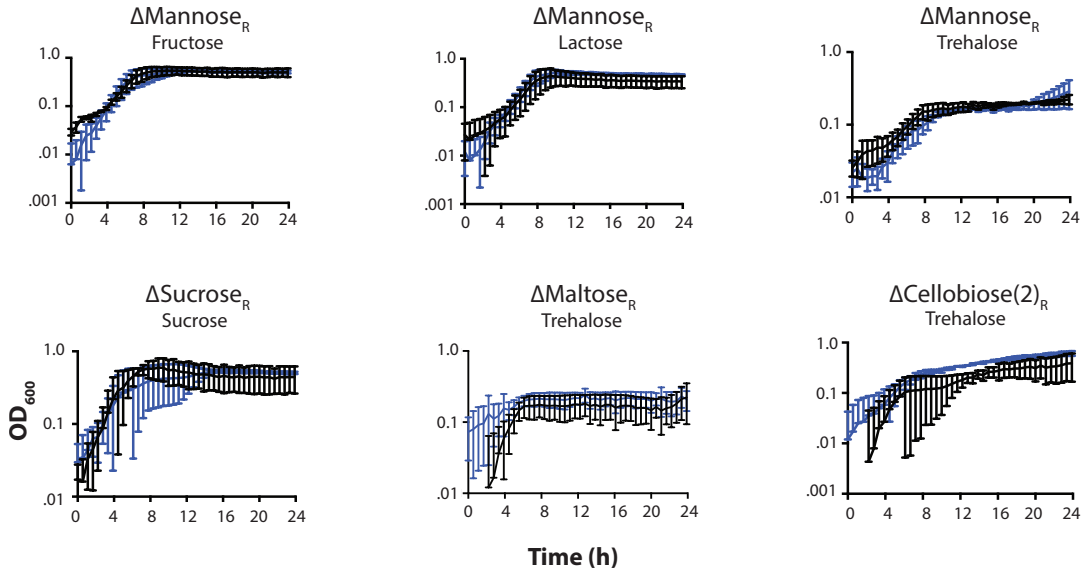

Figure 4.3. Growth of the MGAS5005 EIIC mutant library in 9 PTS carbohydrates. Each growth curve panel represents the average of at least 3 independent biological replicates. **(A-N)** EIIC mutants were grown in CDM + 1% PTS carbohydrate (0.5% for glucose) as indicated in chapter 3. Black lines represent WT MGAS5005 growth, whereas red lines represent growth of the EIIC mutant. **O)** Rescue strains ($EIIC_R$) for each mutant were grown only in carbohydrates for which a significant growth phenotype was observed **(A-N)**. Black lines indicate growth of WT MGAS5005 and blue lines depict growth of each $EIIC_R$ rescue strain. Statistical analyses were carried out as indicated in chapter 3.

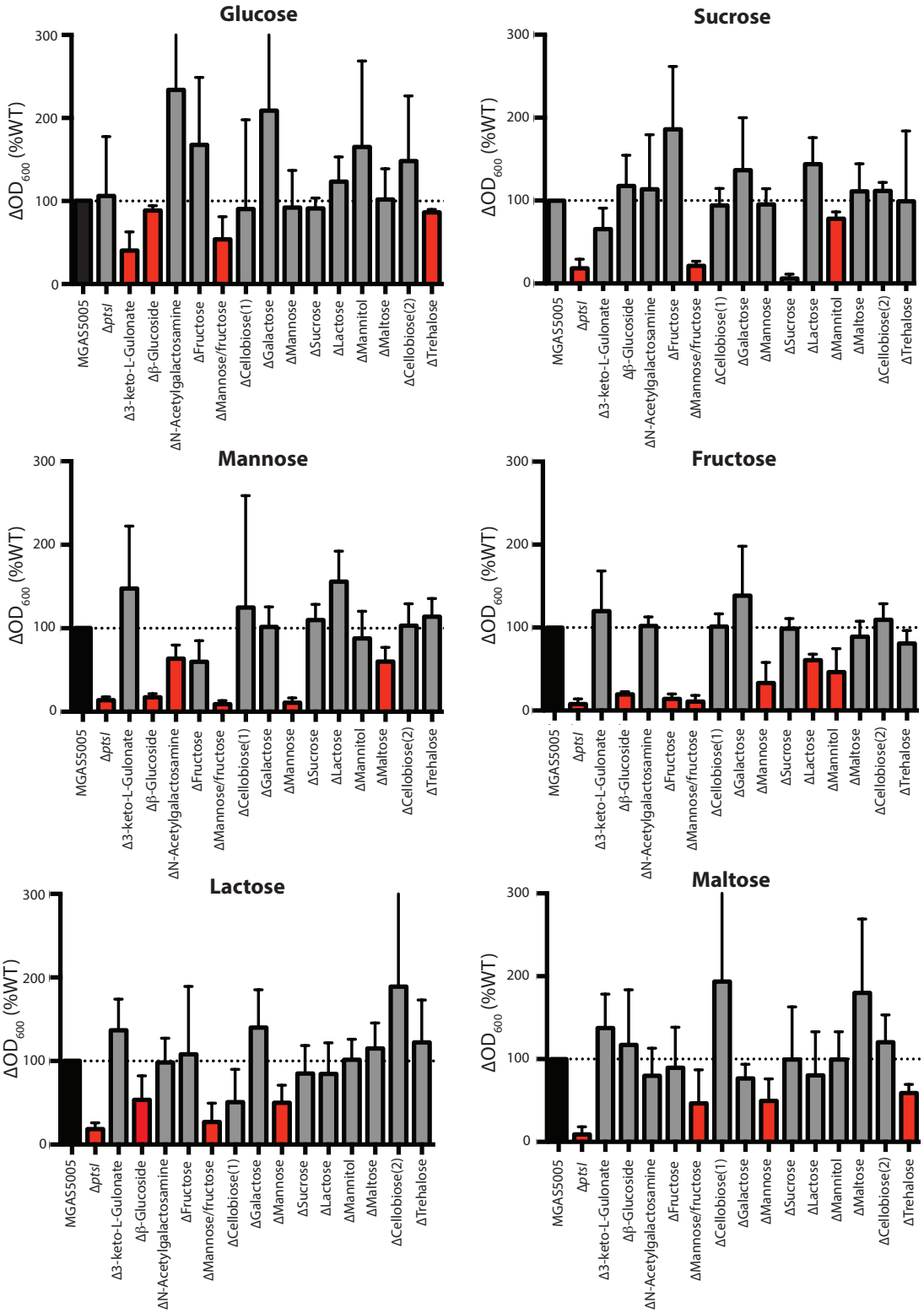
Glucose
Sucrose
Mannose
Fructose
Lactose
Maltose
ΔOD600 (%WT)
0
100
200
300
MGAS5005
Δpts/
Δ3-keto-L-Gulonate
Δβ-Glucoside
ΔN-Acetylgalactosamine
ΔFructose
ΔMannose/fructose
ΔCellobiose(1)
ΔGalactose
ΔMannose
ΔSucrose
ΔLactose
ΔMannitol
ΔMaltose
ΔCellobiose(2)
ΔTrehalose

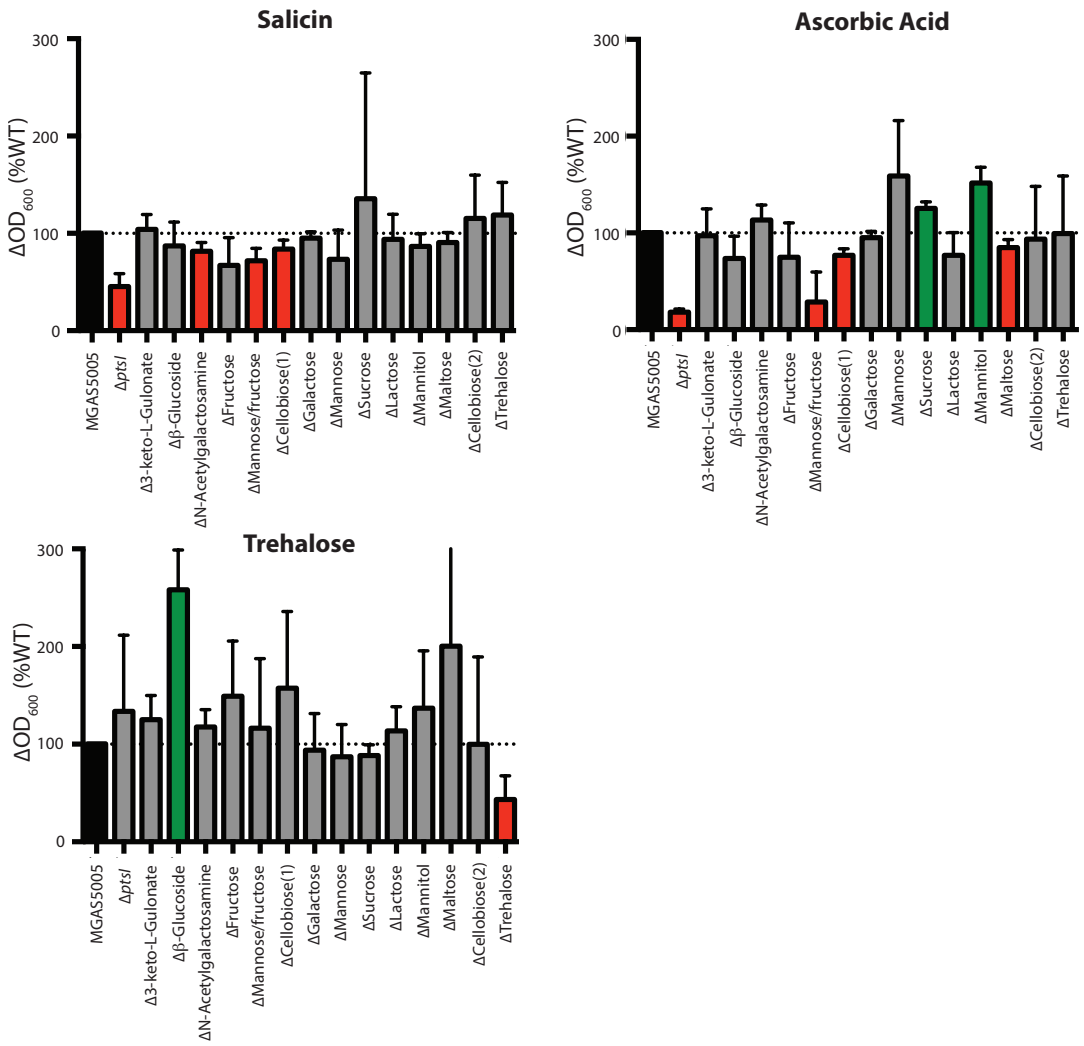

Figure 4.4. ΔOD of the MGAS5005 EIIC mutant library grown in 9 PTS carbohydrates. Each graph represents the average of at least 3 independent biological replicates. Data is normalized to MGAS5005 as indicated in chapter 3. **(A-N)** EIIC mutants were grown in CDM + 1% PTS carbohydrate (0.5% for glucose) as indicated in chapter 3. Black bars represent WT ΔOD, whereas red bars represent ΔOD of the EII mutant that is significantly lower than WT. Green bars represent ΔOD of the EII mutant that is significantly higher than WT. Grey bars depict ΔOD of the EII mutant that is similar to WT.

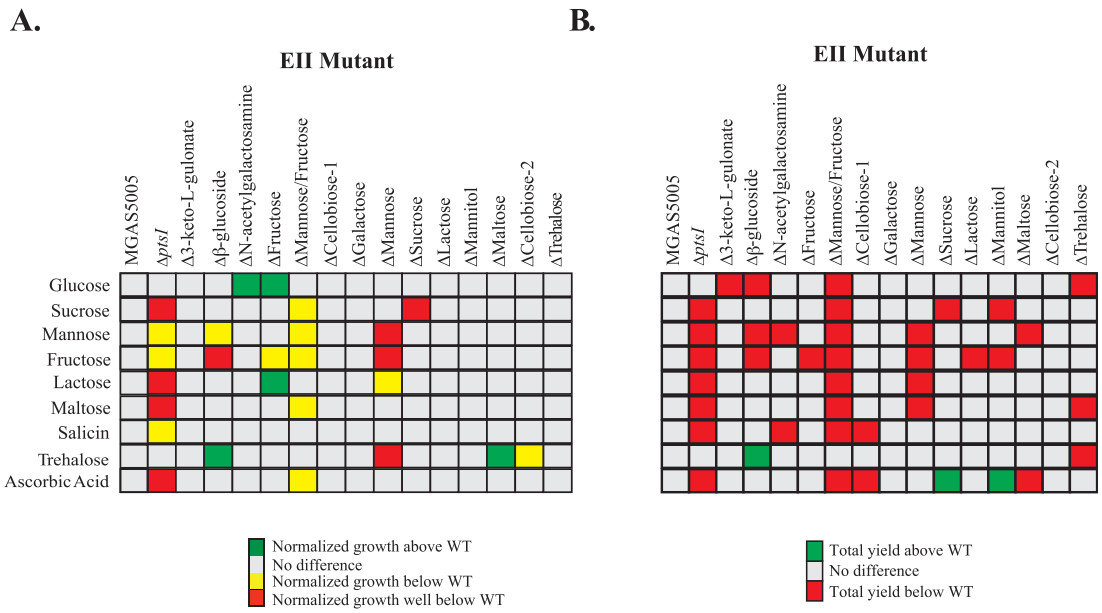

Figure 4.5. PTS EII mutant library growth profiles. (A) As described in chapter 3, growth of each EII mutant was normalized to WT MGAS5005. Growth of the mutant in a PTS sugar above WT (two-fold, green), below WT (two-fold, yellow), well below WT (>two-fold, red) are indicated. **(B)** Total yield (ΔOD) was calculated as described (See Chapter 3). ΔOD in mutants above WT (green) or below WT (red) are indicated (p-value <0.05). All results represent at least three independent biological replicates, and only sugars that facilitate growth of MGAS5005 are shown.

Carbohydrate Utilization profiles of the EIIC mutant library also supports redundancy

To ascertain if the growth phenotypes seen with the EIIC mutants were the result of altered uptake and metabolism of specific carbohydrates, the library was assayed for utilization of 49 different carbon sources using a BioMérieux API®50 CH panel. This system detects changes in pH in the presence of each given carbon source as a sensitive readout for metabolic utilization, but does not require growth (see Chapter 3). As expected, MGAS5005.Δ*ptsI* was unable to utilize most (81%) of the carbon sources metabolized by MGAS5005 (**Fig. 4.6**). Although overall growth in mannose, fructose and trehalose were altered in several EIIC mutants (**Fig. 4.5A and B**), utilization of these carbohydrates was largely unaffected (**Fig. 4.6**). As with the growth assays, overlap was evident among the EIIC loci for their ability to transport and utilize multiple PTS carbohydrates. Moreover, there appears to be significant interplay between different carbohydrate utilization

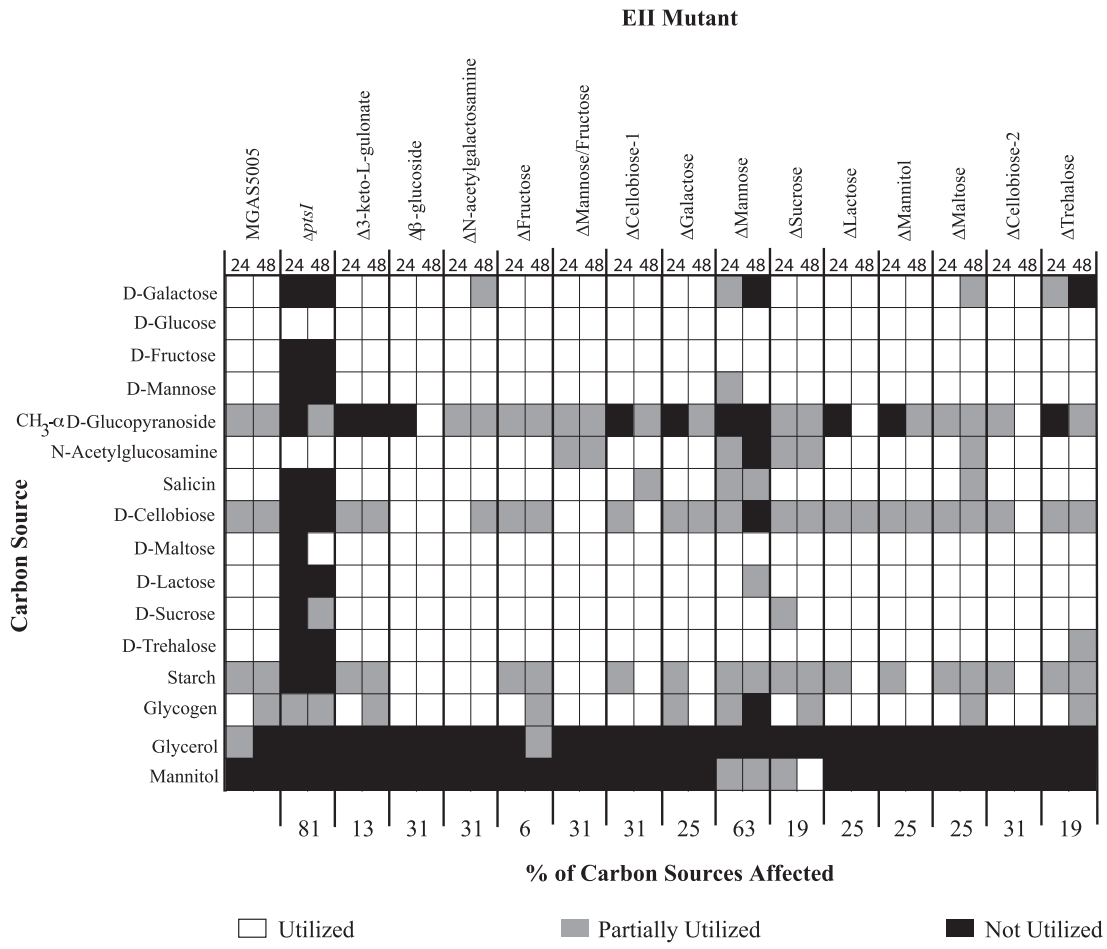

Figure 4.6. Carbohydrate utilization profile of the PTS EIIC mutant library in MGAS5005 . The API®50CH system was used to determine the utilization of select carbon sources as described in chapter 3. Only carbon sources that are utilized by at least one strain tested are displayed. White boxes indicate utilization (+), grey boxes indicate partial utilization (+/-), and black boxes indicate no utilization (-). Readings for each strain presented with the 24h reading on the left box, and the 48h reading on the right box.

pathways, as 10/14 of the EIIC mutants alter utilization of at least 25% of the carbohydrates tested (**Fig. 4.6**). Although neither of the 2 Cellobiose EIIC mutants (**Fig. 4.1**) had an extensive effect on the growth of GAS on PTS carbohydrates, these EIIC mutants showed the second largest effect on carbon utilization (31%), along with ΔMannose/Fructose and Δβ-Glucoside (**Fig. 4.6**). Finally, the mannose-specific EII mutant mutant had the largest effect on carbon utilization (**Fig. 4.6**).

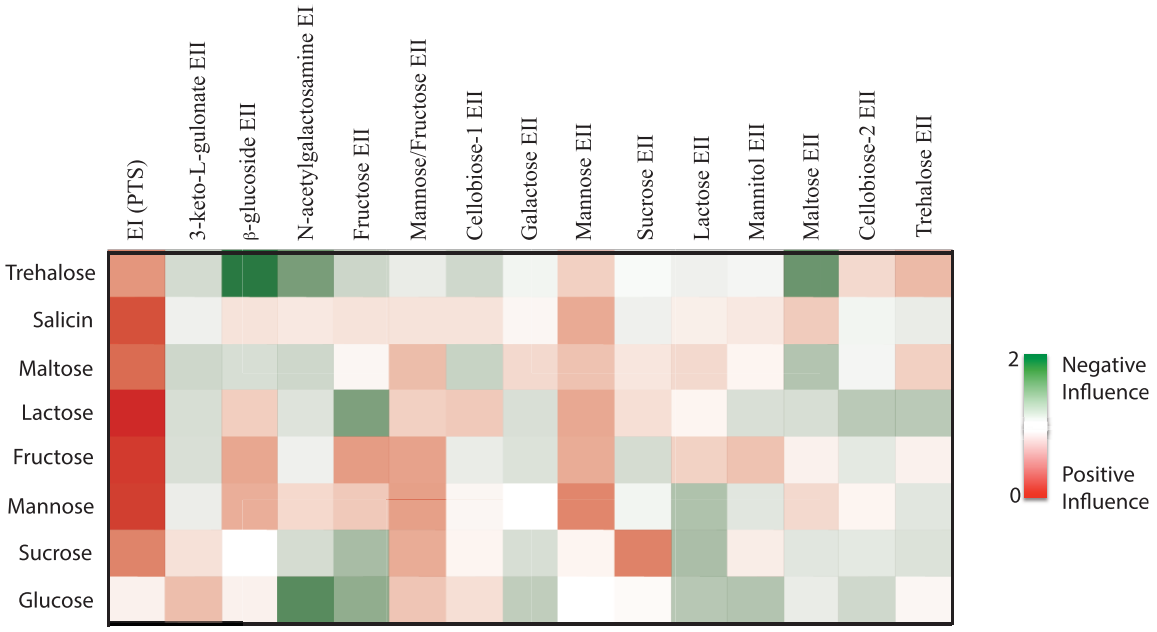

Figure 4.7. Influence of each EII on the metabolism of each PTS sugar. Influence scores for each EII in a particular PTS carbohydrate is represented as a heat map. Green indicates a negative influence of an EII for the metabolism of a PTS sugar, red indicates a positive influence of an EII for the metabolism of a PTS sugar, and white indicates no influence. Intensity of color represents relative influence of an EII.

Influence scores reveal the extensive overlap among PTS proteins on carbohydrate metabolic pathways

To represent the overall effect of an EIIC on the metabolism of PTS carbohydrates by GAS, we developed an Influence Score (**Fig. 4.7**), an arbitrary measure that combines both the growth and utilization data for each EIIC mutant to provide a visual representation of the overall impact of an EIIC protein on the metabolism of a PTS carbohydrate. An EIIC would show a positive influence (red) if its mutation resulted in a growth defect and/or inefficient utilization of a PTS carbohydrate compared with WT MGAS5005. In contrast, an EIIC would have a negative influence (green) if its mutation resulted in a growth/utilization profile above that of WT. Only PTS carbohydrates found in both the growth and utilization assays (**Figs. 4.3-4.6**) were used in determining the Influence Score and intensity of color reflects the relative impact. As expected, the complete PTS strongly influences the metabolism of all the PTS carbohydrates except for glucose (**Fig. 4.7**).

Although there are certain instances where an EII has a strong influence on the metabolism of a given carbohydrate (i.e., Sucrose EII on sucrose), most of the EII complexes have an intermediate to minor influence on the metabolism of several carbohydrates; supporting redundancy among the EIIC systems in MGAS5005 for the transport and utilization of PTS carbohydrates (**Fig. 4.7**).

Multiple EIICs contribute to the early onset of SLS-mediated hemolysis observed in Δ*ptsI*

In previous work, it was shown that Δ*ptsI* exhibited earlier growth phase expression of *sagA* as compared to the WT MGAS5005, which in turn lead to the early onset of SLS-mediated hemolysis (Gera *et al*., 2014). This lead to an increase in lesion size and severity when GAS was injected subcutaneously in CD-1 female mice (a GAS soft tissue infection model) (Gera *et al*., 2014). Although the PTS does participate in signal transduction, it is first and foremost a carbohydrate transport system. Therefore, we hypothesized that one or several specific EIIC mutants potentially contribute to the early onset of hemolysis observed in MGAS5005.Δ*ptsI* as a result of the lack of the metabolism of particular carbohydrates. In an effort to address this question, we compared the onset of hemolysis for the EIIC mutant library to MGAS5005 and MGAS5005.Δ*ptsI*, as described in chapter 3. All EIIC mutants grew similarly to the WT (**Fig 4.8**). As expected, MGAS5005.Δ*ptsI* exhibited high levels of SLS-mediated hemolysis in exponential phase and throughout growth, whereas MGAS5005 only exhibited activity in the transition to stationary phase (**Fig. 4.9**), as previously shown (Gera *et al*., 2014). Although there was not an individual EII that fully recapitulated the hemolytic profile of the PTS mutant, seven EIIC mutants exhibited at least one early hemolytic time point (Δ3-keto-L-Gulonate, Δβ-Glucoside, ΔN-Acetylgalactosamine, ΔMannose/Fructose, ΔCellobiose(1), ΔGalactose, ΔMannose) (**Fig 4.8**). This suggests that multiple EIIs contribute to PTS-regulation of SLS-mediated hemolysis, possibly indicating the incorporation of multiple environmental signals. Of note, two EIIC mutants (ΔTrehalose, ΔCellobiose) produced significantly lower hemolysis

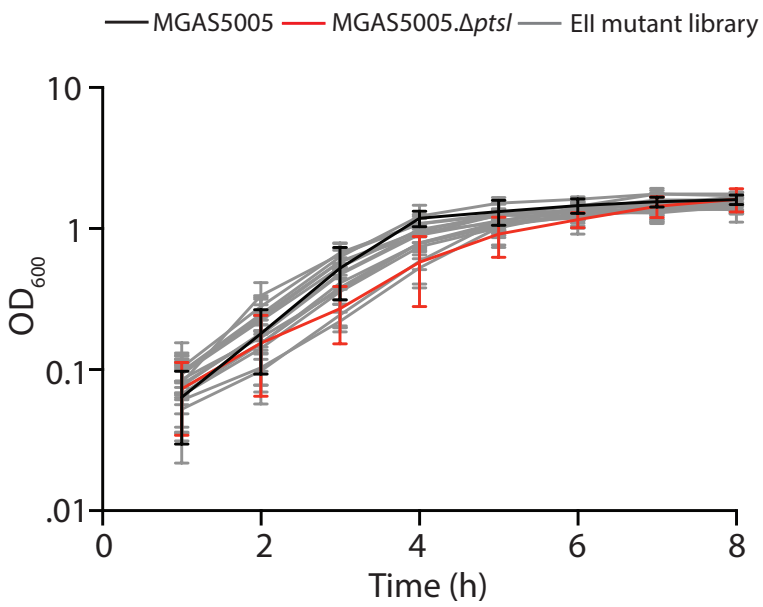

Figure 4.8 Growth of the MGAS5005 EIIC mutant library for hemolysis assays. Each graph represents the average of at least 3 independent biological replicates. Strains were grown in THY as indicated in chapter 3. Black lines represent growth of MGSA5005, red lines depict growth of MGAS5005.Δ*ptsI*, and grey lines represent growth of each EII mutant.

overall compared to MGAS5005 (**Fig 4.8**). The reason for this phenotype is currently unknown. Interestingly, three of the seven EIIC mutants that exhibited early hemolysis belong the the Mannose-family of PTS transporters.

Multiple EIICs are important for the survival of GAS in whole human blood

With the creation of an annotated EIIC mutant library, we had the ability to screen components of the PTS system through different host niches to test the different roles each component plays in GAS pathogenesis. We screened the EIIC mutant library and MGAS5005.Δ*ptsI* in a Lancefield bactericidal assay (see chapter 3) to test the involvement of the PTS system for GAS survival in whole human blood, as this is the environment that iGAS must encounter during systemic infections. We only found two EIIC mutants (Δβ-glucoside and ΔFructose) that have lower survival as compared to MGAS5005 (**Fig 4.10**). However, MGAS5005.Δ*ptsI* has significantly lower fitness in whole

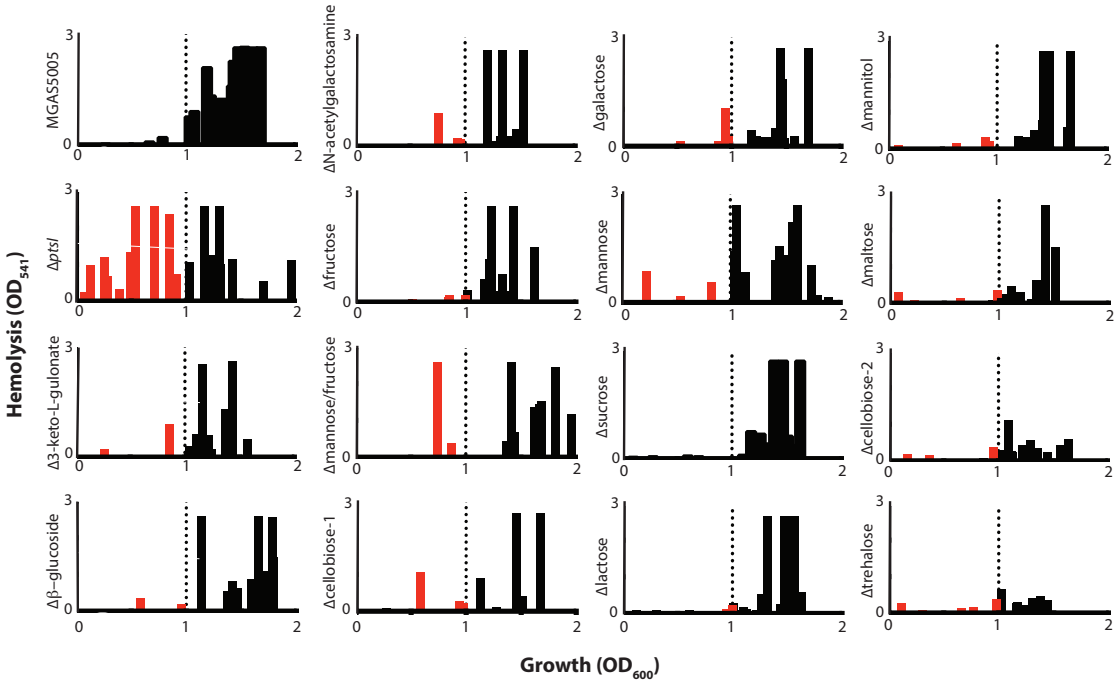

Figure 4.9 Hemolysis profile of the EII mutant library in MGAS5005. Culture lysates were measured for hemolytic activity by incubating them with red blood cells (RBCs) as indicated in chapter 3. Data from three biological replicates are shown. Occurrence of hemolysis (defined as $OD_{541} > 0.2$) on the X-axis and the relative level of hemolytic activity observed on the Y-axis. Dotted line represents an OD_{600} of 1, where positive hemolysis to the left of this line is considered early (red bars). Positive hemolysis to the right of this line is considered normal (black bars).

human blood compared to its parental strain (**Fig 4.10**). This is surprising considering that the main carbohydrate present in human blood is glucose, whose metabolism in MGAS5005.Δ*ptsI* was shown to be unaffected (Wishart *et. al.*, 2013, Wishart *et. al.*, 2009, Wishart *et. al.* , 2007, Gera *et al*., 2014). This suggests that the PTS may influence the expression of other genes that are important for survival in this infection environment, or that the low amount of PTS sugars available in blood affects GAS virulence.

Discussion

In this study, we generated a PTS EIIC mutant library based on the annotated loci in the M1T1 GAS strain MGAS5005 to help assign the carbohydrate-specific targets for

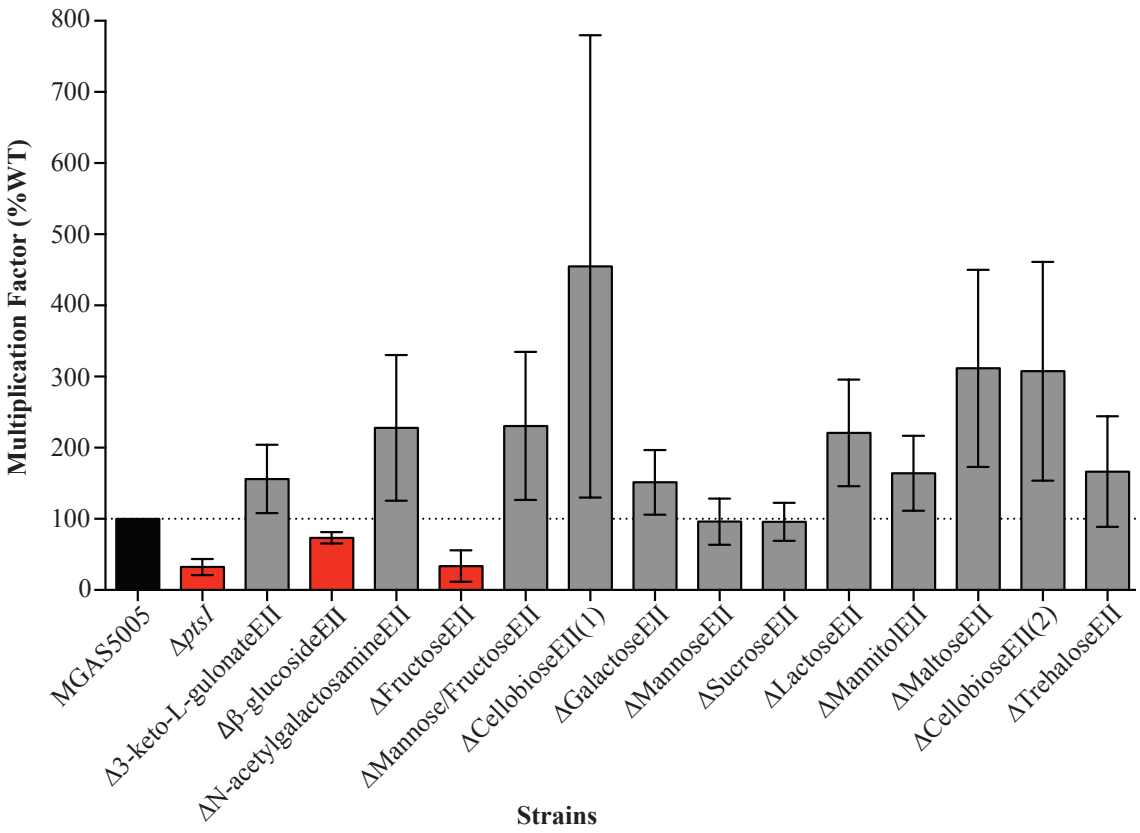

Figure 4.10 EIIC mutant library survival in whole human blood. The EIIC mutant library was subjected to a Lancefield bactericidal assay. Data is the average of three biological replicates. Multiplication factors (MF) were calculated as indicated in chapter 3, and shown compared to MFs from MGAS5005. Red bars indicate MFs of mutants that are significantly different from that of MGAS5005.Grey bars indicate those EIICs that survive in whole human blood similar to WT.

each transporter and to uncover those that contribute to the growth phase expression of Streptolysin S (SLS). By experimentally verifying growth and metabolism of PTS sugars, we discovered that each EII has varying influences on the metabolism of PTS sugars, with Mannose-family EIIs having the broadest influence. Several EIIC mutants, including the Mannose-family EIIs, contributed to an early onset of SLS-mediated hemolysis during growth *in vitro*, as previously observed with the PTS-defective MGAS5005.Δ*ptsI* GAS mutant (Gera *et al.*, 2014).

The sugar-specificities of a few individual EII systems have been assessed in streptococci, revealing imperfect annotations of their carbohydrate targets

(Shelburne *et al*., 2008b, Bidossi *et al*., 2012). Applying an extensive metabolic panel to the full complement of EII loci identified in the GAS genome, we found that the level of influence that any given EII had on the metabolism of each PTS carbohydrate varied (**Fig. 4.7**). In fact, several EIIC transporters appear to have very little influence on PTS sugar metabolism (**Fig. 4.7**), either because they are not involved in sugar transport or that the substrates of these EIIC components are shared between multiple EII complexes. Some of these EIIs (*e.g*., Trehalose-specific EII, N-acetylgalactosamine-specific EII, Cellobiose-specific EII(1)) are either lacking a key component gene or have multiple genes encoding a single subunit; indicating that they may not be involved in sugar transport (**Fig. 4.1**). The annotated Galactose-specific EII appears to have virtually no effect on PTS carbohydrate metabolism (**Fig. 4.7**). The *lacD.1* gene, encoding a tagatose-bisphosphate aldolase, was shown previously to regulate SpeB expression, and no longer participated directly in carbohydrate metabolism (Loughman & Caparon, 2006). Since the Galactose-specific EII is found at this genetic locus, it may no longer be contributing to carbohydrate uptake. Instead, it may have adapted to regulate SLS-mediated hemolysis as the ΔGalactose exhibits early hemolysis (**Fig. 4.9**). Several EIIs negatively influenced the metabolism of PTS carbohydrates, indicating that perhaps GAS uses EIICs to prioritize the hierarchal metabolism of less preferred carbohydrates (**Fig. 4.7**). It is clear, however, that annotation alone does not accurately define the sugar specificity of a particular EII, and that each must be experimentally verified.

Seven different PTS EIIC mutants in M1T1 MGAS5005 were found to result in SLS-mediated hemolytic activity early in the growth phase (**Fig. 4.9**). Since no single EIIC mutant fully recapitulated the early hemolytic activity phenotype seen with the PTS-defective MGAS5005.Δ*ptsI*, there appears to be an additive effect of these EIIs. The mechanism for how these EIICs may influence SLS release is currently being investigated. Given that there are no PTS sugars commonly influenced by all seven EIIC identified, the possibility

that the lack of utilization of a single PTS carbohydrate is responsible for hemolysis is unlikely. This does not rule out the possibility of a non-PTS carbon source that is able to be utilized by these EIIs, a distinct possibility as MGAS5005.Δ*ptsI* and ΔMannose EIIC mutant also affects the utilization of several non-PTS carbon sources (Gera *et al*., 2014) (**data not shown**). It is also possible that these seven EIIs interact with a common set of PTS-regulatory domain (PRD)-containing regulators, where disruption of this regulatory interaction could lead to early hemolysis. Studies have shown that EIIBs are capable of interacting with other regulators that may influence pathogenesis (Joyet *et al*., 2013). Whichever the mechanism, it appears that components of carbohydrate metabolic networks are important for timely hemolytic activity in GAS. Interestingly, GAS mutants in the catabolite control protein CcpA (Δ*ccpA*) exhibited early and sustained hemolysis (Kinkel & McIver, 2008, Shelburne *et al*., 2008a), although this does not appear to involve CcpA directly (Kietzman & Caparon, 2010).

We found two EII mutants (Δβ-glucoside and ΔFructose) as important for survival in whole human blood. Both these EIIs are fusion proteins of all three subunits (EIIABC), and both affect growth of GAS in fructose as the sole carbon source. Although typically thought of as an environment rich in glucose, there are trace amounts of fructose available in blood (Wishart *et. al.*, 2013, Wishart *et. al*, 2009, Wishart *et. al.* , 2007). This would suggest that perhaps fructose metabolism plays a role for GAS survival in whole human blood, a possibility that will be further interrogated in Chapter 6. However, it was curious that although MGAS5005.Δ*ptsI* was unable to survive in human blood as compared to MGAS5005, ΔMannose did survive to the same extent as the wildtype (**Fig 4.10**). This would suggest that perhaps partial utilization of PTS carbohydrates is enough to allow for growth in whole human blood, with the most likely candidate being fructose. In the case of MGAS5005.Δ*ptsI,* GAS is unable to utilize any PTS sugar other than glucose, so this may either hinder its ability to grow in blood, or more likely hinder its expression of other

virulence factors important for survival in whole blood by affecting PRD-containing regulatory proteins.

Chapter 5: The Mannose-Specific EII locus is a central to GAS carbohydrate metabolism and virulence, but in a strain specific manner

Portions of this chapter were published with the following authors: Ganesh S. Sundar, Emrul Islam, Kanika Gera, Yoann Le Breton and Kevin S. McIver (© 2016 John Wiley & Sons Ltd. Molecular Microbiology. doi: 10.1111/mmi.13573.).

Author contributions: GSS, KG, and KSM designed the study, GSS, YLB, and EI acquired and analyzed the data, and GSS, YLB, and KSM wrote the manuscript.

Data contribution: all data presented in this chapter were obtained by GSS

Introduction

Several PTS EII complexes are known to be important for the pathogenic processes of Gram-positive pathogens (Iyer & Camilli, 2007, Shelburne *et al.*, 2008b, McAllister *et al*., 2012, Pridgeon *et al*., 2013). The mannose-specific EII, composed of ManL (EIIAB), ManM (EIIC) and ManN (EIID), repeatedly appears to play important roles in pathogenesis, leading to the suggestion that it helps facilitate bacterial residence in animals (Zuniga *et al*., 2005). Mannose-family EII complexes can have broad substrate specificities, making them potential candidates to influence pathogenesis by incorporating numerous nutritional inputs and acting as a sensor to induce other metabolic operons (Fleming & Camilli, 2016). In *Streptococcus mutans*, Δ*manL* strains are not able to form biofilms in the presence of glucose, show reduced competency, and reduced acid tolerance (Abranches *et al*., 2006). Interestingly, the mannose-specific EII is actually the target for class IIa bacteriocins, highlighting the importance of carbohydrate metabolism to the survival of microbes in the host (Kjos *et al*., 2011) .Therefore, mannose EII subunits have the potential to play important virulence roles in streptococcal pathogens. We identified the mannose-specific EII, encoded by *manLMN,* as an important EII that displayed a wide influence on sugar metabolism (see Chapter 4). Inactivation of this Mannose-family EII contributed to the early onset of SLS activity, and increased lesion severity in a

strain specific manner. Mannose-family members of bacterial EIIC proteins are known to transport the widest range of substrates compared with other PTS EIIC transporters (Zuniga *et al*., 2005). Of the 14 EIIC mutants tested in our MGAS5005 library, only ΔMannose and ΔMannose/Fructose showed growth defects and total yields below or significantly below WT in at least four different PTS carbohydrates (see Chapter 4). Of the two, the mannose EIIC (ManM) exhibited the greatest influence over carbon utilization of any other PTS system, with 63% of carbon sources displaying altered utilization patterns in the ΔMannose mutant compared with MGAS5005 (see Chapter 4). Although ΔN-acetylgalactosamine represents a third mannose family EIIC present in the MGAS5005 genome (see chapter 4), it only impacted one to two substrates for growth and utilization. Therefore, the Mannose and the Mannose/Fructose EIIC transporters have the broadest impact on the metabolism of PTS sugars in MGAS5005 (see Chapter 4), suggesting their central role in GAS physiology. Since ΔMannose had the greatest influence on PTS carbohydrate metabolism, we decided to further examine its role in GAS physiology and virulence in two different M1T1 GAS strains.

Results

***manLMN* forms an operon that is induced in the presence of mannose**

The mannose-specific EII is made up of three distinct subunits: EIIAB (*manL*, cytosolic), EIIC (*manM*, membrane transporter), and an EIID (*manN*, membrane transporter exclusive to Mannose-family EII systems) **(Fig. 5.1A)**. The transcriptional architecture of *manLMN* was interrogated using RT-PCR to determine if these genes are expressed as an operon, using the primers as shown in **Fig. 5.1A.** At the end of the predicted operon is a gene (*manO*) encoding a hypothetical protein; however, only *manLMN* were found to be co-transcribed (**Fig. 5.1B**, data not shown). As a result, insertional inactivation mutants of the *manL* and *manM*, would be expected to be polar, affecting the expression of the

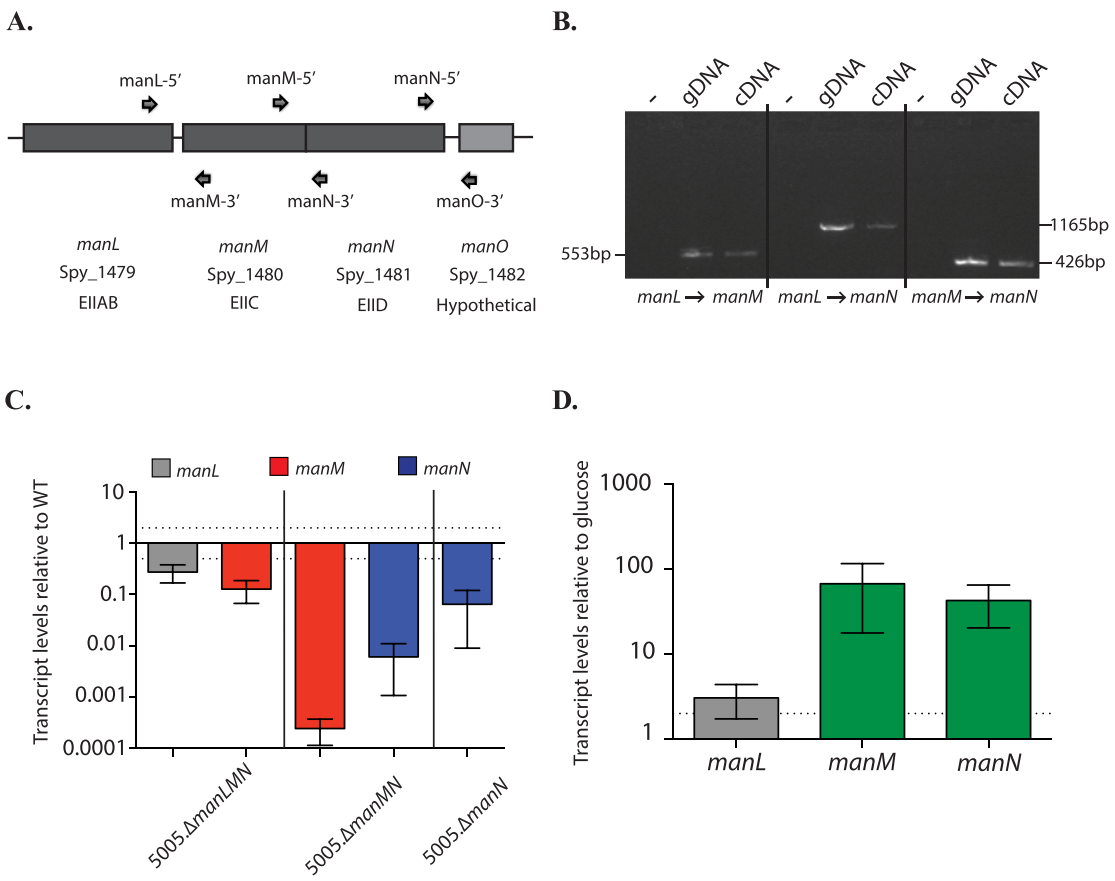

Figure 5.1 The transcriptional architecture of the mannose PTS EII locus. (A) Primers for RT-PCR are shown on the graphical representation of the mannose-specific EII genetic locus. **(B)** RNA was isolated from MGAS5005 grown in THY to late-logarithmic phase. RT-PCR was performed using primers in gene pairs as shown below. Bands indicate presence of transcript, indicating the genes are transcribed together. **(C)** Since mutagenesis approaches were potentially polar, this was assessed using qRT-PCR. Primers are located in the middle of each gene. **(D)** Induction of the mannose operon of GAS cells grown in mannose was determined. MGAS5005 was grown in glucose and mannose, RNA was extracted, and relative transcript levels were compared. Each bar depicts the average of at least three biological replicates with its respective standard error. Dotted lines represent a two-fold difference in expression.

downstream operon genes (**Fig. 5.1C**). Since this EII is annotated as mannose-specific, we hypothesized that the expression of *manLMN* should be induced in the presence of mannose. As expected, *manM* and *manN* are both induced when MGAS5005 is grown in CDM + 1% mannose as compared with growth in glucose (**Fig. 5.1D**). *manL* is not as highly induced as *manM* and *manN* when MGAS5005 is grown in mannose (**Fig. 5.1D**),

suggesting the presence of a second promoter between *manL* and *manM* that is more highly induced in the presence of mannose.

The mannose-specific EII subunits have varying influences on the metabolism of PTS carbohydrates in different M1T1 strains

The mannose-specific EII subunit mutants in MGAS5005 were assayed for their individual influence on the metabolism of PTS sugars. Since the EIIC ManM was established earlier as a promiscuous transporter (see Chapter 4), we were interested to see if this was consistent for the EIIAB and EIID subunits as well. Surprisingly, MGAS5005.Δ*manLMN* did not grow comparable to WT MGAS5005 in glucose, sucrose, maltose, and salicin, despite having no such phenotype in the ΔMannose EIIC mutant (**Chapter 4;Fig. 5.2A** and **Fig 5.3**). MGAS5005.Δ*manLMN* grew in lactose similar to WT, which was not the case for the ΔMannose EIIC mutant (**Fig 5.3**). However, both strains did have a reduced total yield in lactose (**Fig. 5.2AB**; **Fig 5.4**). MGAS5005.Δ*manN* had no effect on the overall growth of GAS in PTS carbohydrates, but did affect the total yield in 4 PTS carbohydrates. Of these, the only sugar that is specific to ManN was ascorbic acid (**Fig. 5.2A and B**). As expected, total yield in mannose was affected in all three mutant strains, further validating this EII as mannose-specific (**Fig. 5.2B; Fig 5.4**).

In contrast, the same *manL*, *manM* and *manN* mutants introduced into another M1T1 strain, 5448 (*covS*$^{+}$), had a different influence on the metabolism of PTS carbohydrates. 5448.Δ*manMN* and 5448.Δ*manLMN* had altered growth in fewer PTS carbohydrates than their respective counterparts in the *covS*-deficient MGAS5005 (**Fig. 5.2A**). In fact, 5448.Δ*manMN* and 5448.Δ*manLMN* grew better in 3 PTS carbohydrates, indicating that ManL and ManM negatively influence the metabolism of these carbohydrates by an unknown mechanism (**Fig. 5.2B**). In addition, although both sets of mutants in MGAS5005 and 5448 appear to influence the utilization of the same number of carbon sources, they do vary in the degree in which they affect utilization (**Fig. 5.2C**). MGAS5005 mannose-specific EII components had a largely positive influence on PTS sugar metabolism,

whereas these proteins in 5448 exhibited either a positive or negative influence, depending on the specific sugar (**Fig. 5.2D**). Overall, the influence of ManL, ManM and ManN on the metabolism of PTS carbohydrates varied between M1T1 GAS strains and suggests a versatile EII that may adapt to the specific needs of the individual genetic background.

ΔMannose EIIC induces hemolysis early in growth, although ManL and ManN contribute in a strain-specific manner

The individual subunits of the mannose-specific EII complex (ManLMN) were interrogated for their role in early onset of hemolysis. In order to more accurately profile the point of growth where hemolysis began for each of the mutants, supernatants from samples taken every 20 minutes were tested. In MGAS5005, early hemolysis was observed in the ΔMannose EIIC mutant, as expected from the initial screen in the EII mutant library, and slightly in MGAS5005.Δ*manN*. The overall level of hemolysis in MGAS5005.Δ*manLMN* was relatively lower compared with WT MGAS5005, which was not the case for 5448.Δ*manLMN* compared with WT 5448. Although 5448.Δ*manMN* also exhibited the early hemolytic activity, 5448.Δ*manN* presented hemolytic profile similar to 5448 and different from that observed for the same mutant in MGAS5005 (**Fig. 5.5**). Therefore, ManM plays a consistent role in the regulation of growth-phase dependent expression of SLS; however the contribution of ManL and ManN to this phenotype appears to be strain specific.

Contribution of ManMN (EIICD) to the pathogenesis of M1T1 MGAS5005 in a soft tissue infection model

The pathogenesis of the ΔMannose EIIC mutant was assessed in a murine soft tissue infection model, where lesion size and survival from invasive disease was monitored as described (see Chapter 3). MGAS5005 lacking a functional PTS (MGAS5005.Δ*ptsI*) was previously shown to elicit larger and more severe lesions than those induced by MGAS5005 in the subcutaneous model (Gera *et al*., 2014). Although the ΔMannose EIIC mutant exhibited similar lesion sizes to that of MGAS5005, the severity of the lesions (see

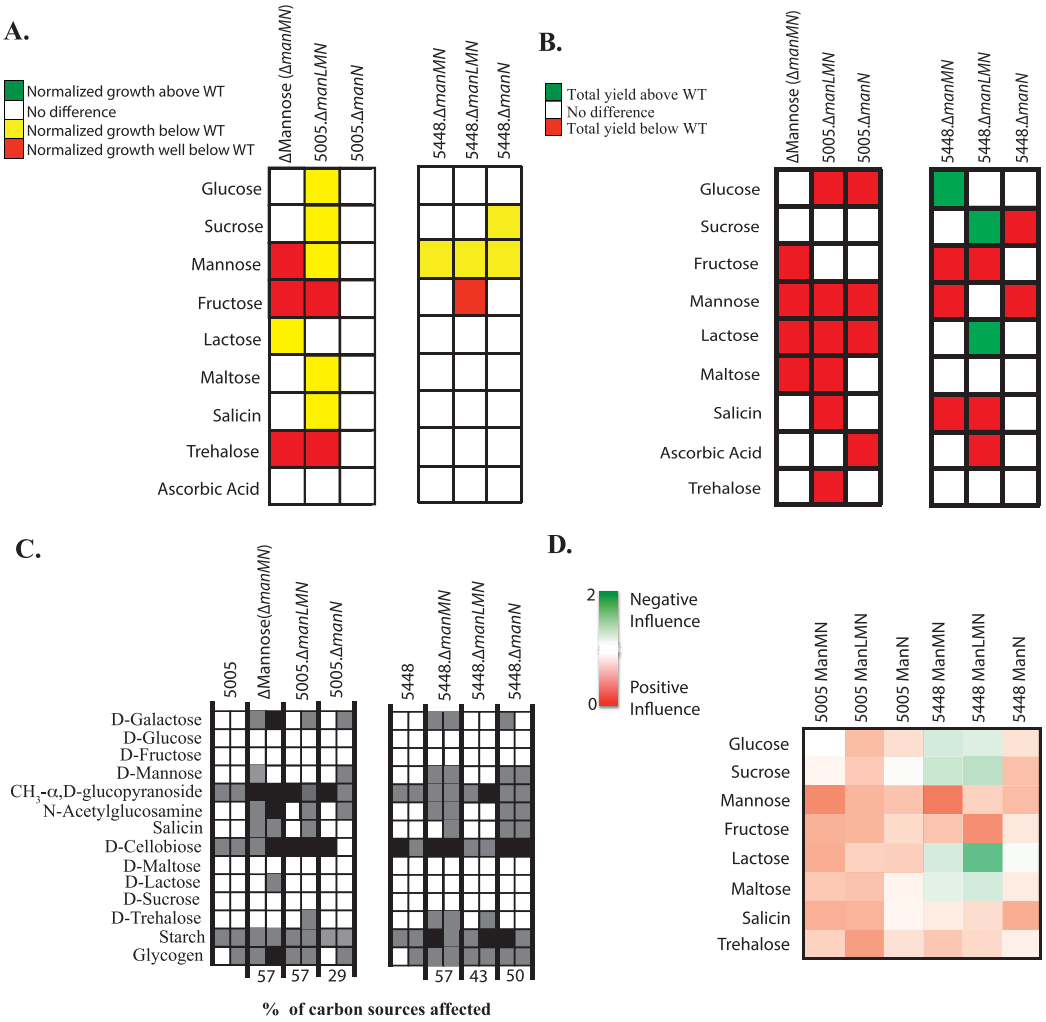

Figure 5.2 Metabolic profile of the mannose-specific EII subunit mutants. (A) Growth curves for the mannose-specific EII subunit mutants were analyzed as described in chpater 3. Normalized growth above WT (green, two-fold above), below WT (yellow, two-fold below), and well below (red, >two-fold below) are indicated. **(B)** Total yield (ΔOD) of the subunit mutants were calculated as indicated in chapter 3. ΔOD significantly above WT were shown in green, whereas ΔOD significantly below WT are shown in red. ΔOD that are not significantly different in the mutant as compared to the WT are shown in white. Significance was determined by Student's t-test (p-value <0.05). Data represent the average of at least three biological replicates. **(C)** The API®50CH system was used to determine the utilization profiles of the mannose-specific EII mutants, as indicated in chapter 3. Carbon sources presented are utilized in at least one strain tested. White boxes indicate utilization (+), grey boxes indicate partial utilization (+/-), and black boxes indicate no utilization (-). Two reading were taken for each strain in each sugar, depicted as 24h on the left and 48h on the right. **(D)** Influence scores for ManLMN in both 5005 and 5448 were calculated as indicated in chapter 3. Positive influence on the metabolism of a PTS carbohydrate is indicated in red, whereas a negative influence is indicated in green. Relative intensity of each color represents the relative degree of influence of each protein on the metabolism of a carbohydrate.

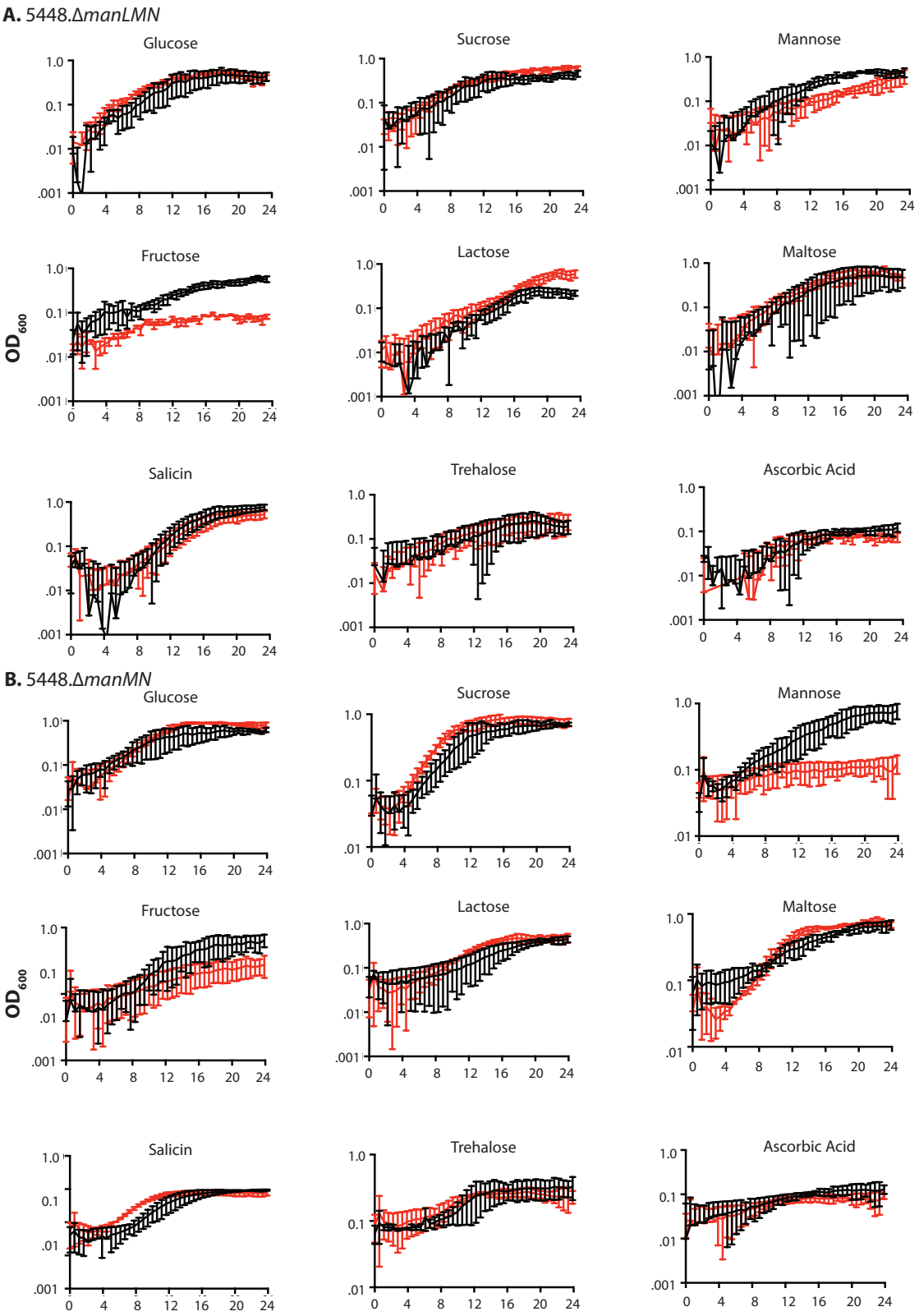
A. 5448.ΔmanLMN
Glucose
Sucrose
Mannose
Fructose
Lactose
Maltose
Salicin
Trehalose
Ascorbic Acid
OD600
B. 5448.ΔmanMN
Glucose
Sucrose
Mannose
Fructose
Lactose
Maltose
Salicin
Trehalose
Ascorbic Acid
OD600

C. 5448.Δ*manN*

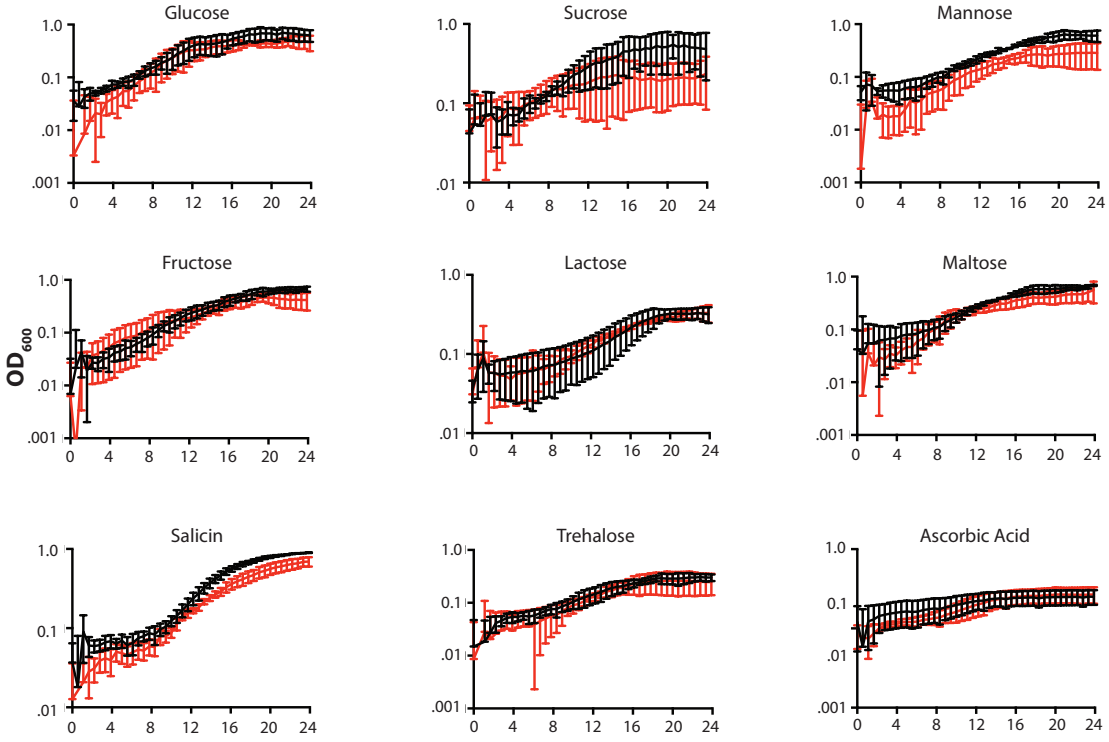

D. MGAS5005.Δ*manLMN*

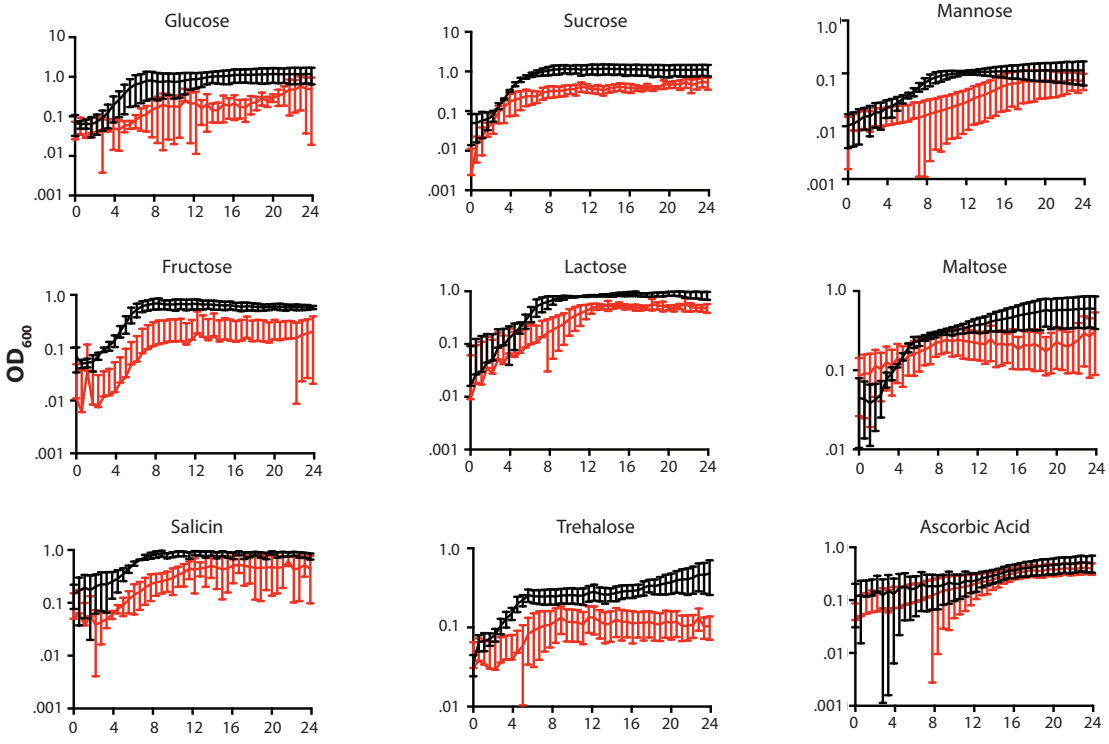

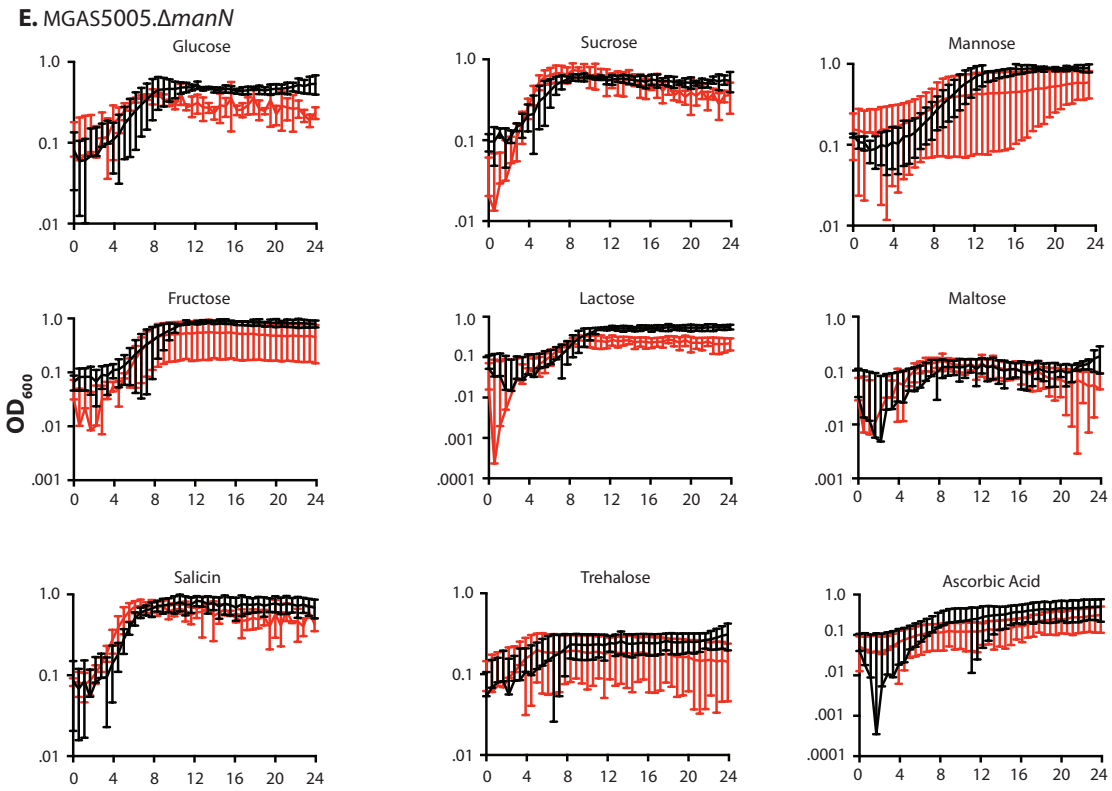

Figure 5.3. Growth of MGAS5005 manLMN EII mutants in 9 PTS carbohydrates. Each graph represents the average of at least 3 independent biological replicates. **(A-E)** EII mutants were grown in CDM + 1% PTS carbohydrate (0.5% for glucose) as indicated in chapter 3. Black lines represent WT growth, whereas red lines represent growth of the EII mutant.

Chapter 3) in the mutant was increased significantly as compared with MGAS5005 and the ΔMannose$_R$ rescued strain (**Fig. 5.6AB; Fig 5.7**). As was the case for MGAS5005.Δ*ptsI* the increased localized lesion severity did not lead to increased mortality (**Fig. 5.7C**). Rather, survival was slightly increased in the ΔMannose EIIC mutant compared with, WT MGAS5005. Thus, the loss of *manMN* (EIICD) results in enhanced necrosis during soft-tissue infection.

Discussion

Characterization of the mannose-specific EIIABCD components (*manLMN*) in two different M1T1 GAS strains revealed that they played a strain-

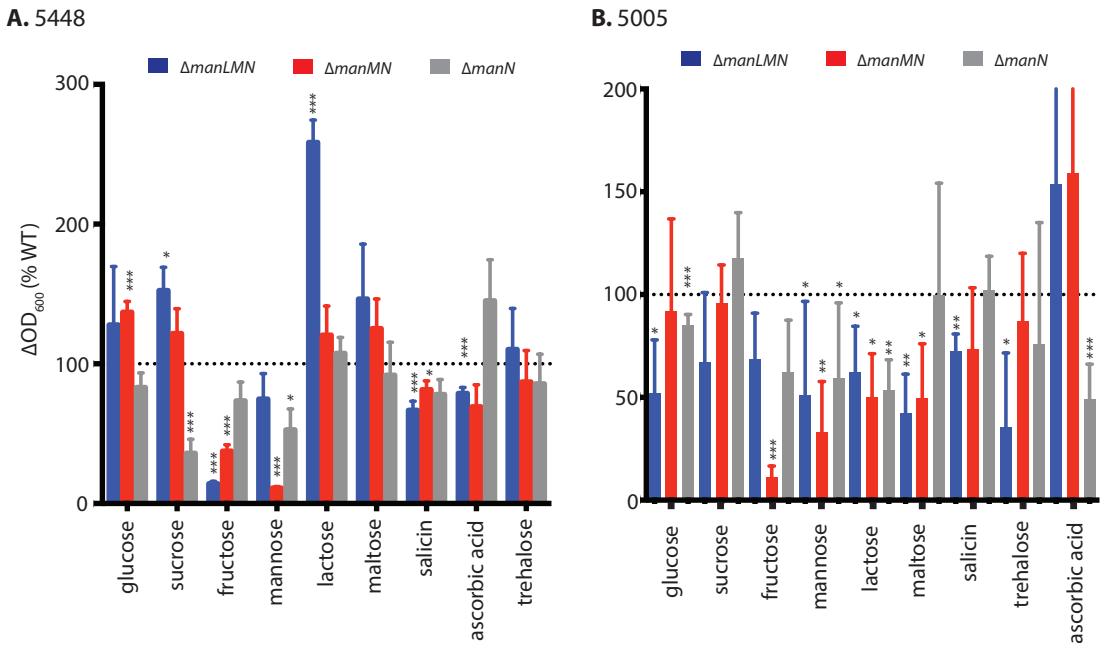

Figure 5.4. ΔOD of the mannose subunit mutant in two M1T1s. Each graph represents the average of at least 3 independent biological replicates. Data is normalized to wildtype as indicated in chapter 3. **(A,B)** Mutants were grown in CDM + 1% PTS carbohydrate (0.5% for glucose) as indicated in chapter 3. Color of bars depict strain as indicated. * p-value < 0.05 ** p-value <0.01 ***p-value <0.005

specific role for PTS sugar metabolism and growth phase-related production of SLS-mediated hemolysis. We identified the Mannose-specific EII system as a central component to the metabolism of a large number of PTS carbohydrates in MGAS5005. In S*treptococcus pneumoniae*, a *manLMN* mutant was recently shown to be unable to grow on non-preferred carbohydrates due to the lack of induction of other metabolic operons (Fleming & Camilli, 2016). In contrast, ManLMN has been shown to have a large number of substrates in other bacteria and plays a more direct role in metabolism of these sugars (Tong *et al.*, 2011, Port *et al.*, 2014). The exact mechanism by which the mannose-specific EII affects the metabolism of other carbohydrates in GAS is not known. In MGAS5005, there were 5 sugars whose metabolism was differentially affected between Δ*manLMN* and the ΔMannose EIICD (Δ*manMN*) mutant (**Fig 5.2; Fig 5.3**). Thus, an intact *manL* (EIIAB) alone facilitates optimal growth of GAS on maltose, salicin, glucose and

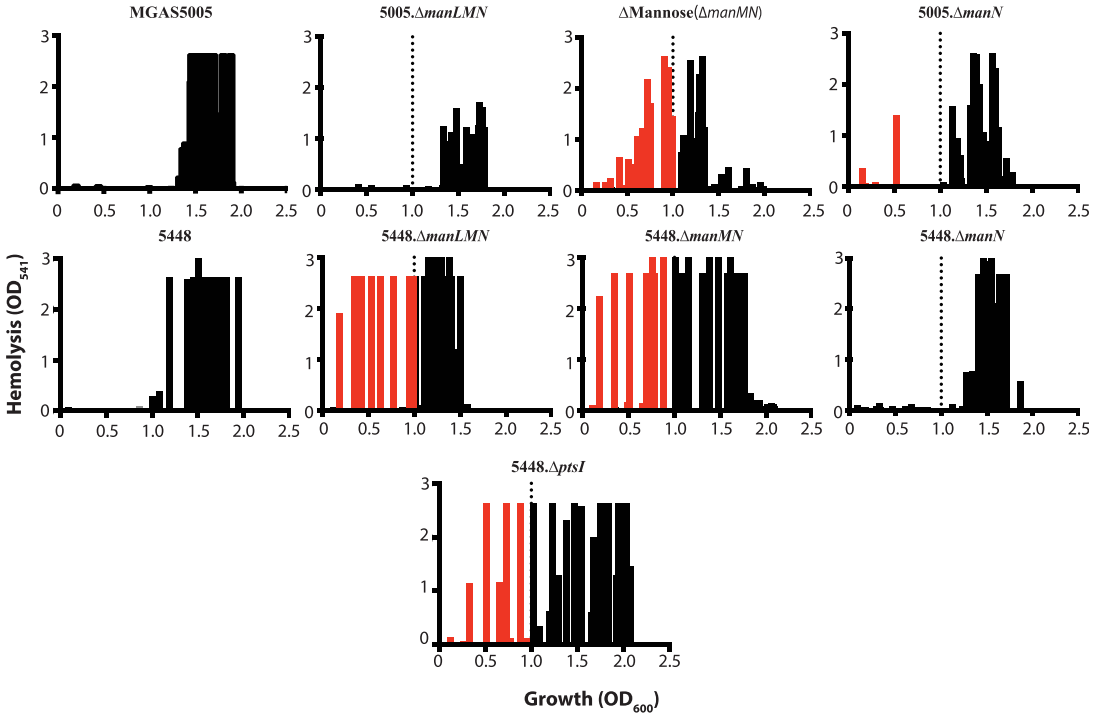

Figure 5.5 Hemolytic activity of the mannose-specific EII subunit mutants. As described in chapter 3, culture lysates from GAS grown cells were incubated with red blood cells (RBCs) to measure hemolytic activity. Data from three biological replicates is shown. The occurrence of hemolysis ($OD_{541} > 0.2$) on the X-axis is compared to the relative amount of hemolytic activity observed on the Y-axis. Red bars (to the left of the dotted line) represent hemolysis at an OD_{600} below 1, indicating early hemolytic activity. Black bars (to the right of the dotted line) represent hemolysis occurring at an $OD_{600} > 1$, which is considered normal based on WT 5448 or MGAS5005.

sucrose. Lack of *manL* prevents GAS from growing in these sugars efficiently, but it does allow for wild type growth in lactose (**Fig 5.2A**). This would suggest that either ManL (EIIAB) can interact with other EII systems, or that ManL (EIIAB) interacts with a protein(s) that influence other metabolic pathways. ManN (EIID) in MGAS5005 had very little influence on PTS sugar metabolism, likely due to the presence of an intact EIIABC that would still allow for transport of PTS substrates (**Fig 5.2D**).

The specific roles of the ManLMN subunits were not consistent between the two M1T1 strains tested, MGAS5005 and 5448, even though their *manLMN* gene sequences are identical. The ΔMannose EIIC mutant had a much more limited effect on the growth of

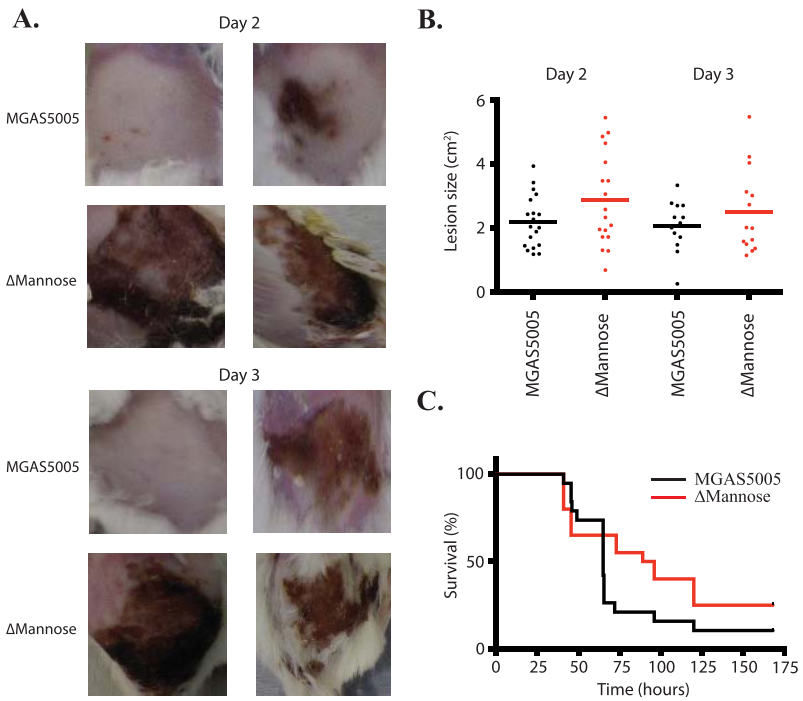

Figure 5.6 Subcutaneous murine infections of ΔMannose. Lesion size and survival of mice were monitored for 7 days. Each strain was tested in at least 10 female CD-1 mice. **(A)** Representative images of lesions taken at 2 and 3 days post infection. **(B)** Lesion size was measured as indicated in chapter 3 at 2 and 3 days post infection using ImageJ. Each data point represents a single mouse lesion **(C)** Mouse survival was monitored for 7 days. Significance was determined as described in chapter 3.

GAS in PTS carbohydrates in 5448 compared with the same *manMN* mutant in MGAS5005 (**Fig. 5.2A; Fig 5.3**). Overall, Mannose EII component mutants in 5448 only affected growth of GAS in 1 or 2 sugars, which was not the case for the same mutants in MGAS5005, with the exception of MGAS5005.Δ*manN* (**Fig 5.2A and B**). Differences in overall PTS sugar metabolism have been observed between different GAS strains, specifically M14 HSC5 and M1T1 MGAS5005 (Port *et al.*, 2014). A mutation in the fructose-specific EII (Δ*fruA*) in MGAS5005 exhibited increased growth in both glucose and lactose, which was not seen for the same mutant in 5448 (chapter 6). We have also observed differences in carbon utilization between MGAS5005 and 5448 (data not shown), indicating that different strains may require different nutrients and have subsequently altered the roles of similar proteins. Thus, GAS strains may be able to infect several different host niches because

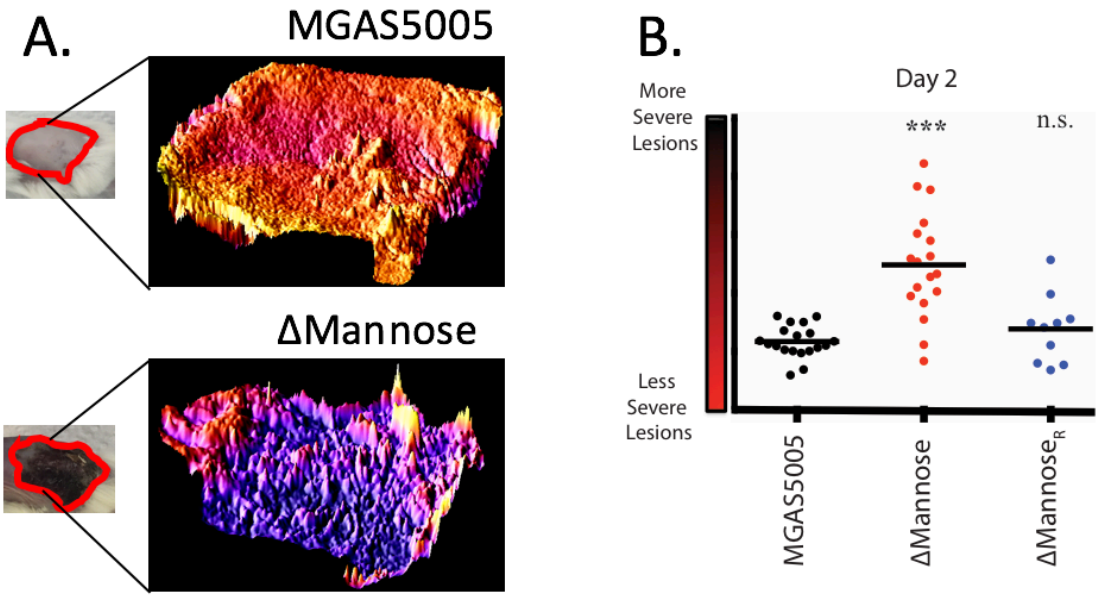

Figure 5.7 ΔMannose subcutaneous murine infections lead to the development of more severe lesions. **(A)** Lesion severity, as described in chapter 3, was determined by analyzing the average red pixel intensity of the lesion selection. Increased tissue necrosis (ΔMannose lesions) lead to scarring which appear darker on the image, making the pixel intensity closer to the black end of the scale. Less necrotic lesions retain the appearance of the body of a mouse (pink/red), therefore the pixel intensity is closer to the light red end of the scale. **(B)** Average pixel intensity for at least 10 independent lesions were scored and displayed. ***p-value < 0.005.

of their metabolic versatility. The role of ManL and ManN, but not ManM, in regulating hemolytic activity is potentially strain specific. A Δ*manLMN* mutant in 5448 exhibited early hemolysis, which was not seen for the same mutant produced in MGAS5005. However, Δ*manN* in MGAS5005 exhibited early hemolytic activity to a certain extent, which was not seen for the same respective mutant in 5448. One explanation could be the *covS* status of each strain. MGAS5005 is a *covS* mutant whereas 5448 is wild type for *covS*, so the presence of a functional CovS may influence the roles of ManL and ManN. To address this possibility, the roles of ManLMN in hemolytic activity are currently being evaluated in 5448AP (*covS*$^-$).

The lesions that develop from ΔMannose EII system GAS infections in a mouse model of soft tissue disease are more severe in their necrosis than those that develop from

a wild type MGAS5005 infection (**Fig. 5.6A; Fig. 5.7**). Although the lesion sizes from ΔMannose mutant infections trend larger than those from MGAS5005 infections, the differences are not statistically significant (**Fig. 5.6B**). Since 6 other EIIC mutants exhibited early hemolytic activity as well, this suggests that the increased lesion sized observed in MGAS5005.Δ*ptsI* infections could be the result of the additive contribution of several EIIs on SLS expression (see chapter 4). As seen with the PTS-defective MGAS5005.Δ*ptsI* mutant (Gera *et al*., 2014), a ΔMannose EIIC mutant does not impact lethality compared with MGAS5005 *in vivo* (**Fig. 5.6C**). Thus, the influence of the PTS on GAS pathogenesis may be localized to the site of infection, indicating the potential for GAS to use specific carbon metabolic pathways in each distinct host niche in order to govern its pathogenesis.

In conclusion, the Mannose-specific EIIC plays a central role in PTS carbohydrate metabolism and regulates SLS-mediated hemolysis. This could be a mechanism to obtain sugars in nutrient poor host conditions. Although ManM acts to reduce the lesion severity in soft tissue infections, the overall role of the PTS to mediate lesion severity appears to be the additive effect of multiple EIIs.

Chapter 6: Comparing the role of the fructose-specific EII in GAS PTS carbohydrate metabolism and virulence between two M1T1s

Portions of this chapter were published with the following authors: Kayla M. Valdes, Ganesh S. Sundar, Luis A. Vega, Ashton T. Belew, Emrul Islam, Rachel Binet, Najib M. El-Sayed, Yoann Le Breton, Kevin S. McIver (© American Society for Microbiology, Infection and Immunity, 84(4): 1016-31. DOI: 10.1128/IAI.01296-15.).

Author contributions: K.M.V., G.S.S., L.A.V., Y.L.B., and K.S.M. conceived and designed the research plan, K.M.V., G.S.S., L.A.V., E.I., and Y.L.B. performed the research, A.T.B. and N.M.E. performed the RNA-Seq bioinformatic analysis, and R.B. provided expertise and access to Biolog. K.M.V., G.S.S., Y.L.B., and K.S.M. wrote the paper. K.M.V. and G.S.S contributed equally to the manuscript

Data contribution: K.M.V obtained data for Fig: 6.2B, 6.3, 6.4, 6.9, and Table 6.1

G.S.S obtained data for Fig: 6.5, 6.6, 6.7, 6.8, and Table 6.2

Y.L.B. obtained data for Fig: 6.2A

L.A.V. obtained data for Fig: 6.1

Introduction

fruA encodes one of the 14 EII PTS sugar transporters found in the GAS M1T1 genome (Shelburne *et al*., 2008b) and is predicted to be located within a conserved three-gene *fru* operon conserved across low GC Gram-positive bacteria. In the model organism *Lactococcus lactis*, the *fru* operon is composed of *fruR*, encoding a DeoR family transcriptional repressor; *fruK (fruB* in GAS), a 1-phosphofructokinase; and *fruA*, an EIIABC PTS sugar transporter (Barriere *et al*., 2005). Interestingly, *fruA* has been implicated in the pathogenesis of other streptococcal species. In the oral pathogen *Streptococcus gordonii*, the fructose EIIABC (*fruA*) has been linked to biofilm formation (Loo *et al*., 2003). In the zoonotic pathogen *Streptococcus iniae*, *fruA* was found in the

genomes of five virulent strains but was absent from nonvirulent strains (Pridgeon *et al*., 2013). In GAS, the transcription of *fruA* was induced in an analysis of global heme stress in GAS (Sachla *et al.*, 2014), a condition likely encountered during bloodstream infection. Therefore, understanding its different roles in GAS virulence is useful to understand the development of invasive disease.

Results

Fructose metabolic operon genes are important for survival from neutrophil killing

In a previous study, the fructose-specific metabolic operon was implicated in resistance to neutrophil killing of GAS (Valdes *et al*., 2016). Neutrophils are the predominant cell type that act as a first line of defense at the site of infection, and they can kill pathogens through multiple extra- or intracellular means, such as antimicrobial peptides, phagocytosis, and DNA neutrophil extracellular traps (NETs). We subjected 5448.Δ*fruR*, 5448.Δ*fruB*, and 5448.Δ*fruA* strains to opsonophagocytic killing assays using the human-derived promyelocytic leukemia cell line HL60 differentiated into neutrophil-like cells (**Fig. 6.1 A**) and freshly isolated human PMNs (**Fig. 6.1B**). Both neutrophil-like HL60 cells and human-isolated PMNs were infected using an MOI of 0.1, and strains were plated for survival and compared to the parental 5448. When either the 5448.Δ*fruR* or 5448.Δ*fruB* mutant was incubated with HL60 cells, each showed a significant decrease in survival compared to that of 5448 (**Fig. 6.1A**). However, the 5448.Δ*fruA* mutant survived at levels comparable to that of the wild-type GAS. Importantly, 5448.Δ$fruR_R$ and 5448.Δ$fruB_R$ revertant strains either partially or completely restored the phenotype to wild-type levels (**Fig. 6.1A**). These phenotypes were recapitulated with freshly isolated human PMNs (**Fig. 6.1B**), supporting a requirement for FruB and FruR, but not FruA, for survival in human neutrophils. There was also a survival defect observed for the 5448.Δ*fruR* or 5448.Δ*fruB* mutant, but not the 5448.Δ*fruA* mutant, in human monocytes, suggesting a role for these *fru*

for a defect in growth for any of the *fru* operon mutants, we also grew each strain in RPMI plus 20% plasma and saw no growth defect compared to the parental 5448 (**Fig 6.1 D and E**). Thus, *fruR* and *fruB*, but not *fruA*, are important for GAS resistance to killing by human neutrophils and primary monocytes.

This suggests that the fructose-specific metabolic operon plays an important role for GAS to survive in whole human blood. This was rather curious, as fructose is not present in high amounts in human blood or in RBCs, although there are trace amounts (Wishart *et. al.*, 2013, Wishart *et. al*, 2009, Wishart *et. al*, 2007). We assayed the components of the fructose metabolic operon in whole human blood, and determined that only *fruR* and *fruB* were required for GAS survival in whole human blood and exhibited small colony phenotypes when streaked on blood agar plates, which was not the case for *fruA* (**Fig 6.2A and B**). Importantly, the revertants have similar survival to wildtype 5448. Interestingly, ΔFructose (Δ*fruA* in MGAS5005; Chapter 4) is impaired in its ability to survive in whole human blood. This would again suggest that there is a strain specific behavior that EIIs possess in their roles in pathogenesis. Similar to ΔMannose (Chapter 5), we sought to determine if this differential phenotype observed was the result of altered metabolic influences of FruA between MGAS5005 and 5448. Since the metabolic influence of FruA was already determined for MGAS5005, we characterized the fructose-specific EII in 5448.

Fructose-Specific EII operon induced by the presence of fructose

As seen in Chapter 4 and 5, EIIs do not always solely affect the metabolism of the PTS carbohydrate based on their respective annotation. This, combined with the fact that fructose metabolic genes were implicated in GAS survival against neutrophil killing, led us to assess the effect of fructose on GAS gene expression, with the hope of elucidating pathways that may provide an explanation for the observed phenotype. We conducted RNA transcriptome sequencing (RNA-Seq) on total RNA isolated from wild-type 5448 grown in chemically defined medium (CDM) supplemented with 0.5% glucose or 1% fructose

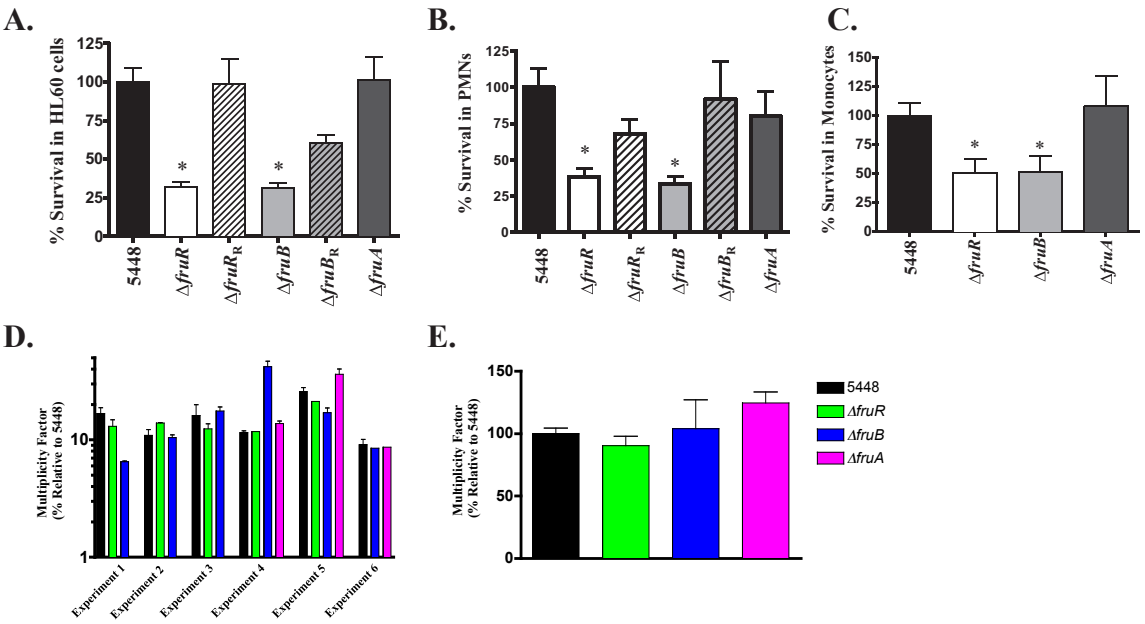

Figure 6.1 Role of fructose-metabolic genes in immune evasion. (A) Survival in neutrophil-like HL60 cells. GAS ($1x10^5$ CFU/well) and HL60 cells ($1x10^6$ CFU/well) were incubated for 2 h at 37°C. Cells were lysed and the percentage of surviving GAS CFU was determined relative to the level of survival for 5448. **(B)** Survival in human neutrophils (PMNs). GAS ($1x10^5$ CFU/well) and neutrophils ($1x10^6$ CFU/well) were incubated for 2 h at 37°C. Neutrophils then were lysed, and the percentage of surviving GAS CFU was determined and is shown as survival relative to that of the WT (5448). **(C)** Survival in human monocytes. GAS ($1x10^5$ CFU/well) and human monocytic cells ($1x10^6$ CFU/well) were incubated for 2 h at 37°C. Cells were lysed, and the percentage of surviving GAS CFU was determined relative to that for survival of 5448. Error bars in panels A to C represent means SD of the results from three biological replicates performed in triplicate. Significance for panels A to C was determined by unpaired t test ($P < 0.05$). Each *fru* mutant was grown along with the parental strain 5448 in RPMI + 20% plasma. Data from 6 independent experiments, with at least three replicates for each *fru* operon mutant in comparison to WT 5448 are shown in **(D)**. The cumulative results of **(D)** are shown as an average of the replicates in **(E)**. *Performed by L.A.V.

to late logarithmic phase in two biological replicates and processed for RNA-Seq. Data obtained from fructose-grown cells were compared to those of glucose-grown cells (WT-glu/WT-fru), with changes in gene expression over 2-fold (log_2 -1.0 or log_2 1.0) being considered significant (**Table 6.1**). A total of 195 genes (103 nonphage genes; 5.5% of genome) were altered (**Table 6.1**). Several predicted and established sugar metabolism operons were highly induced during growth in fructose (**Table 6.1**, shaded gray), including the *lacD.1* and

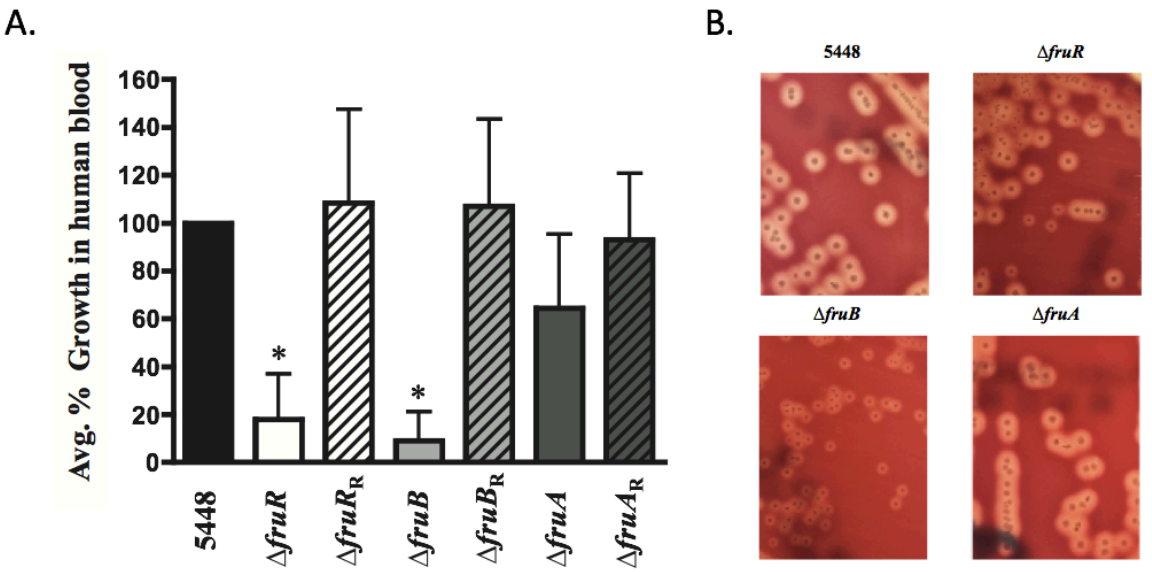

Figure 6.2. *fruR* and *fruB* are important for survival in human blood. Wild-type 5448 (black bars) was compared to 5448.Δ*fruR* (white bars), 5448.Δ*fruB* (light gray bars), and 5448.Δ*fruA* (dark gray bars) mutants for growth and survival. The respective rescued mutant strains are indicated with diagonal lines. **(A)** Lancefield bactericidal assay was performed by monitoring growth in whole human blood with rotation at 37°C for 3 h. Data are presented as percent growth in blood corresponding to the multiplication factor (MF) of the mutant divided by the MF of the wild type times 100. Error bars represent means SD of the results of six independent experiments. **(B)** Colony morphology of each *fru* mutant was streaked on blood agar (TSA + 5% sheep blood) plates, cultured overnight at 37°C + 5% CO_2 and imaged. * Performed by Y.L.B and K.M.V

lacD.2-specific PTS operons, the maltose-specific ABC transport system (*malADC*), and the predicted fructose operon (*fruRBA*). Of these, the putative *fruRBA* operon was the most highly induced by fructose, with more than a 5-fold increase in expression (**Table 6.1**). In addition, several members of the SerR regulon involved in serine metabolism were induced by fructose (LaSarre & Federle, 2011), including genes encoding the putative regulator SloR, the V-type sodium ATP synthase (*ntp*) operon, and the serine dehydratase (*sdhAB*) operon. Interestingly, *sloR* is predicted to encode a transmembrane protein that exhibits homology to the EIIC domain of the putative FruA PTS transporter. Notably, only six genes, including *nagB* and *nagA*, involved in N-acetylglucosamine metabolism, appeared to be repressed in the presence of fructose. Overall, the two largest gene ontology categories found to be induced by fructose were carbohydrate transport and metabolism (33 genes;

32% COGxxxxG) and energy production conversion (9 genes; 9% COGxxxxC). Therefore, the presence of fructose influences the expression of a subset of sugar metabolism genes, particularly the predicted *fruRBA* fructose utilization operon.

***fruRBA* is transcribed as an operon**

In the 5448 genome, the *fru* locus is comprised of three contiguous genes (**Fig. 6.3 and Table 6.1)**: *fruR*, encoding a predicted transcriptional repressor; *fruB*, encoding the enzyme 1-phosphofructokinase; and *fruA*, encoding a predicted fructose-specific EIIABC component of the sugar PTS. Each of the three genes slightly overlap, with the start codon of the gene downstream being found in the upstream gene, suggesting they form an operon. RT-PCR of transcripts from 5448 grown in CDM plus 1% fructose showed transcriptional linkage between *fruB-fruA* and *fruR-fruB,* and a 1.5-kb full- length transcript was detected between *fruR* and *fruA* (**Fig. 6.3A**). These data demonstrate that *fruRBA* genes are expressed as an operon during inducing growth in fructose as the sole carbon source.

To determine the transcriptional start site (TSS) of the *fru* operon, 5'-RACE was used in conjunction with a primer complementary to *fruR* (FruR SP1) (**Table 3.2**). A TSS that was located near the classical -10 (TATAAT) and -35 (TTGACT) promoter hexamers was identified 56 bp upstream of the start codon for *fruR* (**Fig. 6.3B**). A predicted CcpA-binding site (*cre*) site (Kietzman & Caparon, 2010) and FruR-binding site (Barriere *et al*., 2005) also were identified overlapping and upstream of the promoter, respectively (**Fig. 6.3C**). Finally, a putative *rho*-independent terminator was detected downstream of *fruA*, consistent with the generation of the full-length *fruRBA* transcript (**Fig. 6.3C**). Thus, the promoter of the *fruRBA* operon appears to be under CcpA-mediated catabolite repression by glucose and FruR-mediated induction by fructose.

To interrogate each gene in the *fru* operon for its role in fructose metabolism and virulence, we generated nonpolar deletions for *fruR, fruB, and fruA* by allelic exchange in the 5448 genome with an chloramphenicol resistance cassette (*cat*) (Rose, 1988),

Table 6.1. Subset of genes differentially expressed in fructose *Performed by K.M.V

Spy no.	Annotation	Gene name	Log_2 fold change[a]
Induced by fructose			
M5005_Spy_0039	Alcohol dehydrogenase/acetaldehyde dehydrogenase	*adh.2*	−2.10
M5005_Spy_0123	Translation initiation inhibitor		−1.82
M5005_Spy_0124	**Serine catabolism regulator; FruA-like EIIC domain protein**	***sloR***	**−2.32**
M5005_Spy_0125	Hypothetical protein		−1.09
M5005_Spy_0126	V-type sodium ATP synthase subunit I	*ntpI*	−2.01
M5005_Spy_0127	V-type sodium ATP synthase subunit K	*ntpK*	−1.97
M5005_Spy_0128	V-type sodium ATP synthase subunit E	*ntpE*	−2.22
M5005_Spy_0129	V-type sodium ATP synthase subunit C	*ntpC*	−1.79
M5005_Spy_0130	V-type sodium ATP synthase subunit F	*ntpF*	−1.22
M5005_Spy_0131	V-type sodium ATP synthase subunit A	*ntpA*	−1.24
M5005_Spy_0132	V-type sodium ATP synthase subunit B	*ntpB*	−0.96
M5005_Spy_0133	V-type sodium ATP synthase subunit D	*ntpD*	−1.21
M5005_Spy_0150	PTS, 3-keto-l-gulonate-specific IIA	*ptxA*	−0.99
M5005_Spy_0474	Transcription antiterminator, BglG family	*licT*	−1.36
M5005_Spy_0476	6-Phospho-beta-glucosidase	*bglA*	−1.22
M5005_Spy_0521	PTS, *N*-acetylgalactosamine-specific IIB	*agaV*	−1.75
M5005_Spy_0660	**Fructose repressor**	***fruR***	**−1.95**
M5005_Spy_0661	**1-Phosphofructokinase**	***fruB***	**−2.52**
M5005_Spy_0662	**PTS, fructose-specific IIABC**	***fruA***	**−3.33**
M5005_Spy_0798	IFN response binding factor 1		−1.01
M5005_Spy_1062	Maltodextrose utilization protein	*malA*	−1.12
M5005_Spy_1063	ABC cyclomaltodextrin permease protein	*malD*	−1.17
M5005_Spy_1081	PTS, cellobiose-specific IIA component		−0.98
M5005_Spy_1307	Hypothetical membrane spanning protein		−1.02
M5005_Spy_1308	ABC unknown sugar-binding protein		−1.16
M5005_Spy_1309	ABC unknown sugar permease protein		−1.82
M5005_Spy_1310	ABC unknown sugar permease protein		−1.40
M5005_Spy_1395	Tagatose-bisphosphate aldolase; SpeB regulator	*lacD.1*	−1.01
M5005_Spy_1396	Tagatose-6-phosphate kinase; regulatory	*lacC.1*	−1.35
M5005_Spy_1397	Galactose-6-phosphate isomerase LacB subunit; regulatory	*lacB.1*	−1.54
M5005_Spy_1400	PTS, galactose-specific IIB component		−1.45
M5005_Spy_1401	PTS, galactose-specific IIA component		−1.14
M5005_Spy_1509	Pyruvate, phosphate dikinase		−1.36
M5005_Spy_1510	Pyruvate, phosphate dikinase		−1.26
M5005_Spy_1629	Lantibiotic transport ATP-binding protein	*salX*	−1.89
M5005_Spy_1631	Lantibiotic salivaricin A	*salA*	−1.67
M5005_Spy_1632	6-Phospho-beta-galactosidase	*lacG*	−1.66
M5005_Spy_1633	PTS, lactose-specific IIBC component	*lacE*	−2.73
M5005_Spy_1634	PTS, lactose-specific IIA component	*lacF*	−2.22
M5005_Spy_1635	Tagatose-bisphosphate aldolase	*lacD.2*	−2.18
M5005_Spy_1636	Tagatose-6-phosphate kinase	*lacC.2*	−1.49
M5005_Spy_1637	Galactose-6-phosphate isomerase LacB subunit	*lacB.2*	−1.67
M5005_Spy_1638	Galactose-6-phosphate isomerase LacA subunit	*lacA.2*	−1.50
M5005_Spy_1663	PTS, mannitol-specific IIB component		−1.69
M5005_Spy_1744	PTS, cellobiose-specific IIC component	*celC*	−1.34
M5005_Spy_1745	PTS, cellobiose-specific IIB component	*celB*	−0.95
M5005_Spy_1841	l-Serine dehydratase	*sdhB*	−1.06
M5005_Spy_1842	l-Serine dehydratase	*sdhA*	−1.27
Repressed by fructose			
M5005_Spy_0667	Exotoxin type C precursor		2.07
M5005_Spy_1139	Glucosamine-6-phosphate isomerase	*nagB*	0.98
M5005_Spy_1388	*N*-Acetylglucosamine-6-phosphate deacetylase	*nagA*	0.97
M5005_Spy_1574	Universal stress protein family		2.05
M5005_Spy_1575	Quinolone resistance protein	*norA*	2.33
M5005_Spy_1746	PTS, cellobiose-specific IIA component	*celA*	1.02

[a] Log_2 fold changes were determined by comparing CDM-glu/CDM-fru values

[b] Entries in boldface type indicatemthe fruRBA operon

* shading indicates metabolic genes

generating the 5448.Δ*fruR*, 5448.Δ*fruB*, and 5448.Δ*fruA* mutant strains (**Table 3.1**). These mutations subsequently were verified by PCR (data not shown). Due to the translational overlap between the genes in the *fru* operon, we wanted to further ensure that the mutations generated for each individual gene did not influence the expression of the gene downstream.

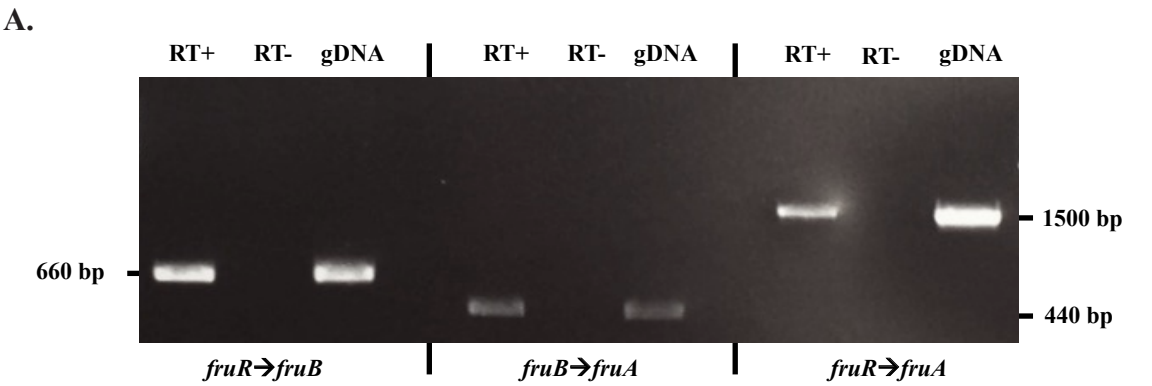
A.
RT+
RT-
gDNA
RT+
RT-
gDNA
RT+
RT-
gDNA
1500 bp
660 bp
440 bp
fruR→fruB
fruB→fruA
fruR→fruA

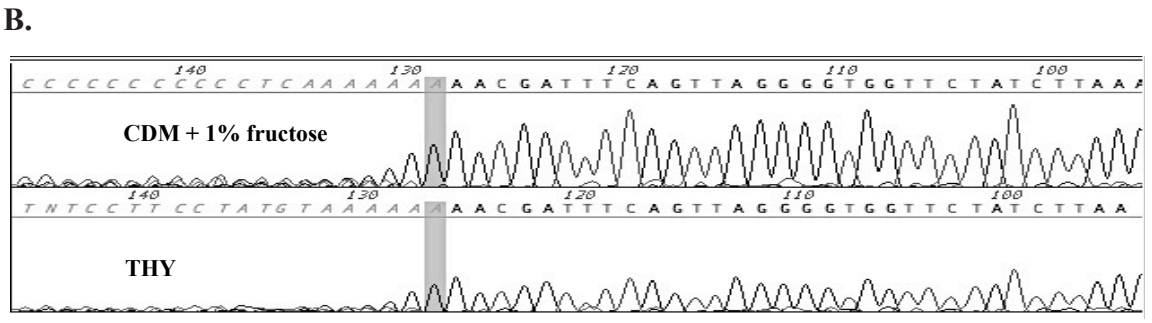
B.
CDM + 1% fructose
THY

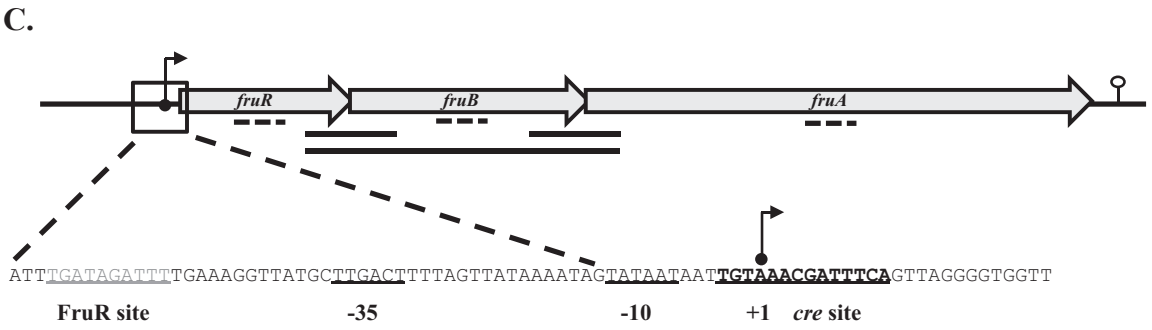
C.
fruR
fruB
fruA
ATTTGATAGATTTTGAAAGGTTATGCTTGACTTTTAGTTATAAAATAGTATAATAATTGTAAACGATTTCAGTTAGGGGTGGTT
FruR site
-35
-10
+1
cre site

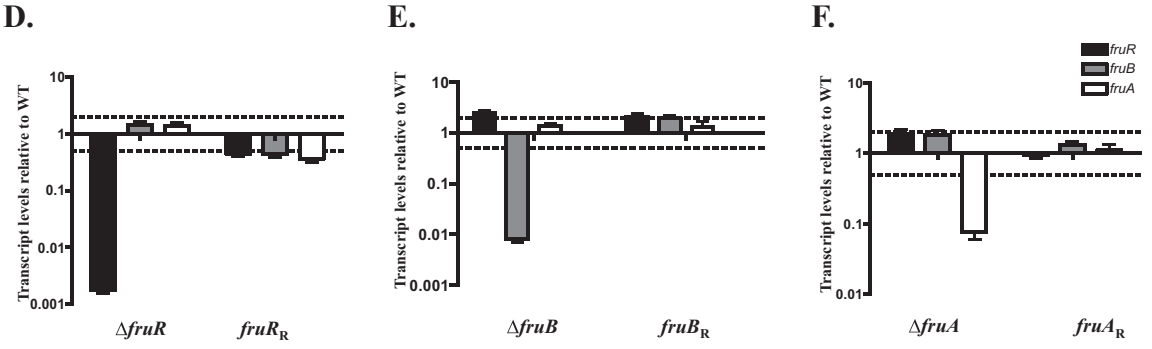
D.
E.
F.
Transcript levels relative to WT
ΔfruR
fruR_R
ΔfruB
fruB_R
ΔfruA
fruA_R
fruR
fruB
fruA

Figure 6.3 *fruRBA* is an operon in GAS M1T1 5448 (A) RT-PCR on RNA isolated from 5448 grown in CDM + 1% fructose demonstrating transcriptional linkage between *fruR/fruB*, *fruB/fruA*, and *fruR/fruA*. Reactions were run using specific primers (**Table 3.1**) either with reverse transcriptase (+RT), without reverse transcriptase (-RT) as a negative control, and using genomic DNA (gDNA) as a positive control. Expected sizes of bands are indicated. **(B)** The transcriptional start site (+1) was determined by 5'-RACE and subsequent DNA sequencing (gray bar) from 5448 grown in THY and CDM + 1% fructose. **(C)** Genetic organization of *fruR* (encoding a transcriptional regulator), *fruB* (encoding 1-phosphofructokinase), and *fruA* (encod ing PTS fructose-specific EIIABC) is shown. The magnified region indicates promoter sequences, including putative FruR and CcpA (*cre*) binding sites (underlined). Solid lines indicate transcription linkage found by RT-PCR. Dashed lines represent probes for qRT-PCR to measure transcript levels. The transcriptional start site is indicated by an arrow, and the 10 and 35 positions are shown. (**D to F**) Real-time qPCR analyses of relative transcript levels for each gene in the *fru* operon in individual mutants and their respective rescue strains in *fruR* (**D**), *fruB* (**E**), and *fruA* (**F**) compared to levels for wild-type 5448 grown in THY to late log phase. Probes targeted gene regions as indicated by the dotted line in panel A. Error bars represent the standard errors from three biological replicates. Dashed lines indicate 2-fold significance. Significance was determined using comparisons of transcript levels relative to those of the *gyrA* gene. *Performed by K.M.V

qRT-PCR was utilized to assess this using probes centered on each gene, as shown in **Fig. 6.3C**, for each individual mutant with RNA isolated during late-logarithmic phase in THY. The data for *fruR, fruB*, and *fruA* mutants show that the transcript levels for each mutant were significantly reduced (**Fig. 6.3D-F**). Revertant strains for each mutant restored the transcript levels of that gene. Importantly, the transcript levels of the other genes in the operon were unaffected by other individual mutations, as expected due to the operon being under CCR in THY. Thus, the mutations made in the *fru* operon genes were nonpolar, and their transcript levels could be restored via reversion (**Fig 6.3D-F**).

FruR is a repressor of the *fruRBA* operon

In other streptococci, *fruR* encodes a putative DeoR-like repressor in the family of carbohydrate regulatory proteins (Loo *et al*., 2003, Barriere *et al.*, 2005, Wen *et al*., 2001). To confirm that FruR is a repressor of the *fru* operon, we grew wild-type 5448 and the 5448.Δ*fruR* mutant under both catabolite-repressing (glucose) and inducing (fructose) conditions in order to isolate RNA for qRT-PCR. Growth in CDM plus 0.5% glucose (**Fig.**

6.4A) was successful; however, when fructose was the sole carbon source available, the *fruR* strain failed to grow (**Fig. 6.4A and 6.8B**). In order to generate appropriate cell density to extract RNA, we applied a modified diauxic growth condition. Both the WT and the *fruR* strain were grown in CDM plus 0.5% glucose to late logarithmic phase, washed twice, and transferred for growth in either CDM plus 1% fructose or CDM plus 0.5% glucose for 1 h. qPCR was used to determine the effect of the 5448.Δ*fruR* mutant on the transcription of *fruB* and *fruA* using RNA from cells grown in either fructose or glucose. When we compared WT 5448 growth in glucose to that in fructose, we saw an increase in transcript levels across the entire operon (**Fig. 6.4B**, black bars), mirroring what we saw in the RNA-Seq results (**Table 6.1**). Comparing WT 5448 grown in fructose to the 5448.Δ*fruR* mutant grown in fructose, an increase in *fruB* and *fruA* transcript levels is observed, indicating that FruR acts as a repressor of this operon (**Fig. 6.4B**, checkered bars). Furthermore, an even larger increase in transcript levels for *fruB* and *fruA* in the 5448.Δ*fruR* mutant was observed when it was grown in glucose than when it was grown in fructose, indicating that the operon is also under carbon catabolite repression (CCR) (**Fig. 6.4B**, diagonal bars).

To confirm the role of FruR in the repression of the *fru* operon, a luciferase reporter assay was performed using the mapped promoter region of the operon (P*fruR*). A significant increase in luciferase activity was observed only when WT 5448 containing the P*fruR*-*luc* construct was grown in CDM plus 1% fructose as opposed to 0.5% glucose or 1% sucrose or mannose (**Fig. 6.4C**), indicating the induction of the operon is fructose dependent. When the same assay was performed in the *fruR* background, there was an overall increase in luciferase activity for all sugars tested (**Fig. 6.4C**). Therefore, both FruR and CcpA negatively control the expression of the *fru* operon, and fructose (after conversion to fructose-1-phosphate) likely acts as an inducer of the operon through inactivation of FruR.

FruA is required for optimal growth and utilization of fructose by GAS 5448

FruA is predicted to be a fusion of the EIIA, EIIB, and EIIC enzyme subunits

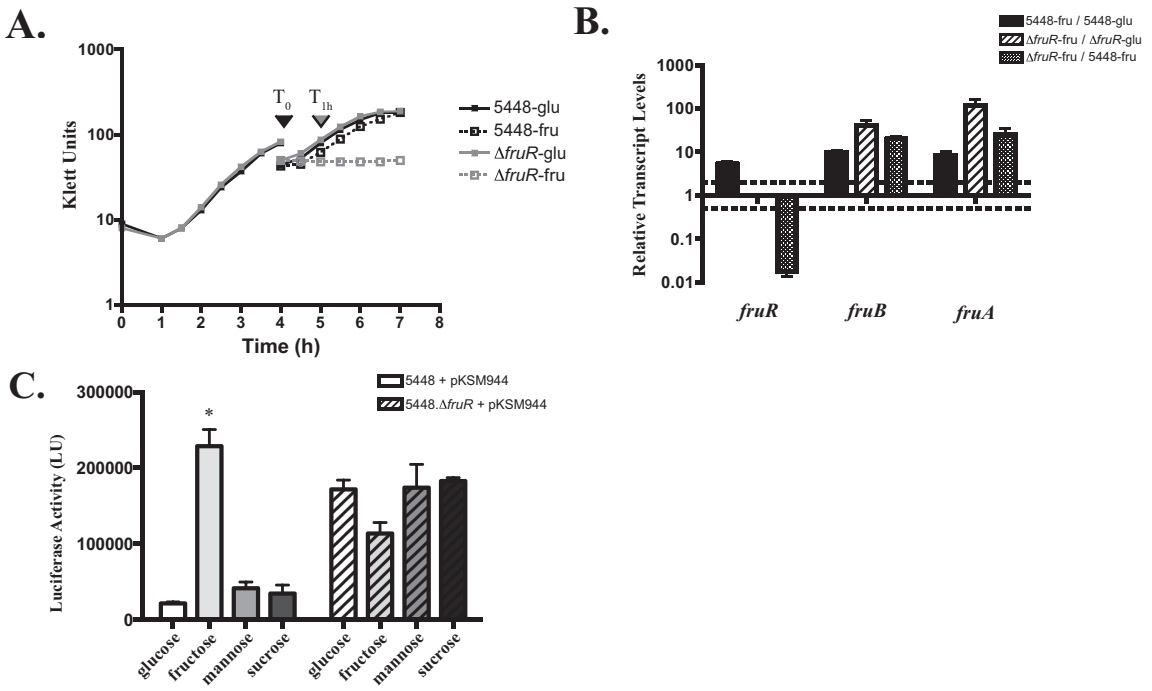

Figure 6.4. FruR represses expression of the *fruRBA* operon. (A) Growth of 5448 (black) or the 5448.Δ*fruR* mutant (gray) strain under modified diauxic conditions. Cells were grown in CDM plus 0.5% glucose (solid line) to late log phase (T_o), washed, and transferred into CDM with either 0.5% glucose (solid line) or 1% fructose (dashed line). Cells were outgrown for 1 h (T_{1h}) in either sugar for RNA extraction. **(B)** Transcript levels of *fru* operon genes were measured by qRT- PCR with respect to growth condition. 5448 grown in fructose compared to growth in glucose (black bars), the 5448.Δ*fruR* mutant grown in fructose compared to growth in glucose (diagonal bars), and the 5448.Δ*fruR* mutant grown in fructose compared to growth in WT 5448 (checkered bars) are shown. Error bars represent the standard errors from two biological replicates. Differences greater than 2-fold in expression for the mutant compared with that of the wild type (denoted by a dashed line) are considered significant. Significance was determined using comparisons of transcript levels relative to those of the gene *gyrA*. (C) P*fruR* promoter activity in WT 5448 containing the P*fruR-luc* luciferase reporter plasmid was grown in CDM containing 0.5% glucose or 1% fructose, mannose, or sucrose. Samples were taken at the mid-logarithmic phase of growth and assayed for luciferase production, expressed in relative luciferase units (LU). Error bars represent means standard deviations (SD) of results from three biological replicates performed in triplicate. Significance for panel C was determined by comparison of results for growth in fructose, mannose, or sucrose to those for growth in glucose using an unpaired t test ($P<0.001$). *Performed by K.M.V.

of a fructose-specific PTS EII involved in import and concomitant phosphorylation of fructose. To confirm the role of FruA in the utilization of fructose, the 5448.Δ*fruA* mutant was grown on a panel of PTS sugars and compared to the parental GAS 5448. In order to establish what PTS sugars are amenable to 5448 growth, growth curves in CDM supplemented with a 1% (0.5% for glucose) concentration of 11 readily available PTS sugars were determined (**Fig. 6.5A**). WT 5448 was able to grow in 9 of the 11 PTS sugars tested; however, mannitol and cellobiose were not conducive to significant growth of 5448 and were eliminated from further analysis. When 5448.Δ*fruA* was grown in the remaining 9 PTS sugars, only fructose resulted in reduced growth (**Fig. 6.5B and C; Fig 6.6**). Importantly, reversion of the *fruA* mutation (5448.Δ$fruA_R$) restored growth in fructose back to wild-type levels (**Fig. 6.5C; Fig. 6.6**). Both 5448.*fruR* and 5448.*fruB* strains also displayed significant growth defects in CDM supplemented with 1% fructose that were restored in the revertant, but had growth comparable to 5448 in the rich media THY (**Fig. 6.7**). These data suggest that FruA is the primary EII transporter of fructose in GAS 5448 and that FruB and FruR also are required for growth on fructose as the sole carbon source.

We also wanted to ascertain if *fruA* affects the utilization of other carbon sources, as many EIIs were shown to affect the metabolism of multiple carbon sources (see Chapter 4). We used Biolog PM1 and PM2A phenotype microarrays (PMs) to monitor the metabolism of 190 different carbon sources of the *fruA* strain. The parental GAS 5448 and 5448.Δ*fruA* strains were different in their utilization of 72 carbon sources (data not shown), 3 of which are designated PTS sugars (N-acetyl-D-galactosamine, cellobiose, and mannitol) (**Table 6.2**). Surprisingly, fructose was not identified in the Biolog assay as having a defect in metabolism (**Table 6.2**). This suggests that there is another PTS transporter that is able to transport fructose, although at levels that do not sustain wild-type growth (**Fig. 6.6**). To confirm this observation, wild-type 5448 and 5448.Δ*fruA* strains also were tested using a bioMérieux API®50 strip that tests the utilization of a subset of 49 carbohydrates (**Fig. 6.8**).

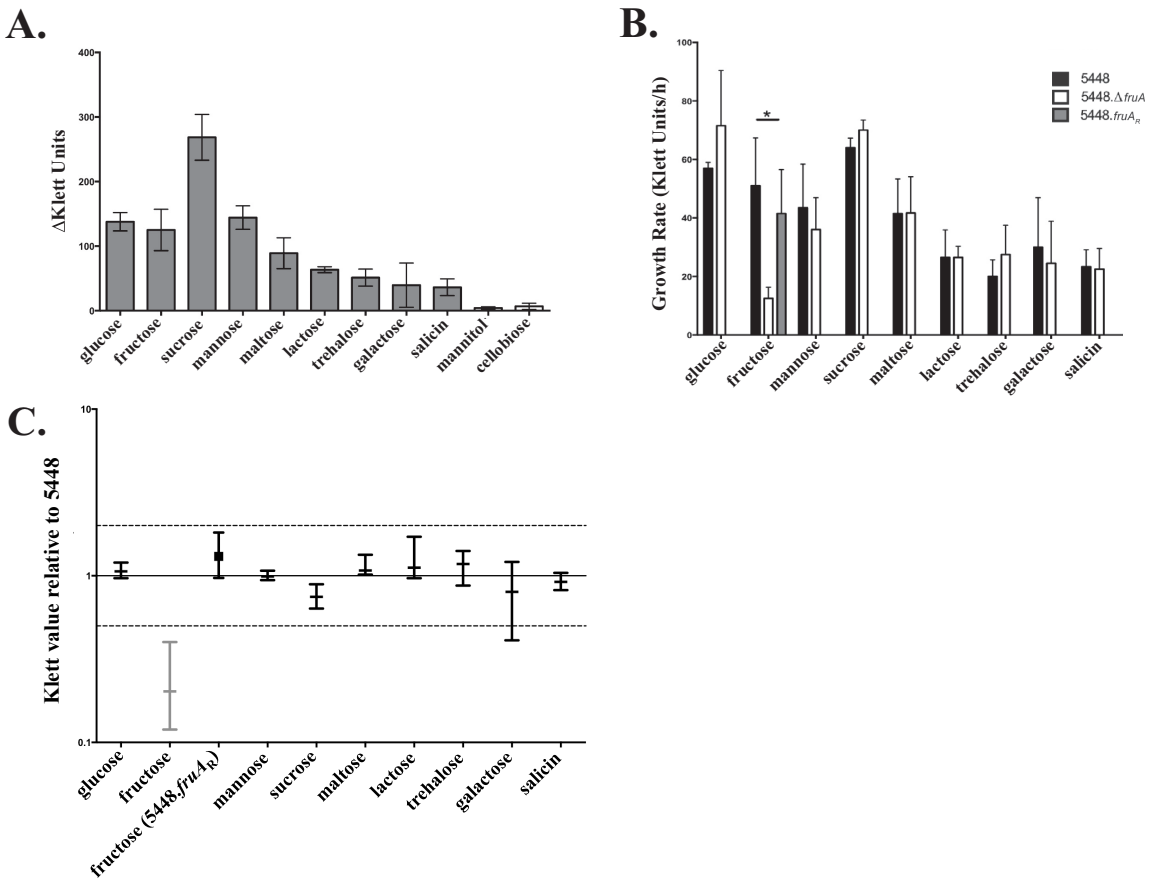

Figure 6.5 Growth analysis of 5448 and *fru* operon mutants in PTS sugars. (A) Total yield was calculated for GAS 5448 grown for 26 h at 37°C with 5% CO2 in various PTS sugars as the sole carbon source. **(B)** Growth rates were determined for 5448 (black bars) and 5448.Δ*fruA* (white bars) strains in 9 PTS sugars. The growth of the $fruA_R$ revertant (gray bar) was assessed for fructose only. Error bars represent standard errors of the means from three biological replicates. Statistical analysis was performed using an unpaired t test. **(C)** Growth curve comparison of 5448 to 5448.Δ*fruA* across time. Klett unit relative to 5448 at each time point was calculated by taking the percent WT of each individual time point, and plotting the median percent WT along with the interquartile range (25-75% of the data set). Black bars represent sugars in which 5448.Δ*fruA* grows similarly to the parental 5448. Gray bars indicate sugars in which 5448.Δ*fruA* grows poorly compared to 5448. Black square represents growth comparison of 5448.Δ$fruA_R$ to wildtype. Dashed lines represent 2-fold growth above and below 5448.

As seen with Biolog, the 5448.Δ*fruA* strain was able to utilize fructose similarly to 5448 in this assay; however, the fructose utilization is insufficient to support growth. We also tested 5448.Δ*fruB* and 5448.Δ*fruR* strains using the API®50 strips. Like the 5448.Δ*fruA* strain, both the *fruR* and *fruB* mutants were able to utilize fructose, even though neither was able to

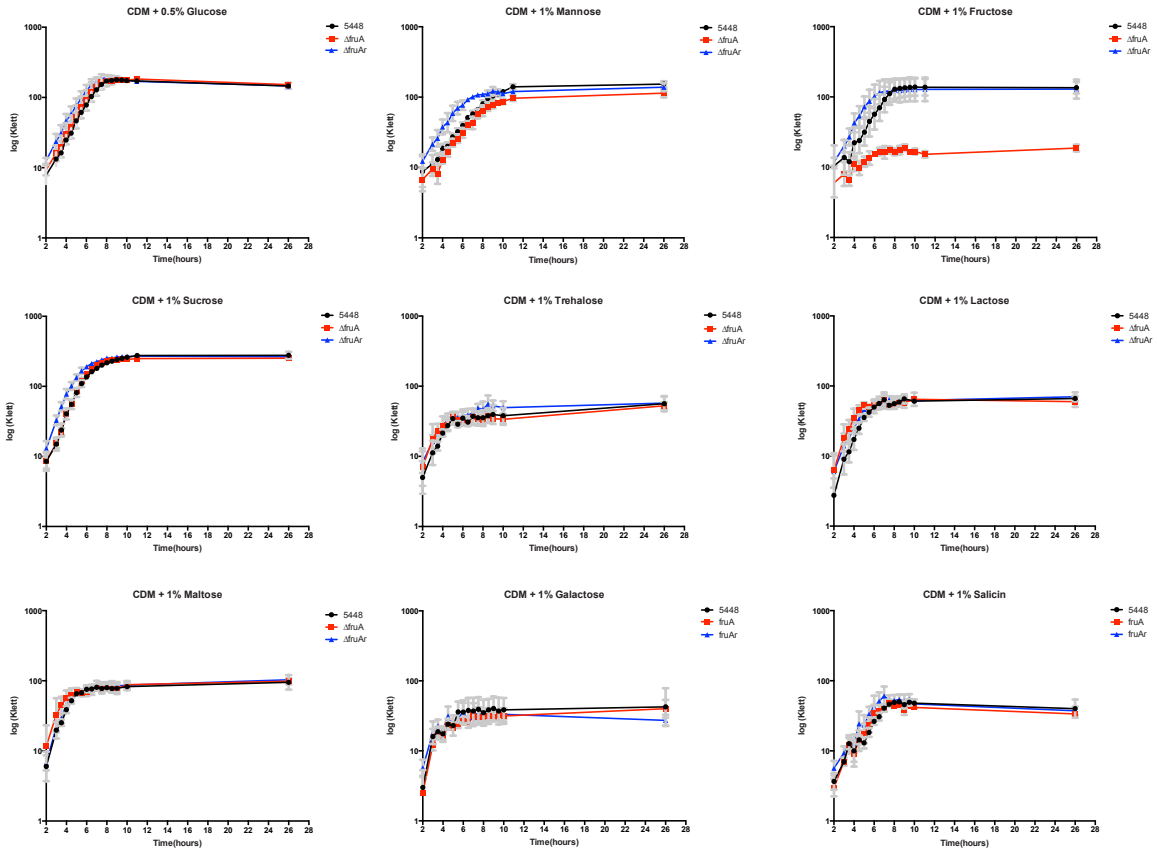

Figure 6.6 Δ*fruA* has diminished growth in fructose as the sole carbon source. 5448 (black), Δ*fruA* (red), and Δ$fruA_R$ (blue) were grown in CDM + 1% PTS carbohydrate (0.5% glucose) for 26 hours. Error bars represent the standard error of the mean of at least three biological replicates. Only carbohydrates that facilitate growth of 5448 are shown.

grow on fructose as the sole carbon source (**Fig. 6.8**). Taken together, these data suggest that *fruA* is required for optimal growth on fructose and that FruA is the main fructose transporter for GAS. Since a PTS-defective mutant (Δ*ptsI*) of M1T1 GAS is defective for the utilization of fructose in the Biolog assay (Gera *et al.*, 2014),there appears to be another PTS EII that is able to transport fructose to be metabolized, albeit not at the levels necessary to support GAS growth on fructose. Finally, the loss of *fruA* affects the utilization of other carbon sources; however, this is unsurprising, because a *ptsI* mutant also affects the utilization of non-PTS carbon sources through currently unknown mechanisms (Gera *et al.*, 2014).

Effect of fructose on *sloR*

The RNA-Seq data (**Table 6.1**) showed that several members of the SerR regulon

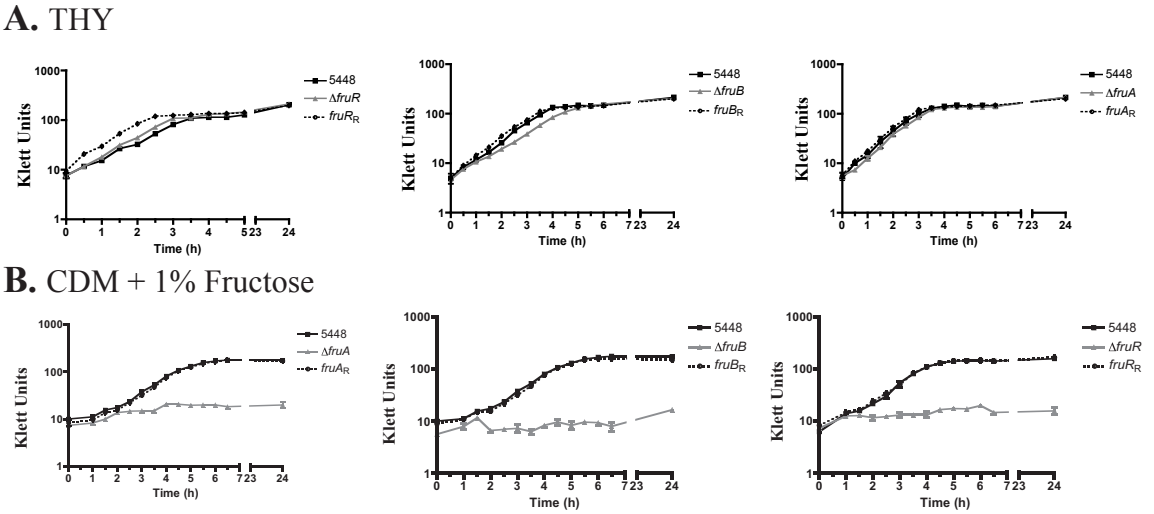

Figure 6.7 Growth curves for the 5448.Δ*fruR* mutant and its 5448.Δ*fruR*$_R$ revertant, 5448.Δ*fruB* mutant and its 5448.Δ*fruB*$_R$ revertant, and 5448.Δ*fruA* and its 5448.Δ*fruA*$_R$ revertant. Growth in **(A)** THY or **(B)** chemically defined medium (CDM) supplemented with 1% fructose were measured by absorbance using a Klett-Summerson colorimeter (Klett units). Data are representative of three independent experiments.

(LaSarre & Federle, 2011) were up-regulated in fructose, including *sloR*, the putative streptolysin O regulator (Savic *et al.*, 2002). *In silico* analysis of SloR showed nine transmembrane domains that exhibited a high degree of homology to a fructose-specific EIIC. Given that a *fruA* mutant still could utilize fructose (**Table 6.2 and Fig. 6.8**), we wanted to explore the role of SloR in fructose utilization and transport in addition to confirming its regulation in fructose. An insertional inactivation mutant of *sloR* (5448. Δ*sloR* strain; **Table 3.1**) was generated using a temperature-sensitive replicating plasmid. The growth of the 5448.Δ*sloR* mutant in CDM plus 1% fructose was found to be comparable to that of wild-type 5448 (**Fig. 6.9B**), suggesting that SloR does not play a role in fructose uptake. We also tested the effect SloR had on the metabolism of other sugar sources using the API®50 assay, and we saw no observable difference between a *sloR* strain and wild-type 5448 (data not shown). Additionally, an expression reporter plasmid was constructed by cloning the promoter of *sloR* (P*sloR*) upstream of the firefly luciferase gene (*luc*), and activity was determined through the quantification of relative luciferase units (LU). A significant increase in P*sloR*-luciferase activity was observed when cells were grown in

Table 6.2. Carbon Sources with altered utilization in 5448.Δ*fruA*

Carbon source[a]	Result for[b]: 5448	5448.Δ*fruA* mutant
***N*-Acetyl-D-galactosamine**	**+**	**+/−**
D-Cellobiose	**+**	**+/−**
D-Mannitol	**+**	**+/−**
D-Galactose	+	+
D-Fructose	+	+
α-D-Glucose	+	+
D-Mannose	+	+
Sucrose	+	+
α-D-Lactose	+	+
Maltose	+	+
Salicin	+	+
D-Trehalose	+	+
β-Methyl-D-glucoside	+	+
Maltotriose	+	+

[a] Only PTS carbon sources are listed.
[b] +, Omnilog value (OV) of >200; +/−, 125 < OV < 200; −, OV < 125. Carbon sources with differences in utilization are set in boldface type.

fructose compared to sucrose (**Fig 6.9A**). To rule out that FruR regulates *sloR*, we also tested *sloR* transcript levels in a Δ*fruR* strain grown in fructose and glucose using qPCR and saw no observable difference (data not shown). Taken together, we show that *sloR* induction is a fructose-specific phenotype; however, this induction is independent of FruR. We also show that *sloR* is not an alternative transporter of fructose.

FruA in 5448 has different role than in 5005

We strived to determine if the differences in the role of *fruA* in the survival of GAS in whole human blood was a result of the different influences in metabolism between MGAS5005 and 5448. Unlike ΔMannose, where the parental strain determined the influence on PTS carbohydrate metabolism, Δ*fruA* was only impaired on growth on fructose in both strains (**Fig 6.6,** see chapter 4). Although ΔFructose seems to grow slightly better in glucose and lactose (see chapter 4), the extent of metabolic differences of the mutant between both M1T1s is relatively small compared to ΔMannose. This can be seen in utilization as well, where although 5448.Δ*fruA* has slightly altered utilization of CH3-αD-Glucopyranoside, cellobiose, starch, and glycogen when compared ΔFructose as both are compared to their respective wildtype (**Fig 6.8**; see chapter 4), these differences

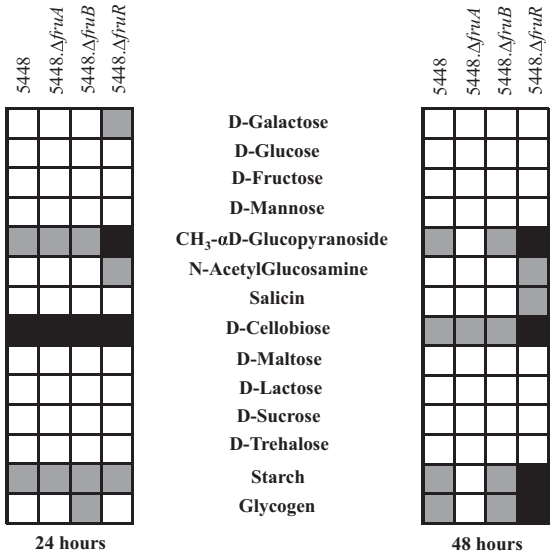

Figure 6.8 Limited carbohydrate metabolism profile of 5448 and the *fru* operon mutants. Wild-type 5448 and the 5448.Δ*fruA*, 5448.Δ*fruB*, and 5448.Δ*fruR* mutants were assayed using API®50 CH results after incubation at 37°C for 24 h and 48 h. Listed are select carbon sources from a panel of 49 carbohydrate sources: complete utilization (white boxes), partial utilization (gray boxes), and no utilization (black boxes) based on the colorimetric indicator dye shown for each.

are not drastic. This suggests that the differences seen with survival of both mutants in whole human blood may be either unrelated to metabolism, or that there may be an indirect perturbation to GAS virulence that accounts for the difference. Either way, it is clear that EIIs play an important role in GAS pathogenesis, even if not the exact same role in all strains.

Discussion

Our results reveal a fructose-induced *fruRBA* operon that was found to be required for the growth of GAS in fructose and implicate FruA as the primary transporter of fructose in GAS. FruR acts as a repressor at the *fru* operon promoter, likely along with CcpA, to allow for fructose induction of the system. 5448 mutants lacking *fruR* and *fruB*, but not *fruA*, exhibited diminished survvial in whole human blood and greater sensitivity to phagocytic killing by neutrophils and monocytes. Interestingly, this was not the case for ΔFructose (Δ*fruA* in MGAS5005) which had impaired survival in whole human blood. However, this

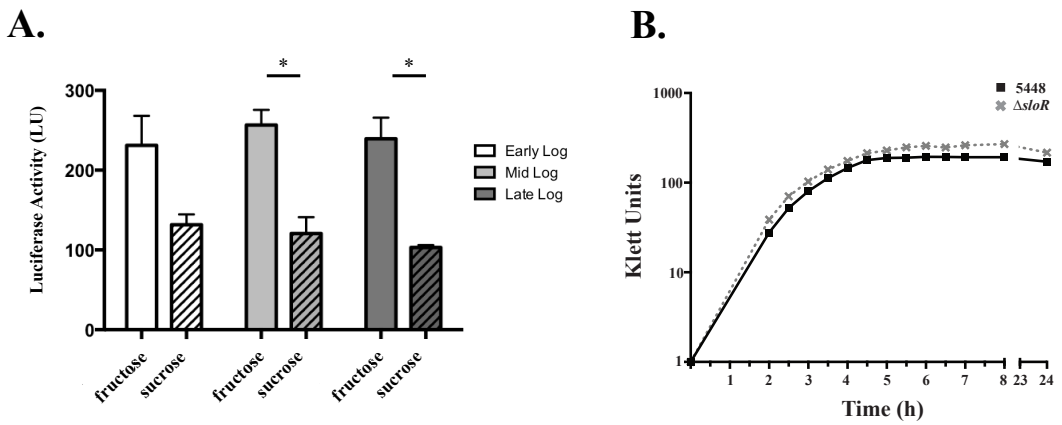

Figure 6.9 The effect of fructose on *sloR*. (A) P*sloR* promoter activity in WT 5448 containing the P*sloR-luc* luciferase reporter plasmid was grown in CDM containing either 1% fructose (solid bars) or sucrose (diagonal bars). Samples were taken at three time points in logarithmic phase of growth (early: white bars; mid: light gray bars; late: dark gray bars) and assayed for luciferase production, expressed in relative luciferase units. Error bars for represent mean ± SD of the results from three biological replicates performed in triplicate. Significance for **(A)** was determined using a Student t test ($p \leq 0.01$). **(B)** Growth of 5448. Δ*sloR* in CDM + 1% fructose compared to 5448. ***(A)** Performed by K.M.V.

discrepancy is most likely not the result of altered metabolic roles of *fruA* in both strains.

Fructose-induced regulon of GAS

Metabolic genes for utilization of alternative (non-glucose) sugars typically are induced only during times of low glucose (derepression of CCR) and in the presence of the inducing sugar. For pathogenic streptococci and related low-GC Gram-positive bacteria, a genome-wide fructose-induced regulon previously has been determined only for *Streptococcus mutans* and the probiotic *Lactobacillus acidophilus* (Ajdic & Pham, 2007, Barrangou *et al.*, 2006). In *S. mutans*, microarray analysis revealed 68 genes (3.5% of genome) that were differentially expressed at least 2-fold in fructose compared to expression in glucose, whereas a similar analysis in *L. acidophilus* found that 110 genes (6% of the genome) were regulated. Our RNA- Seq analysis discovered that GAS in CDM with fructose affected the transcription of roughly 5.5% of the nonprophage genome (102 genes) compared to growth in glucose (**Table 6.1**). This is in line with what was observed in both *L. acidophilus* and *S. mutans*, highlighting a fairly focused fructose-specific response

Table 6.3 Differences in phenotypes between Δ*fruA* mutants in two M1T1 strains

5448Δ*fruA*	ΔFructose (Δ*fruA* in MGAS5005)
Decreased growth in fructose	Decreased growth in fructose
Increased utilization of CH_3-αD-Glucopyranoside (+/- vs +)	Increased growth in glucose
Increased utilization of starch (+/- vs +)	Increased growth in lactose
Increased utilization of glycogen (+/- vs +)	Decreased survival in whole human blood

in these cells.

The most highly fructose-induced genes in GAS were *fruRBA*, followed by several other sugar-specific PTS operons, such as *lacD.1* and *lacD.2*. The comparable *L. acidophilus fruRBA* genes also were highly induced by fructose (Barrangou *et al.,* 2006). In contrast, the *S. mutans* genes for *fruRBA* (Smu.0870-72) were constitutively expressed, and a separate mannose/fructose family PTS was found to be inducible (Ajdic & Pham, 2007). There are three potential mechanisms by which fructose could enter GAS cells. (i) The predominant pathway in Gram-positive bacteria involves the canonical PTS^{fru} EIIABC (*fruA-fruI*), a 1-phosphofructokinase (*fruB-fruK*), and a fructose-responsive regulator (*fruR*). (ii) An alternate PTS recognizes and translocates fructose as fructose-6-phosphate (F6P) with lower affinities than those of pathway i. (iii) Facilitated diffusion transport using a membrane-spanning permease would esterify free fructose at position 6 using ATP (Kornberg, 2001). The induction of *fruRBA* by fructose in GAS suggests pathway i is the main pathway; however, the induction of other PTSs (e.g., *lacD.1* and *lacD.2*) suggests that pathway ii also plays a role in fructose utilization. This is supported by the fact that mutants lacking any of the *fruRBA* genes still are able to metabolize fructose (**Fig. 6.8 and Table 6.2**), albeit not to a level that supports growth (**Fig. 6.7B**). Thus, the role of other PTS operons in the utilization of fructose will need to be explored further.

We also observed an increase in the expression of genes in the serine catabolism regulon, including *sloR, sdhAB*, and *ntpA-K* (LaSarre & Federle, 2011). We further validated the fructose induction of *sloR* expression via qPCR (data not shown) and through promoter-luciferase fusions (**Fig. 6.5A**). SloR initially was implicated in streptolysin O

expression (Savic *et al*., 2002), but more recently it was shown to be involved in serine acquisition (LaSarre & Federle, 2011). However, SloR shows significant homology to a fructose EIIC transporter (Kelley & Sternberg, 2009), suggesting that it plays a role in the transport of fructose (pathway ii described above, i.e., intake as F6P) and potentially aids in signal transduction to coordinate gene expression. However, a *sloR* mutant did not show any significant effect on the utilization of fructose or any other PTS sugar by GAS (data not shown). In other *Streptococcus* and *Listeria* species, orphan EIICs have been suggested to act as environmental sensors that interact with other regulatory proteins to influence gene expression (Van den Bogert *et al*., 2013, Kreft & Vazquez-Boland, 2001). It is possible that SloR serves a similar sensory role in GAS, and this hypothesis is being explored.

Role of the *fruRBA* operon in fructose metabolism in 5448.

(i) FruA. The GAS M1T1 genome is predicted to encode 14 sugar-specific EII translocation components of the PTS. As seen in chapter 4, homology and subsequent annotation do not necessarily clearly indicate functionality. In this study, we characterized fructose utilization and the contribution of the *fruRBA* operon, confirming its annotated role in fructose metabolism. We found that an in-frame mutant of *fruA* (5448.Δ*fruA* strain), encoding the putative PTS EIIABC, exhibited a significant growth defect compared to the WT (5448), but it did show some residual growth on fructose (**Fig. 6.6**). Nonpolar mutants of *fruB* (5448.Δ*fruB* strain), encoding 1-phosphofructokinase, and *fruR* (5448.Δ*fruR* strain), a putative repressor, also showed a comparable defect in growth on fructose, confirming that the entire *fru* operon is necessary for total fructose utilization in GAS. As mentioned above, the residual growth and utilization of fructose may involve other PTS EII pathways (**Fig. 6.7B and Table 6.2**). However, since *fruRBA* is the only operon in the 5448 genome that encodes a 1-phosphofructokinase (M5005_Spy_0061; FruB), it strongly suggests that this operon, through FruA, is the primary operon for fructose transport utilization (Ferenci & Kornberg, 1971). This has been observed in several other other Gram-positive

bacterial species (Loo *et al.*, 2003, Barriere *et al*., 2005, Wen *et al*., 2001, Voigt *et al.*, 2014)

(ii) FruR. The DeoR-family transcriptional regulator FruR is directly involved in the repression of the *fru* operon in *L. lactis* (Barriere *et al*., 2005) and other Gram-positive bacteria (Loo *et al*., 2003, Wen *et al.*, 2001, Voigt *et al*., 2014). Through transcriptional analysis of the 5448.Δ*fruR* mutant and its 5448.Δ$fruR_R$ rescue strain, we demonstrated that FruR represses the transcription of the *fruRBA* operon through the *fru* promoter (P*fru*) and that the promoter is required for fructose induction (**Fig. 6.4**). Furthermore, the expression of the operon exhibits evidence of CCR, likely through a CcpA-mediated CCR mechanism. *In silico* analysis of the *fruR* promoter region identified the presence of a putative FruR binding site (Barriere *et al.*, 2005) upstream of the 35 hexamer and a catabolite response element (*cre*) site for CcpA binding (Kinkel & McIver, 2008, Shelburne *et al*., 2008a, Kietzman & Caparon, 2010) overlapping the start of transcription (**Fig. 5.3C**). The physiological inducer of FruR de-repression is fructose-1-phosphate (F1P), and 1 mM F1P is sufficient to disrupt FruR binding to its operator in *Pseudomonas putida* (Chavarria *et al.*, 2014, Chavarria *et al*., 2011). Fructose-1-phosphate is also the inducer of the *fruRBA* operon in other Gram-positive species, such as *L. lactis* (Barriere *et al.*, 2005). This correlates with FruR being a member of the DeoR family of repressors, which typically are induced by sugar phosphates produced by the regulatory pathway they control (Barriere *et al.*, 2005, Loo *et al.*, 2003, Deutscher *et al*., 2006). Surpringly we found that 5448.Δ*fruR* is unable to grow on fructose. We surmise that this is becaused of the overexpression of *fruB* and *fruA* , leading to an increase in fructose transport and metabolism. This can potentially lead to growth arrest as this would create an imbalance of intracellular metabolites. It is also possible that FruR regulates other importnat genes for GAS growth.

(iii) FruB. 1-phosphofructokinase (*fruB*) converts imported F1P to fructose-1,6-bisphosphate (FBP), and our data show that it is also necessary for GAS growth on fructose

(**Fig. 6.7B**). This is likely due to the fact that the *fruB* mutant (5448.Δ*fruB* strain) would be expected to build up F1P due to an inability to convert it to FBP following transport by FruA. Since the majority of intracellular fructose cannot be further metabolized, the generation of FBP for glycolysis would be blocked, resulting in growth arrest. The *fruB* mutant (5448.Δ*fruB* strain) also exhibited a small-colony phenotype when plated on blood agar (**see Fig.6.2B**) and showed a slightly longer doubling time than the parental 5448 and its 5448.Δ$fruB_R$ revertant, implicating this enzyme in playing a role outside the conversion of F1P to FBP. Although other PTS EII pathways exist in GAS that allow for the transport of fructose as F6P, as demonstrated by both the RNA-Seq and Biolog/API®50 CH metabolic data (**Tables 6.1 and 6.2 and Fig. 6.8**), the efficiency of transport is not able to support growth. In addition, when fructose is transported by alternative PTSs (pathway ii described above), a 6-phosphofructokinase (*pfkA*) enzyme would need to be present to convert F6P to FBP (Kornberg, 2001). However, *pfkA* was not upregulated when GAS was grown in fructose as the sole carbon source (**Table 6.1**).

Alternate influences of *fruA* on GAS survival in whole human blood unlikely to be related to metabolism

We discovered that 5448.Δ*fruA* is unaffected in survival in whole human blood, but was not the case for ΔFructose (Δ*fruA* in MGAS5005). We metabolically characterized 5448.Δ*fruA* to determine if there were drastic alterations in its influence on PTS carbohydrate metabolism. Potentially, this could explain the difference in survival in whole human blood between the two mutants, as could be the case for differences in hemolytic activity with the mannose-specific EII subunit mutants in MGAS5005 and 5448. However, unlike with those mutants, Δ*fruA* in both MGAS5005 and 5448 essentially only affect the metabolism of fructose (**Table 6.3**). Although there are slight differences in some carbohydrates' metabolism between the two mutants as compared to their parental strains, this is unlikely to explain the stark difference seen in survival in whole human blood since they are subtle (**Table 6.3**). Rather, it is more likely that fructose metabolism may influence the GAS

regulon differently in MGAS5005 than in 5448, and preventing fructose metabolism through the deletion of *fruA* subsequently has different impacts in the two strains. Gene regulation and genetic interaction differences between MGAS5005 and 5448 is an area we are currently exploring to understand the importance of a strain background for the context of the role of identical proteins.

Chapter 7: Assessing the Importance of PTS and non-PTS Glucose Utilization Pathways in GAS Pathogenesis

Introduction

Glucose is abundant in nature. In the human body alone, glucose is present in 32 of 43 biofluids or tissues studied so far, with the highest concentrations usually found in blood (Wishart *et. al*, 2013, Wishart *et. al*, 2009, Wishart *et. al*, 2007). As a result, human pathogens possess many mechanisms to transport and metabolize glucose (Cvitkovitch *et al*., 1995, Vitko *et al*., 2016). In *S. aureus*, glucose can be metabolized either through the PTS or through a glucokinase, as a double mutant of both genes was unable to grow in glucose alone. Additionally, alterations to efficient glucose metabolism in this pathogen negatively affected pathogenesis (Vitko *et al.*, 2016). Although little is known about glucose metabolism in GAS, it is hypothesized to be transported through the phosphoenolpyruvate-dependent phosphotransferase system (PTS), as shown in *S. pneumonaie* (Vitko *et al.*, 2016) and deletion of some PTS transporters also leads to altered metabolism of glucose, strengthening this premise (Chapter 4). The GAS genome also encodes for a glucokinase (*nagC*), as well as a non-PTS glucose transporter (*glcU*), presumably for glucose transport and metabolism that is PTS independent. However, the actual contribution of each pathway to overall glucose metabolism has not been investigated.

SLS-mediated hemolysis was shown to be under the influence of the PTS, as a PTS-null mutation (Δ*ptsI*) led to SLS activity during early exponential phase as compared to early stationary phase for the parental strain MGAS5005 (Gera *et al.*, 2014). We screened an annotated EIIC mutant library in a previous study, and discovered 7 EIIC mutants that had early onset hemolysis during growth as compared to MGAS5005 (Chapter 4). We carried out this screen in an effort to determine if the lack of utilization of a particular PTS carbon source was responsible for the dysregulation of SLS-mediated hemolysis.

There was no carbohydrate whose metabolism was commonly affected in all 7 EIIC mutants that displayed early hemolysis (Chapter 4). However, all of these EIIs do appear in the CcpA regulon (DebRoy *et al.*, 2016) and, considering that a MGAS5005.Δ*ccpA* mutant also exhibits early hemolysis (Kinkel & McIver, 2008, Shelburne *et al.*, 2008), we hypothesized that disruption of efficient glucose metabolism could be the trigger for SLS-mediated hemolysis. This is further strengthened by the fact that Mga was shown to regulate SLS and SLO only in conditions of low glucose, but this regulation disappeared once glucose was added (Valdes, 2016). In this study, we characterized the routes of glucose metabolism and compared their influence on hemolysis, GAS survival in whole human blood, and GAS pathogenesis in a murine skin infection model. We also investigated whether glucose can be metabolized either through the PTS or via a non-PTS metabolic pathway or both, and whose expression are correlated with each other.

Results

MGAS5005.Δ*ptsI* does not regulate hemolytic activity based on sugar concentration

Earlier studies from our group showed that MGAS5005.Δ*ptsI* exhibited early hemolytic activity as compared to MGAS5005 (Gera *et al.*, 2014), likely due to the lack of access to a PTS carbohydrate. However, our screen of the GAS PTS pathways found 7 EIIs to exhibit early hemolytic activity that did not affect the metabolism of a particular carbohydrate (Chapter 4), and all of these EII loci are a part of the CcpA regulon (DebRoy *et al.*, 2016). Although MGAS5005 only exhibits hemolytic activity at late log-stationary phase when preferred sugar concentrations are low, a direct correlation between sugar concentration and hemolytic activity has not been explicitly shown in GAS. Therefore, we grew MGAS5005 in three glucose conditions and assayed at which glucose concentration that hemolysis begins to occur. MGAS5005 and MGAS5005.Δ*ptsI* were grown for 8 h in THY +10% horse serum, horse serum alone, and in whole human blood.

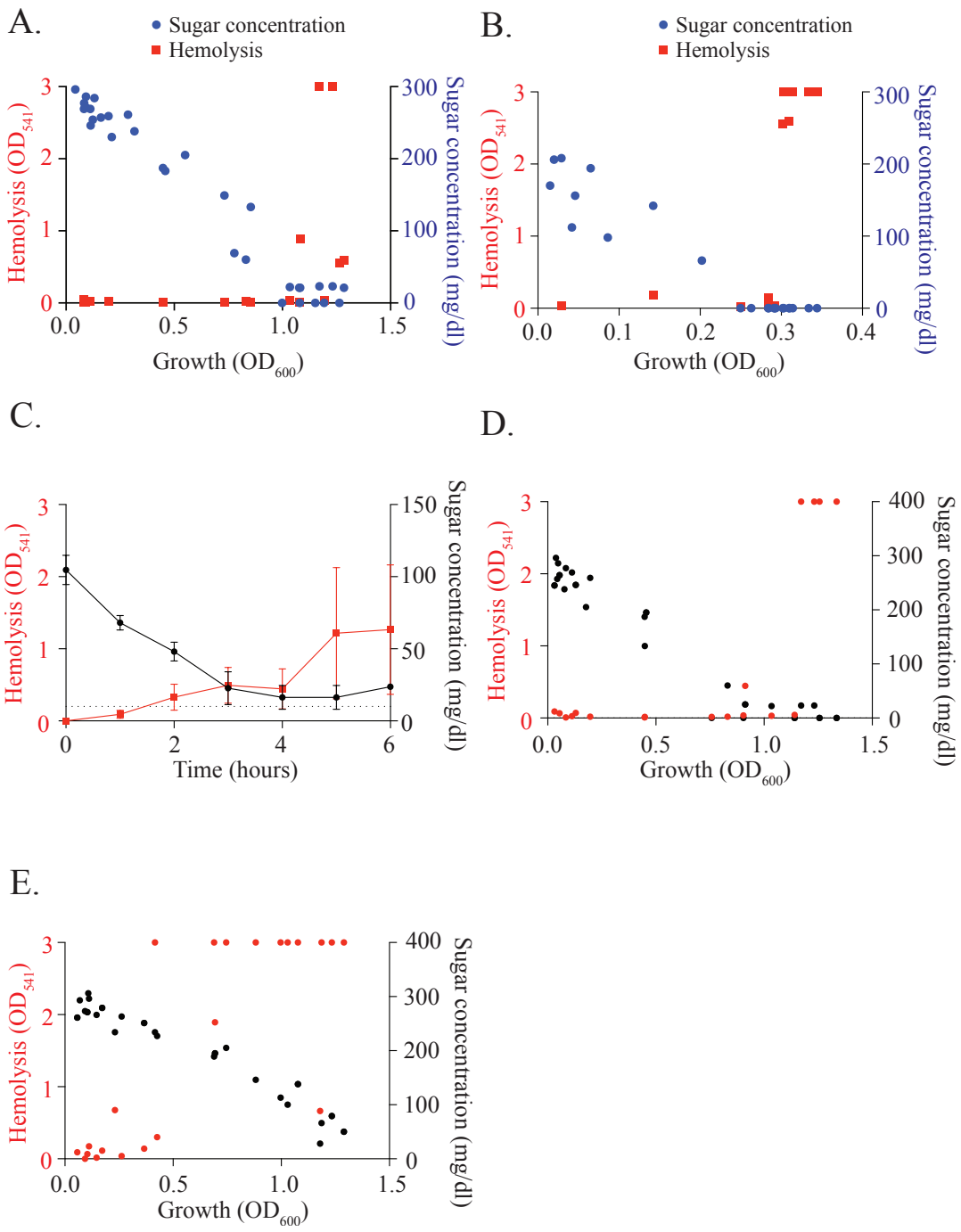

Figure 7.1. Occurrence of hemolysis at low sugar concentration. Sugar concentrations, OD_{600}, and hemolysis was measured as described (see chapter 3). **A)** MGAS5005 grown in THY + 10% horse serum. Blue circles represent sugar concentration. Red squares represent positive hemolysis. **B)** MGAS5005 grown in Horse Serum alone. **C)** GAS grown in whole human blood. **D)** MGAS5005 and MGAS5005.Δ*ptsI* grown in THY + 10% horse serum. Red circles represent hemolytic values, and black circles represent sugar concentrations at each measured OD_{600} for MGAS5005 **(D)** and Δ*ptsI* **(E)**.

Sugar concentrations, hemolytic values, and growth (OD_{600}) were measured as indicated in chapter 3. In all three conditions, MGAS5005 did not display SLS-mediated hemolysis until sugar concentrations was around 50 mg/dl or lower (**Fig. 7.1A-C**). In the MGAS5005.Δ*ptsI* mutant, hemolysis is detectable at sugar concentrations around 200 mg/dl, suggesting that the lack of flux through glucose metabolism may be the trigger for SLS-mediated hemolysis (**Fig 7.1DE**).

Glucose metabolism occurs primarily through the Non-PTS glucokinase NagC

Since regulation of SLS-mediated hemolysis does not seem to be affected by the metabolism of a PTS carbohydrate, but rather by the disruption of glucose-mediated gene regulation, we wanted to characterize the routes of glucose metabolism in MGAS5005. Previously, we had shown that MGAS5005.Δ*ptsI* has no growth defect in CDM + 0.5% glucose, suggesting that the PTS system either does not transport glucose, or that there is an alternate glucose transport system that is specific to glucose in conjunction with the PTS (**Fig 7.2**). To test this theory, we constructed mutants in a putative non-PTS glucose transporter (*glcU*) based on its role in other streptococcal species (Vitko *et al*., 2016), and a putative glucokinase (*nagC*) that would be required to generate glucose-6-phosphate following non-PTS glucose import. The MGAS5005 Δ*glcU* mutant was created by using the pCRS mutagenic system (see chapter 3), while an MGAS5005 Δ*nagC* mutant was created using allelic exchange to replace the glucokinase gene with a kanamycin resistance (*aphA3*) cassette. For both mutants, rescued strains were then created by curing the confirmed mutants of the mutagenic plasmid to restore the wild type genotype. The WT MGAS5005, Δ*glcU*, Δ*nagC* and Δ*ptsI* GAS strains were grown in THY, a glucose-rich media, to evaluate growth defects of each mutant. We included Δ*manMN* (ΔMannose) based on our findings suggesting that the mannose-specific EII is a high affinity glucose transporter (Chapter 5) (Fleming & Camilli, 2016). Growth (ΔOD_{600}) calculated after 24 hours was similar in all strains tested (**Fig 7.3A**). However, the total

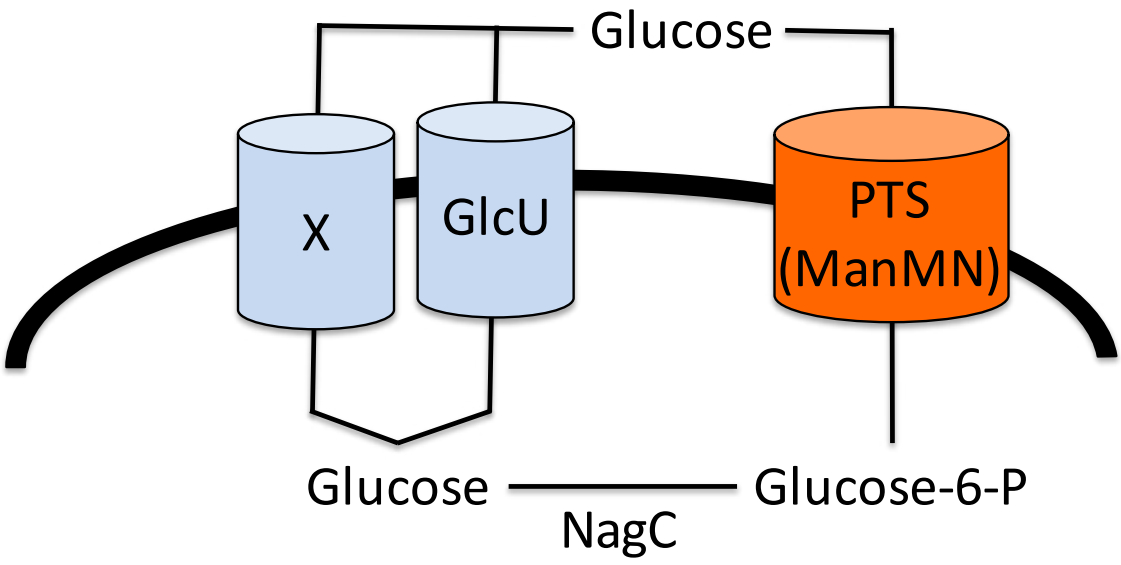

Figure 7.2 Predicted glucose metabolic pathways in MGAS5005. Differential colors (blue/orange) depict the two predicted pathways from glucose transport. ManMN is potentially the main glucose PTS transporter, based on current literature. However, this has yet to be shown in GAS. Black lines depict the routes of glucose transport. GlcU: glucose uptake protein; NagC: glucokinase.

amount of sugar consumed (see chapter 3) was slightly lower in Δ*manMN* and Δ*glcU* as compared to MGAS5005. Since THY is a complex rich media that potentially contains multiple sugars, we tested the same strains in CDM + 0.5% glucose and monitored the amount of sugar consumed to determine if loss of any of these predicted glucose metabolic pathways reduced the efficiency of glucose metabolism. None of the mutants showed significantly increased glucose consumption when the total yield was standardized for all strains (**Fig. 7.3B**). We next determined the total yield of each mutant grown in different concentrations of glucose, where GAS strains were incubated in CDM + X% of glucose as the sole carbon source for 48 hours, and growth and total yield (ΔOD_{600}) was calculated as described in chapter 3. Δ*manMN* and Δ*glcU* had very little effect on GAS growth on glucose (**Fig 7.3C**).

The Δ*ptsI* mutation led to a consistent growth defect when grown in 2% glucose (**Fig 7.3C**), while at 0.5%, 0.75%, and 1% glucose, growth was only affected early (12 h) and late (48 h) (**Fig 7.3C**). However, when looking just the total yield at 12, 24, 36 and 48

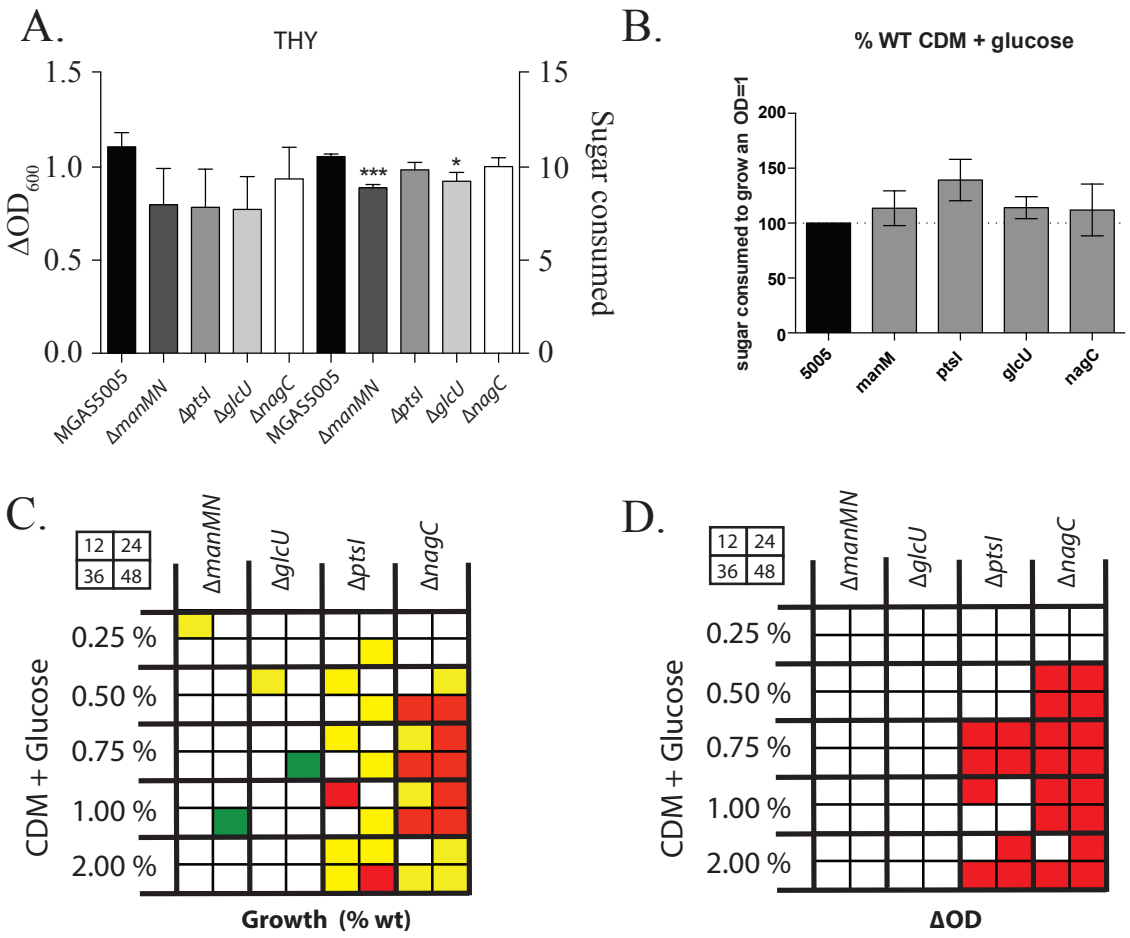

Figure 7.3. Growth of various predicted glucose metabolic gene mutants in MGAS5005. **A)** GAS strains were grown in THY for 24 h. ΔOD_{600} is plotted on the left Y-axis. The total sugar consumed during growth in THY over 24 h was calculated as indicated in chapter 3, and plotted on the right Y-axis. Shading is indicative of strains. *p-value <0.5. ***p-value <0.005. **B)** Strains grown in CDM + 0.5% glucose for 24 h. We calculated the total amount of sugar that would be consumed for a particular GAS strain to grow to an OD600 of 1 from an OD600 of 0 (see Chapter 3). Grey bars depict strains with similar sugar consumption to MGAS5005. Red bars depict strains that were statistically significantly different from MGAS5005. **C)** Strains were grown in CDM + various % glucose. Each growth curve was analyzed at 12, 24, 36, and 48 h and plotted as indicated. Green boxes depict growth above WT, yellow boxes depict growth 2 fold below WT, and red boxes depict growth more than 2 fold below WT. White boxes depict growth similar to MGAS5005 **D)** ΔOD_{600} of growth performed in **(C)**, and depicted similarly. White boxes depict ΔOD_{600} similar to MGAS5005. Red boxes depict ΔOD_{600} significantly lower than MGAS5005.

h, growth of GAS on 0.75% glucose had the most drastic effect (**Fig 7.3D**). In contrast, Δ*nagC* had the lowest growth in all concentrations of glucose compared to wild type for all the mutants assayed over 48 h (**Fig 7.3D**). This would suggest that either the main route of glucose transport occurs through the non-PTS glucose transport system, or that deleting the glucokinase gene (Δ*nagC*) somehow affects the expression of the PTS system, hindering overall glucose transport.

Deletion of *nagC* leads to the inability of GAS to grow on certain PTS carbohydrates as the sole carbon source

To investigate if the non-PTS alternate glucose metabolic pathway affects PTS function, we grew Δ*nagC* and Δ*glcU* in CDM + 1% of a PTS carbohydrate as the sole carbon source for 48 h (see chapter 3). Surprisingly, the Δ*nagC* glucokinase mutant did not grow as well as wild type in glucose, fructose, sucrose and maltose (**Fig 7.4A**). The Δ*glcU* permease mutant actually grew slightly better than MGAS5005 in both lactose and maltose, while both strains had reduced growth in mannose as compared to MGAS5005 (**Fig 7.4A**). However, when these strains were grown in C media + 1% of a PTS carbohydrate (0.5% glucose), all of these phenotypes disappeared (**Fig 7.4A**). C-media contains a low concentration of glucose (0.05% w/v), suggesting that Δ*nagC* and Δ*glcU* have growth defects in some PTS sugars only when it is presented as the sole carbon source. These growth defects were rescued by in the presence of 0.05% (w/v) of glucose (**Fig 7.4A**) and this was reflected when comparing the total yield of these strains grown in these two different conditions (**Fig 7.4B**). However, since there are many differences between CDM and C-media (see chapter 3), it is also likely that other factors contribute to the rescue of the growth defects observed. Finally, Δ*nagC* had reduced growth and total yield in C media, further confirming that glucose metabolism seems to occur primarily through glucokinase (**Fig 7.4AB**). We next interrogated the utilization profile of the Δ*nagC* mutant to see if it reflected what was observed with growth. Using the API®50CH carbon utilization strips, we determined

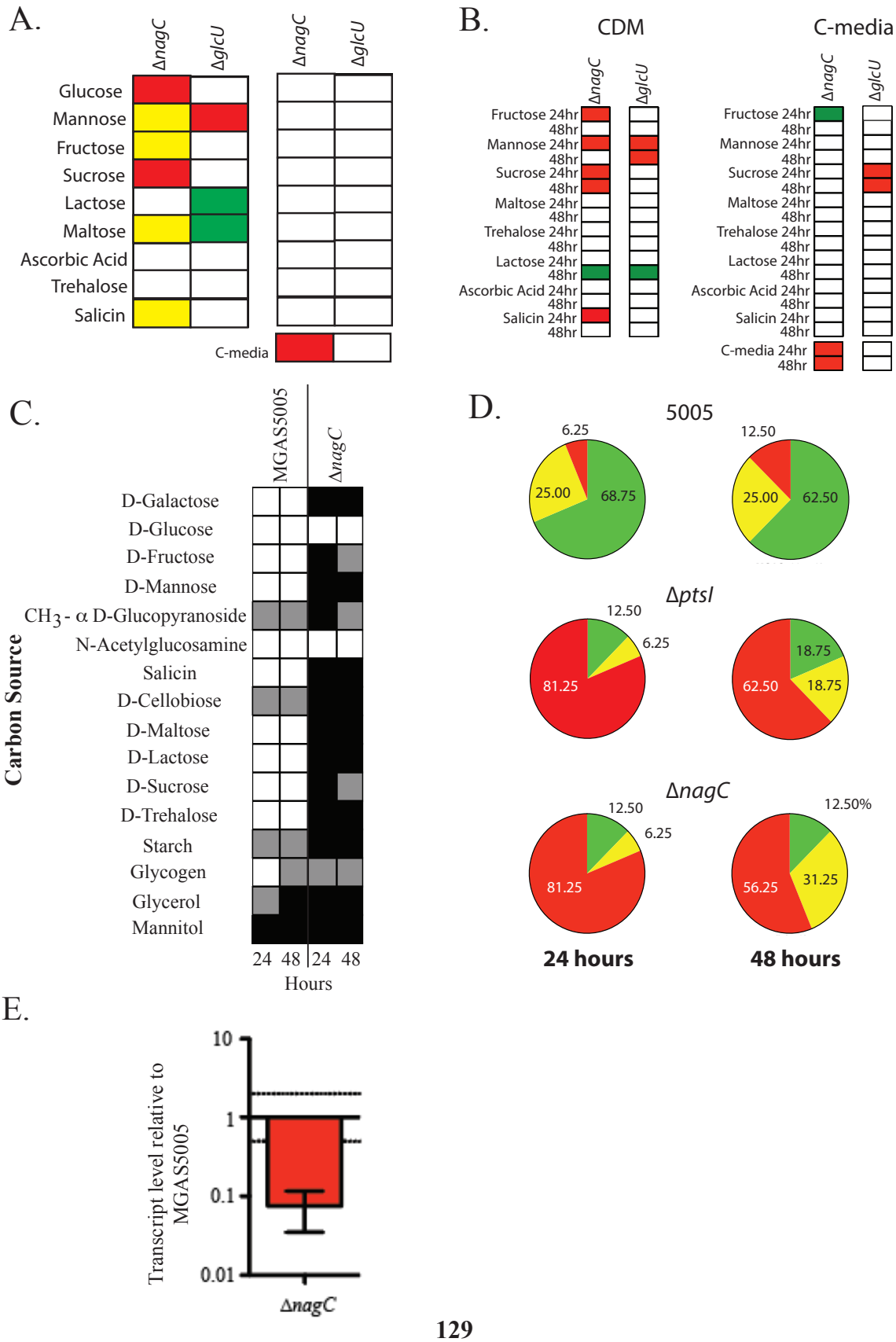
A.
ΔnagC
ΔglcU
ΔnagC
ΔglcU
Glucose
Mannose
Fructose
Sucrose
Lactose
Maltose
Ascorbic Acid
Trehalose
Salicin
C-media
B.
CDM
C-media
ΔnagC
ΔglcU
Fructose 24hr
48hr
Mannose 24hr
Sucrose 24hr
Maltose 24hr
Trehalose 24hr
Lactose 24hr
Ascorbic Acid 24hr
Salicin 24hr
C-media 24hr
C.
MGAS5005
ΔnagC
Carbon Source
D-Galactose
D-Glucose
D-Fructose
D-Mannose
CH3 - α D-Glucopyranoside
N-Acetylglucosamine
Salicin
D-Cellobiose
D-Maltose
D-Lactose
D-Sucrose
D-Trehalose
Starch
Glycogen
Glycerol
Mannitol
24 48 24 48
Hours
D.
5005
6.25
25.00
68.75
12.50
25.00
62.50
ΔptsI
12.50
6.25
81.25
18.75
62.50
18.75
ΔnagC
12.50
6.25
81.25
12.50%
56.25
31.25
24 hours
48 hours
E.
Transcript level relative to MGAS5005
10
1
0.1
0.01
ΔnagC

Figure 7.4. Deletion of *nagC* prohibits GAS growth in several PTS sugars. A) Growth of Δ*nagC* and Δ*glcU* in CDM + PTS sugar (left boxes). Color scheme similar to Fig 7.3C. Growth was also carried out in C-media plus PTS sugar (right boxes), similarly to CDM. Growth curves were analyzed after 48 hours. **B)** ΔOD_{600} was calculated after 24 and 48 h of growth in CDM or C-media + 1% PTS sugar. Color scheme similar to Fig 7.3D. **C)** Utilization profile of Δ*nagC* in MGAS5005. Utilization of select carbon sources as determined by the API®50CH system. White boxes indicate utilization (+), grey boxes indicate partial utilization (+/-), and black boxes indicate no utilization (-). Readings for each strain are given for 24 and 48 h (left and right box respectively). **D)** Utilization patterns where analyzed by determining the percent of carbon sources listed that fall into utilization (green), partial utilization (yellow), and no utilization (red). **E)** Transcript level of *ptsI* in a Δ*nagC* mutant compared to MGAS5005, measured through qRT-PCR. Data presented are the average of three biological replicates.

that Δ*nagC* had impaired utilization of 88% of the carbon sources tested (**Fig. 7.4C**). Comparing the utilization profile of Δ*nagC* to Δ*ptsI*, it is evident that both mutants have a drastic reduction in overall carbon utilization, as over 81% of carbon sources could not be utilized at 24 h, and over 56% at 48 h (**Fig 7.4D**). This suggests that similar to the PTS, NagC positively influences the metabolism of multiple carbohydrates. To investigate whether these metabolism defects in PTS sugars was observed due to lower PTS expression, we assessed the transcript levels of *ptsI* in Δ*nagC* and compared it to MGAS5005. We performed qRT-PCR on RNA isolated from both strains grown in THY to late log, as indicated in chapter 3. *ptsI* expression was significantly lower in Δ*nagC* than in MGAS5005, suggesting that this is the possible reason for the lack of growth on PTS sugars in the glucokinase mutant (**Fig 7.4E)**. The mechanism by which this occurs, however, is currently unknown.

Route of glucose metabolism is important for survival of GAS in whole human blood, but not for SLS-mediated hemolysis

Considering MGAS5005.Δ*ptsI* exhibited early onset of hemolytic activity, we assayed whether Δ*nagC* and Δ*glcU* would also affect the timing of hemolysis during GAS growth. Surprisingly, both Δ*glcU* and, to a slightly greater extent, Δ*nagC* exhibited hemolytic activity early in growth (**Fig. 7.5AB**). Neither of these mutants resembled the level of early hemolytic activity observed by MGAS5005.Δ*ptsI*, suggesting a lesser role for the alternate glucose metabolic pathway in regulating the timely expression of SLS; however,

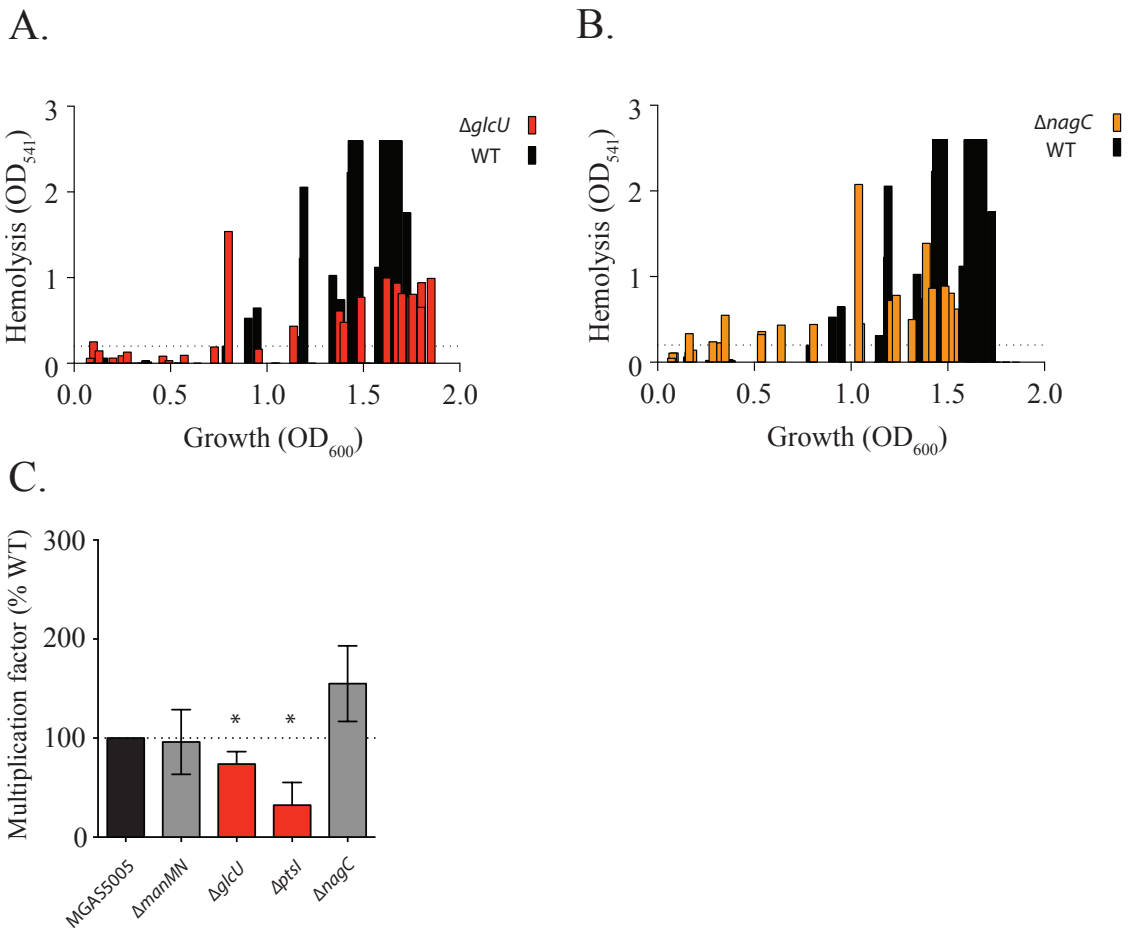

Figure 7.5. Deletion of the alternate glucose metabolic pathway components leads to altered blood phenotypes. (A,B) Black bars represent hemolytic values of MGAS5005. Red bars represent hemolytic values of Δ*glcU*. Orange bars depict hemolytic values of Δ*nagC*. **(C)** Lancefield Bactericidal Assay. Multiplication factors are shown as compared to MGAS5005. Grey bars indicate strains where the MF is similar to wildtype. Red bars indicate strains where the the MF is statistically significantly different from MGAS5005. Data shown represent the average of at least three biological replicates. *p-value <0.05.

this does suggest that SLS-mediated hemolysis is linked to glucose metabolism. Since both glucose transport and metabolic pathways exhibited some degree of early hemolytic activity, we wanted to determine if this would translate to increased survival in whole human blood, as producing more SLS should mean successful evasion of immune cells and access to nutrients. We found that although Δ*nagC* survives similarly to MGAS5005 when exposed to whole human blood for 3 h, Δ*ptsI* had severely reduced survival (**Fig 7.5C**). Additionally, Δ*glcU* has a slightly reduced survival in whole human blood, suggesting

that the route of glucose transport affects how GAS is able to survive in an important host environment. Although the reason for this discrepancy is unknown, there may be a difference in gene expression that could contribute to GAS survival in whole human blood. Despite the Δ*manMN* mutant exhibiting increased lesion severity in a murine subcutaneous infection model (Chapter 5), there was no phenotype observed in whole human blood (**Fig 7.5C**), indicating that the contribution of the mannose-specific EII to GAS pathogenesis is restricted to the skin.

A Δ*nagC* mutant exhibits increased lesion severity compared to MGAS5005

To determine if the route of glucose metabolism affects overall GAS pathogenesis, we injected MGAS5005, Δ*nagC*, and Δ*ptsI* subcutaneously in CD-1 female mice and measured lesion size, severity, and total CFUs per mg of spleen for all three strains as indicated in chapter 3. As observed previously by our group (Gera *et al*., 2014), Δ*ptsI* exhibited larger lesions as compared to MGAS5005; however, Δ*nagC* mice showed lesions comparable in size to wild type at 48 h post infection (**Fig 7.6A**). Still, the lesions associated with Δ*nagC* infection were more severe than those of MGAS5005, and more similar to those of Δ*ptsI*-infected mice (**Fig 7.6BC**). These results correlate with the hemolytic profile of all three strains, where Δ*ptsI* shows early and robust hemolysis, while Δ*nagC* was early but not as robust as Δ*ptsI* (**Fig 7.5B**). All three strains showed similar CFUs/mg of spleen at 48 h from all mice tested, suggesting that dissemination from the local site of infection was similar (**Fig 7.6D**). This was somewhat unexpected as Δ*ptsI* did not survive in whole human blood and may indicate a human-specific phenotype. It also suggests that the PTS and *nagC* help control hemolytic activity at the local site of skin infections, but this does not translate to greater dissemination (**Fig 7.6E**). In conclusion, glucose metabolism through the PTS is important for survival in whole human blood. However, impaired glucose utilization in general leads to the early production of Streptolysin S, resulting in a more severe lesion in a subcutaneous skin infection model.

A.

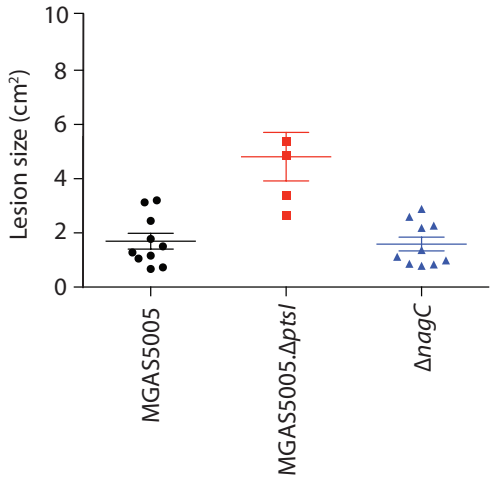
Lesion size (cm²)
10
8
6
4
2
0
MGAS5005
MGAS5005.ΔptsI
ΔnagC

B.

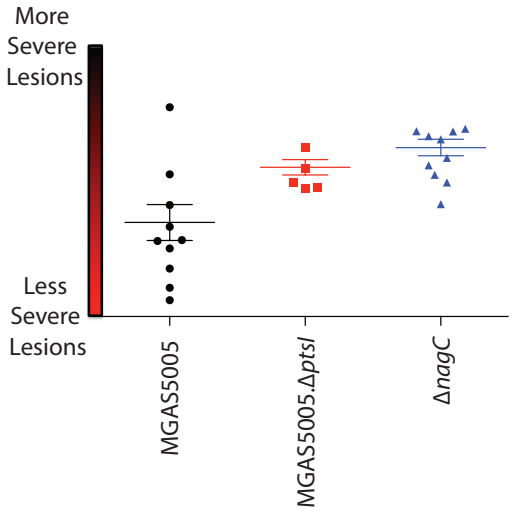
More Severe Lesions
Less Severe Lesions
MGAS5005
MGAS5005.ΔptsI
ΔnagC

C.

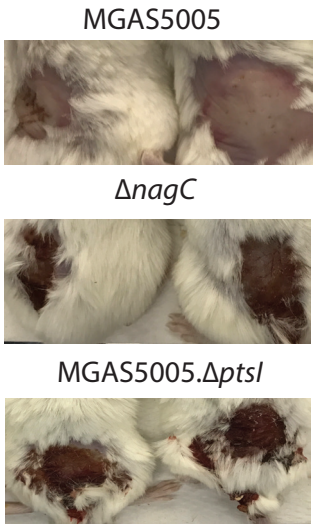
MGAS5005
ΔnagC
MGAS5005.ΔptsI

D.

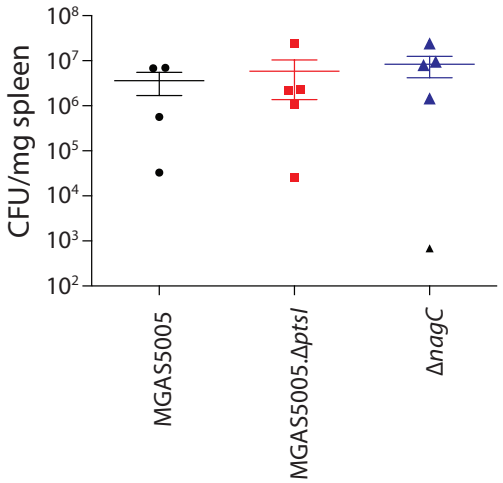
CFU/mg spleen
10⁸
10⁷
10⁶
10⁵
10⁴
10³
10²
MGAS5005
MGAS5005.ΔptsI
ΔnagC

E.

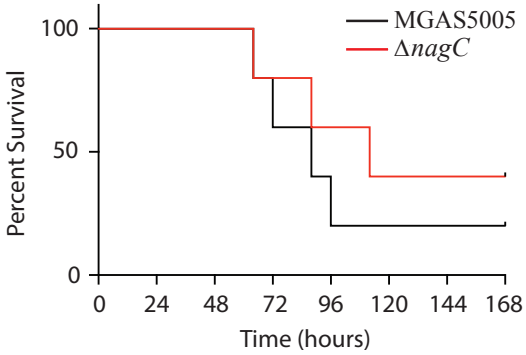
Percent Survival
100
50
0
0
24
48
72
96
120
144
168
Time (hours)
MGAS5005
ΔnagC

Figure 7.6. Contribution of glucose pathway mutants in GAS pathogenesis in a murine subcutaneous infection model. MGAS5005, Δ*ptsI*, and Δ*nagC* were injected subcutaneously into CD-1 mice (See Chapter 3). Lesion size **(A)** and severity **(B)** shown for MGAS5005-infected (black), Δ*ptsI*-infected (red), and Δ*nagC*-infected (blue) mice at 48 hours post infection. **(C)** Representative images of lesions associated with infection from each strain was taken at 48 hpi. **(D)**. CFUs/mg spleen were graphed to assess diseemination. **(E)** Survival of mice associated with each infection that were not sacrificed for spleen CFU counts were monitored for survival over 7 days.

Discussion

In this chapter, we generated mutants in predicted glucose utilization pathways and compared the contribution of the non-PTS pathway (*nagC*) to the PTS pathway for overall glucose metabolism. We found that elimination of the alternate glucose metabolic pathway led to a more drastic reduction in growth on glucose as the sole carbon source as compared to effects of eliminating the PTS. Interestingly, we discovered that deletion of the glucokinase *nagC* also lead to decreased growth in PTS sugars, likely resulting from the decreased expression of *ptsI* in this background. Altering metabolic pathways for glucose metabolism affected the activity of SLS, as both Δ*nagC* and Δ*glcU* showed an early hemolytic profile during growth. Although the route of glucose metabolism did not affect the onset of early hemolysis, it did affect survival in human blood as the Δ*ptsI* mutant is unable to survive whereas the Δ*nagC* mutant did. Early onset of hemolysis translated to an increased lesion severity, but not increased lesion size, at the site of infection when mice were infected with Δ*nagC*. However, there was no observable dissemination defect (spleen) nor was there a significant reduction of lethality with Δ*nagC*. We established that there are at least two metabolic routes for glucose metabolism that are interconnected and influence the expression of the toxin SLS.

In GAS, there are two main routes hypothesized for glucose utilization: (1) PTS and (2) a non-PTS transporter. Elimination of both *nagC* and *ptsI* ablated glucose metabolism in *S. aureus* (Vitko *et al.*, 2016), so it is unlikely that GAS does have any

additional alternative glucose metabolic pathways. Both the glucokinase (Δ*nagC*) and PTS (Δ*ptsI*) mutants were grown in different concentrations of glucose over 48 h to monitor which pathway was more important in the overall metabolism of glucose and found that disruption of the non-PTS glucose pathway (Δ*nagC*) lead to a greater loss of growth in all concentrations of glucose as compared to Δ*ptsI*. This suggests that the non-PTS glucose metabolic pathway is the preferred route of glucose metabolism at most concentrations, we identified a non-PTS glucose transporter gene (*glcU*) in GAS based on homologous to the *S. aureus* transporter important in glucose metabolism (Vitko *et al*., 2016). Inactivation of *glcU* lead to very modest growth defect in all glucose concentrations tested. Coupled with the fact that a Δ*glcU*Δ*ptsI* double mutant was still able to grow on glucose (data not shown), this strongly indicates the presence of a third glucose transporter(s) that has yet to be identified. Ideally, a Δ*nagC*Δ*ptsI* double mutant would allow us to confirm this as was used for *S. aureus* (Vitko *et al*., 2016). However, *S. aureus* has a much more robust metabolic network compared to GAS, and therefore substrates to grow the double mutant are more readily identifiable. We have yet to find a carbon source that would facilitate growth of a GAS Δ*ptsI*Δ*nagC* double mutant.

Unexpectedly, Δ*nagC* also had trouble growing on the PTS sugars mannose, fructose, sucrose, and maltose, likely due to its reduction of the expression of *ptsI*. The mechanism of this repression is unknown, but it is possible that the intracellular PEP pool is low in a Δ*nagC* mutant, leading to lowered PTS activity. Reduced PEP level may also fail to stimulate adequate induction of *ptsI*; however, the regulators involved are not known. Since growth defects of the Δ*nagC* mutant in PTS sugars disappeared when C media (low glucose-high peptide) was used in place of CDM (no carbon source), it is possible that growing Δ*nagC* in low glucose allows for the generation of enough PEP to stimulate PTS expression and allow for growth on PTS sugars. As CDM has no additional carbon source, the levels of PEP would remain low in this condition. Oddly, Δ*nagC* was able to grow in

lactose and trehalose, even though in the utilization assay they are unable to utilize these sugars. One limitation of the utilization assay is that the readout for positive utilization is a drop in pH based on a pH indicator dye. In GAS, this is largely due to the generation of lactic acid at the end of the fermentation of a sugar. In Δ*nagC*, it is possible that there is a shift in the metabolic network, where fermentation of lactose and trehalose may now lead to a different end metabolite, causing the utilization assay to present a false negative.

Invasive GAS (iGAS) uses the bloodstream to disseminate from the local site of infection to other sterile sites in the body, leading to life-threatening systemic infection. Since human blood is glucose rich, we interrogated if the route of glucose metabolism affected survival of GAS in whole human blood. Surprisingly, the non-PTS transporter mutant (Δ*nagC*) was able to survive, while the PTS mutant (Δ*ptsI*) was not, strongly suggesting that glucose being transported through the PTS is important for GAS survival during bacteremia. One caveat is that that Δ*ptsI* mutant not only affects the glucose transport, but also impacts the metabolism of many carbon sources. Therefore, it is certainly possible that Δ*ptsI* has more far reaching perturbations outside of glucose transport that are required for survival in blood. This assertion is further strengthened by the fact that Δ*ptsI* would also not be able to phosphorylate PRD-containing virulence regulators, which can have a multitude of different consequences.

Deletion of the glucokinase gene *nagC* lead to an increase in lesion severity in a subcutaneous murine infection model as compared to infection with wild type MGAS5005. This was expected, as Δ*nagC* exhibits early hemolysis, but at lower level than that of the Δ*ptsI*. One explanation could be that there are fewer bacteria in the lesion, as Δ*nagC* may not be able to grow inside the skin as well as Δ*ptsI*. It could also be the consequence of having a lower magnitude of hemolysis early in growth as compared to Δ*ptsI*. This suggests not only that lesion severity correlates with production of SLS, as was shown previously (Gera *et al*., 2014), but that the regulation of PTS-mediated SLS activity is indirectly affected by Δ*nagC*.

Dissemination of MGAS5005, Δ*ptsI*, and Δ*nagC*, based on CFU/mg spleen in infected mice after 2 days, was quite similar (**Fig. 7.6D**). This was unexpected for Δ*ptsI*, as in whole human blood, it does not survive nearly as well as MGAS5005 or Δ*nagC* (**Fig 7.5C**). A phenotype in human blood and not in mice can indicate a human-specific trait, which may not be surprising as our PTS fructose-metabolic operon mutants (Δ*fruBAC*) also showed a human-specific role in survival in whole human blood (Chapter 6). Since that operon is part of the larger PTS network, this may explain the overall human-specificity seen with Δ*ptsI*. Survival, lesion size, and dissemination of mice infected with MGAS5005 and Δ*nagC* were similar.

Overall, this suggests that the importance of the route of glucose metabolism varies with the host and specific environment in GAS pathogenesis. Forcing glucose to be metabolized in one route versus the other impacts the ability of GAS to survive. This can be due to (1) efficiency of glucose metabolism and (2) expression of other important pathogenic networks. Forcing glucose to be metabolized through the PTS may be inefficient, and therefore may affect survival in a glucose rich environment. However, this cannot be the case as Δ*nagC* has similar survival in blood as the wild type. The more likely scenario is that forcing glucose through the PTS changes glucose from a preferred sugar to a PTS-inducing sugar that can affect the phosphorylation of PRDs on PCVRs, thereby changing their activity. This would not be the case in the Δ*ptsI* mutant, where PTS phosphorylation of PRDs cannot occur, and would again change the activity of PCVRs. GAS may use the affinity of both systems for glucose transport, coupled with the ability to phosphorylate PCVRs in response to inducing sugars to regulate virulence programs in different environments. This process would be disrupted in a Δ*nagC* mutant, but to a higher degree in Δ*ptsI* and would lose regulation completely.

Chapter 8: Conclusions and Future Directions

In this dissertation, we aimed to determine the root cause of the early SLS-mediated hemolytic activity that was observed in MGAS5005.Δ*ptsI*. We had originally hypothesized that this was the result of the lack of transport of a particular PTS carbon source, as a Δ*ptsI* mutant has no PTS transport function. To tackle the question of which carbon source was primarily responsible, we insertionally inactivated each of the individual EIICs, as these are the carbohydrate transporters that provide sugar-specificity to the PTS (Chapter 4). Establishing an EIIC mutant library in MGAS5005 allowed us to not only metabolically characterize each one, but allows for screening of each EIIC mutant in host niches to determine if a transporter or a carbohydrate they specifically affect are important for GAS pathogenesis. We put this to the test by screening the library in survival in whole human blood, and discovered two EIIC mutants that have reduced survival compared to the parental strain MGAS5005. One of the EIICs discovered (FruA) did not have a reduction of survival in whole human blood in another M1T1 strain 5448 (Chapter 6). Differences in phenotypes between EII subunits in MGAS5005 and 5448 was also found with the mannose-specific EII, where the relative influence on metabolism and hemolysis varied between the two strains (Chapter 5). We additionally screened the EII library for early hemolytic activity, and found seven EIIC mutants that exhibit early hemolysis (Chapter 4). However, there was no sugar in common whose metabolism was affected by all the EIIs. We did observe that hemolysis occurs at low nutrient concentrations, so we investigated the nature of glucose metabolism in MGAS5005 by making mutants in the non-PTS and PTS glucose metabolic pathway (Chapter 7). The deletion of both Δ*ptsI* and the glucokinase (Δ*nagC*) affected glucose metabolism, although the glucokinase had a much larger influence. Interestingly, these two mutants had different phenotypes when grown in whole human blood, where Δ*nagC* survived better than Δ*ptsI*, even though both strains show early hemolytic activity (Chapter 7). Unexpectedly, the Δ*nagC* mutant also had a

growth defect on several PTS sugars, the result of lowered expression of *ptsI*. Finally, Δ*nagC* had more severe lesions than MGAS5005 when GAS was injected subcutaneously, although the lesions were similar sizes which is not the case for Δ*ptsI* (Chapter 7). This dissertation established a useful tool to screen for the importance of carbohydrate metabolic pathways in different infection environments, established the redundancy of many of these pathways, showed differences in the roles of identical proteins in different backgrounds, established the glucose metabolic pathway in MGAS5005, and allowed us to more clearly hypothesize the trigger for SLS-mediated hemolysis.

Different roles of EIICs in GAS physiology between two M1T1s

We discovered that although the mannose-specific (*manLMN*) and the fructose-specific (*fruA*) EIIs have the 100% same sequences in both MGAS5005 and 5448, their specific roles in metabolism and virulence are somewhat different. The differences observed in the mannose-specific EII roles between the two M1T1 strains is much larger than that of *fruA*, although this may be the result of the fact that the mannose-specific EII has a greater role in virulence and certainly in PTS carbohydrate metabolism, hence the greater possibility for variation. The greatest difference between the mannose-specific EII subunits between the two strains was seen with metabolism, where the MGAS5005 version had a much larger positive influence than the 5448 version. Other than SNPs, one of the main differences between these two strains is the presence (or absence) of a functional CovS. Since the CovRS regulon includes many metabolic genes, it's possible that an intact CovS in 5448 limits the role of the mannose-specific EII in 5448 since there is still another layer of regulation. However, in MGAS5005 which is *covS*$^{-}$, deletion of the mannose-specific EII has a more drastic effect in an already altered metabolic background. To test this hypothesis, we would create the mannose-specific EII subunit mutants in both the animal passaged 5448 strain 5448AP (*covS*$^{-}$), and a 5448.Δ*covS* knockout mutant and

characterize the influence on GAS PTS carbohydrate metabolism. This would elucidate if the reason for the differences we observed is due to an intact CovRS system. Secondly, we would extend this out to all of the EIICs, by making the annotated EIIC mutant library in both 5448 and 5448AP as well, and comparing the influence of each of the remaining EIIs on PTS carbohydrate metabolism in all three strains (MGAS5005, 5448, 5448AP). If CovS plays a role in shaping the role of each EIIC, we would expect the influence of each EII to be similar in MGAS5005 and 5448AP as compared to 5448. This idea is further strengthened by the fact that CovS seems to play a role in the influence of the PTS on the expression of *hasA* (capsule production and *speB*) (Gera, 2014).

Both EIIC mutants that are impaired for their survival in whole human blood have altered fructose metabolism

Survival in whole human blood is a necessary step for an invasive infection to spread from the localized site of infection to other sterile sites. Since these types of infections are often the most dangerous, it is of great interest to identify genes important for GAS survival in this environment. Screening the EIIC mutant library for survival in whole human blood identified both the Δβ-glucoside-specific EII and the fructose-specific EII as important for survival. Both of these EIIs contribute to efficient fructose metabolism, as their respective mutants have defects in growth on fructose as the sole carbon source. Although fructose is present in blood, it is at much lower concentrations than glucose (Chapter 2). However, *fruA* is upregualted in the presence of heme stress (Sachla *et al*., 2014), so it is possible that fructose metabolism may play an important role in combating both the immune response, as seen with *fruB* and *fruR*'s role in evading neutrophil killing, as well as metal stress. Interestingly, *fruA* was only important for survival in blood in MGAS5005, not 5448. To ascertain if this is the case for the Δβ-glucoside-specific EII as well, we would make a 5448 version of this mutant. Addtionally, we would characterize its metabolic operon, as it is predicted to be transcribed with a PRD containing antiterminator (*licT*) and a beta-glucosidase (*bglA*). We would

also characterize the EIIC mutant metabolically and in a Lancefield bactericidal assay to determine if there are differences between the two strains. To further elucidate the impact that fructose metabolism has on survival in whole human blood, we would perform a TNseq essentiality screen, similar to the transposon mutagenesis screen carried out by Le Breton *et. al* (2015), to identify genes that are required for optimal fitness for surviving in blood. This could either strengthen the hypothesis that fructose metabolism plays an important role in this environment, or could identify other pathways whose efficiency is affected by fructose, or its downstream metabolites.

Routes of glucose metabolism in GAS

We made mutants in the two glucose metabolic pathways predicted in GAS (Δ*nagC* & Δ*ptsI*) and assessed their ability to grow in glucose. Deletion of *nagC* lead to a more drastic reduction in growth, suggesting that it is the preferred route of glucose metabolism. Although the *ptsHI* operon is not in the CcpA regulon, it does have a *cre* site, and therefore may be catabolite repressed. This would fit our model that the PTS is a less preferred glucose transport system. The lack of growth of Δ*nagC* on PTS sugars was surprising. However, the fact that *ptsI* expression was lower in a Δ*nagC* mutant coupled with the fact that a slow growing Δ*nagC* mutant strain may have less PEP, could explain why growth on PTS sugars was impaired when they are the sole carbon source, but not in a media where there is low glucose. The levels of glucose metabolic intermediates and PEP in both of these backgrounds would be investigated via mass spectrometry to see if there are drastic alterations that may explain the phenotypes observed. This would also lend insight into how these two pathways may interact with each other, as metabolites are often cofactors for GAS gene regulation.

There is a third unidentified glucose transport mechanism present in GAS, as a Δ*ptsI*Δ*glcU* mutant is still able to grow in glucose, although at a lower rate. To identify a third potential transport mechanism, we would carry out a screen using MGAS5005 and

grow it in CDM + 2DG as a carbon source. 2DG is a glucose analog that is not metabolizable in GAS, therefore prevents growth, and usually kills GAS cells. 2DG is transported through similar mechanisms as glucose, therefore, the hypothesis is that suppressors would appear that prevent transport of 2DG in MGAS5005 to allow the cell to survive. This strain should then be a glucose transport-null strain. However, to allow for growth in CDM + 2DG, we would need to introduce another carbon source to facilitate growth, as using 2DG as the sole carbon source would prevent any cell from surviving, even if a suppressor mutation occurs. Rather, we would change the ratio of 2DG to the alternate carbon source in CDM to allow for baseline growth, but still select for suppressors. A second method would be to make a conditional mutant of Δ*nagC* using Δ*ptsI* as the background strain. This should get rid of both glucose-metabolic pathways, therefore rendering this strain as glucose-null. However, deletion of *ptsI* would eliminate growth on multiple other carbon sources as well, so no inferences can be made about solely glucose metabolism in this mutant, and therefore may not be useful.

Occurrence of hemolysis in Group A Streptococcus M1T1 MGAS5005

We observed that deletion of the PTS leads to the early activity of SLS, occurring during exponential phase rather than in late-log phase during growth. Seven EIIC mutants displayed early hemolysis as well, although none to the level of a Δ*ptsI* mutant (Chapter 4). This suggests that all the EIICs identified contribute to the overall early hemolytic phenotype observed in Δ*ptsI*, a notion also backed by the fact that ΔMannose has severe lesions similar to Δ*ptsI* in a murine skin infection model, but does not display the increased lesion size (Chapter 5). We did observe that all these EIICs identified fall into the CcpA regulon (DebRoy *et al.*, 2016). This suggests that perhaps the early hemolytic phenotype observed is not the result of the lack of PTS carbohydrate metabolism, but rather the disruption of efficient glucose metabolism. This is further strengthen by the fact that Δ*ccpA*

also displays SLS-mediated hemolysis in exponential phase of growth. Additionally, we demonstrate that in MGAS5005, hemolysis only occurs in low nutrient conditions, regardless of the media used. Δ*nagC* and Δ*glcU* also display an extent of early hemolysis, and Δ*nagC* displays severe lesions similar to Δ*ptsI* in a murine skin infection model. Similarly to ΔMannose, these lesions are similar in size to MGAS5005 and not to Δ*ptsI*.

As a result of all of the data we have collected in this dissertation, we propose the following model for the induction of SLS-mediated hemolysis, and how each perturbation results in the observed early hemolytic activity.

MGAS5005 high vs low glucose (Fig 8.1). Glucose can enter the cell both through the PTS and non-PTS transport systems. When a high amount of glucose is present in the environment (**Fig 8.1A**), we hypothesize that glucose is transported primarily through the non-PTS glucose transporters (Blue section), as these enzymes are active in early exponential phase of growth (unpublished). Transport may still occur through the PTS, however, this is unlikely as *ptsI* is actively expressed during late log-phase of growth (unpublished). The rapid uptake of glucose would lead to a buildup of fructose-1,6-bisphosphate, a known trigger for HprK to phosphorylate HPr on its Serine-46 residue) (Deutscher, 2008). HPr-Ser~P would then be a cofactor for CcpA to repress SLS-mediated hemolysis by preventing expression of the *sag* operon (DebRoy *et al.*, 2016). The exact mechanism for this is currently unknown, in that even though the *sag* operon is included in the CcpA regulon (DebRoy *et al.*, 2016) and binding of CcpA to the *sag* operon promoter occurs *in vitro* (Kinkel & McIver, 2008), it does not occur *in vivo* (Kietzman & Caparon, 2010). Therefore, CcpA-mediated repression of the *sag* operon is likely indirect. Additionally, since glucose would primarily be transported by the non-PTS metabolic pathway, EIIs would likely remain phosphorylated, which could present the opportunity to phosphorylate Mga on it's PRD2 domain (Hondorp *et al.*, 2013). However, when glucose levels become low, the PTS becomes the primary mode of glucose transport, as the mannose-specific EII

A.

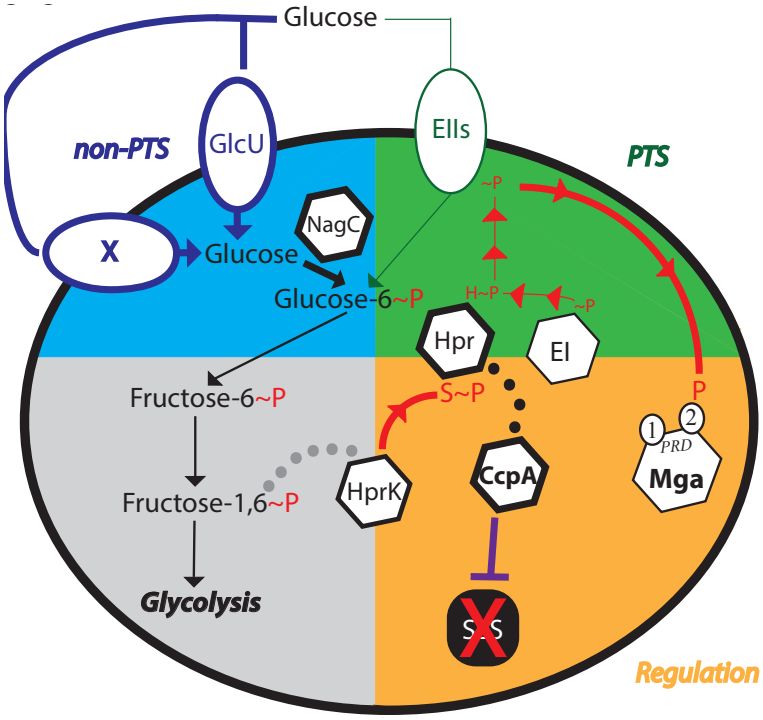

NO Lysis

B.

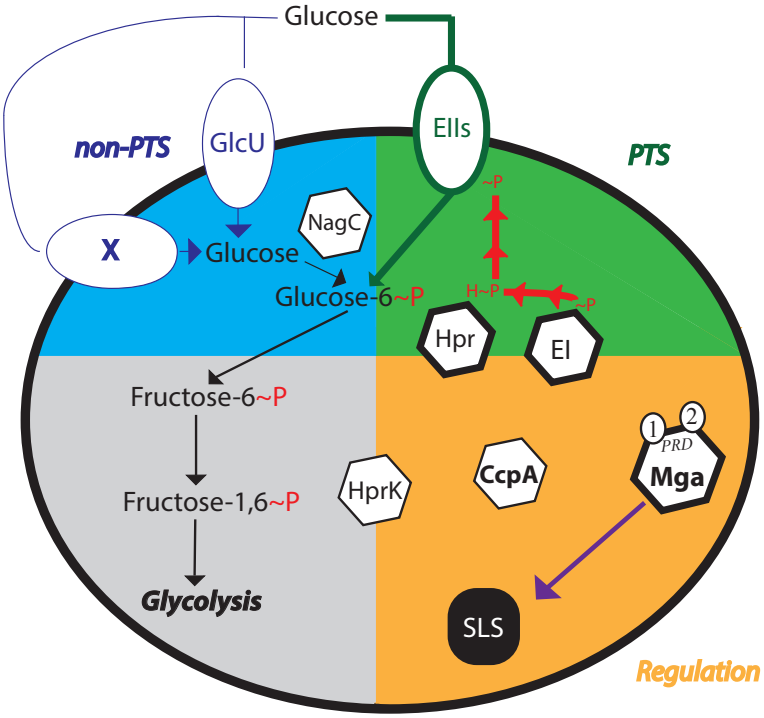

Host Cell Lysis

Figure 8.1 Regulation of SLS-mediated hemolysis in MGAS5005 in both high (A) and low (B) glucose. Dotted lines represent protien interactions. Solid lines depict either metabolic reactions or influence on regulation of SLS. the grey portion of the cell represents glycolysis. The blue and green portions of the cell deptict the non-PTS and PTS glucose metabolic pathways respectively. The orange portion of the cell represents the the effect of the metabolic pathways on the regulation of SLS through the actions of CcpA and Mga. P represent phosophates. X represents the alternate set of unidentified transporters for glucose. H~P represents the histidine that is phosphorylated, and S~P represents the serine that is phosphorylated. (1) and (2) depict the PRDs 1 and 2 respectively present on Mga. Bold lines and dotted lines represent likely preferred routes of metabolism and the proteins that participate in them.

was shown to be a high affinity glucose transporter in other bacteria (Fleming & Camilli, 2016). Also, expression of many EIIs begin to occur in late-log phase, which correlates with low glucose levels. As glucose levels lower and PTS activity ramps up (**Fig 8.1B**), HPr-Ser~P can either be phosphorylated by EI, or the phosphate on the serine can be cleaved by HprK. This leads to the derepression of the *sag* operon, as CcpA is no longer interacting with HPr. As the phosphorelay continues to shuttle phosphates to the EIIBs which phosphorylate the incoming sugar, Mga can no longer be phosphorylated on its PRD2, leading to further activation of the *sag* operon. This is thought to occur as Mga was shown to activate *sag* expression in low glucose conditions (Valdes, 2016), although direct regulation has not been shown. This leads to robust SLS-mediated hemolysis in low-glucose conditions, as we observed in this dissertation. This system would rely on multiple inputs, so we will discuss below what we think occurs when we start to eliminate components that

components that mediate SLS activity.

Δ***ptsI*** (**Fig 8.2**). Δ*ptsI* has robust SLS-mediated hemolysis even in high glucose conditions. Based on our model, elimination of the PTS would force glucose to only be metabolized by the non-PTS glucose pathway. Factoring in our growth data with Δ*ptsI*, the buildup of fructose-1,6-bisphoshate may not be as high, as glucose is forced into only one pathway which allows for adequate but not optimal growth. HprK may not phosphoryalte

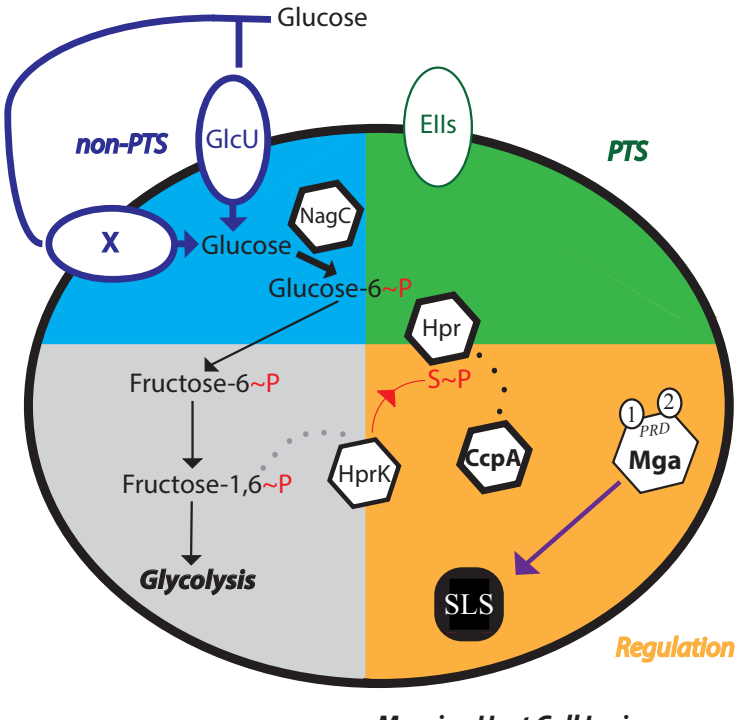

Figure 8.2 Effect of the loss of *ptsI* on SLS-mediated hemolysis. EI is removed from the model, representing a Δ*ptsI* mutant.

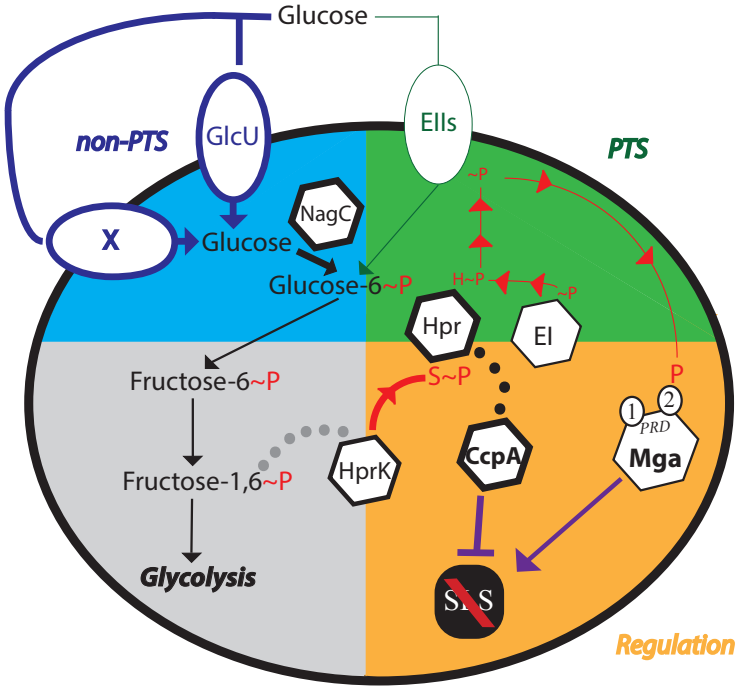

Figure 8.3 Effect of the loss of an EII on SLS-mediated hemolysis. The same color scheme from Fig 8.1 was used.

HPr on its serine residue in this situation. This suggests that CcpA again would not efficiently be able to mediated repression of *sag* operon. Lack of CCR in a PTS mutant is also shown with the expression of *speB* (catabolite repressed), which is higher in Δ*ptsI* than MGAS5005 (Gera, 2014). Finally, since Mga is phosphorylated on its PRDs by the PTS, and Mga activates *sag* expression in low glucose environments (where Mga is not phosphorylated), a Δ*ptsI* mutant would lock Mga in a non-phosphorylated state which permanently activates sag expression. This would explain the robust SLS-mediated hemolysis that was observed early in growth for the Δ*ptsI* mutant, and the subsequent massive tissue destruction observed in the murine subcutaneous infection model.

ΔEII (Fig 8.3). Predicting the impact of each EII that contributes to SLS activity is complicated, as each EII has a varied influence on PTS carbohydrate metabolism. The seven EIIC mutants that exbihit early hemolysis could be the result of the fact that these EIIs may be the interacting partners for Mga that phosphorylate its PRD2. In this case, an EIIC mutant would prevent phosphorylation of PRD2, and Mga would remain unphosphorylated. This would then induce SLS-mediated hemolysis. However, since CcpA is still intact, CCR is still possible as glucose levels are still high when these mutants are grown in THY. However, it is unknown how both CcpA and Mga regulate SLS expression, therefore it is unknown if an unphosphoryalted Mga could outcompete CcpA when exerting its influence on SLS expression. This would suggest that the seven EIIs, whose mutantions lead to early hemolysis, can provide a signal to the cell through Mga, which is feasible as all three mannose-family EIIs fall into this category, encompassing the metabolism of most of the PTS carbohydrates. However, interaction between EIIs and Mga have not been tested in GAS. In this case, using Phos-tag gels to determine the phosphorylation state of Mga in each mutant, and using qPCR to determine the influence each EII has on Mga activity (assay Mga regulon expression), would indicate the extent to which each EII affects Mga activity. We could then build on this model to determine which EIIs have a greater influence on Mga activity, and if this translates to an increase in magnitude of SLS-mediated hemolysis.

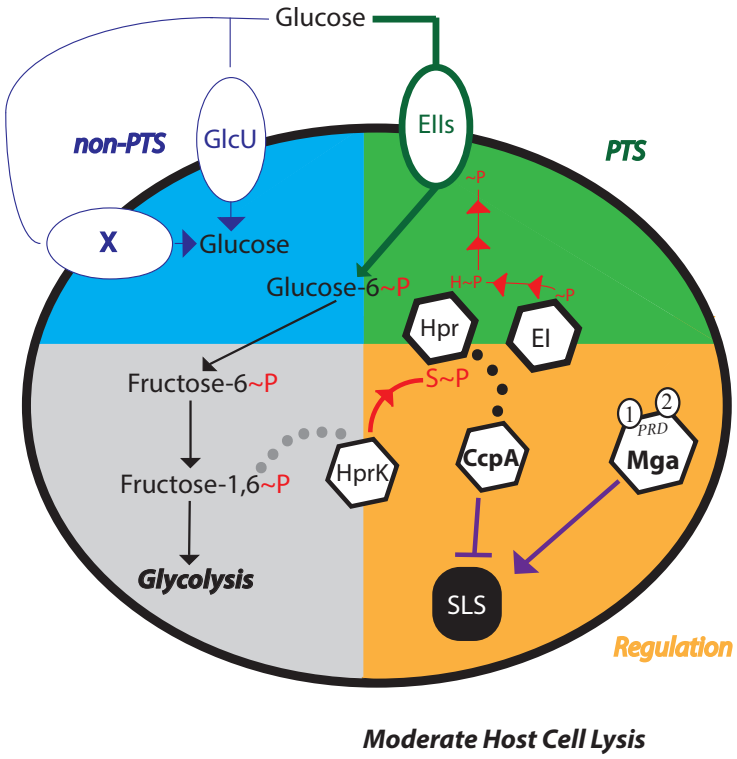

Figure 8.4 Effect of the loss of *nagC* on SLS-mediated hemolysis. NagC is removed from the model, to simulate the conditions in Δ*nagC*.

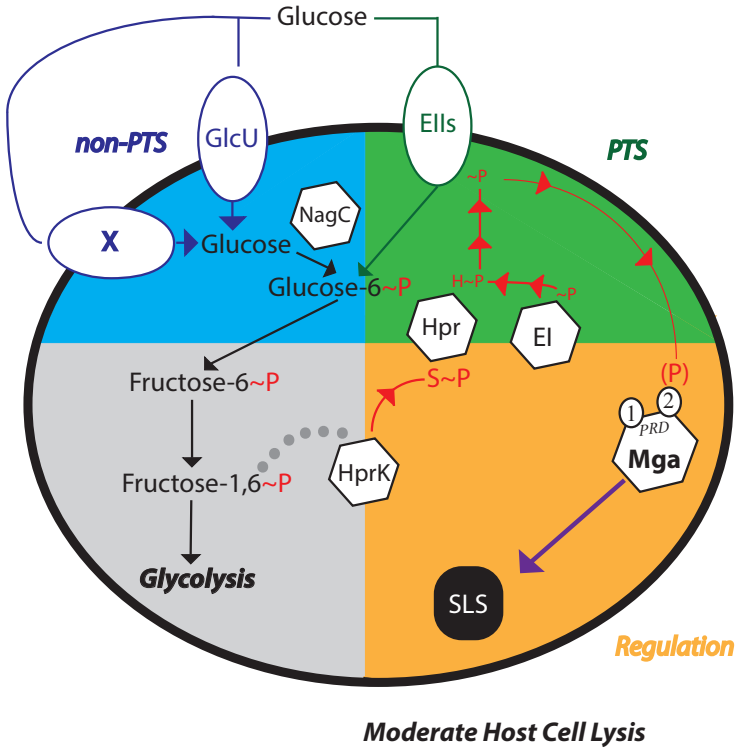

Figure 8.5 Effect of the loss of *ccpA* on SLS-mediated hemolysis. CcpA is removed form the model, to simulate a Δ*ccpA* mutant.

Δ*nagC* (Fig 8.4). Glucose in Δ*nagC* is forced through the PTS, meaning that PTS enzymes in our model would be dephosphorylated, because these phosphates will be shuttled onto glucose. This would mean that the PTS would not pass its phosphate to any PRDs, and in our case Mga, which would mean that Mga would be unphosphorylated and activate the expression of SLS. Additionally, Hpr would be predominately phosphorylated on its histidine residue, and not its serine residue, which would mean that Hpr-Ser~P would be present in very low quantities. Therefore, it would not be present in high enough levels to be used as a cofactor by CcpA to represses SLS expression. This would lead to the early activity of SLS observed in Δ*nagC*. However, unlike Δ*ptsI*, Mga is not locked into a unphosphorylated state, which could explain why the early hemolytic activity is not as robust as with Δ*ptsI*.

Δ*ccpA* (Fig 8.5). Δ*ccpA* also exhibits early hemolytic acitivty (Kinkel & McIver, 2008). This scenario is fairly straightforward, as not having CcpA to repress SLS activity leads to the increased expression of SLS as compared to the wildtype. Deletion of *ccpA* also increases the expression of many PTS enzymes. If this increased expression leads to the increased PTS activity, then Mga may not be phosphorylated on its PRDs, since these phosphates are shuttled to incoming sugars. This leads to early and sustained hemolysis, as observed previously (Kinkel & McIver, 2008).

Future experiments to validate the model

As this is a model based on the data currently available, there are still gaps in our knowledge of SLS regulation. Many of the hypotheses generated from the model rest on the fact that the differences in Mga regulation of the *sag* operon (directly or indirectly), are contingent on the fact that a phosphorylated Mga will not activate expression. I propose using the different phosphomimetic and phosphoablative forms of Mga in MGAS5005 to simulate the different phosphorylation conditions possible for Mga. In these strains, *sag* expression and SLS activity would be measured to determine in which simulated conditions

lead to SLS activity. Additionally, Phos-tag gels on Δ*ptsI*, Δ*nagC*, and Δ*ccpA* to assay the phosphorylation state of Mga would be carried out, again to determine if Mga is indeed unphosphorylated in each of these mutants as hypothesized in the model.

To identify other potential triggers for SLS-mediated hemolysis, we would carry out a screen to identify other mutants (regulators or carbon metabolic genes) that also exhibit early hemolytic activity. To do this, we would screen the master Tnseq transposon mutant library (Le Breton *et al.*, 2015) to look for mutants that displayed early hemolytic activity. When hemolysis occurs, RBCs burst and the cell contents seep into the medium fairly evenly. By using the well scanning mode on the Omega FLOUstar microplate reader, we can measure when hemolysis occurs in a high throughput fashion by screening individual mutants per well to assess if hemolysis begins earlier than WT. This would then be confirmed using a traditional hemolysis assay, and using AP-PCR and sequencing would identify the gene that was inactivated.

On the other side, we would also screen for potential substrates that may trigger SLS-mediated hemolysis. Because *sag* expression is under CCR, and CCR is both CcpA-dependent and independent, it is possible that other carbohydrates may trigger SLS activity. To interrogate this possibility, we would grow GAS transformed with a plasmid expressing GFP under the *sag* promoter in the Biolog panel of carbon sources (190 different ones) in the Omega FLOUstar microplate reader, and measure the induction of GFP. This would allow us to determine if there are other carbon sources that can elicit CCR, and if groups of carbon sources lead to quicker induction of *sag* expression as compared to others, potentially establishing a hierarchy of preferred and non-preferred carbon sources.

Significance

In this dissertation, we have established that early hemolytic activity is not the result of the lack of access of a PTS sugar, but rather the the potential premature relief of CCR based on the underappreciated signaling roles of the PTS. In addition, we have also

determined that gene annotations do not always define function, and that identical proteins may have different roles in different backgrounds. This highlights that although meta-genomic analyses play an important role in learning about human pathogens, it is still important to characterize potentially important genes at the molecular level in more than one strain. This also suggests that inferences made of a protein's function may not be easily extendable to other strains even if their respective gene sequences are identical. Finally, we have established an annotated EII mutant library that can now be used in further screens to determine the role of carbohydrate transport, metabolism, and signaling in different pathogenic scenarios.

Appendix A: Media Compositions

*Media compositions as adapted from Gera *et al.*, 2013

Todd Hewitt Broth (rich media)

1) 30g Todd-Hewitt (TH) broth:

20g peptone

3.1g beef heart infusion

2.5g sodium carbonate

2g dextrose

2g sodium chloride

0.4g disodium phosphate

2) 2g Yeast extract

3) 1L H_2O

C-media (low glucose, high peptide)

0.5% (w/v) Protease peptone 3

1.5% (w/v) Yeast extract

17 mM NaCl

0.4 mM $MgSO_4$

10 mM K_2HPO_4

Distilled H_2O

Chemically Defined Media (CDM, carbon free media)

0.0200 g/L	Adenine Sulfate, $2H_2O$
0.1000 g/L	DL-Alanine
0.1000 g/L	L-Arginine, FB
0.1000 g/L	L-Asparagine, Anhydrous
0.1000 g/L	L-Aspartic Acid
0.0002 g/L	Biotin
0.0005 g/L	Calcium Chloride, Anhydrous
0.0020 g/L	D-Calcium Pantothenate
0.0001 g/L	Cyanobalamin
0.0652 g/L	L-Cystine, 3HCl
0.0008 g/L	Folic Acid
0.1000 g/L	L-Glutamic Acid
0.2000 g/L	L-Glutamine
0.1000 g/L	Glycine
0.2000 g/L	Guanine, HCl, H_2O
0.1000 g/L	L-Histidine, FB
0.1000 g/L	Hydroxy L-Proline
0.1000 g/L	L-Isoleucine
0.1000 g/L	L-Leucine
0.1249 g/L	L-Lysine, HCl
0.3419 g/L	Magnesium Sulfate, Anhydrous
0.1000 g/L	L-Methionine
0.0010 g/L	Niacinamide
0.0025 g/L	β-NAD, 3 H_2O
0.0002 g/L	Para-Aminobenzoic Acid

0.1000 g/L	L-Phenylalanine
0.2000 g/L	Potassium Phosphate, Dibasic, Anhydrous
1.0000 g/L	Potassium Phosphate, Monobasic, Anhydrous
0.1000 g/L	L-Proline
0.0010 g/L	Pyridoxal, HCl
0.0010 g/L	Pyridoxamine, 2HCl
0.0020 g/L	Riboflavin
0.1000 g/L	L-Serine
2.7126 g/L	Sodium Acetate, Anhydrous
7.3500 g/L	Sodium Phosphate, Dibasic, Anhydrous
3.1950 g/L	Sodium Phosphate, Monobasic, H_2O, ACS
0.0010 g/L	Thiamine, HCl
0.2000 g/L	L-Threonine
0.1000 g/L	L-Tryptophan
0.1442 g/L	L-Tyrosine, 2Na, $2H_2O$
0.0200 g/L	Uracil
0.1000 g/L	L-Valine

Bibliography

Abranches, J., M.M. Candella, Z.T. Wen, H.V. Baker & R.A. Burne, (2006) Different roles of EIIABMan and EIIGlc in regulation of energy metabolism, biofilm development, and competence in *Streptococcus mutans*. *J. Bacteriol.* **188**: 3748-3756.

Afzal, M., S. Shafeeq, B. Henriques-Normark & O.P. Kuipers, (2015) UlaR activates expression of the *ula* operon in *Streptococcus pneumoniae* in the presence of ascorbic acid. *Microbiol.*: 41-49.

Ajdic, D. & V.T. Pham, (2007) Global transcriptional analysis of *Streptococcus mutans* sugar transporters using microarrays. *J. Bacteriol.* **189**: 5049-5059.

Ake, F.M., P. Joyet, J. Deutscher & E. Milohanic, (2011) Mutational analysis of glucose transport regulation and glucose-mediated virulence gene repression in *Listeria monocytogenes*. *Molecular Microbiololgy* **81**: 274-293.

Alexa, A., J. Rahnenfuhrer & T. Lengauer, (2006) Improved scoring of functional groups from gene expression data by decorrelating GO graph structure. *Bioinformatics* **22**: 1600-1607.

Anders, S., P.T. Pyl & W. Huber, (2015) HTSeq--a Python framework to work with high-throughput sequencing data. *Bioinformatics* **31**: 166-169.

Antunes, A., I. Martin-Verstraete & B. Dupuy, (2011) CcpA-mediated repression of *Clostridium difficile* toxin gene expression. *Mol. Microbiol.* **79**: 882-899.

Aziz, R.K. & M. Kotb, (2008) Rise and persistence of global M1T1 clone of *Streptococcus pyogenes*. *Emerging Infect. Dis.* **14**: 1511-1517.

Barrangou, R., M.A. Azcarate-Peril, T. Duong, S.B. Conners, R.M. Kelly & T.R. Klaenhammer, (2006) Global analysis of carbohydrate utilization by *Lactobacillus acidophilus* using cDNA microarrays. *Proc. Natl. Acad. Sci. USA* **103**: 3816-3821.

Barriere, C., M. Veiga-da-Cunha, N. Pons, E. Guedon, S.A. van Hijum, J. Kok, O.P. Kuipers, D.S. Ehrlich & P. Renault, (2005) Fructose utilization in *Lactococcus lactis* as a model for low-GC gram-positive bacteria: its regulator, signal, and DNA-binding site. *J. Bacteriol.* **187**: 3752-3761.

Beall, B., R.R. Facklam, J.A. Elliott, A.R. Franklin, T. Hoenes, D. Jackson, L. Laclaire, T. Thompson & R. Viswanathan, (1998) Streptococcal *emm* types associated with T-agglutination types and the use of conserved *emm* gene restriction fragment patterns for subtyping group A streptococci. *J. Med. Microbiol.* **47**: 893-898.

Beissbarth, T. & T.P. Speed, (2004) GOstat: find statistically overrepresented Gene Ontologies within a group of genes. *Bioinformatics* **20**: 1464-1465.

Bernheimer, A.W.R., M., (1948) The effect of nucleic acids and of carbohydrates on the formation of streptolysin. *J. Exp. Med.*: 149-168.

Bernish, B. & I. van de Rijn, (1999) Characterization of a two-component system in *Streptococcus pyogenes* which is involved in regulation of hyaluronic acid production. *J. Biol. Chem.* **274**: 4786-4793.

Bernstein G. A., V.A.M., Pipal A. J., Williams K. A., (2010) Comparison of clinical characteristics of pediatric autoimmune neuropsychiatric disorders associated

with streptococcal infections and childhood obsessive-compulsive disorder. *Journal of Child and Adolescent Psychopharmacology.* **20**: 333-340.

Bidossi, A., L. Mulas, F. Decorosi, L. Colomba, S. Ricci, G. Pozzi, J. Deutscher, C. Viti & M.R. Oggioni, (2012) A functional genomics approach to establish the complement of carbohydrate transporters in Streptococcus pneumoniae. *PLoS One* **7**: e33320.

Bolger, A.M., M. Lohse & B. Usadel, (2014) Trimmomatic: a flexible trimmer for Illumina sequence data. *Bioinformatics* **30**: 2114-2120.

Carapetis, J.R., A.C. Steer, E.K. Mulholland & M. Weber, (2005) The global burden of group A streptococcal diseases. *Lancet Infect. Dis.* **5**: 685-694.

Casabon, I., Couture, M., Vaillancourt, K., Vadeboncoeur, C., (2006) Synthesis of HPr(Ser-P)(His-P) by Enzyme I of the Phosphoenolpyruvate: Sugar Phosphotransferase System of *Streptococcus salivarius*. *Biochemistry* **45**: 6692-6702

Centers for Disease Control and Prevention. 1997. Active Bacterial Core Surveillance Report, Emerging Infections Program Network, Group A Streptococcus, 1997.

Centers for Disease Control and Prevention. 1998. Active Bacterial Core Surveillance Report, Emerging Infections Program Network, Group A Streptococcus, 1998.

Centers for Disease Control and Prevention. 1999. Active Bacterial Core Surveillance Report, Emerging Infections Program Network, Group A Streptococcus, 1999.

Centers for Disease Control and Prevention. 2000. Active Bacterial Core Surveillance Report, Emerging Infections Program Network, Group A Streptococcus, 2000.

Centers for Disease Control and Prevention. 2001. Active Bacterial Core Surveillance Report, Emerging Infections Program Network, Group A Streptococcus, 2001.

Centers for Disease Control and Prevention. 2002. Active Bacterial Core Surveillance Report, Emerging Infections Program Network, Group A Streptococcus, 2002.

Centers for Disease Control and Prevention. 2003. Active Bacterial Core Surveillance Report, Emerging Infections Program Network, Group A Streptococcus, 2003.

Centers for Disease Control and Prevention. 2004. Active Bacterial Core Surveillance Report, Emerging Infections Program Network, Group A Streptococcus, 2004.

Centers for Disease Control and Prevention. 2005. Active Bacterial Core Surveillance Report, Emerging Infections Program Network, Group A Streptococcus, 2005.

Centers for Disease Control and Prevention. 2006. Active Bacterial Core Surveillance Report, Emerging Infections Program Network, Group A Streptococcus, 2006.

Centers for Disease Control and Prevention. 2007. Active Bacterial Core Surveillance Report, Emerging Infections Program Network, Group A Streptococcus, 2007.

Centers for Disease Control and Prevention. 2008. Active Bacterial Core Surveillance Report, Emerging Infections Program Network, Group A Streptococcus, 2008.

Centers for Disease Control and Prevention. 2009. Active Bacterial Core Surveillance Report, Emerging Infections Program Network, Group A Streptococcus, 2009.

Centers for Disease Control and Prevention. 2010. Active Bacterial Core Surveillance Report, Emerging Infections Program Network, Group A Streptococcus, 2010.

Centers for Disease Control and Prevention. 2011. Active Bacterial Core Surveillance Report, Emerging Infections Program Network, Group A Streptococcus, 2011.

Centers for Disease Control and Prevention. 2012. Active Bacterial Core Surveillance Report, Emerging Infections Program Network, Group A Streptococcus, 2012.

Centers for Disease Control and Prevention. 2013. Active Bacterial Core Surveillance Report, Emerging Infections Program Network, Group A Streptococcus, 2013.

Centers for Disease Control and Prevention. 2014. Active Bacterial Core Surveillance Report, Emerging Infections Program Network, Group A Streptococcus, 2014.

Centers for Disease Control and Prevention. 2015. Active Bacterial Core Surveillance Report, Emerging Infections Program Network, Group A Streptococcus, 2015.

Chatellier, S., Ihendyane, N., Kansal, R. G., Khambaty, F., Basma, H., Norrby-Teglund, A., Low, D. E., McGeer, A., Kotb, M. (2000). Genetic relatedness and superantigen expression in group A streptococcus serotype M1 isolates from patients with severe and nonsevere invasive diseases. *Infection and Immunity* **68**(6): 3523-3534.

Chavarria, M., G. Durante-Rodriguez, T. Krell, C. Santiago, J. Brezovsky, J. Damborsky & V. de Lorenzo, (2014) Fructose 1-phosphate is the one and only physiological effector of the Cra (FruR) regulator of Pseudomonas putida. *FEBS Open Bio* **4**: 377-386.

Chavarria, M., C. Santiago, R. Platero, T. Krell, J.M. Casasnovas & V. de Lorenzo, (2011) Fructose 1-phosphate is the preferred effector of the metabolic regulator Cra of *Pseudomonas putida*. *J. Biol. Chem.* **286**: 9351-9359.

Chen, S., Oldham, M.L., Davidson, A.L., Chen, J. , (2013) Carbon catabolite repression of the maltose transporter revealed by X-ray crystallography. *Nature*: 1-6.

Conway, T., (1992) The Entner-Doudoroff pathway: history, physiology and molecular biology. *FEMS Microbiol. Rev.* **103**: 1-28.

Courtney, H.S., Hasty, D.L., Dale, J.B., (2003) Serum opacity factor (SOF) of Streptococcus pyogenes evokes antibodies that opsonize homologous and heterologous SOF-positive serotypes of group A streptococci. *Infect. Immun.* **71**: 5097-5103.

Cox, C.J., M. Sharma, J.F. Leckman, J. Zuccolo, A. Zuccolo, A. Kovoor, S.E. Swedo & M.W. Cunningham, (2013) Brain human monoclonal autoantibody from sydenham chorea targets dopaminergic neurons in transgenic mice and signals dopamine D2 receptor: implications in human disease. *J. Immunol.* **191**: 5524-5541.

Cunningham, M.W., (2000) Pathogenesis of Group A Streptococcal infections. *Clin. Microbiol. Rev.* **13**: 470-511.

Cunningham, M.W., (2008) Pathogenesis of Group A Streptococcal infections and their sequelae. *Adv. Exp. Med. Biol.* **609**: 29-42.

Cunningham, M.W., (2016) Post- Streptococcal Autoimmune Sequelae: Rheumatic Fever and Beyond. In: *Streptococcus pyogenes*: Basic Biology to Clinical Manifestations. D.L.S. Vincent A. Fischetti, Joseph J. Ferretti (ed). University of Oklahoma Health Sciences Center University of Oklahoma Health Sciences Center Library, pp. 837-874.

Cvitkovitch, D.G., D.A. Boyd, T. Thevenot & I.R. Hamilton, (1995) Glucose transport by a mutant of *Streptococcus mutans* unable to accumulate sugars via the phosphoenolpyruvate phosphotransferase system. *J. Bacteriol.* **177**: 2251-2258.

Dale, J.B.B., M.R.; Cleary, P.P.; Courtney, H.S.; Good, M.F.; Grandi, G.; Halperin, S.; Margarit, I.Y.; McNeil, S.; Pandey, M.; Smeesters, P.R.; Steer, A.C., (2016) Current Approaches to Group A Streptococcal Vaccine Development. In: *Streptococcus pyogenes*: Basic Biology to Clinical Manifestations. D.L.S. Vincent A. Fischetti, Joseph J. Ferretti (ed). University of Oklahoma Health Sciences Center University of Oklahoma Health Sciences Center Library, pp.

Datta, V., S.M. Myskowski, L.A. Kwinn, D.N. Chiem, N. Varki, R.G. Kansal, M. Kotb & V. Nizet, (2005) Mutational analysis of the group A streptococcal operon encoding streptolysin S and its virulence role in invasive infection. *Mol. Microbiol.* **56**: 681-695.

DebRoy, S., M. Saldana, D. Travisany, A. Montano, J. Galloway-Pena, N. Horstmann, H. Yao, M. Gonzalez, A. Maass, M. Latorre & S.A. Shelburne, (2016) A Multi-Serotype Approach Clarifies the Catabolite Control Protein A Regulon in the Major Human Pathogen Group A Streptococcus. *Sci. Rep.* **6**: 32442.

Deutscher, J., (2008) The mechanisms of carbon catabolite repression in bacteria. *Curr. Opin. Microbiol.* **11**: 87-93.

Deutscher, J., C. Fischer, V. Charrier, A. Galinier, C. Lindner, E. Darbon & V. Dossonnet, (1997) Regulation of carbon metabolism in gram-positive bacteria by protein phosphorylation. *Folia Microbiol.* **42**: 171-178.

Deutscher, J., C. Francke & P.W. Postma, (2006) How phosphotransferase system-related protein phosphorylation regulates carbohydrate metabolism in bacteria. *Microbiol. Mol. Biol. Rev.* **70**: 939-1031.

Evans, A.C.., (1936) Studies on Hemolytic Streptococci: II. *Streptococcus pyogenes*. *J. Bacteriol.* **31**: 611–624.

Facklam, R.B., B.;Efstratiou,A.; Fischetti,V.;Johnson, D.; Kaplan, E.; Kriz,P.;Lovgren,M.;Martin,D.; Schwartz, B.; Totolian,A.; Bessen,D.; Hollingshead,S.; Rubin, F.; Scott, J.; Tyrrell, G., (1999) emm Typing and Validation of Provisional M Types for Group A Streptococci. *Emerging Infect. Dis.* **5**: 247-253.

Federle, M.J., K.S. McIver & J.R. Scott, (1999) A response regulator that represses transcription of several virulence operons in the group A streptococcus. *J. Bacteriol.* **181**: 3649-3657.

Ferenci, T. & H.L. Kornberg, (1971) Role of fructose-1,6-diphosphatase in fructose utilization by *Escherichia coli*. *FEBS Lett.* **14**: 360-363.

Ferretti, J.K.h., W. , (2016) History of Streptococcal Research. In: *Streptococcus pyogenes*: Basic Biology to Clinical Manifestations. D.L.S. Vincent A. Fischetti, Joseph J. Ferretti (ed). University of Oklahoma Health Sciences Center University of Oklahoma Health Sciences Center Library, pp. 1-26.

Fleming, E. & A. Camilli, (2016) ManLMN is a glucose transporter and central metabolic regulator in *Streptococcus pneumoniae*. *Mol. Microbiol.*

Forster, A.H., Gescher, J., (2014) Metabolic engineering of Escherichia coli for production of mixed-acid fermentation end products. *frontiers in Bioengineering and Biotechnology* **2**: 1-12.

Foster, A.J., J.M. Jenkinson & N.J. Talbolt, (2003) Trehalose synthesis and metabolism are required at different stages of plant infection by *Magnaporthe grisea*. *EMBO J.* **22**: 225-235.

Gera, K., (2014) Role of the Phosphoenolpyruvate: Carbohydrate Phosphotransferase System in the Virulence of the Group A Streptococcus. ProQuest, University of Maryland.

Gera, K., T. Le, R. Jamin, Z. Eichenbaum & K.S. McIver, (2014) The Phosphoenolpyruvate Phosphotransferase System in Group A Streptococcus Acts To Reduce Streptolysin S Activity and Lesion Severity during Soft Tissue Infection. *Infect. Immun.* **82**: 1192-1204.

Gera, K. and K. S. McIver (2013). Laboratory growth and maintenance of *Streptococcus pyogenes* (the Group A Streptococcus, GAS). *Current Protocols in Microbiology* **30**: Unit 9D.2.

Goldmann, O., Sastalla I., Wos-Oxley, M., Rohde, M.m Medina, E. , (2009) *Streptococcus pyogenes* induces oncosis in macrophages through the activation of an inflammatory programmed cell death pathway. *Cell microbiology* **11**: 138-155.

Gorke, B. & J. Stulke, (2008) Carbon catabolite repression in bacteria: many ways to make the most out of nutrients. *Nature Reviews Microbiology* **6**: 613-624.

Graham, M.R., L.M. Smoot, C.A. Migliaccio, K. Virtaneva, D.E. Sturdevant, S.F. Porcella, M.J. Federle, G.J. Adams, J.R. Scott & J.M. Musser, (2002) Virulence control in group A streptococcus by a two-component gene regulatory system: global expression profiling and in vivo infection modeling. *Proc. Natl. Acad. Sci. USA* **99**: 13855-13860.

Graham, M.R., K. Virtaneva, S.F. Porcella, W.T. Barry, B.B. Gowen, C.R. Johnson, F.A. Wright & J.M. Musser, (2005) Group A Streptococcus transcriptome dynamics during growth in human blood reveals bacterial adaptive and survival strategies. *American Journal of Pathology* **166**: 455-465.

Hay, R.J., N.E. Johns, H.C. Williams, I.W. Bolliger, R.P. Dellavalle, D.J. Margolis, R. Marks, L. Naldi, M.A. Weinstock, S.K. Wulf, C. Michaud, J.L.M. C & M. Naghavi, (2014) The global burden of skin disease in 2010: an analysis of the prevalence and impact of skin conditions. *J Invest Dermatol* **134**: 1527-1534.

Heath, A., V.J. DiRita, N.L. Barg & N.C. Engleberg, (1999) A two-component regulatory system, CsrR-CsrS, represses expression of three *Streptococcus pyogenes* virulence factors, hyaluronic acid capsule, streptolysin S, and pyrogenic exotoxin B. *Infect. Immun.* **67**: 5298-5305.

Higashi, D.L.B., N.; Donahue, D.L.; Mayfield, J.A.; Tessier, C.R.; Rodriguez, K.; Ashfeld, B.L.; Luchetti, J.; Ploplis, V.A.; Castellino, F.J.; Lee, S.W., (2016) Activation of band 3 mediates group A streptococcus streptolysin S-based beta-hemolysis. *Nature Microbiology* **1**: 1-6.

Hondorp, E.R., S.C. Hou, L.L. Hause, K. Gera, C.E. Lee & K.S. McIver, (2013) PTS phosphorylation of Mga modulates regulon expression and virulence in the group A streptococcus. *Mol. Microbiol.* **88**: 1176-1193.

Hondorp, E.R. & K.S. McIver, (2007) The Mga virulence regulon: infection where the grass is greener. *Mol. Microbiol.* **66**: 1056-1065.

Hu, M.C., M.A. Walls, S.D. Stroop, M.A. Reddish, B. Beall & J.B. Dale, (2002) Immunogenicity of a 26-valent group A streptococcal vaccine. *Infect. Immun.* **70**: 2171-2177.

Hynes, W., Sloan, M, (2016) Secreted Extracellular Virulence Factors. In: *Streptococcus pyogenes*: Basic Biology to Clinical Manifestations. D.L.S. Vincent A. Fischetti, Joseph J. Ferretti (ed). University of Oklahoma Health Sciences Center University of Oklahoma Health Sciences Center Library, pp. 405-444.

Iyer, R. & A. Camilli, (2007) Sucrose metabolism contributes to in vivo fitness of *Streptococcus pneumoniae*. *Mol. Microbiol.* **66**: 1-13.

Joyet, P., H. Bouraoui, F.M.D. Ake, M. Derkaoui, C. Zebre, T.N. Cao, M. Ventroux, S. Ness;er, M. Noirot-Gros, J. Deutscher & E. Milohanic, (2013) Transcription regulators controlled by interaction with enzyme IIB componentsof the phosphoenolpyruvate:sugar phosphotransferase system. *Biochimica et Biophysica Acta* **1834**: 1415-1424.

Kapur, V., J.T. Maffei, R.S. Greer, L.L. Li, G.J. Adams & J.M. Musser, (1994) Vaccination with streptococcal extracellular cysteine protease (interleukin-1 beta convertase) protects mice against challenge with heterologous group A streptococci. *Microb. Pathog.* **16**: 443-450.

Kawabata, S., E. Kunitomo, Y. Terao, I. Nakagawa, K. Kikuchi, K. Totsuka & S. Hamada, (2001) Systemic and mucosal immunizations with fibronectin-binding protein FBP54 induce protective immune responses against *Streptococcus pyogenes* challenge in mice. *Infect. Immun.* **69**: 924-930.

Kelley, L.A. & M.J. Sternberg, (2009) Protein structure prediction on the Web: a case study using the Phyre server. *Nature Protocols* **4**: 363-371.

Kenny, J.G., J. Moran, S.L. Kolar, A. Ulanov, Z. Li, L.N. Shaw, E. Josefsson & M.J. Horsburgh, (2013) Mannitol Utilization is Required for Protection of *Staphylococcus aureus* from Human Skin Antimicrobial Fatty Acids. *PLoS One* **8**.

Kietzman, C.C. & M.G. Caparon, (2010) CcpA and LacD.1 affect temporal regulation of *Streptococcus pyogenes* virulence genes. *Infect. Immun.* **78**: 241-252.

Kinkel, T.L. & K.S. McIver, (2008) CcpA-mediated repression of streptolysin S expression and virulence in the Group A Streptococcus. *Infect. Immun.* **76**: 3451-3463.

Kjos, M., I.F. Nes & D.B. Diep, (2011) Mechanisms of Resistance to Bacteriocins Targeting the Mannose Phosphotransferase System. *Applied and Environmental Microbiology* **77**: 3335-3342.

Kornberg, H.L., (2001) Routes for fructose utilization by Escherichia coli. *J. Mol. Microbiol. Biotechnol.* **3**: 355-359.

Kreft, J. & J.A. Vazquez-Boland, (2001) Regulation of virulence genes in *Listeria*. *Int. J. Med. Microbiol.* **291**: 145-157.

Krzywinski, M., J. Schein, I. Birol, J. Connors, R. Gascoyne, D. Horsman, S.J. Jones & M.A. Marra, (2009) Circos: an information aesthetic for comparative genomics. *Genome Res.* **19**: 1639-1645.

Kurlan, R., D. Johnson & E.L. Kaplan, (2008) Streptococcal infection and exacerbations of childhood tics and obsessive-compulsive symptoms: a prospective blinded cohort study. *Pediatrics* **121**: 1188-1197.

Lancefield, R.C., (1962) Current knowledge of type-specific M antigens of group A streptococci. *J. Immunol.* **89**: 307-313.

Langmead, B., (2010) Aligning short sequencing reads with Bowtie. *Current Protocols in Bioinformatics* **11**.

Langmead, B. & S.L. Salzberg, (2012) Fast gapped-read alignment with Bowtie 2. *Nat. Methods* **9**: 357-359.

LaSarre, B. & M.J. Federle, (2011) Regulation and consequence of serine catabolism in *Streptococcus pyogenes*. *J. Bacteriol.* **193**: 2002-2012.

Le Bouguenec, C., Schouler, C. , (2010) Sugar metabolism, and additional virulence factor in *enterobacteria*. *Int. J. Med. Microbiol.* **301**: 1-6.

Le Breton, Y., A.T. Belew, K.M. Valdes, E. Islam, P. Curry, H. Tettelin, M.E. Shirtliff, N.M. El-Sayed & K.S. McIver, (2015) Essential Genes in the Core Genome of the Human Pathogen *Streptococcus pyogenes*. *Sci. Rep.* **5**: 9838.

Le Breton, Y. & K.S. McIver, (2013) Genetic Manipulation of *Streptococcus pyogenes* (The Group A Streptococcus, GAS). *Curr. Prot. Microbiol.* **In Press**.

Le Breton, Y., P. Mistry, K.M. Valdes, J. Quigley, N. Kumar, H. Tettelin & K.S. McIver, (2013) Genome-wide identification of genes required for fitness of Group a Streptococcus in human blood. *Infect. Immun.* **81**: 862-875.

Leckman, J.F., R.A. King, D.L. Gilbert, B.J. Coffey, H.S. Singer, L.S.t. Dure, H. Grantz, L. Katsovich, H. Lin, P.J. Lombroso, I. Kawikova, D.R. Johnson, R.M. Kurlan & E.L. Kaplan, (2011) Streptococcal upper respiratory tract infections and exacerbations of tic and obsessive-compulsive symptoms: a prospective longitudinal study. *Journal of the American Academy of Child and Adolescent Psychiatry* **50**: 108-118 e103.

Levin, J.C. & M.R. Wessels, (1998) Identification of *csrR*/*csrS*, a genetic locus that regulates hyaluronic acid capsule synthesis in group A streptococcus. *Mol. Microbiol.* **30**: 209-219.

Li, H., B. Handsaker, A. Wysoker, T. Fennell, J. Ruan, N. Homer, G. Marth, G. Abecasis, R. Durbin & G.P.D.P. Subgroup, (2009) The Sequence Alignment/Map format and SAMtools. *Bioinformatics* **25**: 2078-2079.

Loo, C.Y., K. Mitrakul, I.B. Voss, C.V. Hughes & N. Ganeshkumar, (2003) Involvement of an inducible fructose phosphotransferase operon in *Streptococcus gordonii* biofilm formation. *J. Bacteriol.* **185**: 6241-6254.

López-Garrido, J., E. Puerta-Fernández, I. Cota & J. Casadesús, (2015) Virulence Gene Regulation by L-Arabinose in *Salmonella enterica*. *Genetics* **200**: 807-819.

Loughman, J.A. & M. Caparon, (2006a) Regulation of SpeB in *Streptococcus pyogenes* by pH and NaCl: a model for in vivo gene expression. *J. Bacteriol.* **188**: 399-408.

Loughman, J.A. & M.G. Caparon, (2006b) A novel adaptation of aldolase regulates virulence in *Streptococcus pyogenes*. *EMBO J.* **25**: 5414-5422.

Lowe, R.G., M. Lord, K. Rybak, R.D. Trengove, O. R.P. & P.S. Solomon, (2009) Trehalose biosynthesis is involved in sporulation of *Stagonospora nodorum*. *Fungal Genet Biol* **46**: 381-389.

Lun, S., Willson, P.J., (2004) Putative mannose-specific phosphotransferase system component IID represses expression of suilysin in serotype 2 *Streptococcus suis*. *Vet. Microbiol.* **105**: 169-180.

Lyon, W.R., J.C. Madden, J.C. Levin, J.L. Stein & M.G. Caparon, (2001) Mutation of *luxS* affects growth and virulence factor expression in *Streptococcus pyogenes*. *Mol. Microbiol.* **42**: 145-157.

Martin, D.R., (2000) Laboratory evaluation of *streptococci*. In: Streptococcal Infections: Clinical Aspects, Microbiology, and Molecular Pathogenesis. D.L. Stevens & E.L. Kaplan (eds). New York: Oxford University Press, pp. 266-279.

McAllister, L.J., A.D. Ogunniyi, U.H. Stroeher & J.C. Paton, (2012) Contribution of a genomic accessory region encoding a putative cellobiose phosphotransferase system to virulence of *Streptococcus pneumoniae*. *PLoS One* **7**: e32385.

McIver, K.S., (2009) Stand-alone response regulators controlling global virulence networks in *Streptococcus pyogenes*. *Contributions to Microbiology* **16**: 103-119.

Molloy, E.M., P.D. Cotter, C. Hill, D.A. Mitchell & R.P. Ross, (2011) Streptolysin S-like virulence factors: the continuing sagA. *Nature Reviews Microbiology* **9**: 670-681.

Moye, Z.D., Zeng, L., Burne, R.A., (2014) Modification of Gene Expression and Virulence Traits in *Streptococcus mutans* in Response to Carbuhydrate Availability. *Applied and Environmental Microbiology* **80**: 972-985.

Murphy, T.K., Storch, E. A., Lewin, A. B., Edge, P. J., Goodman, W. K., (2012) Clinical factors associated with Pediatric Autoimmune Neuropsychiatric Disorders Associated with Streptococcal Infections. *The Journal of Pediatrics* **160**: 314-319.

Ngamskulrungroj, P., U. Himmelreich, J.A. Breger, C. Wilson, M. Chayakulkeeree, M.B. Krockenberger, R. Malik, H.M. Daniel, D. Toffaletti, J.T. Djordjevic, E. Mylonakis, W. Meyer & J.R. Perfect, (2009) The trehalose synthesis pathway is an integral part of the virulence composite for *Cryptococcus gattii*. *Infect. Immun.* **77**: 4584-4596.

Nicolas, G.G.F., M., Lavoie, M.C., (2010) *Streptococcus salivarius* mutans defective in mannose phosphotransferase systems show reduced sensitivity to mutacins I-T9 and R-3B. *Can. J. Microbiol./Rev. Can. Microbiol.* **56**: 692-696.

Nizet, V., B. Beall, D.J. Bast, V. Datta, L. Kilburn, D.E. Low & J.C. De Azavedo, (2000) Genetic locus for streptolysin S production by group A streptococcus. *Infect. Immun.* **68**: 4245-4254.

Ogata, H., S. Goto, K. Sato, W. Fujibuchi, H. Bono & M. Kanehisa, (1999) KEGG: Kyoto Encyclopedia of Genes and Genomes. *Nucleic Acids Res.* **27**: 29-34.

Orefici, G.C., F.; Cox,C.; Cunningham, M.W., (2016) Pediatric Autoimmune Neuropsychiatric Disorders Associated with Streptococcal Infections (PANDAS). In: *Streptococcus pyogenes*: Basic Biology to Clinical Manifestations. D.L.S. Vincent A. Fischetti, Joseph J. Ferretti (ed). University of Oklahoma Health Sciences Center University of Oklahoma Health Sciences Center Library, pp. 771-812.

Pancholi, V., Caparon, M., (2016) *Streptococcus pyogenes* Metabolism. In: *Streptococcus pyogenes*: Basic Biology to Clinical Manifestations. D.L.S. Vincent A. Fischetti, Joseph J. Ferretti (ed). University of Oklahoma Health Sciences Center University of Oklahoma Health Sciences Center Library, pp. 109-170.

Petzold, E.W., U. Himmelreich, E. Mylonakis, T. Rude, D. Toffaletti, G.M. Cox, J.L. Miller & J.R. Perfect, (2006) Characterization and regulation of the trehalose synthesis pathway and its importance in the pathogenicity of *Cryptococcus neoformans*. *Infect. Immun.* **74**: 5877-5887.

Pfoh, E.W., M.R.; Goldmann, D.; Lee, G.M., (2008) Burden and Economic Cost of Group A Streptococcal Pharyngitis. *Pediatrics* **121**: 229-234.

Port, G.C., L.A. Vega, A.B. Nylander & M.G. Caparon, (2014) *Streptococcus pyogenes* Polymyxin B-Resistant Mutants Display Enhanced ExPortal Integrity. *J. Bacteriol.* **196**.

Pridgeon, J.W., Y. Li, M. Yildirim-Aksoy, L. Song, P.H. Klesius, K.K. Srivastava & P.G. Reddy, (2013) Fitness cost, *gyrB* mutation, and absence of phosphotransferase system fructose specific IIABC component in novobiocin-resistant *Streptococcus iniae* vaccine strain ISNO. *Vet. Microbiol.* **165**: 384-391.

Ritchie, M.E., B. Phipson, D. Wu, Y. Hu, C.W. Law, W. Shi & G.K. Smyth, (2015) limma powers differential expression analyses for RNA-sequencing and microarray studies. *Nucleic Acids Res.* **43**: e47.

Robinson, J.T., H. Thorvaldsdóttir, W. Winckler, M. Guttman, E.S. Lander, G. Getz & J.P. Mesirov, (2011) Integrative genomics viewer. *Nat. Biotechnol.* **29**: 24-26.

R**odriguez-Iturbe, B.H., M., ,** (2016) Post-Streptococcal Glomerulonephritis. In: *Streptococcus pyogenes*: Basic Biology to Clinical Manifestations. D.L.S. Vincent A. Fischetti, Joseph J. Ferretti (ed). University of Oklahoma Health Sciences Center University of Oklahoma Health Sciences Center Library, pp. 813-836.

Rose, R.E., (1988) The nucleotide sequence of pACYC184. *Nucleic Acids Res.* **16**: 355.

Roy, D.J., Casabon, I., Vaillancourt, K., Huot, J.L., Vadeboncoeur, C., (2008) *Streptococci* and *lactococci* synthesize large amounts of HPr(Ser-P)(His-P). *Can. J. Microbiol./Rev. Can. Microbiol.* **54**: 941-949.

Sachla, A.J., Y. Le Breton, F. Akhter, K.S. McIver & Z. Eichenbaum, (2014) The crimson conundrum: heme toxicity and tolerance in GAS. *Front. Cell. Infect. Microbiol.* **4**: 159.

Saier, M.H., Jr., (2015) The Bacterial Phosphotransferase System: New Frontiers 50 Years after Its Discovery. *J. Mol. Microbiol. Biotechnol.* **25**: 73-78.

Saier, M.H., Jr., S. Chauvaux, G.M. Cook, J. Deutscher, I.T. Paulsen, J. Reizer & J.J. Ye, (1996) Catabolite repression and inducer control in Gram-positive bacteria. *Microbiology* **142 (Pt 2)**: 217-230.

Sanyahumbi, A.S.C., S.; Wyber, R., Carapetis, J.R., (2016) Global Disease Burden of Group A Streptococcus. In: *Streptococcus pyogenes*: Basic Biology to Clinical Manifestations. D.L.S. Vincent A. Fischetti, Joseph J. Ferretti (ed). University of Oklahoma Health Sciences Center University of Oklahoma Health Sciences Center Library, pp. 661-704.

Savic, D.J., W.M. McShan & J.J. Ferretti, (2002) Autonomous expression of the slo gene of the bicistronic nga-slo operon of *Streptococcus pyogenes*. *Infect. Immun.* **70**: 2730-2733.

Schulze, K., Medina, E., Guzman, C.A., (2006) Intranasal immunization with serum opacity factor (SOF) of *Streptococcus pyogenes* fails to protect mice against lethal mucosal challenge with a heterologous strain. *Vaccine* **24**: 1446-1450.

Shelburne, S.A., 3rd, D. Keith, N. Horstmann, P. Sumby, M.T. Davenport, E.A. Graviss, R.G. Brennan & J.M. Musser, (2008a) A direct link between carbohydrate utilization and virulence in the major human pathogen group A Streptococcus. *Proc. Natl. Acad. Sci. USA* **105**: 1698-1703.

Shelburne, S.A., 3rd, D.B. Keith, M.T. Davenport, N. Horstmann, R.G. Brennan & J.M. Musser, (2008b) Molecular characterization of group A Streptococcus maltodextrin catabolism and its role in pharyngitis. *Mol. Microbiol.* **69**: 436-452.

Slade, H.D., G.A. Knox & W.C. Slamp, (1951) The amino acid nutrition of group A hemolytic *streptococci*, with reference to the effect of glutathione on the cysteine requirement. *Journal of Biochemistry* **62**: 669-675.

Stevens, D.L.B., A.E., (2016a) Impetigo, Erysipelas, and Cellulitis. In: *Streptococcus pyogenes*: Basic Biology to Clinical Manifestations. D.L.S. Vincent A. Fischetti, Joseph J. Ferretti (ed). University of Oklahoma Health Sciences Center University of Oklahoma Health Sciences Center Library, pp. 723-740.

Stevens, D.L.B., A.E., (2016b) Severe Group A Streptococcal Infections. In: *Streptococcus pyogenes*: Basic Biology to Clinical Manifestations. D.L.S. Vincent A. Fischetti, Joseph J. Ferretti (ed). University of Oklahoma Health Sciences Center University of Oklahoma Health Sciences Center Library, pp. 741-770.

Stevens, M.J., D. Molenaar, A. de Jong, W.M. de Vos & M. Kleerebezem, (2010) Involvement of the mannose phosphotransferase system of *Lactobacillus plantarum* WCFS1 in peroxide stress tolerance. *Appl. Environ. Microbiol.* **76**: 3748-3752.

Stincone, A., A. Prigione, T. Cramer, M.M. Wamelink, K. Campbell, E. Cheung, V. Olin-Sandoval, N.M. Gruning, A. Kruger, M. Tauqeer Alam, M.A. Keller, M. Breitenbach, K.M. Brindle, J.D. Rabinowitz & M. Ralser, (2015) The return of metabolism: biochemistry and physiology of the pentose phosphate pathway. *Biol. Rev. Camb. Philos. Soc.* **90**: 927-963.

Stulke, J., M. Arnaud, G. Rapoport & I. Martin-Verstraete, (1998) PRD--a protein domain involved in PTS-dependent induction and carbon catabolite repression of catabolic operons in bacteria. *Mol. Microbiol.* **28**: 865-874.

Sumby, P., S.F. Porcella, A.G. Madrigal, K.D. Barbian, K. Virtaneva, S.M. Ricklefs, D.E. Sturdevant, M.R. Graham, J. Vuopio-Varkila, N.P. Hoe & J.M. Musser, (2005) Evolutionary origin and emergence of a highly successful clone of serotype M1 group A streptococcus involved multiple horizontal gene transfer events. *J. Infect. Dis.* **192**: 771-782.

Sumitomo, T., (2011) Streptolysin S contributes to group A streptococcal translocation acorss an epithelial barrier *J. Biol. Chem.* **286**: 2750-2761.

Sung, K., S.A. Khan, M.S. Nawaz & A.A. Khan, (2003) A simple and efficient Triton X-100 boiling and chloroform extraction method of RNA isolation from Gram-positive and Gram-negative bacteria. *FEMS Microbiol. Lett.* **229**: 97-101.

Swedo, S.E., H.L. Leonard, M. Garvey, B. Mittleman, A.J. Allen, S. Perlmutter, L. Lougee, S. Dow, J. Zamkoff & B.K. Dubbert, (1998) Pediatric autoimmune neuropsychiatric disorders associated with streptococcal infections: clinical description of the first 50 cases. *Am. J. Psychiatry* **155**: 264-271.

Todd, E.W., (1938) The differentiation of two distinct serological varieties of streptolysin, streptolysin O and streptolysin S. *Journal of Pathology and Bacteriology* **47**: 423.

Tong, H., L. Zeng & R.A. Burne, (2011) The EIIABMan Phosphotransferase System Permease Regulates Carbohydrate Catabolite Repression in *Streptococcus gordonii*. *Applied and Environmental Microbiology* **77**: 1857-1965.

Tournu, H., A. Fiori & P. Van Dijck, (2013) Relevance of Trehalose in Pathogenecity: Some General Rules, Yet Many Exceptions. *PLoS Path.* **9**: e1003447.

Trapnell, C., A. Roberts, L. Goff, G. Pertea, D. Kim, D.R. Kelley, H. Pimentel, S.L. Salzberg, J.L. Rinn & L. Pachter, (2012) Differential gene and transcript expression analysis of RNA-seq experiments with TopHat and Cufflinks. *Nature protocols* **7**: 562-578.

Valdes, K., (2016) Functional Characterization of the Link Between Carbohydrate Metabolism and the Pathogenesis of the Invasive M1T1 Group A Streptococcus, p. 287. ProQuest.University of Maryland.

Valdes, K.M., G.S. Sundar, L.A. Vega, A.T. Belew, E. Islam, R. Binet, N.M. El-Sayed, Y. Le Breton & K.S. McIver, (2016) The *fruRBA* operon is necessary for Group A Streptococcal growth in fructose and for resistance to neutrophil killing during growth in whole human blood. *Infect. Immun.*

Van den Bogert, B., J. Boekhorst, R. Herrmann, E.J. Smid, E.G. Zoetendal & M. Kleerebezem, (2013) Comparative genomics analysis of Streptococcus isolates from the human small intestine reveals their adaptation to a highly dynamic ecosystem. *PLoS One* **8**: e83418.

Vitko, N.P., M.R. Grosser, D. Khatri, T.R. Lance & A.R. Richardson, (2016) Expanded Glucose Import Capability Affords *Staphylococcus aureus* Optimized Glycolytic Flux during Infection. *MBio* **7**.

Voigt, C., H. Bahl & R.J. Fischer, (2014) Identification of PTS(Fru) as the major fructose uptake system of *Clostridium acetobutylicum*. *Appl. Microbiol. Biotechnol.* **98**: 7161-7172.

Watanabe, S., Shimomura, Y., Ubukata, K., Kirike, T., Miyoshi-Akiyama, T., (2013) Concomitant Regulation of Host Tissue-Destroying Virulence Factors and

Carbohydrate Metabolism During Invasive Diseases Induced by Group G Streptococci *The Journal of Infectious Diseases* **208**: 1482-1493.

Wen, Z.T., C. Browngardt & R.A. Burne, (2001) Characterization of two operons that encode components of fructose-specific enzyme II of the sugar:phosphotransferase system of *Streptococcus mutans*. *FEMS Microbiol. Lett.* **205**: 337-342.

Wessels, M.R., (2016) Pharyngitis and Scarlet Fever. In: *Streptococcus pyogenes*: Basic Biology to Clinical Manifestations. D.L.S. Vincent A. Fischetti, Joseph J. Ferretti (ed). University of Oklahoma Health Sciences Center University of Oklahoma Health Sciences Center Library, pp. 705-722.

Willenborg, J., A. de Greeff, M. Jarek, P. Valentin-Weigand & R. Goethe, (2014) The CcpA regulon of *Streptococcus suis* reveals novel insights into the regulation of the streptococcal central carbon metabolism by binding of CcpA to two distinct binding motifs. *Mol. Microbiol.* **92**: 61-83.

Wishart, D.J.T., Guo AC, Wilson M, Knox C, Liu Y, Djoumbou Y, Mandal R, Aziat F, Dong E, Bouatra S, Sinelnikov I, Arndt D, Xia J, Liu P, Yallou F, Bjorndahl T, Perez-Pineiro R, Eisner R, Allen F, Neveu V, Greiner R, Scalbert A., (2013) B 3.0--The Human Metabolome Database in 2013. *Nucleic Acids Res.* **41**: 801-807.

Wishart DS, K.C., Guo AC, Eisner R, Young N, Gautam B, Hau DD, Psychogios N, Dong E, Bouatra S, Mandal R, Sinelnikov I, Xia J, Jia L, Cruz JA, Lim E, Sobsey CA, Shrivastava S, Huang P, Liu P, Fang L, Peng J, Fradette R, Cheng D, Tzur D, Clements M, Lewis A, De Souza A, Zuniga A, Dawe M, Xiong Y, Clive D, Greiner R, Nazyrova A, Shaykhutdinov R, Li L, Vogel HJ, Forsythe I., (2009) HMDB: a knowledgebase for the human metabolome. *Nucleic Acids Res.* **37**: 603-610.

Wishart DS, T.D., Knox C, Eisner R, Guo AC, Young N, Cheng D, Jewell K, Arndt D, Sawhney S, Fung C, Nikolai L, Lewis M, Coutouly MA, Forsythe I, Tang P, Shrivastava S, Jeroncic K, Stothard P, Amegbey G, Block D, Hau DD, Wagner J, Miniaci J, Clements M, Gebremedhin M, Guo N, Zhang Y, Duggan GE, Macinnis GD, Weljie AM, Dowlatabadi R, Bamforth F, Clive D, Greiner R, Li L, Marrie T, Sykes BD, Vogel HJ, Querengesser L., (2007) HMDB: the Human Metabolome Database. *Nucleic Acids Res.* **35**: 521-526.

Wu, M., Chen, Y., Lin, T., Hsieh, P., Wang, J., (2012) Cellobiose-Specific Phosphotransferase System of *Klebsiella pneumoniae* and its Importance in Biofilm Formation and Virulence. *Infect. Immun.* **80**: 2464-2472.

Yang, Y., L. Zhang, H. Huang, C. Yang, S. Yang, Y. Gu & W. Jiang, (2017) A Flexible Binding Site Architecture Provides New Insights into CcpA Global Regulation in Gram-Positive Bacteria. *MBio* **8**.

Young, M.D., M.J. Wakefield, G.K. Smyth & A. Oshlack, (2010) Gene ontology analysis for RNA-seq: accounting for selection bias. *Genome Biology* **11**: R14.

Yu, G., L.G. Wang, Y. Han & Q.Y. He, (2012) clusterProfiler: an R package for comparing biological themes among gene clusters. *OMICS* **16**: 284-287.

Zeng, L. & R.A. Burne, (2010) Seryl-phosphorylated HPr regulates CcpA-independent carbon catabolite repression in conjunction with PTS permeases in *Streptococcus mutans*. *Mol. Microbiol.* **75**: 1145-1158.

Zuniga, M., I. Comas, R. Linaje, V. Monedero, M.J. Yebra, C.D. Esteban, J. Deutscher, G. Perez-Martinez & F. Gonzalez-Candelas, (2005) Horizontal Gene Transfer in the Molecular Evolution of Mannose PTS Transporters. *Mol. Biol. Evol.* **22**: 1673-1685.